AGH
Akademia Górniczo-Hutnicza im. Stanisława Staszica w Krakowie

DZIEDZINA NAUK INŻYNIERYJNO-TECHNICZNYCH

DYSCYPLINA : AUTOMATYKA, ELEKTRONIKA, ELEKTROTECHNIKA I TECHNOLOGIE KOSMICZNE

ROZPRAWA DOKTORSKA

Metodyka kontroli uszkodzeń w dźwigarach skrzynkowych suwnic pomostowych

Autor: mgr inż. Arun Kumar Yadav

Promotor: prof. dr hab. inż. Janusz Szpytko

Praca wykonana:
Akademia Górniczo-Hutnicza im. Stanisława Staszica w Krakowie
Wydział Inżynierii Mechanicznej i Robotyki
Katedra Systemów Wytwarzania

Kraków, 2025

AGH University of Krakow

FIELD OF SCIENCE ENGINEERING AND TECHNOLOGY

SCIENTIFIC DISCIPLINE: AUTOMATION, ELECTRONICS, ELECTRICAL ENGINEERING AND SPACE TECHNOLOGIES

DOCTORAL THESIS

Crack inspection methodology for box girders the overhead crane

Author: M.Sc. Eng. Arun Kumar Yadav

Supervisor: Prof. Dr hab. C. Eng. Janusz Szpytko

Completed in:
AGH University of Krakow
Faculty of Mechanical Engineering and Robotics
Department of Manufacturing Systems

Krakow, 2025

ABSTRACT

Suwnice pomostowe pełnią kluczową rolę w cyklicznych procesach przemieszczania ładunków o zróżnicowanych masach i różnym poziomie ich zagrożenia dla otoczenia, w ograniczonej przestrzeni o zróżnicowanych warunkach środowiskowych. Suwnice pomostowe niejednokrotnie są krytycznymi urządzeniami w procesach technologicznych. Są urządzeniami podlegającymi dozorowi technicznemu.

Charakter pracy suwnic pomostowych i warunki ich użytkowania (intensywność i dynamika) skutkują w szczególności degradacjami stanu technicznego dźwigarów (konstrukcja nośna), które w połączeniu z trudnymi warunkami otoczenia (gradienty temperatury, wilgotność, pole magnetyczne, inne źródła agresywnego oddziaływania, drgania) mają najczęściej charakter zmęczeniowy i przeciążeniowy (stany nieustalone, skoszenia, inne). Z praktyki eksploatacji suwnic możliwe jest stwierdzenie, że 80% uszkodzeń w konstrukcjach nośnych (dźwigarach) jest skutkiem zmęczenia materiału, a 20% jest skutkiem przeciążeń statycznych i dynamicznych zachodzących w procesie użytkowania.

Obserwowanymi skutkami uszkodzeń dźwigarów skrzynkowych suwnic pomostowych (trwałe zmiany w ich geometrii w płaszczyznach poziomych i pionowych oraz pęknięcia i inne zmiany w strukturze materiału dźwigarów, korozja) są dodatkowe naprężenia i odkształcenia, które mają swoje przełożenie na bezpieczeństwo i niezawodność eksploatacyjną urządzenia oraz jego trwałość eksploatacyjną (w szczególności żywotność konstrukcji nośnej suwnicy) oraz koszty eksploatacji. Dlatego też istotnym zagadnieniem jest bieżąca ocena stanu technicznego dźwigarów suwnic pomostowych, w szczególności możliwych zmian w strukturze materiału konstrukcji.

Przedmiotem badań są dźwigary skrzynkowe suwnic pomostowych oraz możliwość identyfikacji (kontroli) możliwych uszkodzeń. Realizacja badań zmian zachodzących w strukturze materiału dźwigarów suwnic pomostowych jest zagadnieniem czasochłonnym, trudnym i złożonym, z uwagi na wielkogabarytowość konstrukcji mostu suwnicy pomostowej, instalację urządzenia w miejscu zabudowy (użytkowania) na znacznej wysokości, możliwe trudne warunki otoczenia, ograniczony czas dostępności urządzenia dla potrzeb badań, możliwe zagrożenia w zakresie bezpieczeństwa dla personelu wykonującego badania stanu technicznego dźwigarów. Dlatego też badania dźwigarów suwnic pomostowych są realizowane w praktyce zazwyczaj nieregularnie.

Przedmiotem pracy jest projekt i wykonanie specjalistycznego robota (narzędzia) umożliwiającego zdalną niedestrukcyjną inspekcję (uszkodzeń)

struktury materiałowej dźwigarów skrzynkowych suwnic pomostowych o złożonej geometrii, a ponadto opracowanie metody wnioskowania o stanie technicznym konstrukcji. Celem naukowym pracy jest koncepcja i projekt specjalistycznego robota umożliwiającego samodzielne przemieszczanie się po złożonym geometrycznie dźwigarze (w poziomie i w pionie, na i pod konstrukcją) umiejscowionym w przestrzeni roboczej. Celem aplikacyjnym pracy jest wykonanie specjalistycznego robota wyposażonego w czujnik GMR (Giant Magneto-Resistance) z elastyczną ramą wspomagającą przemieszczanie się po złożonej geometrycznie konstrukcji dla potrzeb zdalnej niedestrukcyjnej oceny stanu technicznego (uszkodzeń struktury materiałowej) dźwigarów skrzynkowych suwnic pomostowych.

Teza pracy: możliwe jest zautomatyzowanie prac inspekcyjnych dźwigarów suwnic pomostowych skrzynkowych w rezultacie zastosowania specjalistycznego robota. W rezultacie realizacji badań konstrukcji dźwigarów suwnic w układzie online możliwe jest zwiększenie ich trwałości eksploatacyjnej.

Wykorzystanie specjalistycznego zdalnie sterowanego robota inspekcyjnego do automatyzacji procesu oceny stanu technicznego dźwigarów suwnic pozwala skrócić całkowity czas badania konstrukcji, umożliwia dostęp do wcześniej niedostępnych obszarów, zwiększa bezpieczeństwo procesu badań. Pod tym względem proponowane rozwiązanie jest oryginalne. Trwałe uszkodzenia konstrukcji i korozja są głównymi przyczynami degradacji stalowych mostów podsuwnicowych, co zmniejsza ich wytrzymałość i żywotność.

Opracowano i wykonano zautomatyzowany specjalistyczny robot do wykrywania pęknięć, korozji i innych rodzajów defektów dźwigarów suwnic z wykorzystaniem techniki badań nieniszczących. Robot jest wyposażony w szereg gigantycznych czujników magnetooporowych (GMR), może również przenosić czujniki specjalistyczne innego typu, zbierać dane pomiarowe i przesyłać je do zdalnej stacji gromadzenia i przetwarzania wyników badań w czasie rzeczywistym dla potrzeb decyzyjnych.

Istotnym elementem robota są jego koła magnetyczne, które nie tylko pomagają w „wspinaniu" się po stalowych konstrukcjach, ale także generują pole magnetyczne umożliwiające wykrywanie uszkodzeń elementów stalowych. Układ czujników typu GMR kalibruje każdą zmianę gęstości strumienia magnetycznego. Technika detekcji koncentruje się na analizie zjawiska strumienia pola magnetycznego, które w przypadku uszkodzenia elementu stalowego zmienia przewodność elektryczną i gęstość pola magnetycznego. Czujnik matrycowy GMR monitoruje niewielkie różnice w gęstości strumienia pola magnetycznego w rezultacie których możliwe jest wykrycie defektu konstrukcji.

Opracowano i wykonano robot mobilny zdalnie sterowany, z możliwością planowania obszaru badawczego konstrukcji dźwigara, z nawigacją w zakresie pozycjonowania w przestrzeni roboczej, sensorami dla potrzeb rejestracji parametrów eksploatacyjnych użytecznych w ocenie stanu technicznego konstrukcji (lasery, czujniki GMR, kamery), ze systemem przetwarzania i analizy oraz prezentacji wyników badań, algorytmami lokalizacji i planowania trasy. Robot z wynikiem pozytywnym został przetestowany w praktyce.

ABSTRACT

Overhead traveling cranes play a key role in the cyclical processes of moving loads of various weights and varying levels of their risk to the environment, in a limited space with various environmental conditions. Overhead cranes are often critical devices in technological processes. They are devices subject to technical supervision.

The nature of the operation of overhead cranes and the conditions of their use (intensity and dynamics) result, in particular, in the degradation of the technical condition of the girders (supporting structure), which, combined with difficult environmental conditions (temperature gradients, humidity, magnetic field, other sources of aggressive impact, vibrations), most often have fatigue and overload character (transients, skews, other). From the practice of crane operation, it is possible to state that 80% of damage to load-bearing structures (girders) is the result of material fatigue, and 20% is the result of static and dynamic overloads occurring in the process of use.

The observed effects of damage to the box girders of overhead cranes (permanent changes in their geometry in horizontal and vertical planes as well as cracks and other changes in the structure of the girders material, corrosion) are additional stresses and deformations that affect the safety and operational reliability of the device and its service life (in particular, the service life of the crane supporting structure) and operating costs. Therefore, an important issue is the ongoing assessment of the technical condition of overhead crane girders, in particular possible changes in the structure of the construction material.

The subject of the thesis are box girders of overhead travelling cranes and the possibility of identifying (controlling) possible damage. Execution of tests of changes in the material structure of bridge crane girders is a time-consuming, difficult and complex issue, due to the large-size structure of the bridge crane bridge, installation of the device at the place of installation (use) at a considerable height, possible difficult environmental conditions, limited time of availability of the device for tests, possible safety hazards for the personnel performing technical condition tests of the crane girder. Therefore, tests of overhead crane girders are usually carried out irregularly in practice.

The subject of the thesis is the design and implementation of a specialized robot (tool) enabling remote non-destructive inspection (of damage) of the material structure of box girders of overhead cranes with complex geometry, and also the development of a method for inferring the technical condition of the structure. The scientific goal of the work is the concept and design of a specialized robot that allows independent movement on a geometrically

complex girder (horizontally and vertically, on and under the structure) located in the working space. The application purpose of the work is to make a specialized robot equipped with a GMR (Giant Magneto-Resistance) sensor with a flexible frame supporting movement on a geometrically complex structure for the purposes of remote non-destructive assessment of the technical condition (damage to the material structure) of box girders of overhead cranes.

Thesis of the work: it is possible to automate the inspection works of box crane girders as a result of using a specialized robot. As a result of carrying out tests on the structure of overhead crane girders in the online system, it is possible to increase their service life.

The use of a specialized remotely controlled inspection robot to automate the process of assessing the technical condition of crane girders allows you to shorten the total time of structure testing, enables access to previously inaccessible areas, and increases the safety of the testing process. In this respect, the proposed solution is original. Permanent structural damage and corrosion are the main causes of degradation of steel crane bridges, which reduces their strength and service life.

An automated specialized robot for detecting cracks, corrosion and other types of defects in crane girders using non-destructive testing techniques was developed and build. The robot is equipped with a series of giant magnetoresistance (GMR) sensors, it can also carry other types of specialized sensors, collect measurement data and send them to a remote station for collecting and processing test results in real time for decision-making purposes.

An important element of the robot are its magnetic wheels, which not only help in "climbing" on steel structures, but also generate a magnetic field that allows detecting damage to steel elements. The GMR sensor system calibrates each change in the magnetic flux density. The detection technique focuses on the analysis of the magnetic field flux phenomenon, which changes the electrical conductivity and magnetic field density in the event of damage to the steel element. The GMR matrix sensor monitors small variations in the magnetic flux density, as a result of which it is possible to detect a structural defect.

A remotely controlled mobile robot was developed and build, with the possibility of planning the testing area of the girder structure, with navigation in the field of positioning in the working space, sensors for recording operating parameters useful in assessing the technical condition of the structure (lasers, GMR sensors, cameras), with a system for processing and analysis and presentation of inspection results, location and route planning algorithms. The robot with a positive result has been tested in practice.

Table of content PAGES

LIST OF FIGURES **Page**

LIST OF TABLES

Page

ABBREVIATIONS

CASES

AMR:	Anisotropic magneto resistors
AUV:	Autonomous underwater vehicles
CMAA:	Crane Manufacturers Association of America
DCE:	Data communication equipment
DoF:	Degree of freedom
DPT:	Dye penetrates testing
DTE:	Date terminal equipment
DCE	Data Communication Equipment
EC:	Eddy Current
ECT:	Eddy current testing
ESC:	Electronic speed control
ESPI:	Electronic Speckle Pattern Interferometry
FEM:	European Federation Standard
GMR:	Giant magneto resistance
GPS:	Global Positioning System
GSM:	Global Systems for Mobile Communication
HMI:	Hoist Manufacturers Institute
HROV:	Hybrid Remotely Operated Vehicle
ISO:	International Organization for Standardization
MF:	Magnetic field
MF:	Magnetic flux
MFL:	Magnetic flux leakage
MMM:	Metal Memory method
MPT:	Magnetic Particle Testing
NDFeb:	Neodymium Iron Boron
NDT:	Non-destructive testing
ROS:	Robot operating System
ROV:	Remotely operated vehicles
SCC:	Stress corrosion cracking
SCZ:	Stress concentration zones
SHM:	Structural health monitoring
SLAM:	Self-localization and mapping
SmCo:	Samarium Cobalt
SMLF:	Self-magnetic leakage fields
UAV:	Unmanned aerial vehicles

ACKNOWLEDGEMENTS

This research work has been co-financially supported by the UNESCO Fellowship Programme in Engineering, coordinated by the UNESCO AGH Chair and the AGH University of Krakow research grant (Faculty of Mechanical Engineering and Robotics), as well as the Polish Ministry of Education and Science.

A few Word for the Journey……………………………………

I'd like to thank Professor Janusz Szpytko for his attentive attention and great mentoring during my PhD studies. I consider myself extremely fortunate to have had his advice and extensive backing from day one when I arrived at the AGH University of Science and Technology in Krakow. I additionally gained academic expertise and technical abilities from his rigorous instruction, but he also developed my thinking as a competent researcher and responsible instructor via our daily debates.

I am humbled to him for numerous opportunities to engage in many initiatives, cooperate with many intelligent people, and widen my views. It had been a delight to collaborate with such a wonderful group of colleagues in his laboratory, including Dr. Agnieszka, Dr.Pawel, Dr. Jaroslaw and Mr. Jun Aguila. Several individuals who have aided me in my academic endeavours, both directly and indirectly.

Finally, I would be negligent if I did not acknowledge my Family, particularly my sister and mother. Their confidence in me has maintained my enthusiasm and drive strong throughout the process. I'd also want to thank my colleagues Dagmara, Sahil, Sushil, and Dr.Aayush for their entertaining and emotional backing.

DECLARATION

I hereby declare that I, under the supervision of Prof. Dr. hab. inż. Janusz Szpytko in the Manufacturing Systems Department under the Faculty of Mechanical Engineering and Robotics at AGH University of Science and Technology, Krakow, have entirely conceived, planned, executed, and documented the contents of this dissertation and the wording contained in it. It is also worth noting that significant sections of the dissertation were extracted straight from the following publications, which are extracts of the broader research study's conclusions and have not been presented to be evaluated for any other academic or professional award.

1. **Yadav, A., & Szpytko, J. (2020).** Development of Portable Wireless Non-Destructive Crack Identification Method by Using GMR Sensor Array for Overhead Crane Bridges. 11th International Symposium on NDT in Aerospace, Nov 2019, Paris-Saclay, France. e-Journal of Non-destructive Testing Vol. 25(2). https://www.ndt.net/?id=25059
2. **Yadav, A., & Szpytko, J. (2020)**. Magnetic Wheeled Automated Robot for Structural Health Monitoring of Overhead Crane by using NDT method. Singapore International NDT Conference & Exhibition, 4-5 Dec 2019. e-Journal of Non-destructive Testing Vol. 25(4). https://www.ndt.net/?id=25147
3. **Yadav, A., & Szpytko, J. (2019)**. Design of an automated magnetic wheeled robot for crack inspection of overhead cranes by using NDT GMR sensor. NDE 2018 Conference & Exhibition of the society for NDT (ISNT), 19-21 December 2018, Mumbai, India. e-Journal of Non-destructive Testing Vol. 24(6). https://www.ndt.net/?id=24361
4. **Yadav, Arun Kumar, and Janusz Szpytko (2022).** "Method of increasing reliability of large dimensional bridge-type structures." Journal of KONBiN 52.2 (2022): 47-62.
5. **YADAV, Arun Kumar and SZPYTKO Janusz (2020)** Interoperability tool to the non-destructive testing: crane bridge case study W: Projektowanie i eksploatacja maszyn roboczych, Cz. 2 / red. nauk. Tadeusz Łagoda, Marta Kurek, Andrzej Kurek. — Opole: Oficyna Wydawnicza Politechniki Opolskiej, 2020. — (Studia i Monografie Politechnika Opolska; ISSN 1429-6063; z. 542). — ISBN: 978-83-66033-84-9. — S. 283-294.
6. **YADAV, Arun Kumar and SZPYTKO Janusz (2024)** An Innovative fault detection robotic tool for overhead cranes in industries: Magnetic wheel modelling and experimental validation./ / Arun K. YADAV, Janusz SZPYTKO// International Conference on Innovative Intelligent Industrial Production and Logistics, Springer CCIS series, ISSN 1865-0937.

Arun Kumar Yadav

Prof. dr hab.inż Janusz Szpytko

CHAPTER 1

INTRODUCTION

A timely assessment of an overhead cranes, a structural health is required for almost all transportation infrastructure in order to forestall some kind of functional collapse and, eventually, catastrophic accidents. Overhead crane structures may be found in a wide range of places, some of which are not even considered to be part of the civil, mechanical, or any other kind of infrastructure. Because of their extreme size and weight, many of these transportation structures make it hard to do the regular health monitoring that is required of them. In the absence of monitoring and inspection, there are terrible ramifications. According to the reports, there were twenty-four people hurt as a result of the fall of a tower crane in New York City in August of 2008. Eleven of those wounded were first responders. During the month of August in 2008, a tower crane in China fell on top of a kindergarten, causing the deaths of five children and injuries to three more.

The breakdown of the crane's structural integrity was a contributing factor in a number of tragic incidents that took place in the year 2008, including those listed below. There were total of 81 collapses that took place between the years 1992 and 2006, which ultimately led to the deaths of 81 people. It is not known what caused the bulk of the 81 failures, which together account for 51% of all crane collapses. Uneven surfaces, collapses of bridges, and other variables have been related to some of the known instances (Shin,2015), (eLCOSH,2022). Figure 1.1 provides a more in-depth discussion of the factors that led to the collapse.

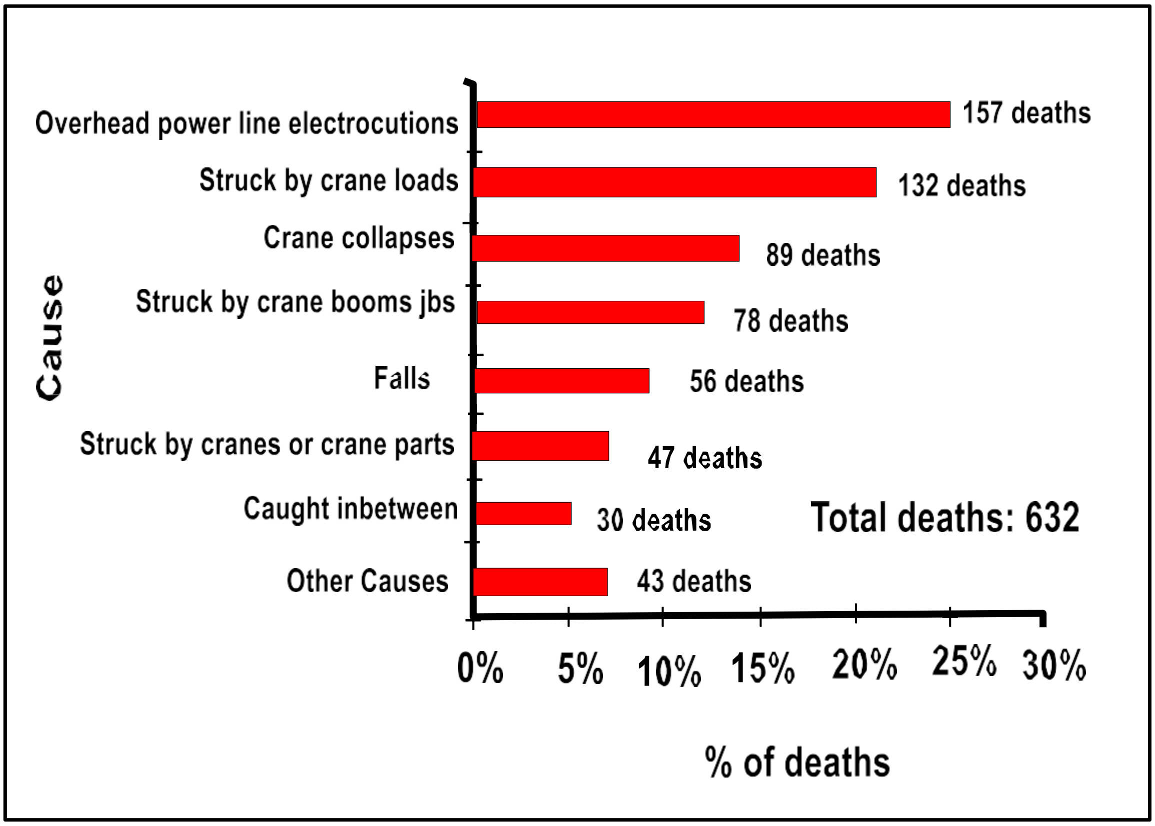

Fig1. 1 Statics of crane failure & death rates (Modified after Shin,2015).

The risks of structural failure and the timing requirements for monitoring structural health have been brought into sharp focus by a number of recent events. Overhead cranes at ports spend much of their days out in the open, where they are subjected to the weather conditions, direct loading and unloading, and chemical reactions. The below Fig. 1.2 depicts the number of incidents occurred from year 2013 to 2019, on sea ports crane in fixed and motion scenario. From the graph it can be seen clearly the incident rates is growing yearly.

Human error and negligence are the primary causes of 90% of accidents, according to the Crane Inspection and Certification Bureau (CICB). The Census of Fatal Occupational Injuries (CFOI), another publication from the Bureau of Labour Statistics, shows that there were 297 crane-related deaths between 2011 and 2017, making the average yearly death toll from these incidents 42.

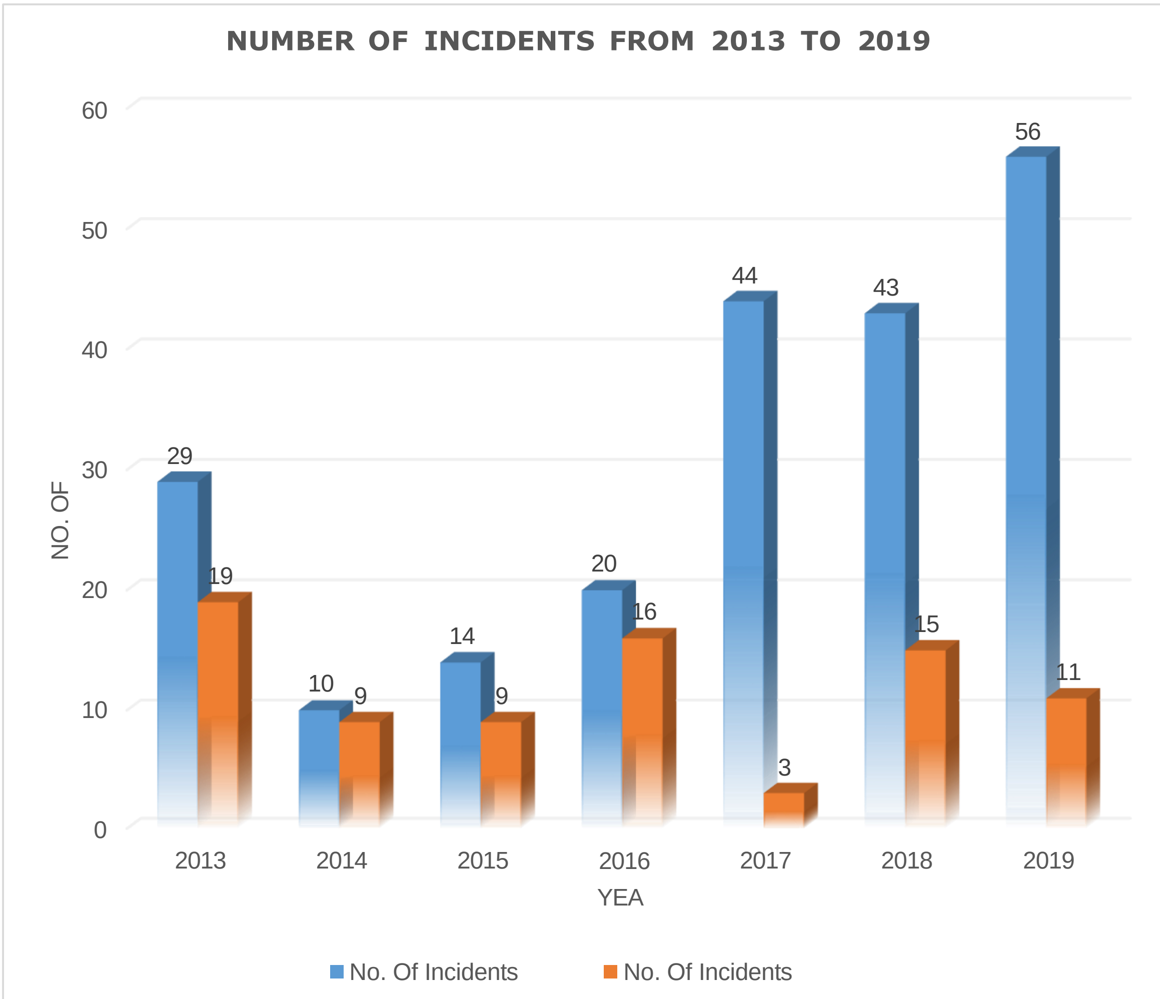

Fig1. 2 Statics of Crane incident during year 2013 to 2019 (Self)

Figure 1.3 below shows further data from 1992 to 2006. Despite the fact that the data is outdated, it is presented here to emphasize the 50% incidence of other reasons. It has occasionally been challenging to determine the incident's cause in the past. It can be due to cracks, fatigue, fatigued crane parts, or a combination of these.

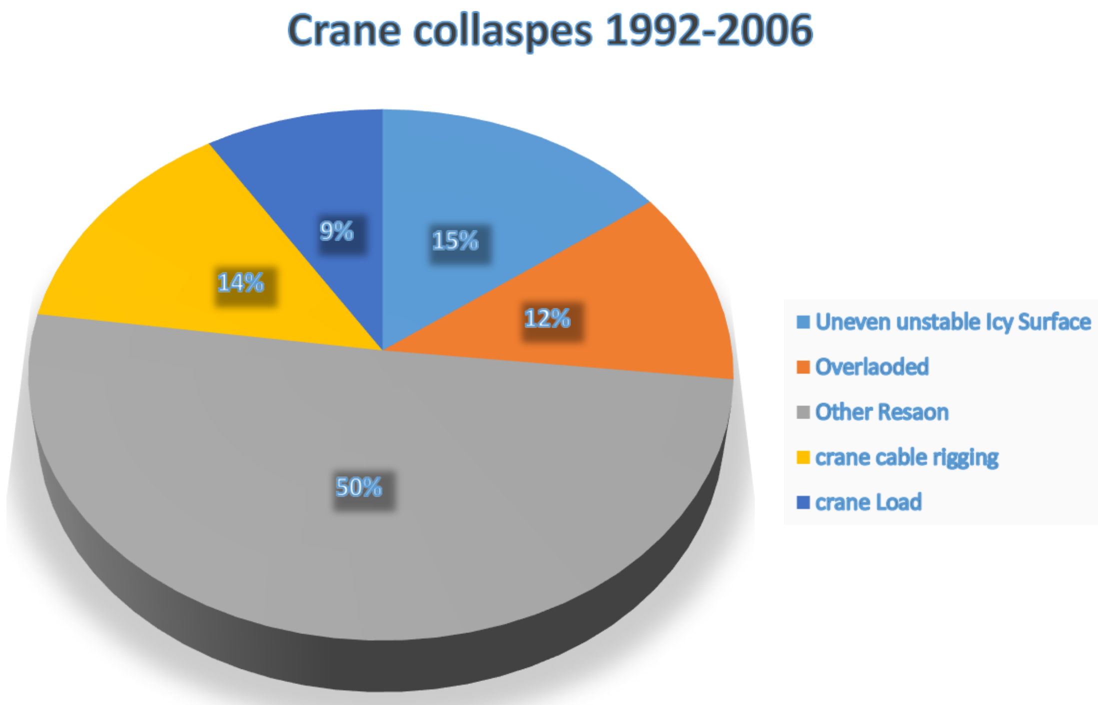

Fig1. 3 Crane Collapses statics (Modified after Michael M. (2010)

Therefore, it is essential to keep up with routine maintenance to assure the cranes' continued safe operation. The majority of the facility's overhead cranes are now inspected visually. Ropes, hooks, the sway control, and any visible fractures are a few of the primary components inspected during a visual inspection of overhead cranes. In addition, they tried to ensure the crane was in working order generally. Due to their importance to the functioning of cranes, these components undergo frequent inspections. Crane girder, visual inspections cannot be performed often due to their enormous size. Some elements of the crane can't be visually inspected since they're too thin or too high up for the inspector to reach.

A skilled engineer must undertake a visual examination in order to discover the cracks and defects. Nonetheless, there are a number of drawbacks to visual techniques, including the following:

1) A lack of visual ability on the part of the inspector results in very poor accuracy.
2) Errors are possible due to the inherent fallibility of humans.
3) It is time-consuming and inefficient, and the outcomes are less precise.

In order to prevent functional malfunctions and catastrophic impacts in the case of an accident, it is crucial to monitor the structural health of almost all manufactured transportation infrastructure on a regular basis. Talking about particularly about steel industries every manufacturing line in the steelworks utilizes a large number of overhead cranes for a variety of activities, including conveying molten steel, hauling steel slabs, transporting goods, etc. The building's two walls are supported by an overhead crane. It consists of three components: a row girder (sometimes referred to as a runway girder), a crane girder, and a crab trolley.

A crane girder is a movable girder that supports weights by carrying the crab trolley. Additionally, referred to as a "running girder," In the majority of situations, the weight of the items to be carried in conjunction with the weight of the girder creates a repeating stress on a moving girder, resulting in multiple instances (Tachibana and Maeda, 1996; Shimura and Uno, 1986). Damage to the overhead crane's running girder, which is one of its components, is likely to result in catastrophic accidents and have a substantial effect on the production line.
Steel bridges of overhead cranes are an essential component of the infrastructure for material/goods transportation, and their maintenance and repair need fast decision-making. Cranes suspended from the ceiling play a vital role in the transportation business across a variety of industries. Numerous overhead cranes are installed in the majority of steel producing facilities to simplify the manufacture of steel. The components of an overhead crane are beam girders, crab trolleys, and runway girders. The

beam girder-mounted crab trolley transports the weight. The runway girder bears the whole weight of the beam girder. When working with a heavy load, the overhead cranes' permanent structures are exposed to a range of strains and loads. The beam girder receives a large degree of fluctuating stress and a lot of varying loads corresponding to the tremendous applied loads.

Due to the high levels of stress and the repeated application of varying loads, a high-stress-concentrated zone forms in the steel structure. These stress-concentrated zones initiate the formation of fractures in the metal body.

Corrosion of the steel structure causes structural breakdown, resulting in severe financial loss. Corrosion can be continually and efficiently monitored, resulting in failure prevention and cost savings. Corrosion and structural fatigue are the primary causes of crane failure.

Corrosion is induced by the environment and may lead to structural collapse if left unchecked (Nguyen & La, 2018). It is, nevertheless, not difficult to judge. The development of structural fatigue in the steel body structure of an overhead crane when exposed to varied loads is known as structural fatigue. As a consequence of fatigue, several cranes have experienced structural failures. Steel is used in overhead cranes for many reasons, including its high strength, durability, ease of production, and cheap cost (Wang & Kawamura, 2016). Steel is also employed in various industries, including building. However, when employed in hostile environments, its corrosion and rust resistance is poor, which is one of the reasons for the possible threat to structural security (Lu et al. 2020).

The structures grow increasingly brittle with time, increasing the chance of fatigue. The most efficient way to prolong the life of overhead crane steel structures is to do a complete examination and analysis of these structures. Overhead crane maintenance and inspection, on the other hand, bring a host of challenges and worries.

The cost of inspection is the first item to consider, followed by labor and material expenses. Crane inspections are a time-consuming and costly activity that requires a significant amount of labor and resources. It is not incorrect to state that every steel company uses a big number of overhead cranes for a variety of tasks, and no industry is prepared to spend a considerable money for frequent overhead crane inspection.

The second problem is a lack of competent inspectors on the task. It is difficult to find a significant number of expert inspectors accessible at the same time. In addition, while checking overhead crane bridges, the inspection team employed visual examination to search for surface flaws, which is a novel approach. Crack inspection techniques include visual examination, ultrasonic methods, magnetic particle defect detection, penetrating flaw identification, and eddy current methods. When it comes to inspecting large buildings, most of the non-destructive testing (NDT) approaches are very expensive (Faroq Howlader & Sattar, 2015). As a result, the most effective technique is to automate the inspection process employing certain automated robots equipped with sensors and non-destructive testing technologies. We can enhance inspection speed and safety while cutting costs and incident rates by automating the process and integrating robots.

This research project's main goal is to construct an autonomous inspection robotic too for use in overhead crane testing and supervision. This will provide

- Improve inspection quality
- Improve inspection speed and frequency
- Reduce the cost of periodic inspections;
- Improve safety and dependability throughout the inspection and monitoring process
- Time saving by reducing overhead crane downtime.

The key benefit of the developed robotic system is that it can check the confined passages, vertical surfaces, and horizontal surfaces of overhead crane bridges. It may reach the bottom surface of the girder as well as the base of overhead crane pillars. The inspection robot's integration of many sensors and a high-definition camera allows it to take close-up images of cracks and faults and transmits them to remote places for additional examination. The robot's real-time live streaming video functions provide live footage of the inspection area as well as a live GMR sensor output graph. This robot is capable of inspecting and monitoring overhead cranes in both autonomous and semi-autonomous mode. The system's detailed characteristics will be explored in the next chapters. Meanwhile, a brief description to highlight the general concepts of cranes for proper perception and how it is related to the subject of the study are presented in the subsequent subsections.

1.1 Introduction of cranes

An overhead crane is a heavy machine that can raise and lower huge objects and transport them to other locations. Most overhead cranes have three basic motions.

- The first action is the lifting and lowering of the material by the hoist.
- With the help of the cross traverse (trolley), the hoist may be positioned directly above the load.
- The crane may be moved around the work area in a circular motion thanks to the lengthy trip of the gantry or bridge action.

A crane and a hoist are two different machines; a crane lifts objects, while a hoist moves objects laterally. Based on their key operational criteria—crane structure motion type, load type and weight, crane location, geometric characteristics, operating regimes, and climatic conditions—overhead crane designs differ greatly from one another. Selecting the appropriate overhead crane is crucial for streamlining processes and increasing productivity.

1.2 Classification of overhead cranes

While many distinct varieties of overhead cranes exist, the most majority of installations may be categorized into four broad types

- *Single-girder cranes*: A single bridge girder is held up by two end trucks. The bridge's flanged bottom provides access to a trolley hoist system.
- *Double Girder Bridge Cranes*: Two bridge girders and a pair of end trucks make up this kind of bridge crane. The trolley travels along tracks attached to the bridge girders.
- *Gantry Cranes*: These cranes are similar to standard overhead cranes in that the bridge supporting the trolleys is securely supported by two or more legs that work on fixed rails or other runways.
- *Monorail:* A trolley hoist is all that is needed for certain applications, such as a factory assembly line or a service line. This kind of crane is built of I-beams, which are common in factory ceiling systems. The trolleys glide down the flat surface on the bottom horizontal bars of the beam. The hoisting mechanism is identical to the one of a single-girder crane, with the notable exception of the permanent girder and the lack of a moving bridge.

1.3 Classification of crane based on configurations

- Down Running or Under (U/R)
- Above Running Top (T/R)

1.3.1 Under-running cranes

An under-running or underslung crane has a suspension system fastened to the underside of the frame. Serving as the crane rail, the bottom flange of the crane beams frequently only covers a portion of the structure's column-to-column distance, giving the crane wheels' stability. An under-run crane can typically lift 1 to 10 tons, with certain configurations being able to lift up to 25 tons and span more than 90 feet. If available space permits, runways suspended from pre-existing building components may be used to support under-hung cranes, providing optimal side approaches with ample headroom. Below is a diagram of the under-running crane configuration from Figure 1.4.

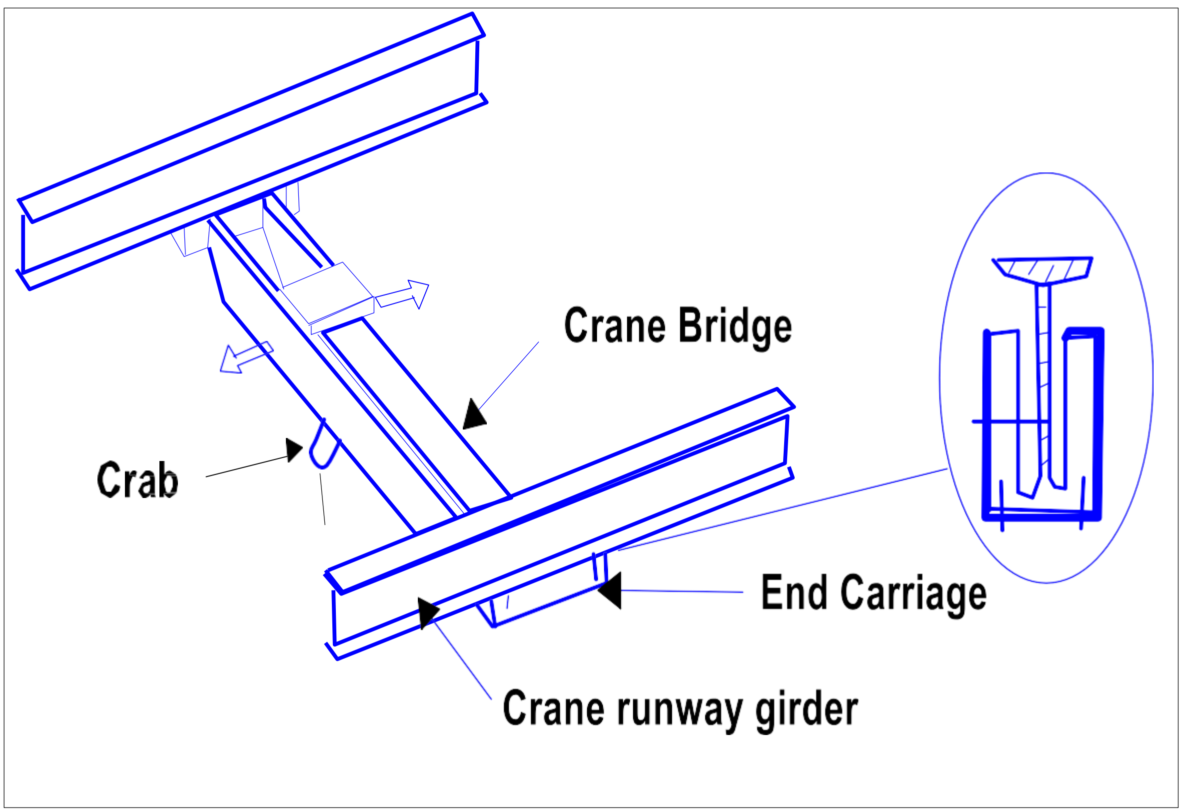

Fig1. 4 Below Running Crane (Modified after Shin, 2015)

1.3.2 Above or Top running cranes

The building's columns or specially designed columns for the crane support the runway beam on which the crane bridge is mounted. The most common type of crane design for transferring crane weights to building columns or standalone structures is one with top-running canes. These cranes are the most variable in terms of capacity, span, and service class; they frequently span across the entire width of the frame supports. There are options for single and double girder constructions (Shin 2015). An illustration of the configuration of a top running crane is shown in fig. 1.5 below.

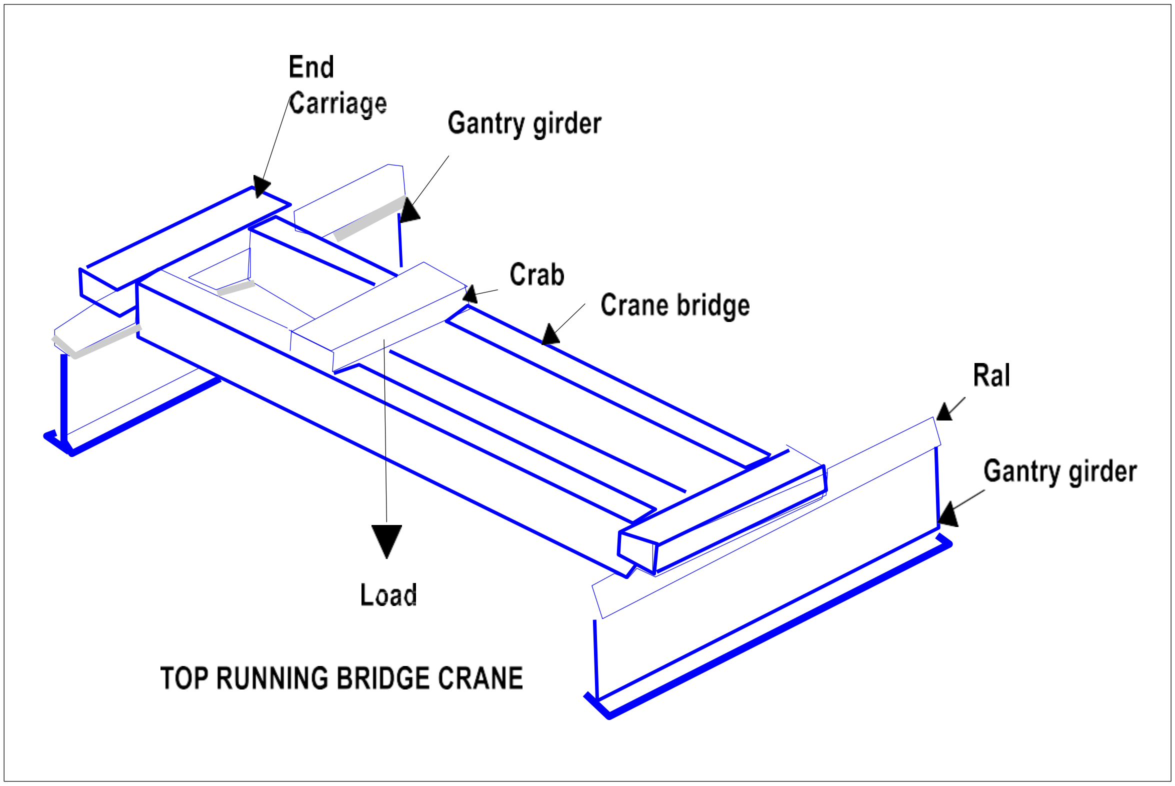

Fig1. 5 Above running crane (Modified after Shin 2015)

1.4 Classification of cranes based on manufacturers' association standard

The "service class" of a crane and/or hoist is determined by a number of factors. The Crane Manufacturers Association of America (CMAA) classifies bridge cranes according to average load intensities and cycle counts. On the other hand, stricter rules—such as the maximum number of starts and maximum operating duration per hour—are used by the International Organization for Standardization (ISO), the European Federation Standard (FEM), and the Hoist

Manufacturers Institute (HMI) to classify hoists. The following subsection presents a summary of the CMMA.

1.4.1 CMAA (Crane Manufacturers Association of America) service classification

Based on the crane's duty cycle, CMAA has classified cranes into six classes; three of these classes are shown here.

1. *Class A (Stand-by or Infrequent Service)* - With regard to duty cycle, this is the lightest crane in the market. This service class is intended for cranes that require precise equipment handling at a leisurely pace, with extended periods of inactivity in between lifts. It is possible to control capacity loads during equipment installation and periodic maintenance. Transformer stations, nuclear power plants, wind turbine halls, engine rooms, utilities for the public, etc. are among the locations where this type of crane is employed.
2. *Class B (Light Service)* **-** Cranes in this service class have slow speeds and low maintenance requirements. Loads can vary from empty to occasionally fully loaded, with two to five lifts every hour and an average lift distance of ten feet (3 meters). Facilities for light assembly, repair, maintenance, storage of light, and other uses can all use class B cranes.
3. *Class C (Moderate Service)* - Cranes classified as class C have somewhat high servicing requirements. With five to ten lifts each hour at an average height of fifteen feet (4.6 meters), and a maximum of fifty percent of the lifts at rated capacity, these cranes can carry loads that average fifty percent of their rated capacity. Cranes used in machine shops and machine rooms of paper mills are examples of class C cranes.

1.5 Main components of overhead crane

The hoisted weight must be moved both horizontally and longitudinally inside the building using a crane. To assist with the weight being hoisted, a hook that is cable-attached to a hoist is sometimes utilized. The crane bridge is supported by a trolley that moves horizontally to support the hoist. The total amount of crane trucks at either end of the crane bridge varies based on the length and carrying capacity of the bridge. Wheel count on crane trucks can range from two to eight, depending on the size of the crane. The wheels are directed by a crane rail that is secured by runway beams. Figure 1.6 depicts crane components in their most basic configuration.

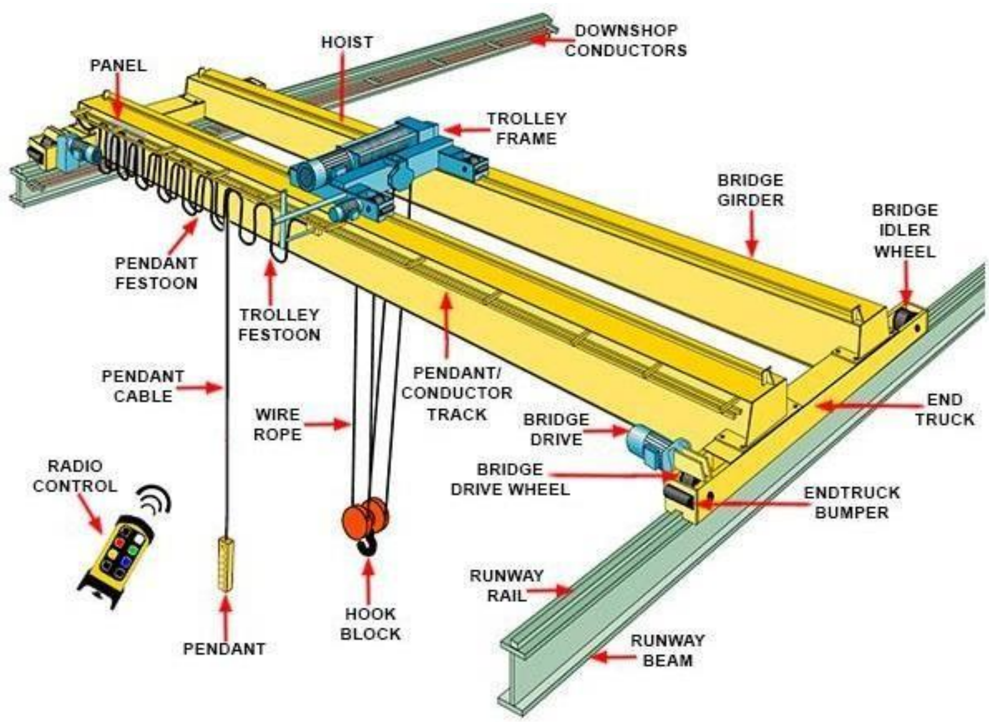

Fig1. 6 Double Girder Overhead Crane (Shin, 2015)

Bridge **-** The main transportable building spans the whole bay. Two end trucks and either one or two bridge girders make up the bridge, depending on the equipment Type.

End trucks **-**The crane's wheels are housed in the end trucks, one on each end of the span. Because these wheels roll along the beam of the runway, the whole length of the bay may be reached.
Bridge Girder(s) **-**It is supported by the end trucks; the trolley is the primary horizontal part of the crane bridge.
Trolley Hoist **-**The hoist and trolley frame come as a single unit. When a crane requires more than one hoist, the hoists may either share a single trolley or be mounted on their own.
Trolley **-** The hoist is moved across the bay on the bridge trolley (s)
Hoist -The hoist, which is mounted on the trolley, is responsible for lifting operations and makes use of a hook or other kind of lifting attachment. Two primary hoist categories exist. In terms of durability, the Munck Wire Rope Hoist excels. The second kind of hoist is the chain hoist (Shin, 2015).

2. Motivation

Visual inspection and monitoring systems have long been used to assess system health. In actuality, health monitoring of any structure is a crucial obligation for keeping a safe environment for people to occupy. Because of the enormous and hefty steel construction of overhead cranes, current eye inspection seems to be a poor signal of the need for more comprehensive quality checks. Robots are incredibly helpful and vital equipment for making any work simpler, and they are growing more popular. Most robots include controls, sensors, and actuators to perform a particular purpose, protecting humans from hazardous or inaccessible places.
Industries must hire expensive, professional inspectors to check and monitor overhead cranes. Machine downtime during inspection reduces output and costs businesses a lot. This study proposes an automated robotic system to examine overhead cranes, minimizing downtime, inspection cost, inspection time, and enhances the safety and quality.

This magnetic-wheeled inspection robot can move horizontally and vertically against gravity. Adhering to steel surfaces requires no extra energy as the wheels are made up of permanent magnets. Because of its lightweight structure and adjustable shape, it can move freely across weld joints without causing any damage. Because of the use of magnetic sensors and cameras, the system is independent and can be handled from a distant area, which is useful. This robot is capable to examine fractures in large steel structures like overhead cranes.

3. Problem statement

In recent years, several authors have suggested inspection robots, but reachability and inspection quality have been the key limitations. Historically, the majority of designed devices could only examine horizontal surfaces. In addition, the inspection was confined to surface flaws and did not include subsurface flaws or fractures. Another drawback of the previously designed inspection system was that it was not real-time and could only inspect a certain surface thickness.

In this research work, the magnetic wheel robotic tool was created exclusively for the inspection of overhead crane bridges and girders, primarily container-loading cranes at seaports. The robot's adaptable structure and degree of freedom allow it to maneuver on horizontal, vertical, and inverted surfaces. The Giant magneto resistance (GMR) sensor array contributes to the inspection of the inspection area's surface, sub-surface, and corrosion. A real-time monitoring feature and live video streaming make this robotic system for the inspection of overhead cranes more precise and efficient. This robot may be used instead of overhead cranes to check any steel structure, including steel bridges, ship superstructures, and other similar structures. Nonetheless, the major function of this robot is to examine the overhead crane's structure for cracks.

4. Objective

The primary purpose of the investigation is to identify faults in the steel structure of the port's overhead cranes girders. Generally, overhead cranes at seaports are exposed to a number of environmental factors, such as moisture impact due to high humidity and coating by dust, which lead to corrosion. The formation of microscopic cracks in the steel sections of cranes as a result of repeated heavy loading and unloading results in the catastrophic destruction of the structure. The planned and constructed magnetic wheeled robot is equipped with a sensing unit and cameras, allowing it to climb freely on steel surfaces. It transmits real-time data and live streaming to a distant site for real-time monitoring and additional analysis while analyzing the steel construction. To simplify user contact, this built system is compatible with Android mobile phones. This robot will discover surface and subsurface defects in large steel structures by considering many parameters.

- Immense maneuverability
- High-reaching velocity.
- Flexibility to a practical range of curvature.
- Simplicity

5. Justification/Significance of the study

The conception of the study is borne out of the versatility of robotic adaptations. Essentially the use of robot has gained popularity in recent time due to the sensitivity of its adoptions in lieu of manual and other automatic operations.

The creation of a robot for monitoring of overhead crane girders is crucial in this research initiative since it aims to enhance the safety and efficiency of industrial operations. Overhead crane bridges are largely utilized in various sectors such as manufacturing, construction, and transportation, but they are susceptible to wear and tear, corrosion, and structural defects that can adversely affect their performance and reliability.

Presently, the method of inspection of overhead crane bridges is manually done by human workers. This method is tedious, time-consuming, costly, and hazardous.

However, a robot tool that can autonomously navigate and inspect the overhead crane bridges would offer several advantages over the manual method. First and foremost, it would reduce the human exposure to high-risk environments and potential accidents. Second, it would enhance the precision and rate of inspection, and thus, allows prompt and early assessment, evaluations, detection and prevention of failures. And finally, use of robot for detection would be swift and economical via eradicating the need for scaffolding, ladders, or other conventional equipment hitherto used. Therefore, this research study is justified by its potential to enhance the quality and safety of industrial operations that rely on overhead crane bridges. It is expected that stakeholders in the manufacturing, transportation and other allied sectors may find the outcome of the study useful particularly in policy and decision making.

CHAPTER 2

LITERATURE REVIEW

Several industries, such as power plants, pipeline inspection, aerospace, railway, steel, and many other similar product manufacturing industries, non-destructive testing is routinely used and applied. Because of its non-destructive character, non-destructive testing (NDT) contributes to a significant and distinctive position in quality policy, along with the secure and steady procedure of system components. Some standards and codes must be validated and authorized by the members of the society for NDT techniques to be used for quality inspection (Sahari et al. 2012).

2.1 Inspection robots review

Steel structures can develop cracks over time as a result of corrosion and exposure to the weather. It is necessary to conduct a complete inspection of overhead cranes for them to work safely. It is now being utilized in India to detect the existence of cracks in huge steel constructions such as overhead cranes using a visual method for diagnosing fractures. However, when it comes to evaluating and locating cracks in complex and extensive infrastructure, this technology is not nearly as precise or valuable as it could be.

During an on-site inspection of overhead steel bridges, it is necessary to conduct structural monitoring. We can prevent cracking in steel bridges by detecting cracks in steel bridges early on, which increases the likelihood of averting catastrophic incidents (La, et al. 2019). When you look at them, dust and corrosion are the most reliable indicators of whether or not there are cracks. However, as time passes, dust accumulates on the broken area, necessitating the implementation of further safety precautions. Fracture detection can be accomplished in a variety of methods using non-destructive testing (NDT). Here are a few illustrations: Technology based on vibration, eddy current imaging, ultrasonic techniques, holographic interferometers (holographic interferometry), acoustic emission, photo elasticity, and Electronic Speckle Pattern Interferometry(ESPI) are just a few of the tools available to you.

Building structure monitoring has been increasingly popular in recent years, with many wireless sensor networks and mobile sensor networks being employed to keep a check on things (Deraemaeker, 2010).

Cracking is one of the most common and major types of steel building flaws, and it harms the entire structure when it occurs. There are many distinct types of cracks that might emerge, ranging in size and shape from surface-breaking cracks to stress corrosion cracking (SCC), and they can appear in any combination. Corrosion cracks and stress corrosion cracks can appear in a variety of shapes and sizes in steel. Some of the most common types of steel cracks are longitudinal cracks, transverse fractures, crater cracks, branching cracks, and stress corrosion cracks.

Corrosion, in addition to these forms of cracks, can result in a range of other problems in steel construction structures. It is the result of chemical reactions between steel structures and the surrounding environment that rust develops in them. The formation of pits in steel buildings is a result of the significant localization of corrosion in steel (Khan, et al. 2020).

To prevent failures and extend the service life of overhead crane steel bridges, it is required to inspect them for flaws regularly. The availability of corrosive testing standards for steel body parts is a common occurrence nowadays. This section contains some of the standards released by organizations like the American Society of Testing and Materials (ASTM), the American Society of Mechanical Engineering (ASME), and the International Standards Organization (ISO). The detection of surface cracking faults can be accomplished using eddy current testing, which comprises eddy current array, magnetic particle testing (MT), Dye penetrates testing (DPT), ultrasonic testing (UT) by following these specifications. [Lu, et al. 2020]. The use of ECA sensors for non-destructive testing of steel welds is governed by the ASTM E3052-16 standard, that is acknowledged by the name of the American Society for Testing and Materials (Eich & Vogele, 2011). Specifically, it entails the detection and measurement of surface fractures in joints that can tolerate non-magnetic and non-conductive coatings up to 5 mm in thickness between the sensor and the joint, among other things. Many computer vision approaches are presented in this literature that has the capability of detecting and monitoring structural degeneration. Although most of them have advantages, they also have drawbacks, such as the capacity to detect flaws on the outer surface of steel but not on the subsurface (Ahmed et al. 2015).

2.2 Category of inspection robots

In the field of professional service robots, inspection robots are one of the newest innovations. Automation of surveillance and inspections in locations where inspectors are unable to reach and where the inspection site is hazardous to human health is accomplished through the use of inspection robots (Liu et al. 2011). As a result, inspection robots contribute a significant role in the handling and inspection of these potentially hazardous places. Robots are classed in a variety of ways, depending on where they are intended to function.

Inspection robots are primarily grouped into four categories from the standpoint of the market (Nguyen & La, 2018).

(1) Remotely operated vehicles (ROV)

(2) Unmanned aerial vehicles (UAV)

(3) Unmanned ground vehicles (UGV)

(4) Autonomous underwater vehicles (AUV)

2.3 Unmanned Aerial Vehicles (UAV) or aerial robots for inspection

Due to the increasing age of infrastructures such as steel bridges and heavy steel machinery, a large amount of effort is required to check them in such a way that serious damage can be discovered early and a preventative maintenance step can be carried out. The majority of countries now deploy flying robots to examine infrastructure. This type of robot allows access to inspection places that are inaccessible to inspectors and some ground robots.(Nguyen & La, 2018, La et al.,2019, Kalra & Gu, 2007).
They can be used for a variety of inspections ; however, they are most commonly employed for visual examination. They are outfitted with a high-resolution camera and an array of sensors to provide an exact view of the structure. It is outfitted with a laser and infrared sensors to generate a three-dimensional (3D) map of the examined area. This navigation strategy can be carried out in a variety of ways, including SLAM (Self-localization and mapping), mapping, and so on. It has a wide range of applications, including water bridge inspection, large and tall pipes, and oil rig platforms. In comparison to traditional inspection methods, aerial robotic inspection is significantly less expensive, faster, and safer. In recent years, some researchers have made efforts to develop airborne vehicles for bridge inspection that are fitted with laser sensors for mapping. In this subsection, review on some earlier works on aerial vehicles for the examination are presented.

Roberts et.al, (2021), in their article introduced a quad-rotor concept that was outfitted with an array of sensors such as an ultrasonic sensor and an infrared sensor for an obstacle-free environment. Limited sensors were used in this work to make the system autonomous for landing and takeoff, anti-drift control, and collision avoidance. The inspection design for the city-flyer quadrotor is presented in figures 2.1.

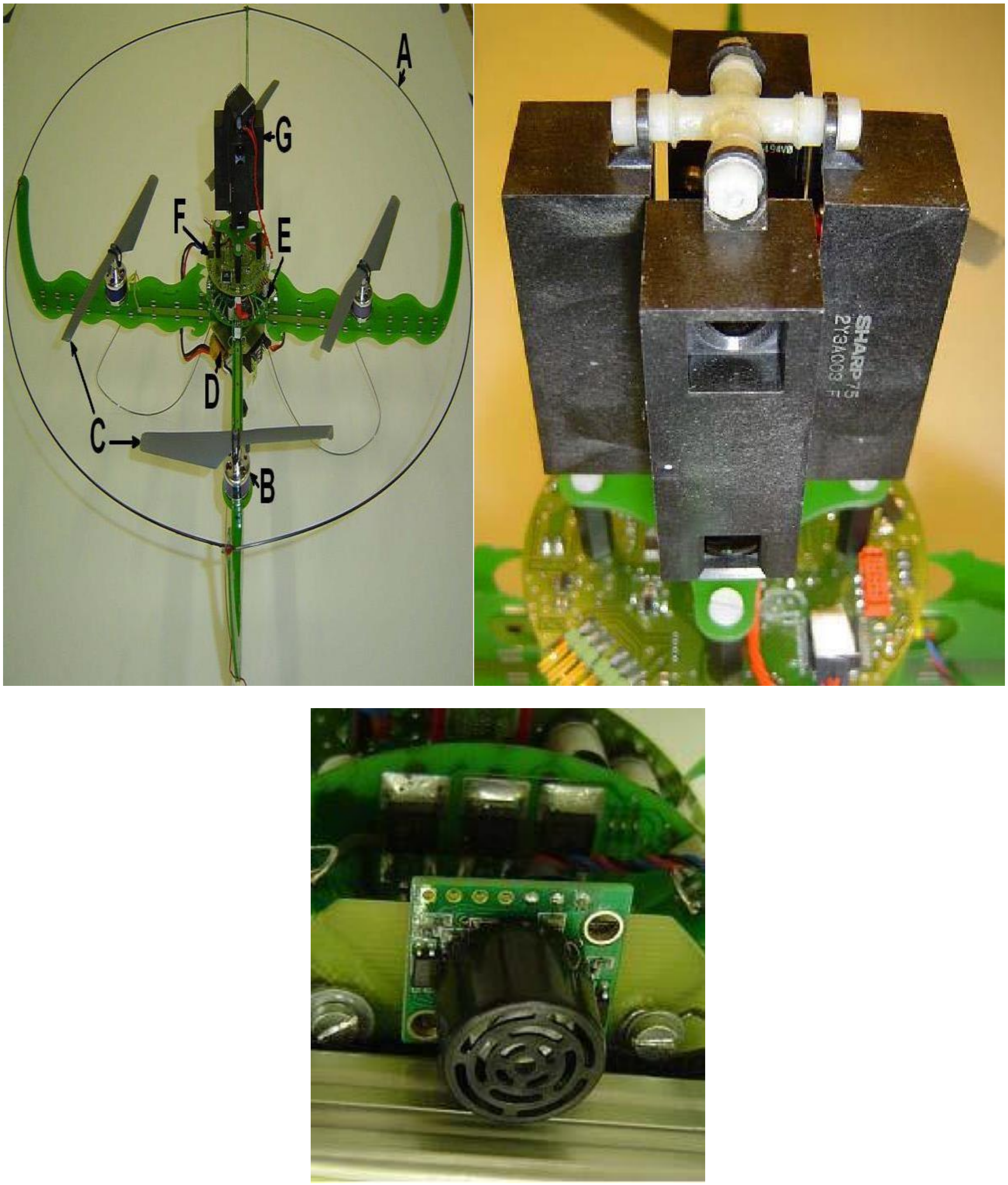

Fig.2. 1 The sensor used for the robot (after Roberts et.al, (2021)

In the research work of (Dryanovski et al. 2013), they proposed a fully autonomous quadrotor system that was introduced in the ROS (Robot oprating System) framework. This quadrotor, as shown in figure.2.2 is equipped with wide variety of laser sensors that integrate it with the existing ROS navigation tools for 2D SLAM and 3D mapping (Xiao et al, 2013). The system is equipped with nominal number of sensors such as planer laser range finder and an inertial measurement unit.

Fig.2. 2 The City-Flyer MAV (Dryanovski et al. 2013)

2.4 Robots for structural health monitoring

In recent days, mostly huge steel structures inspection process to identify the defects and flaws relies on the skilled inspectors i.e., by visual inspection method. A skilled inspector observes the defect location manually that results in lower accuracy of inspection due to subjective nature of human decision power and skillset.

Liu & Liu (2013) list the drawbacks of manual inspection as being subjective, costly, labor-intensive, and dangerous. Massive attempts have been made to conceptualize an autonomous monitoring and inspection system that can provide the highest level of precision, safety, and dependability at the lowest possible operating cost in order to minimize these constraints (Jahanshahi et al., 2017). Large infrastructure can benefit from the installation of an autonomous monitoring and inspection system as an improved option to manual inspection methods, which are primarily time-consuming, costly, and prone to error. In addition to providing increased precision, an autonomous robot monitoring and inspection system enables regular infrastructure system inspection at a much reduced cost. The following subsections provide summaries and illustrations of a few instances of robots that have been employed as non-destructive techniques(Stramigioli et al., 2010).

2.4.1 Omni-Climbers: Wheeled climbing robots with magnetic omnidirectional capabilities for ferromagnetic structural assessment [Roberts et.al, (2021)]

Climbing robots have been developed during the past two decades to facilitate some jobs such as periodical inspections for detection of cracks, corrosion, material degradation and welding defects on tanks and piping. Other applications of interest include ship hull grooming, cleaning and painting of such structures (San-Millan, 2015). The special case of the Omni-Climbers, gas and oil tanks, wind turbines, pipelines and marine vessels are examples of structures that are targets of the use of this robot (Hillenbrand & Berns, 2006). According to Shin et al., 2013, the reason is that

- They need a periodical inspection, maintenance or cleaning,
- Their exterior circumference is convex,
- The cost is built from ferromagnetic material.

The Omni-Climber's main novelties

The two primary issues that this robot's creators attempted to tackle were mobility on the framework and adaptation to various structures. Thus, the primary innovations in the present design are as follows:

- Flexible chassis for improved curvature adaptation: by combining innovative chassis designs with a passive bending system, the robot can passively adjust to a variety of curvatures.
- Omni-directional wheels for enhanced mobility: Mobile robots have made extensive use of omni wheels.
- Their great agility for mobile robots is the major reason behind their appeal. The robot can move in the (x, y) direction and rotate around its central axis by using omni-directional wheels that are positioned at a 120° angle.
- Adjustability: In order to make the design more flexible to different constructions, the adjustability of the mechanisms in all design aspects.

Magnetic attraction force and central magnet unit

The robot need to be secured to the structure by the primary magnetic unit. This suggests two prerequisites:

- When the robot moves on the structure, the magnet's attraction force needs to exert enough normal forces to keep it connected. Consequently, the normal force plus the sliding friction coefficient between the steel wheel and framework (rubber and steel) should be more than the weight of the robot.

- The total of the moments about each contact point should be zero in order to maintain all three wheels fixed to the framework and prevent rotation around any of the contact points. The first requirement results in a minimum normal force of 24 N when taking into account the robot's weight (1200gr) and the mass center. These circumstances also lead to a minimum normal force of 13.9 N. The designed Omni climber robot id depicted in below Fig.2.3.

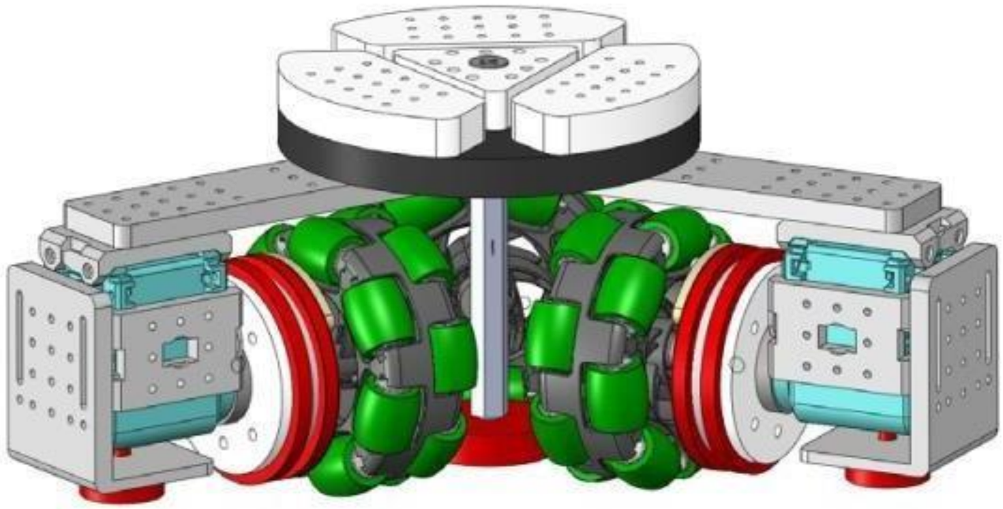

Fig.2. 3 The first version of the Omni-Climber used an elastomer with ABS reinforcement as a chassis (Hillenbrand & Berns, 2006)(Lim et al. 2013).

Table 2-1 MAIN CHARACTERISTICS OF THE TWO VERSIONS OF THE OMNI-CLIMBER ROBOT (AFTER HILLENBRAND & BERNS, 2006

Item		**Omni-Climber I**	**Omni-Climber II**
Dimensions		ϕ 250 mm, Hei 102mm	ϕ 246mm, Heigh 90mm
Weight without battery controller		1099 gr	804 gr
Weight with battery and control		1241 gr	946 gr
Maximum climbing speed		11 cm/s	11 cm/s
Actuation		3 AX-12 rotary actua	3 AX-12 ro actuators
Battery		Lithium Polymer 1 mAh	Lithium Polymer 1 mAh
Wheel		Omni - Directional	Omni – Directional
Controller		Robotis CM-510	Robotis CM-510
Operating voltage		12 V	12 V
Communication		TTL	TTL

Control:

The TTL network links the three actuators to the CM-510 Robotics controller. The controller is supplied with the omnidirectional robot's inverse kinematics. The CM-510 has an infrared receiver built in. Currently, a joystick is used to operate the robot. It transmits high-level motion commands (such as speed, forward, backward, right, left, rotate CW, and rotate CCW) to the controller, which then controls the velocity of each actuator using the CM-510. Robots require a 12 V input voltage to power their controller and motor, which may be supplied by an AC/DC converter or a 1000 mAh Lithium-Polymer battery.

2.4.2 MagneBike compacts magnetic wheeled robot for power plant inspection

A magnetic wheeled robot called the MagneBike was created specifically to examine ferromagnetic components in power plants, particularly steam chests. This robot is a magnetic wheeled robot that can examine power plant facilities, with the intention of concentrating on the steam chests' interiors for a particular case study.

The robot is made up of two magnetic wheel units that are aligned and have integrated lateral lever arms. These arms have two complementing purposes: when gravity is not in favor, they may be employed to laterally balance the robot or to slightly raise the wheel in order to locally reduce the magnetic attraction force while traversing concave edges. A free joint on the fork provides surface adaptability, while an active degree of freedom (DoF) on the front wheel ensures steering with its extremely high mobility, this form of locomotion allows driving in intricate 3D industrial environments—environments that aren't always meant for robots.

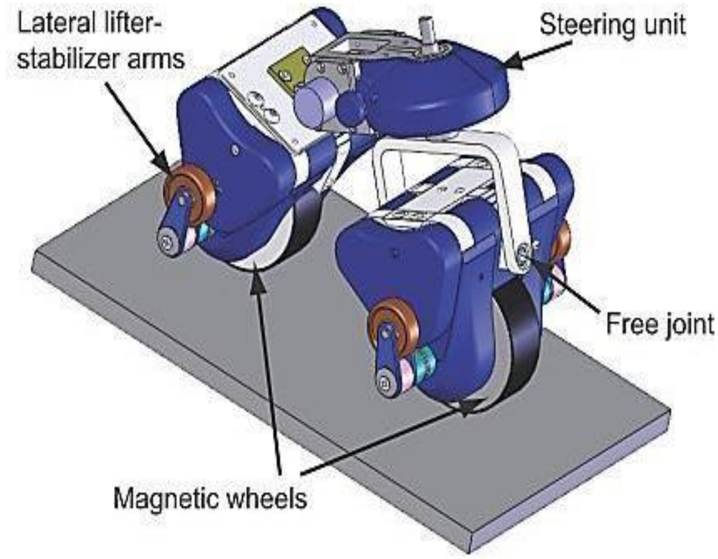

Fig.2. 4 MagneBike locomotion concept: CAD model (Ishizu et al. 2012)

The robot can navigate intricate arrangements of convex and concave step barriers with nearly any slope with respect to gravity. It can even scale vertical walls and navigate circular circuits within pipe structures. It can turn on a point around the back tire, so it only needs a little amount of space to navigate. The author of the paper (Nguyen & La, 2018) presents and analyzes in detail the high mobility locomotion idea of the small and lightweight climbing robot (185× 131 × 153 mm 31, 3.5 kg). The robot's design is shown in Fig. 2.4.

2.4.3 A non-destructive sensing robot for crack detection and deck maintenance [3]

Systems perform poorly in crack detection because to varying lighting circumstances, poor illumination, and limited stability to sustain high temperatures. A robotic device known as a non-destructive sensing robot for crack identification and deck repair has been developed to get around the problem (Nguyen & La, 2018). Figure 2.5 depicts this robot in illustration form. Table 2.2 displays the device's specifications.

Table 2-2 LIDAR CHARACTERISTICS

S/no	Parameter	Values
1	Size of machine, W×L×H	50×67.5×55 mm3
2	Mass with/ without Hokuyo	0.34 kg/0.18 kg
3	Backlash on the main shaft	<10
4	Absolute encoder resolution	0.090
5	3D Scanner resolution	Ajustable
6	3D scan time (for 0.36o resolution)	50s (180o Rotation)
7	Number of points (for 0.36o Resolution)	683×500=341,500 points
8	Maximum rotation speed	3 RPM

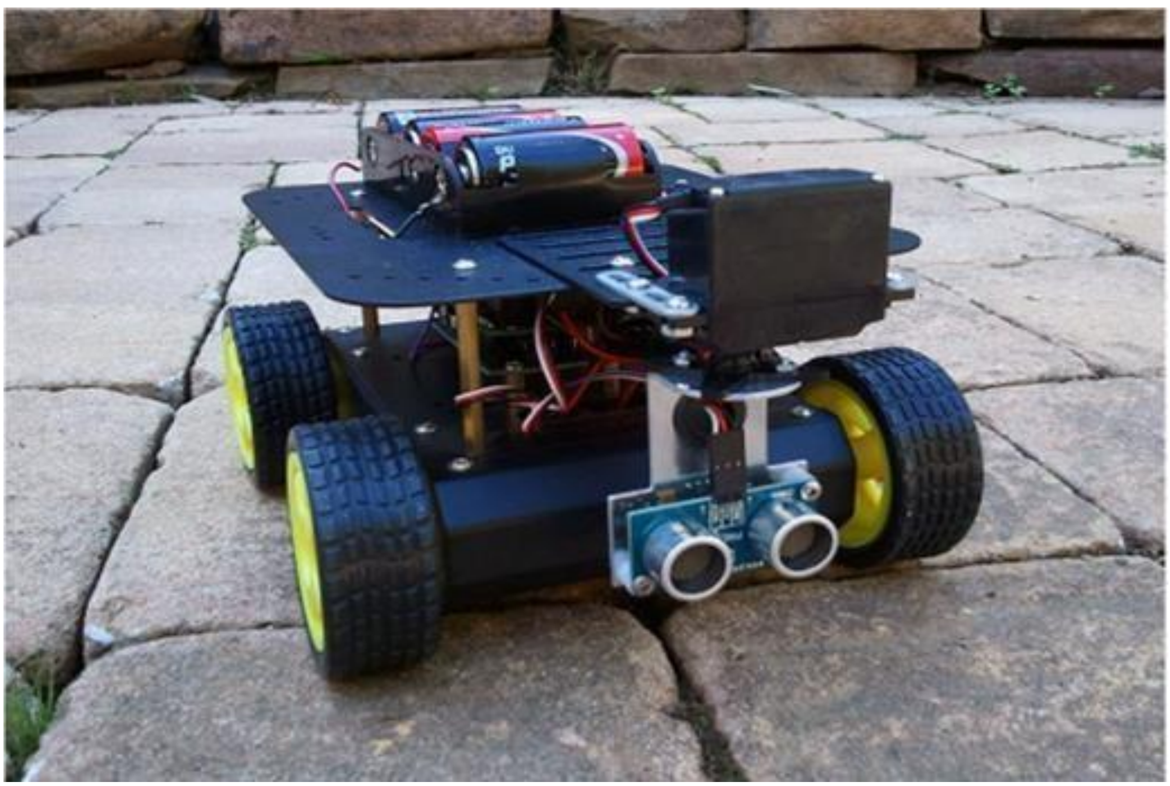

Fig.2. 5 Wheel crack detecting robot (Lim et al., 2013)

Other parts of the robot are reviewed and highlighted in the following subsections.

Sensors:

The mini kit has sensor programs installed for infrared and ultrasonic sensors. The superstructure fracture is located by an infrared sensor. The initial ultrasonic and infrared sensors are positioned above the moving robot. Once each sensor recognizes that the other is operating, it will begin to emit radiation continually. After detecting vibrations or excessive radiation, the infrared sensor will release infrared radiation into the road in order to identify fractures using instructions that are stored in the CPU. The GSM program will go into alert mode when the infrared sensor program has been triggered. It will alert the CPU and turn on the GSM program signal after identifying the fracture. The cached message "CRACK IS DETECTED" will be sent over GSM by using SIM card facilities.

Waves of sound that are continually emitted are used by ultrasonic sensors. when the signal interacts with the object and causes the sensor to receive an echo signal back. It detects the echo signal and evaluates its length in relation to the sent signal. One can determine the obstacle distance by detecting the signal intensity. This invention uses an ultrasonic sensor that generates waves of sound and is mounted inside the robot frame.

Robot commanding:

Both the 4-wheel DC motor and the arm-based CPU utilize universal asynchronous transmission as well as reception to function. For transmission and receiving, it makes use of a number of instructions, including DCE (Data Communication Equipment) and DTE (Data Terminal Equipment). Typically, data communication equipment is utilized to communicate with various interface units, such as sensors, robotics, and GSM devices. The project uses data communication equipment, or DCE, to send orders from the computer to the sensor. In order to allow GSM via data connection equipment, the sensor will simultaneously send the computer a feedback signal indicating that a crack has been spotted. The DTE (date terminal equipment) signal is activated via the UART port when the message has been sent to the observer.

The DTE signal is mainly utilized to inform the arm processor of new signals or messages. It takes a few moments for a signal to be concurrently transferred from the DCE to the DTE units. To allow for the transmission of signals, the equipment is grounded.

All auctions employ AT instructions, also known as attention commands, and the two ports are condensed on the robotic kit's signaling unit. Both units receive attention when the DCE unit is turned on. Using a module's UART port, which may be utilized for implementing an AT command, DTE, such as a microcontroller unit or the external device controller, can connect with it. The UART port interface has a voltage level of 2.8 volts.

Robot operation:

It is made up of four distinct units: a computer unit, a robotics unit, a workspace, and a sensor unit. The computing unit is used to program and operate the robot and sensor programs. An actual structure where activities such as workplace and robot actions are created in real time. The first robotic unit is permitted to be placed in a road tunnel or bridge where it performs crack detection tasks. The sensor device watches actions and reports back to the computer. GSM unit and computer unit linked. The robot will be guided by the computer. It's a repetitive procedure. In the meanwhile, the sensor unit may be directly controlled by computers and robots alike. The robotic unit is in charge of all activities. The subsequent operations are carried out by it (as shown in figure 2.6) (Lim et al., 2013) using specific algorithms:

- Step 1: Use UART to calculate the robotic unit's command.

- Step 2: The robot operates on bridges, roadways, etc.
- The sensor unit makes a sensor observation in step three.
- Step 4: Two infrared sensors and one ultrasonic sensor make up the sensor feedback.
- Step 5: The GSM application will be activated to deliver signals when infrared sensors identify fractures in the workplace.
- Step 6: The operator receives a "crack is detected" message from the GSM unit.
- Step 7: The computer will get a signal to take a different course from the ultrasonic sensor.
- Step 8: The four-wheel DC motor will turn left or right in accordance with the instruction after receiving a signal
- Step 9: The computer will reset the sensor following the transmission of the message signal.
- Step 10: The activities can be performed by a robot by directly activating the sensor unit.

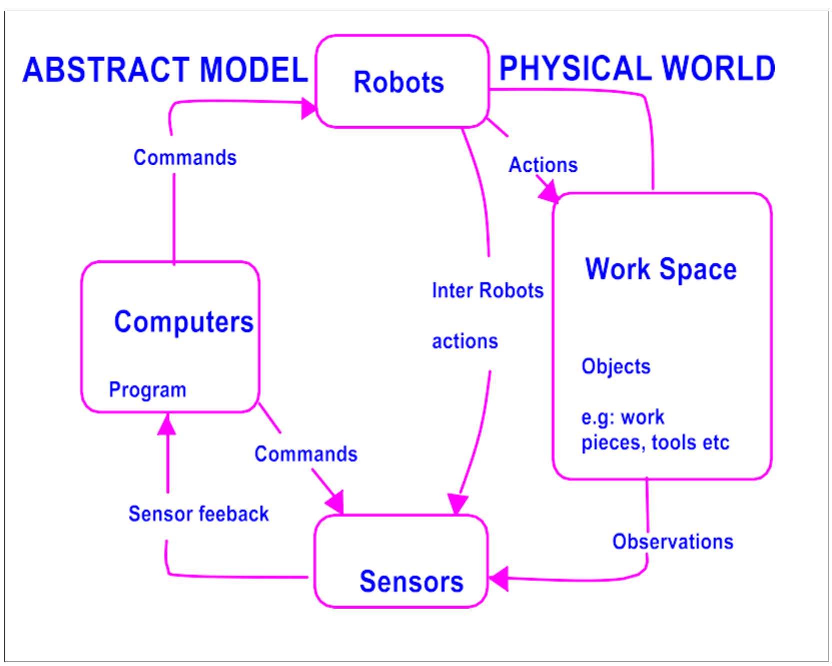

Fig.2. 6 Algorithms to perform the robot operation

2.4.4 Pipe inspection robot

One major application area for autonomous vehicles is pipeline inspection. Different mobile robots are used for in-pipe inspection since access to a specific pipeline segment is typically restricted. The mobile platform consists of three drives per track, two-track modules with integrated motors installed on a positioning frame. The robot may function on flat surfaces or in pipes and ducts with both circular and rectangular cross sections that are oriented vertically and horizontally. Online modifications to the robot's construction are possible through the use of an adjustable track positioning system.

Mechanical structure:

Two-track drives are used by the robot to provide appropriate stability and mobility. The 60x50x170 mm Inuktun Microtrac track modules were used for this research (Ciszewski, et al., 2015). They are primarily made for tiny monitoring stations and are intended only for pipe examination. The robot's body's axis serves as the center of rotation for both of the independently rotating rings that make up the track position system. Each of these rings has arms connected for rotational joints. Each track has these arms installed in a similar manner on both sides. This arrangement enables the robot body's tracks to be oriented in different ways. Three drives are used to modify each truck unit. The robot's body axis may be rotated by both motors, and the third motor turns the outside. The inner and outer arms are attached to the revolving rings.

The robot is made up of more than 230 parts and has 8 drives in total: Six tracks positioning servomotors and 2 tracks. Based on the 3D model, the robot's projected total weight is 5.15 kg, which does not include the camera, illumination, or connections. Figure 2.7 illustrates that the CAD designed model of robotic model.

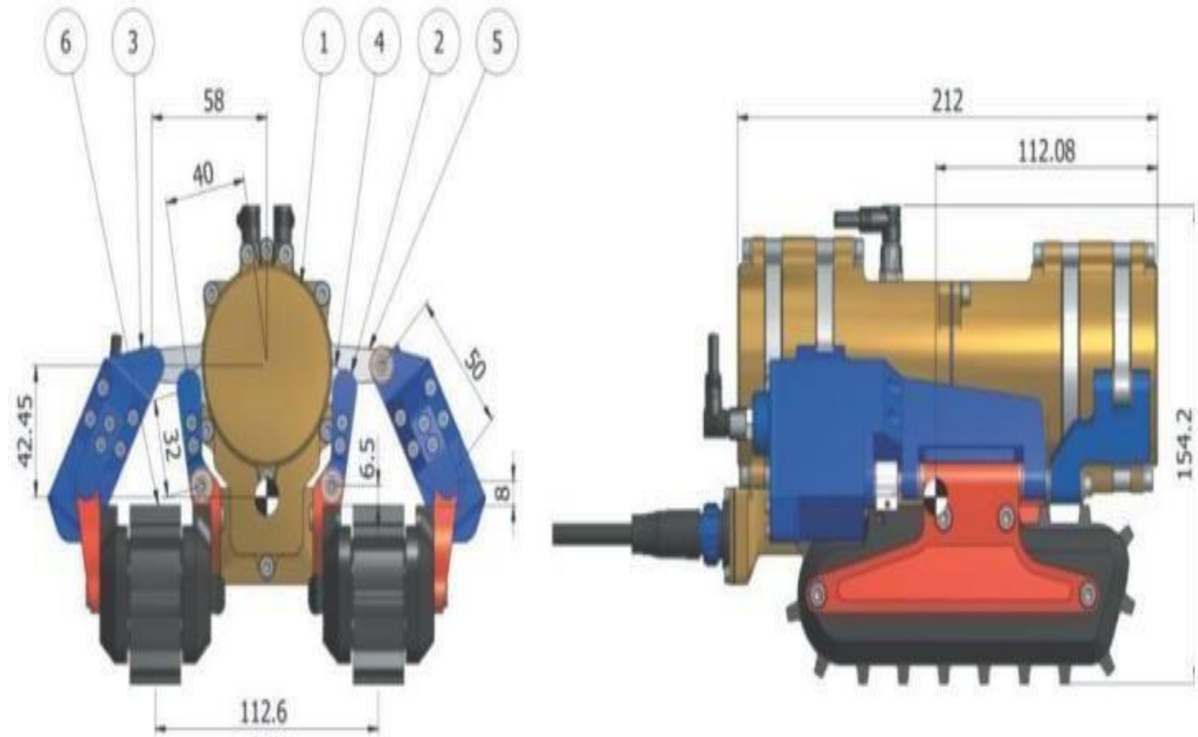

Fig.2. 7 The robot CAD model – general view1 – robot body, 2 – front arm, 3 – rear arm, 4 – front rotating ring, 5 – . rear rotating ring, 6 – track drive unit. (Ciszewski, et al., 2015).

Prototype of the robot:

The prototype weighs 6.5 kg in total. Depending on the multibody simulations findings and the kinematic model, the prototype's operation may be regulated in various conditions. The driving mechanism of the robot may be positioned in different ways to accommodate different inspection duties. In its smallest setup, the robot can function in 210 mm-diameter pipes. The robot is shown in a horizontal 235 mm pipe in Figure 2.8a. The vision system's capabilities define the horizontal pipe's maximum size limit. Additionally, the robot may function in ducts and pipelines with a rectangular cross-section. The examination of flat surfaces is likewise done from the same posture.

Fig.2. 8 Operational environments: a) horizontal pipe, ø235 mm, b) vertical pipe, ø235 mm (Ciszewski, et al., 2015).

Power consumption:

The robot construction was modified in the first set so that it could function on a level surface. The final examination had been carried out in a vertical pipe of the identical diameter, but the second kind of environment was a horizontal pipe with a diameter of 242 mm. The current drain for both the 24 volts and 6.4 volts DC voltage was measured concurrently throughout each test. Robot controlling electronics were powered by the lower voltage servomotors, while the tracks were supplied with a greater voltage.

For three hours on level surfaces, six hours on horizontal pipes, and two and a half hours on vertical pipes, the robot should run on a designated battery power supply. With relation to the following statistics, this value would be enough for typical operating circumstances during pipeline inspection.

2.4.5 Underwater robotic vehicle for ship hull inspection (Ishizu et al. 2012)

One unusual and difficult robotics usage that has come to light is the thickness examination of underwater structures. To locate fractures in these structures accurately, underwater robots equipped with adhesion systems are needed. The hybrid remotely operated vehicle, or HROV, is made up of a polypropylene plate mechanical frame, a pressure container containing controlling electronic devices, a collection of sensors, six thrusters, two motor tracks, an acoustic detecting arrangement, and umbilical connections.

The vehicle's two modes of operation—free-flying and crawling—qualify it as a hybrid robot. Figure 2.9 depicts the average running period for the robot on a battery power source on both the horizontal and vertical surfaces of the pipe.

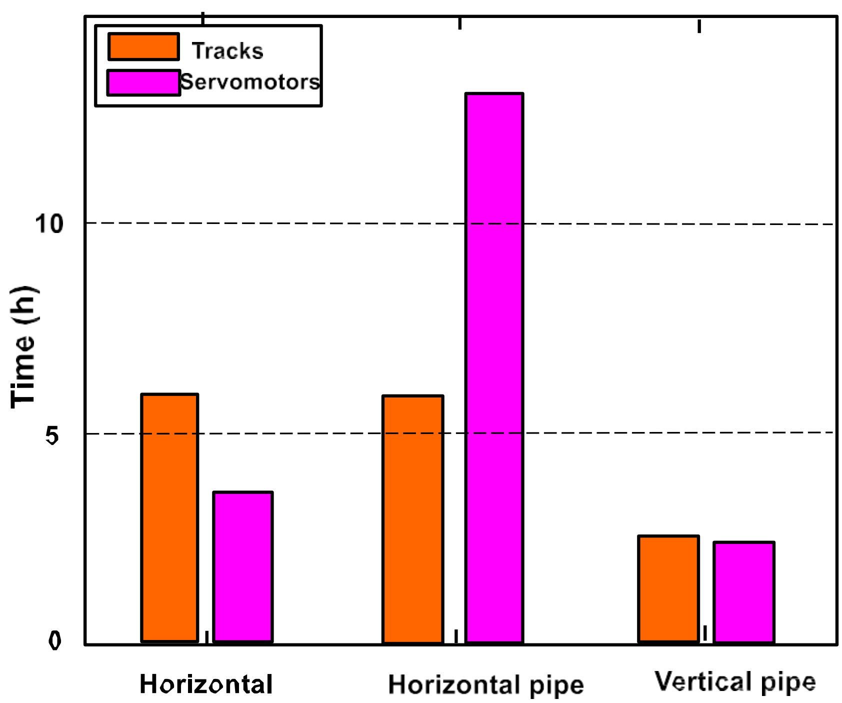

Fig.2. 9 Mean operating time of robots on the battery power supply(Ishizu et al, 2012).

Mechanical design:

The HROV (Hybrid Remotely Operated Vehicle) is composed of a mechanical construction constructed of polypropylene plates that is separated into two portions for ease of use: upper and lower. The vehicle's upper section has a polypropylene flotation case, an acoustic locating system comprised of two transponders, a pressure tank housing the control electronics and sensors, and four vertical thrusters.

The vehicle's bottom section is made up of two horizontal thrusters and two motorized tracks. DC brushless electric motors power the thrusters and motorized tracks. Some navigation sensors are attached to the vehicle's construction. An umbilical connection connects to an isolated 4.5 kW DC power supply for power delivery and data transfer.

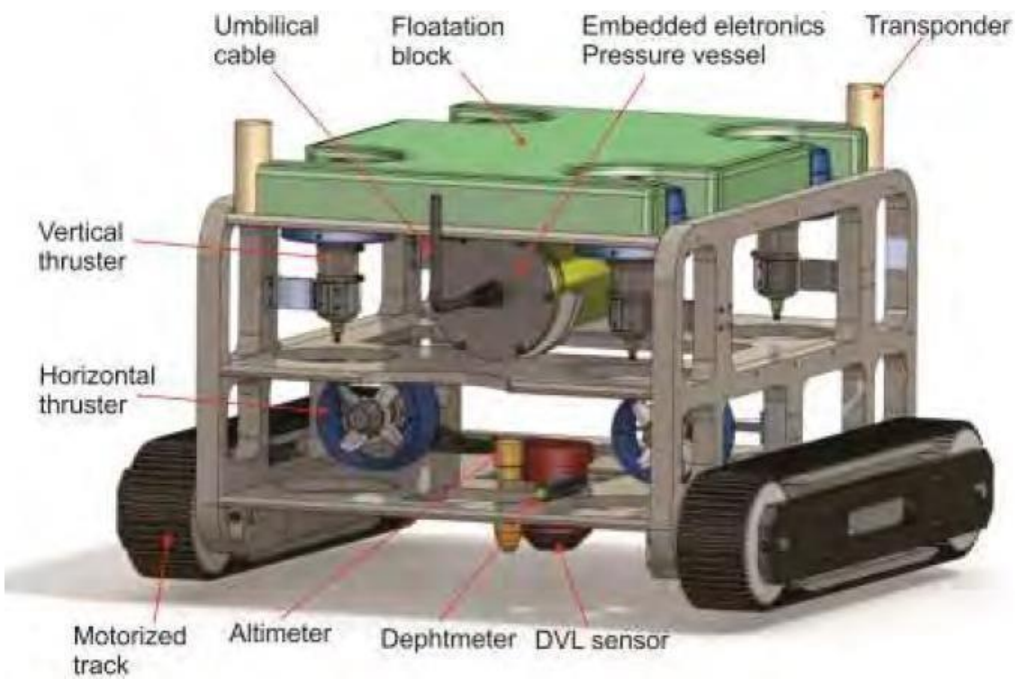

Fig.2. 10 The HROV underwater robotic system (Ishizu et al, 2012)

HROV is made possible by modular structural components. The HROV has a replaceable design that is modular and was developed to function in offshore environments. The vehicle's overall framework can be approximated as symmetric in the longitudinal and transverse planes. It weighs around 125 kg and has a positive buoyancy force of 25 N. The placements of the mass distribution and buoyancy centres are offset by 111 mm, giving the vehicle inherent roll and pitch stability as presented in Fig. 2.10 (Ishizu et al., 2012).

Control architecture:

According to the paper (Ferreira et al., 2014), the HROV's control architecture was created to enable quick creation of data collection, Systems for controlling things, navigational devices, and estimation of state systems are all examples of control systems. The two key elements that comprise the HROV's control architecture are the on-surface computing infrastructure and the undersea computer system. The laptop that powers the surface computing system is powered by the Microsoft Windows XP OS. This is accomplished through the use of task-level controlling instructions, which are linked to a subsea computer via a 4-26 AWG cable and an Ethernet TCP/IP protocol. For task-level definition, a specific metaprogramming language has been developed. This metaprogramming language is used in script files to define necessary moves. The highest level task orders are then converted into low-level command control directives via an interpreter on the subsea computer to which the file is then sent. The subsea computer system handles position and velocity estimations, as well as the lower-level system of controls (which comprises positioning and/or movement control feedback cycles).

Sensors:

Equipped with a suite of sensors, the HROV is able to gauge the vehicle's motion in six dimensions. The vehicle's location and orientation for an earth-fixed reference frame are to be provided by the sensor system, according to the specifications. In Table 2.3, we provide an overview of the vehicle's sensors. The ultrasonic altimeter calibrates the amount of space within the vehicle and the ship's hull.

The DVL sonar provides the vehicle's velocity in the surge, sway, and heave directions. The height of the seafloor and the degrees of freedom are noted in the article (Ferreira et al., 2014). The robot is equipped with a navigation device that determines the direction of movement by measuring rolling and pitching angles with attitude sensors and a compass. In addition, device gives the vehicle's linear acceleration in the surge, sway, and heave directions. When combined with DVL data, this information will allow for an accurate position estimation. The depth is determined using a pressure transmitter. Table 2.3 shows the sensor specs for the HROV.

Table 2-3 TECHNICAL SPECIFICATIONS OF NAVIGATION SENSORS (AFTER FERREIRA ET AL., 2014)

Variable	Sensor	Precision and updat rate	Output
Forward distanc	Altimeter, PA5006-PS	1mm, 10 Hz	Digital
XYZ linearv elocit Height	DVL - Doppler velocity Lo	1%± 1mm/s, 5 Hz	Digital
XYZ angular veloci roll and pitch angl heading	Altitude and HeadingRefere System, AHRS-S305	2%, 0.025% resolutio ±0.5o, 0.02o resolutio ±1o, 0.02o resolution 71 Hz	Digital
Depth	Pressure transmitter, TW-	5 mm, 20 Hz	Digital

2.5 Design of permanent magnetic wheel

The magnetic wheel's design is vital to the functioning of the robot as it is the one that will be carrying out the climbing action. For assurance that the robot sticks to the metal body, the adhesion force among its wheel and the ferrous metal core must be determined. For climbing operations, robots have to satisfy some conditions.

- Adhesion force of magnets will be the same all the time in all directions
- Wheel size and weight should be appropriate to adhere to the metal surface
- Magnetic wheels must have a good coefficient of friction between wheel and metal surface

Instead of electromagnets, permanent magnets are taken into account while designing the magnetic wheels. By switching the magnetic field on and off, the magnetic field may even be controlled in electromagnets. However, electromagnets need a power source to maintain their stickiness, and integrating them into wheels is a little difficult. Due to the high magnetic field intensity of permanent magnets, powerful forces may be generated. Avoiding the modification of the magnetic field throughout the rotation of the magnetic wheel owing to changes in the external power source is another justification for choosing permanent magnets over electromagnets. Adhesion forces alter as a result of the magnetic field changing owing to variations in the power supply. Integrating the interior of the electromagnets is a significant task.

It is observed that the payload capacity, power consumption, and system dependability of robots are strongly impacted by the magnetic circuit design with magnetic attraction force computation of magnetic wheel. Magnetic wheels are essential to this effort in order to provide sufficient adhesion forces for the robot as it is currently configured.

Commonly utilized iron magnets include:

1. Neodymium Iron Boran (NDFeb)
2. Samarium Cobalt (SmCo)
3. Ceramic and Alnico

As was described in the preceding section, several locomotion methods have been examined, and overall, it is obvious that wheeled robots move more quickly and continuously across a variety of terrain. Wheeled locomotion is taken into consideration for the developed robot's mobility because the inspection robot's job is to check huge steel construction bridges.

Robots must have the necessary adhesion forces to maintain the robotic body on the surface of the inspection area in order to complete the climbing function. Permanent wheels on the robot produce the adhesion forces required to move it past various barriers while still carrying all of the sensor equipment. In numerous climbing robots for a variety of purposes, magnetic wheels have been employed for a very long time. Here, magnetic wheels not only offer adhesion and frictional forces but also assist in a non-destructive method of defect detection by producing a magnetic field that aids in locating the fractures in the inspection surface.

The primary duty of the created robot is to climb onto steel bridges and check them for any defects or fractures. Thus, the design of magnetic wheels that can offer enough adhesion and frictional forces for the robot's smooth and flexible motion is entirely reliant on how well they perform in terms of climbing.

The second essential emphasis aspect was the dimensions and weight of the steering wheel, which should be small and light in order to decrease drag. The dimensions and mass of the wheel, which should be less and light in weight while simultaneously maintaining a steady magnetic field throughout rotation, were the second significant concentration factors. NeFeB is one of the strongest types of permanent magnets made up of neodymium, iron and boron. For commercial use, it provides high magnetic field intensity, which overall provides high adhesion forces. Like electromagnets, it doesn’t require any external power to generate a magnetic field and provides constant magnetic field intensity during the rotation of the wheel at any position. It is well resistant to environmental corrosion and has high mechanical properties which make this magnet suitable for the wheel assembly design. Talking about the integration into wheel track, it is quite easier than the integration of electromagnets. These key points made it easy to select the permanent magnets into the wheel track of the inspection robot.

2.5.1 Literature survey of magnetic wheels for climbing robots

In the last few years, many successful types of research have been done by researchers in the field of inspection and climbing robots for many applications. Many robots have been developed with magnetic wheeled locomotion systems to climb and pass the obstacles. This subsection highlights only some of the magnetic wheeled locomotion robots.

Designing a magnetic wheel seems like easy talk, but technically it is not so easy. The most basic magnetic wheel consists of a magnetic ring mounted on a rotating shaft. To generate proper adhesion forces, the magnetic lines and magnetic poles have to face the inspection surface area and also maximum magnetic lines have to pass through the surface. If a magnet is not generating enough adhesion forces, then one of the reasons can be that only a few magnetic lines are passing through the inspection area.

Omni climbers: In their research, Balaguer et al. (2006) constructed an omnidirectional magnetic wheeled climbing robot to evaluate ferromagnetic designs. It was mentioned that a wide range of surfaces might be fitted with this design. As shown in Figure 2.11, the wheel is constructed as a collection of 14-cylinder magnets with a 12 mm diameter and a movable distance.

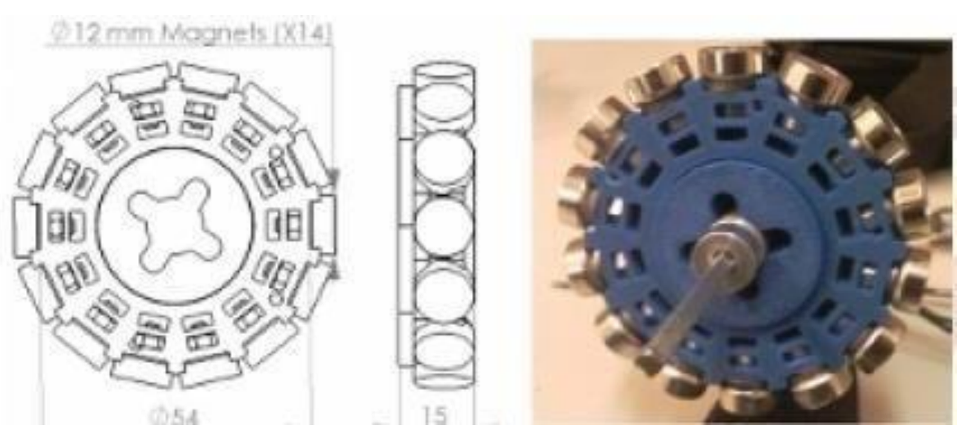

Fig.2. 11 Magnetic wheel of Omni climber robot [Balaguer,et al. (2006)(Tavakoli et al. 2013)

The strongest magnet on the robot is located in the center, where it generates enough force to keep the mechanism attached to the surface. The curvature adaption mechanism is facilitated by three side magnets, which provide the force required to bend the chassis. This robot's primary use is for oil tank and pipeline inspections.

This wheel is made to last four generations in order to solve the issues. An adhesion magnet fixed to the wheel hub and two magnets make up the first generation. In the second version, fourteen magnets are integrated inside the wheel to boost traction forces. By sandwiching the twelve magnets between the rollers, the tilting issue from the previous generation was resolved in the third generation. Fourteen magnetic rollers per wheel are arranged in two rows in the fourth generation. However, this system's drawback is the usage of highly frictional material, which lowers the magnetic force.

Furthermore, Fischer et al., 2007 used a series of magnetic-wheeled wall-climbing robots to develop a robot for checking an extremely thin and sensitive surface. It was discovered that the robot's stickiness is provided by magnetic wheels. Few of the robots are supplied with specific systems within their frameworks to address the majority of the challenges. Furthermore, it is made up of ten parallel magnetic wheels that provide a force of 580 N. This amount is somewhat less than the force provided by ten independent wheels (about 700N). The saturation effect in the surrounding magnetic wheel causes this drop in force. Increasing the distance between the wheels increases force but also weight and bulk. Figure 2.12 depicts the intended construction of the magnetic wheel.

Fig.2. 12 Magnetic wheel unit.(Fischer et al., 2007)

The highest level of efficiency was obtained with a unit composed of ten wheels separated by a 5mm gap. In this paper, a robotic system with a mother-child configuration is given, demonstrating a new approach for increasing speed and reducing bulk.

The authors of the article Fernandez et al.,2010 demonstrated a magnetic-wheeled climbing robot for tank inspection. The design permits the magnetic wheel structure to be made up of a cylindrical nylon framework with 12h holes that wrap the Neodymium (NeFBe) magnet. Three rubber or ring rings are wrapped around the nylon framework to increase frictional force. The diameter of the wheel is 120mm, and the thickness is 20mm. One magnetic wheel weighed one kilogram in total. Figure 2.13 depicts the selected wheel (Nguyen & La, 2018).

The proposed system can climb on oil tanks and navigate welded lines. In article written by San-Millan, (2015) authors presented a climbing robot with wheeled locomotion which uses permanent magnets as an adhesion mechanism. The designed robot is indented for many ferromagnetic structures such as fuel tanks, ships, bridges and turbines to detect the presence of any defect in the structure due to corrosion and fatigue. In the design of the magnetic wheel, he used mainly two different approaches to enhance the effectiveness of the adhesion mechanism.

According to this research, by moving the wheel away from the wheel, the shape of the wheel is not limited by the size of the wheel. In this work the designed robot does not have magnetic wheels, the motor and wheels are mounted on a 144mm long aluminum profile and magnets are placed inside the aluminum profile. figure, 2.14 shows the location of the permanent magnet into the aluminum profile (San-Millan, 2015).

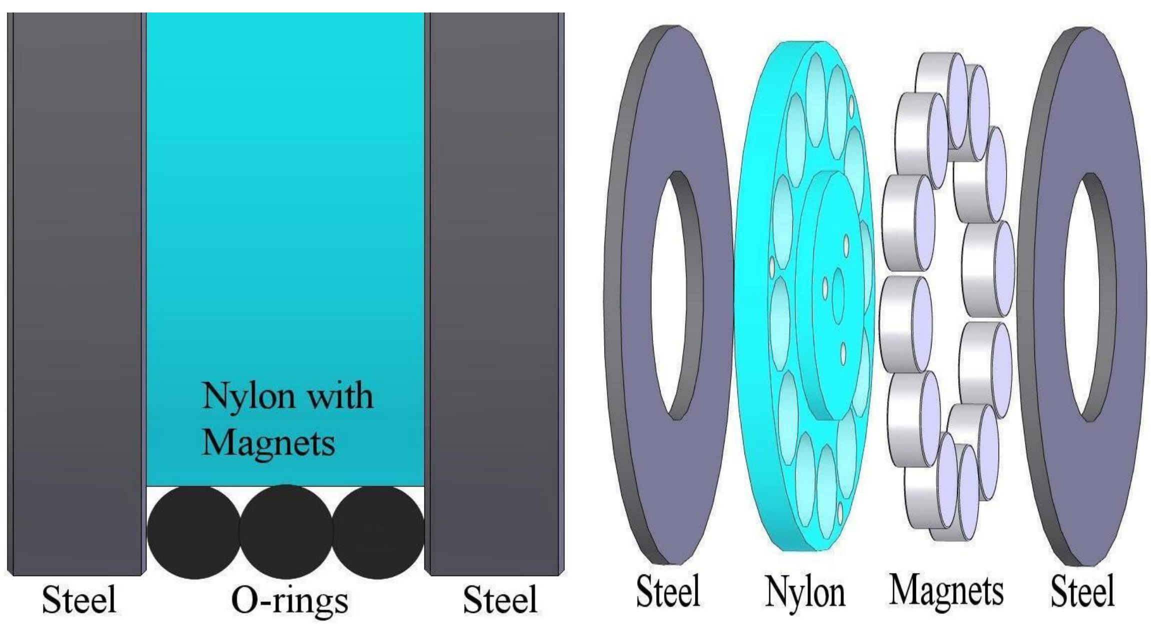

Fig.2. 13 Magnetic wheel structure Nguyen & La, 2018

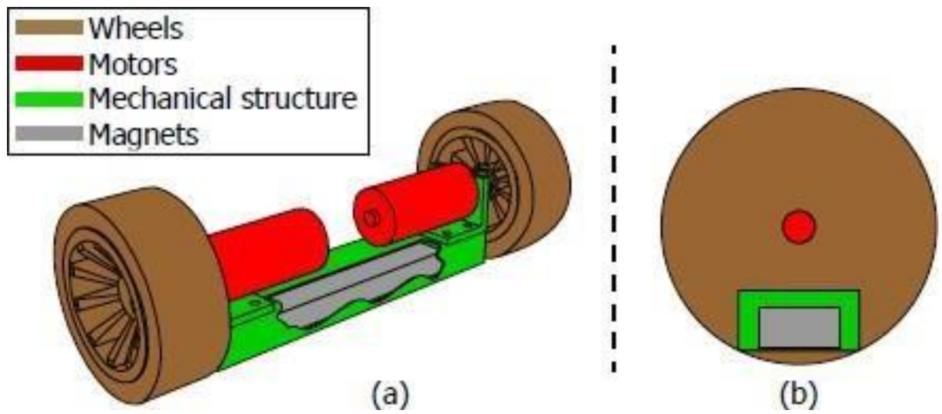

Fig.2. 14 Mechanical design of magnetic adhesion mechanism (a) overall view (b) Axial view (San-Millan, 2015)

The magnets utilized in the structure are commercially available neodymium cubes of 10x10x10x. Magnetic property testing is performed using FEM methods for different arrangements of magnets.

In article of Fondahl et al., (2012), they developed a magnetic climbing robot for the inspection of marine services. In this research work, a basic design of a lightweight crawler is presented that can climb on the vertical walls of the vessel. The robot will provide a video stream as well as offline images for later inspection.

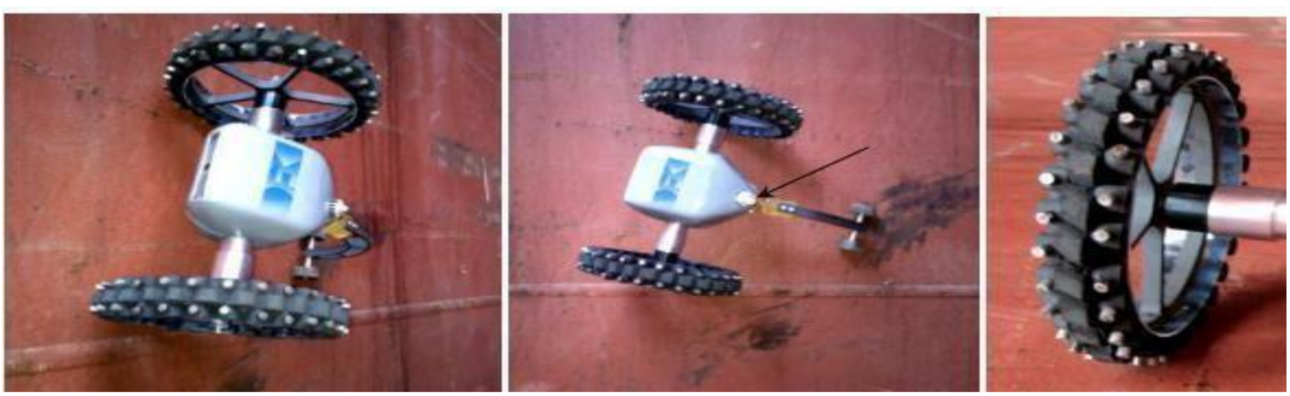

Fig.2. 15 A lightweight magnetic crawler with a designed magnetic wheel (Fondahl et al., (2012))

In many previous versions, silicon rubber is used as a tread and many tests were done on it in cold seasons. The galvanized rubber is a waterjet cut to form the distinct anchor points for the magnets mounting thus providing a better higher adhesion force to the wall. Neoprene foam is mounted between the two strips of rubber to provide additional friction. These three stripes are glued onto a polycarbonate sheet that connects the tread to the rim as shown in figure 2.15

In this design, 112 neodymium magnets are embedded into a flexible rubber outside the wheel hub to enhance the adhesion and traction forces. The polarities of magnets were changed alternatively to boost up the adhesion forces. The main disadvantage of this design is that the magnets are in direct contact with the environment and can get corrosion easily. When dusty and muddy surfaces accumulate, the dust and overall adhesion forces decrease.
Cai et al., (2017) introduced a permanent magnetic wheeled wall-climbing robot to overcome the shortcomings of existing designs of climbing robots. The adhesion mechanism was established by using three large magnetic wheels with a special structure. The three magnetic wheels are isosceles triangle arranged. As illustrated in figure 2.16, the magnetic wheel is made up of a circular NeFeB permanent magnet, copper rings, a yoke iron, a wheel hub, an outside covering, and a protective sleeve.

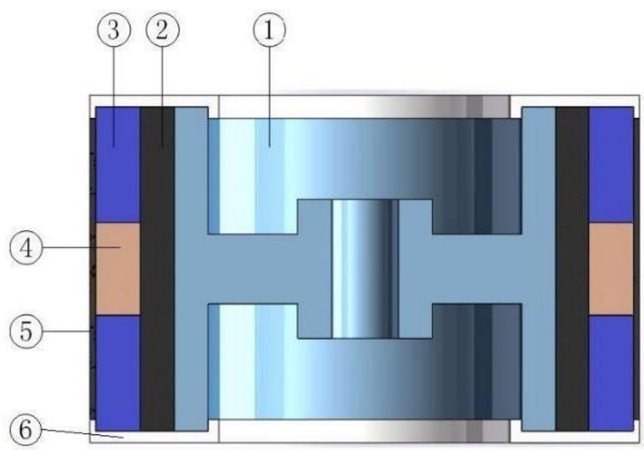

(a)

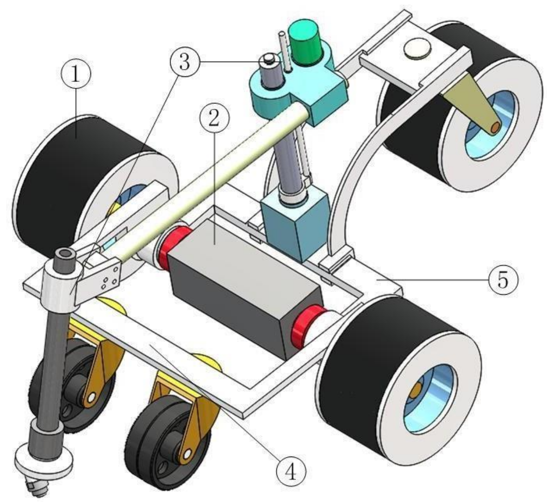

(b)

Fig.2. 16 (a) The structure of the magnetic wheel (b) structure of climbing robot (Cai et al., 2017).

The wheel hub is connected to the driving shaft. The toroidal ring magnet is divided into two pieces which are radially magnetized in opposite direction and symmetrically arranged on both sides of copper rings. There is outer wheel support and coverage to protect the wheel from damage.

Burmeister et al. (2014) proposed a design for a multi-segmented robot with magnetic wheels for hull climbing. Such robots will be able to climb on the hull of the ship, provide covert perch and stare surveillance of the deck area and wirelessly transmit the video. The role of the magnetic wheel in this system provides necessary adhesion between the robot and the surface of climbing.

Here a flux-plate wheel is used which consists of an elastomer wheel, two flux plates, a flux plate locator, a rigid hub, and an array of magnets oriented parallel to the center axis of the wheel. The magnets are positioned with all the north poles facing one side of the wheel, and the south poles facing the other side. The elastomer is made up of 1inch thick neoprene. The rigid hub in the wheel transmits the torque from the output shaft of the motor to the wheel for motion. The designed prototype is 1.25 inches wide, 4 inches in diameter and has a measured adhesion of 21lbf shown in figure 2.17 (Burmeister et al, 2014).

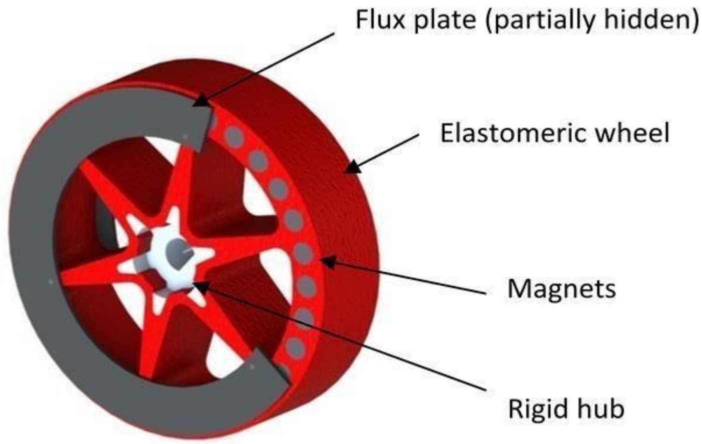

Fig.2. 17 Magnetic wheel with a flux-plate design (Burmeister et al.2014)

In this flux plate which is partially hidden, a series of magnets are positioned parallel to the wheel's central axis. This wheel design is quite good and a bigger wheel can be fabricated by this technique. But in this research, the author did not provide the adhesion forces and effect of elastomeric on the adhesion forces of the wheel.

In other advancement, Schoeneich et al. (2013) created published the creation of Tubulo-a train-like small monitoring climber robot for ferromagnetic tube examination. It is able to climb on tubes with a diameter of 25mm and navigate around curves having a bend radius of 150mm using magnetic rollers. The entire robot is divided into four sections: movement, energy, communication, and visual examination. Instead of using any other kind of mechanical adherence in the locomotion segment, a magnetic wheel was used. The magnetic wheel is built with a center magnet and two iron flux guides on the sides.

A magnetic wheel with an axis at its center has the major advantage of increasing the grasping force. The proposed wheel measures 12mm in diameter and 10mm in length. It is capable of withstanding 2.5 N with rubber seals, as seen in figure 2.18.

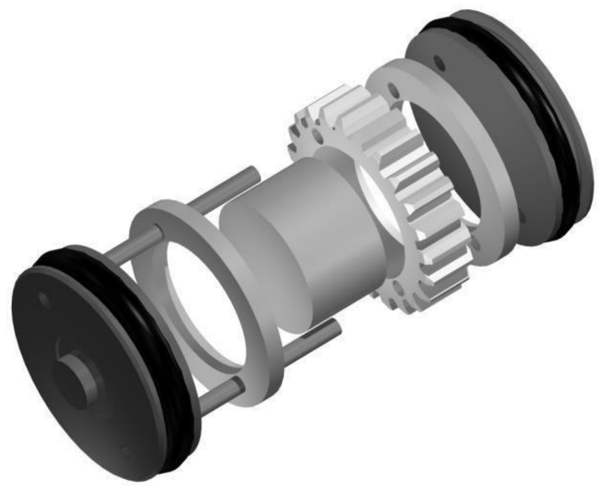

Fig.2. 18 Central axis design for a magnetic wheel. (Schoeneich et al, 2013)

2.5.2 Limitation of previous research

By examining these earlier designs, it can be seen that some of them have drawbacks. For instance, a robot with two magnetic wheels is made of cylindrical magnets fitted with a spring mechanism, allowing the magnets to roll radially on the surface while the spring can also return the magnets to their normal neutral position. The fact that magnets are in close contact with the environment, which correlates to corrosion, is a drawback of this type of magnetic wheel. Due to strong adhesion forces, the wheel's motor must exert a lot of torque in order to rotate the wheel by removing the magnets from the surface. A magnet makes a lot of noise and vibrations that can interfere with the inspection findings because of the uneven surface of the examination area. Because some of the anticipated magnetic wheels are heavy and must be able to sustain substantial adhesion forces in order to spin on a surface, a large amount of motor torque is required.To overcome the drawbacks, it is critical to build a magnetic wheel with continuous magnetic flux throughout the wheel's rotation. The problem of uneven and discontinuous adhesion forces can be overcome by utilizing a cylindrical permanent magnet with the N pole on the curved surface and the south pole at the magnet's centre.

2.6 The outcome of the literature review

After conducting a thorough analysis and reviewing several previous research articles, it was discovered that traditional inspection techniques are still used for overhead cranes. Flexibility was lacking in earlier research on robotic system design for inspecting steel structures. An irregular, concave, or curved surface makes inspection difficult. Robots in the past could only inspect a plane's surface. The accuracy and dependability of the results were the second issue found during the literature review. More accurate results couldn't be obtained because of the lift-off effect during calibration.

Despite decades of research, it is clear from a closer look at the literature that traditional inspection methods, such as visual inspection, are still used for overhead crane inspection. It has been determined through careful reading of the literature that non-destructive technique (NDT) methods with some automation technology are not currently being used. In this research, a climbing four-wheeled robot with permanent magnets for an overhead crane has been developed, and an automated NDT method using a GMR sensor array for crack detection has been implemented on that robot.

The novel aspect of this research is the adaptable robot design, which enables it to climb on plane, curved, and inverted surfaces while reducing lift-off values. The accuracy of the data produced by the specially crafted GMR sensor array is another novel feature. The system is user-friendly and interactive thanks to the ability to stream live video and display live graphs on an Android mobile device. Cost reduction, dependability, and safety that this automated solution will provide to industries are three more promising research areas.

CHAPTER 3

METHODOLOGY: DESIGN AND ANALYSIS OF ROBOTIC MAGNETIC WHEELS

3.1 Initial Design Concept of Magnetic Wheel

It is evident from reading the literature on magnetic wheels that little weight and simplicity of design are necessary for smooth steering and tilting at any angle. Reading this study—which has been discussed by other authors—makes it clear that the design of the wheels should be straightforward and lightweight. After considering all relevant elements, the initial design of a magnetic wheel using two neodymium magnets and ferromagnetic rings is shown in figure 3.1. Neodymium magnets are sandwiched between two rings made of stainless steel (SS) to replicate the fundamental design of a wheel.

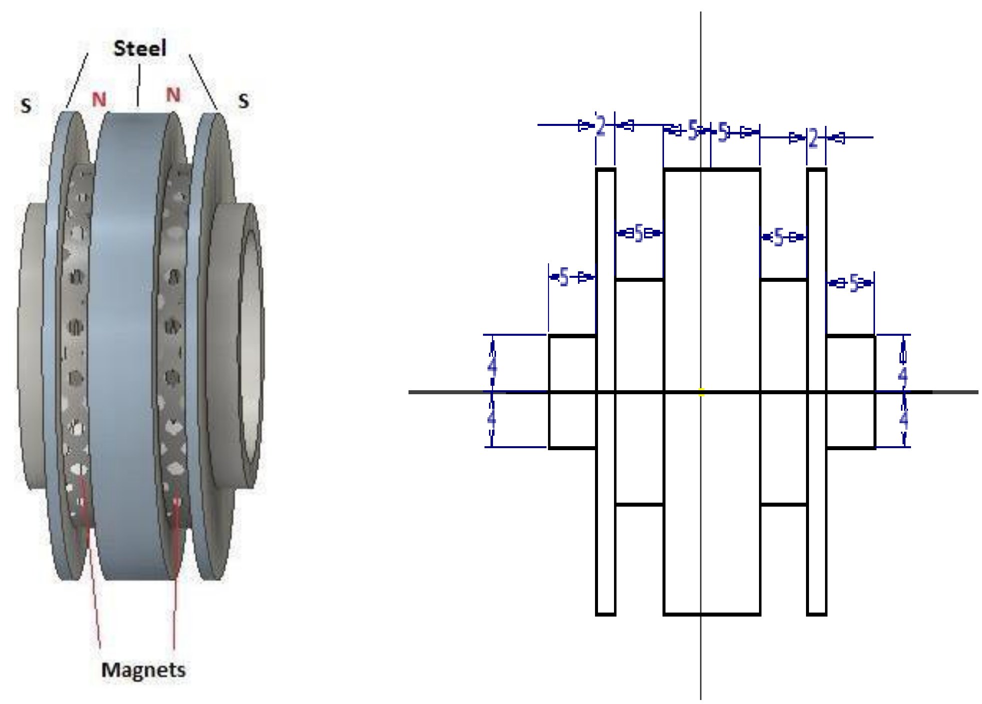

Fig.3. 1 Designed prototype of robotic magnetic wheel

The ferromagnetic rings' dimensions are noticeably smaller than the middle ring's. The main cause of the center ring's continued greater thickness than the side rings is the high concentration of magnetic line propagation through the thick plate. The locations of the thick and side ferromagnetic rings are also depicted in Figure 3.1

Two neodymium magnets are maintained between the ferromagnetic rings of the magnetic wheel so that they may make direct contact with them. These rings are appropriately magnetized by direct contact, which also increases the adhesion force. The purpose of employing two permanent magnets and sandwiching them between steel rings is to create a magnetic field loop that propagates from one magnet through the steel rings, back to the magnet, and then back again. Using this simple technique, the adhesion force may be increased by a factor of two to three.

It is evident from Figure 3.1 that the size of the two permanent magnets are less than those of the outer side ferromagnetic rings. Thus, only the outer ferromagnetic rings and not the permanent magnet will have direct contact with the examination region. Thus, magnets may be safeguarded from environmental harm such as corrosion. The diameters of the wheel and the size of the magnet are two crucial components in the generation of adhesion forces. The dimensions of the wheel are illustrated in Figure 3.2, and its characteristics are presented in table 3.1.

Table 3-1 CHARACTERISTICS OF WHEEL

Part| Description		**Dimensions**	**Material**
Side rings		Radius = ϕ 60 Thickness = 2mm	Stainless steel (SS)
Middle part		Radius = ϕ 60 Thickness= 10mm	Stainless steel (SS)
Magnets		Outer radius = ϕ 30 Inner Radius =ϕ 14 Thickness = 5mm	Neodymium NeFeB

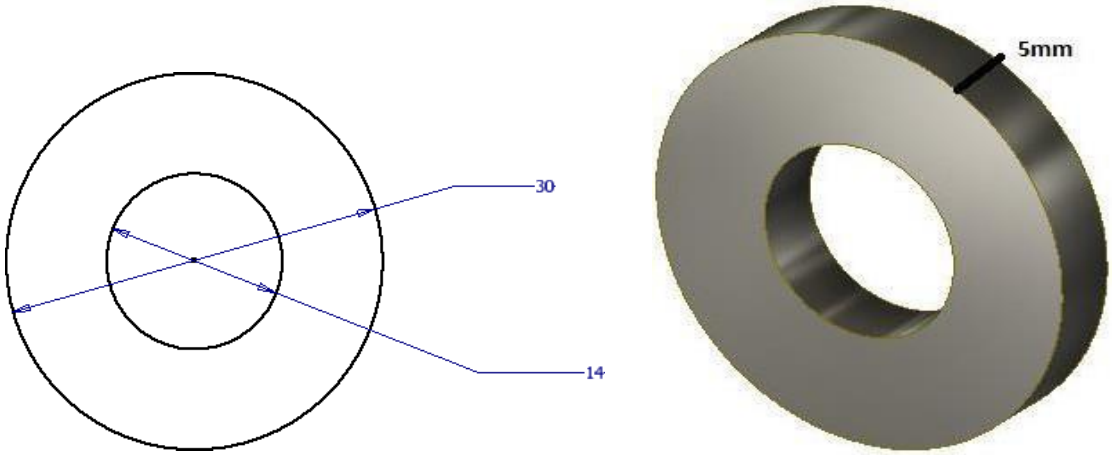

Fig.3. 2 Dimensions of wheel outer and inner diameter

Table 3-2 CHARACTERISTICS OF MAGNET PROPERTIES

Materials	**Grade**	**ResidualMagnetism Br Gauss (G)**	**Tesla**	**Corecievfieldstrength**
Neodymium	N35	11700-12100	1.17 1.12	10.8- 11-.5

Because the magnetic wheel must move over the steel surface, it must provide sufficient adhesion and traction forces to ensure that the body of the robot remains adhered to the inspection area. It is sometimes necessary for it to tilt the wheel and the body of the robot overall in order to navigate around the obstacles that are in its path. Calculating adhesion force and frictional forces is required in the design process because of the consideration of the factors outlined above.

Figure 3.3 depicts the configuration of the magnetic field lines entering the wheel as well as the contact area between the steel surface and the magnetic wheel. It is essential that there be an adequate amount of frictional force to prevent the wheel from slipping while it is being moved over the inspection area. Only then will the movement of the wheel be as smooth as possible. A study found that the frictional forces that exist between steel and steel surfaces are very little, with a value of μ=01.15 (Meystre, 2008).

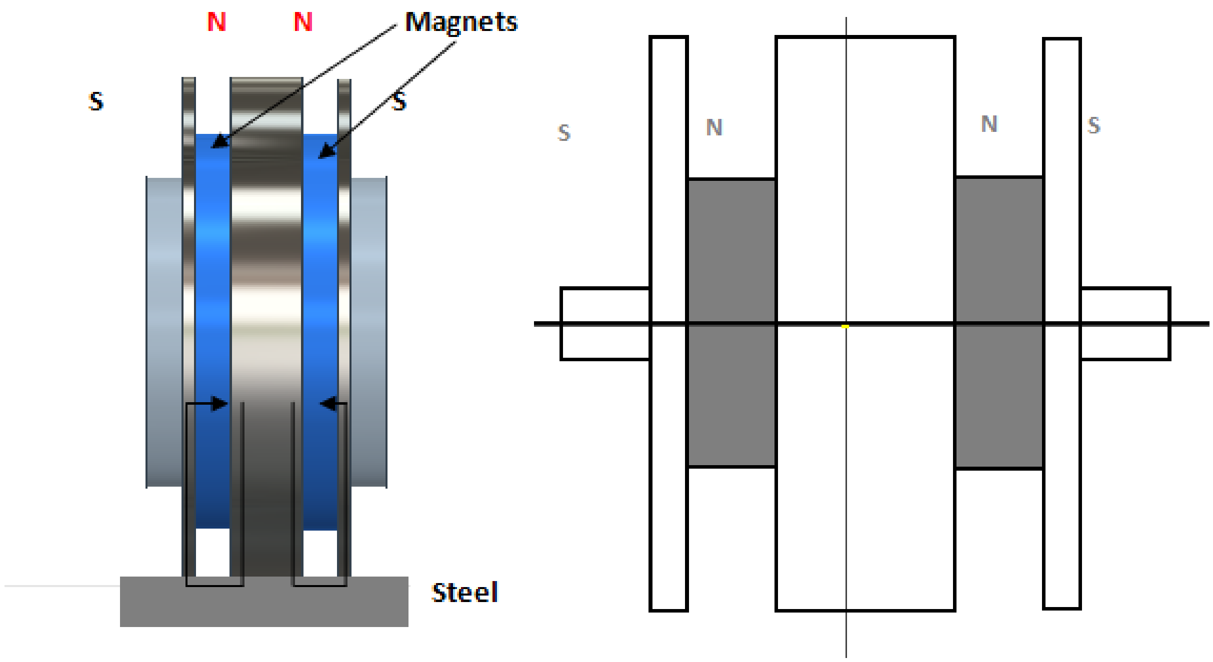

Fig.3. 3 3D model of wheel and steel contact (b) 2D model of magnet poles of the wheel

3.1.1 Adhesion force calculation

An assessment of the adhesion forces between the magnetic wheel and the inspection zone must be made. To find the adhesion force that the given magnet displayed in relation to each of the three contact zones, a number of experiments were conducted:

Case A. Magnet and the steel surface

Case B. Between two steel plates

Case C. Between magnet and magnet

Case A: Magnet and Steel Surface:

These rings of Neodymium and ferromagnetic steel make up the magnetic wheel. Very little research has been conducted with the magnetic wheel and inspection area of steel surface in order to produce the necessary adhesion forces and frictional forces. Figure 3.4 present an illustration of the relationship between distance (in) and pulling force(lb). Maximum draw force of 19.90lb is needed to separate magnetic wheel from steel surface in case of direct contact.

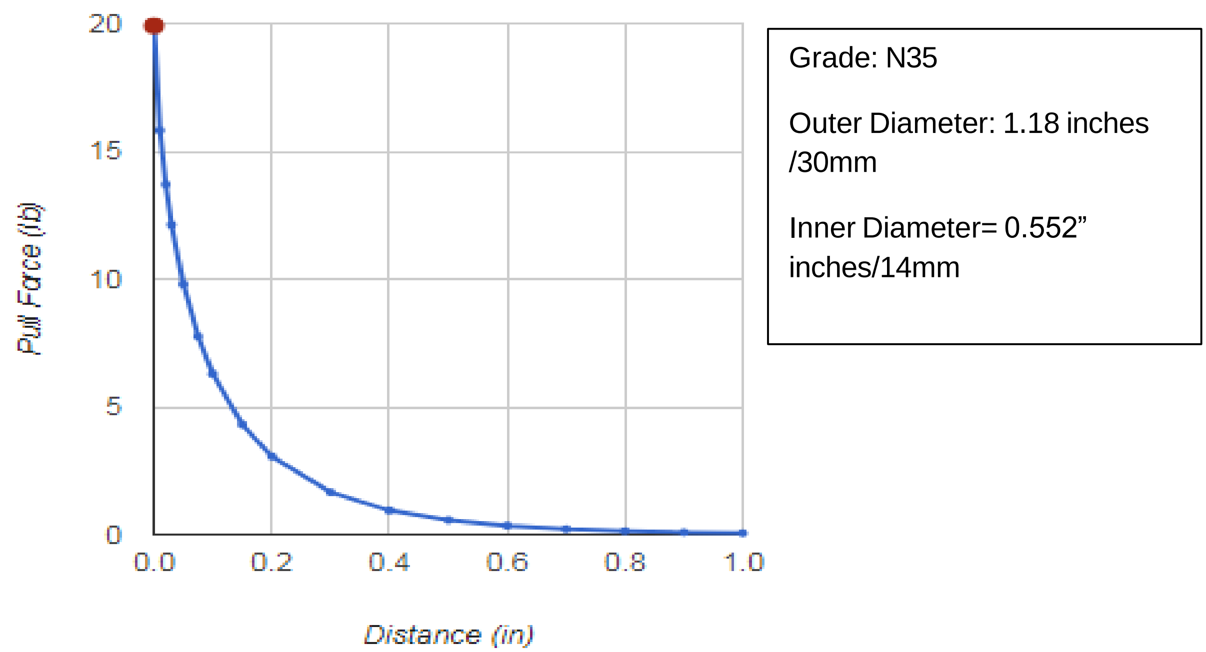

Fig.3. 4 Graphical representation of Adhesion force between magnet and steel surface(Yadav, A., & Szpytko, J. (2019).

Case B: Between two steel plates:

Another experiment established a steel surface contact in place of direct magnet contact, and the draw force was determined on the magnetized wheel. With this setup, the maximum draw force of 52.55(lb.) has been reached. You can see the relationship between the draw force and the separation of the two steel surfaces in figure 3.5. Observations made in the lab indicate that the magnets of a magnetic wheel must be kept away from the steel surface.

Instead, the inspection area should be in direct contact with steel ferromagnetic ring(s) since it takes greater draw forces to detach the wheel from the surface, which implies it creates more adhesion force on the steel.

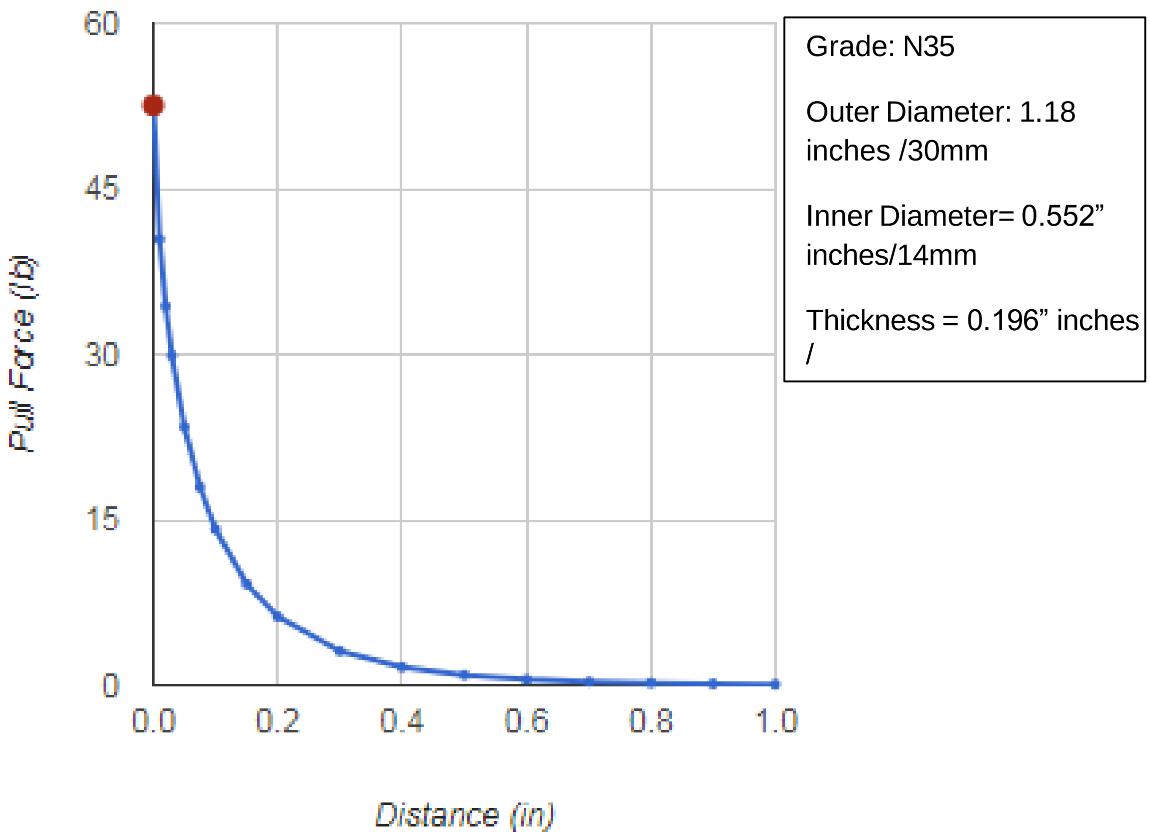

Fig.3. 5Adhesive force between Steel and steel surface

Case C: Between magnet and magnet:

Similar to the draw force and distance between the two magnetic surfaces shown in figure 3.6, these data were gathered by experimental means. When two natural Neodymium magnets are in close proximity to one another, the combined draw between them may reach a maximum of 19.20 lbf (lb.).

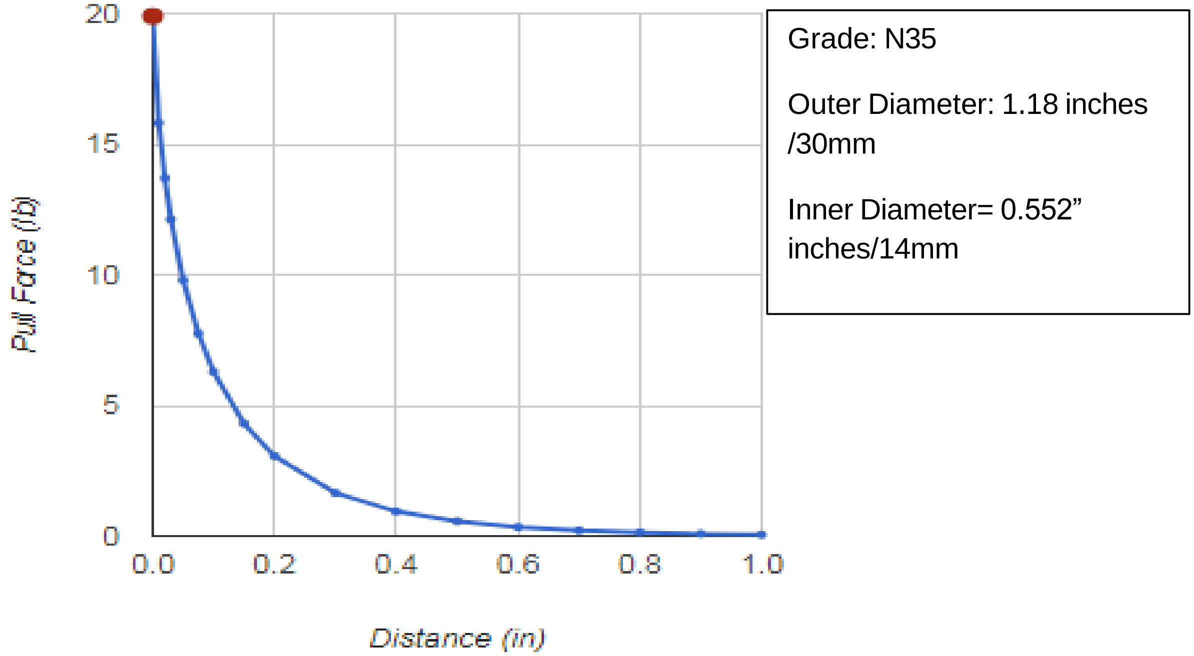

Fig.3. 6 a Adhesion force between Magnet and Magnet

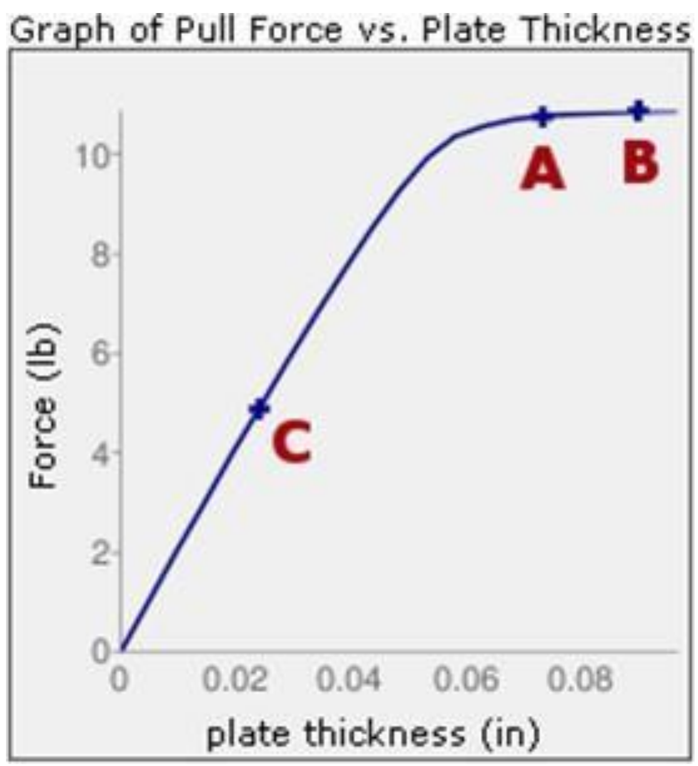

Fig. 3.6 (B) Graphical Representation between pull force and thickness of inspection area

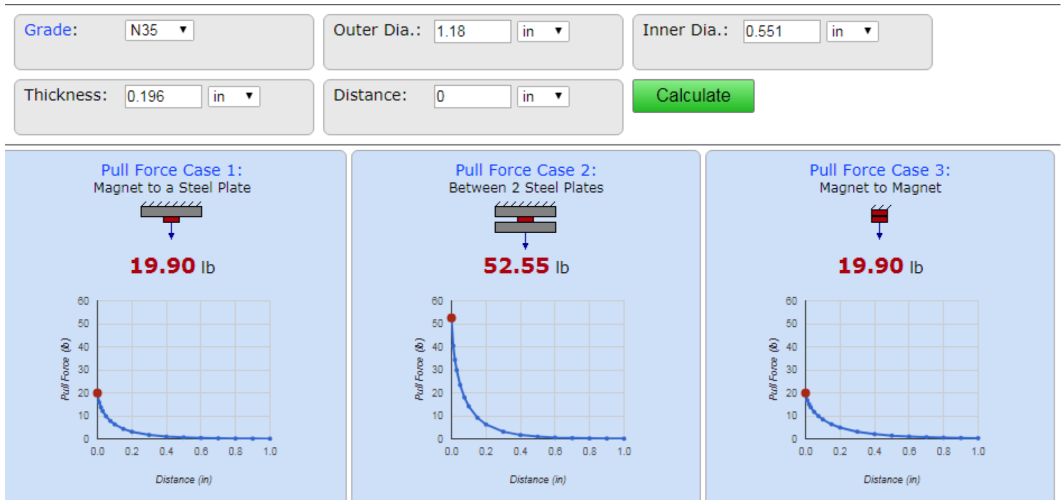

Fig.3.6 c Adhesion force replication in three instances

In order to comprehend the Neodymium magnet N35 grade, table 3.2 outlines its features. The demagnetization curve of a N35 grade magnet is shown in figure 3.7.

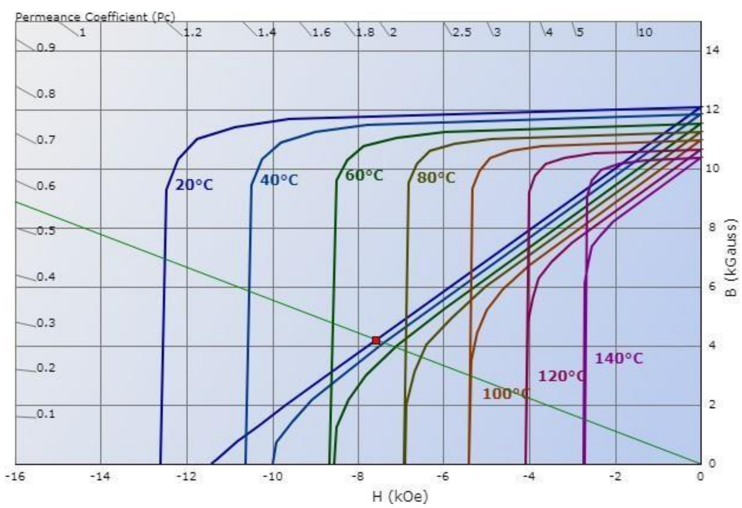

Permeance coefficient (Pc)=

0.55 B= 4.2 Kilogauss

H= -7Killoersted

BH= 38.1 maga-gauss-oersted

Fig.3. 7 Demagnetization curve of Neodymium magnet N35

To prevent corrosion and vibrations in magnetic wheels, direct contact between wheel magnets and steel surface is avoided. The ferromagnetic steel rings in this design will make direct contact with the inspection area. To increase the frictional forces between the Ferromagnetic ring and the inspection region, it is advised to wrap the ferromagnetic rings with a nylon rubber coating. Low adhesion forces are the primary disadvantage of the designed wheel.

Table 3-3 ROLE OF THE THICKNESS OF THE SURFACE PLATE IN ADHESION FORCES

Thickness of steel plates	Adhesion force	Distance between mag and steel surface
10mm	90.527	0mm
15 mm	90.684	0mm
20mm	90.664	0mm
25mm	90.409	0mm
30mm	90.702	0mm

Table 3-4 FORCE CALCULATION

FORCE CALCULATION		
Dimensions Outer Diameter= 60mm Innerdiameter= 14mm Magnet outer dia.= 30mm Inner dia.= 14mm Rubberthickness= 1mm	Wheel without Nylon cove 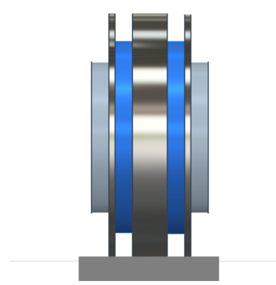	Wheel with nyloncover 
Adhesion force	64.09	41.99
Frictional force	11	18
Friction coefficient	0.12	0.36

Due to the great distance between the inspection area and the magnets, the adhesion forces were insufficient to hold the robot to the surface. On table 3.3, the influence of surface plate thickness in adhesion force is shown. According to the table, adhesion force slightly increases as steel plate thickness increases.

Table 3.4 shows the experimental results and according to that it can concluded that by using a rubber layer on wheel a significant increase in coefficient of friction from 0.12 to 0.36. But due to of the large distance between the magnets and the inspection area, adhesion forces are reduced. Therefore, the future design will place a greater emphasis on adhesion force and frictional force.

3.2 Multi-magnet shaped magnetic wheel

Low adhesion and frictional forces were the principal flaws of the previously built wheel. The rubber layer coating on the ferromagnetic rings increased the coefficient of friction but decreased the adhesion forces overall. As a solution, the newly built magnetic wheel allows the robot to travel smoothly on both flat and uneven terrain. Instead of a huge ring-shaped magnet, many tiny cylindrical magnets were proposed for this concept. The dimensions of cylindrical magnets are shown in figure 3.8. Utilizing cylindrical Neodymium N35 grade natural magnets makes the concept particularly adaptable to wheels of varying diameters. Using the same magnets, a large magnetic wheel may be created.

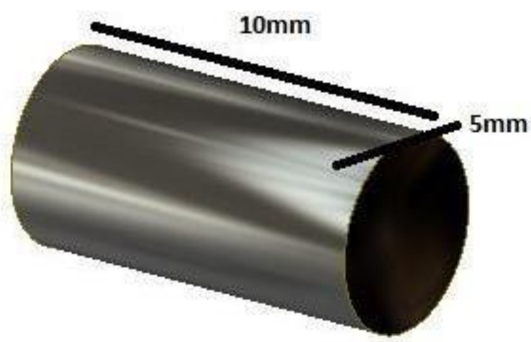

Fig.3. 8 Magnet dimensions

3.2.1 Mechanical design

The most significant distinctions between the multi-magnet wheel and the magnetic wheel that was built most recently are those pertaining to the form and number of magnets. Cylindrical, round-shaped magnets are used instead of inserting a big, ring-shaped magnet in between ferromagnetic rings in order to create a sandwich between two steel rings. Instead of using a single huge ring magnet, this design utilizes two sets of 15 magnets each that are implanted in the wheel flange. This results in a total of 30 magnets being used. It is possible to change the size of the wheel while maintaining the magnets' size by using a strategy that uses smaller magnets. The wheel is primarily made up of thirty magnets, as well as two rubber rings, three steel rings, and an aluminium hub that is used to join the wheel.

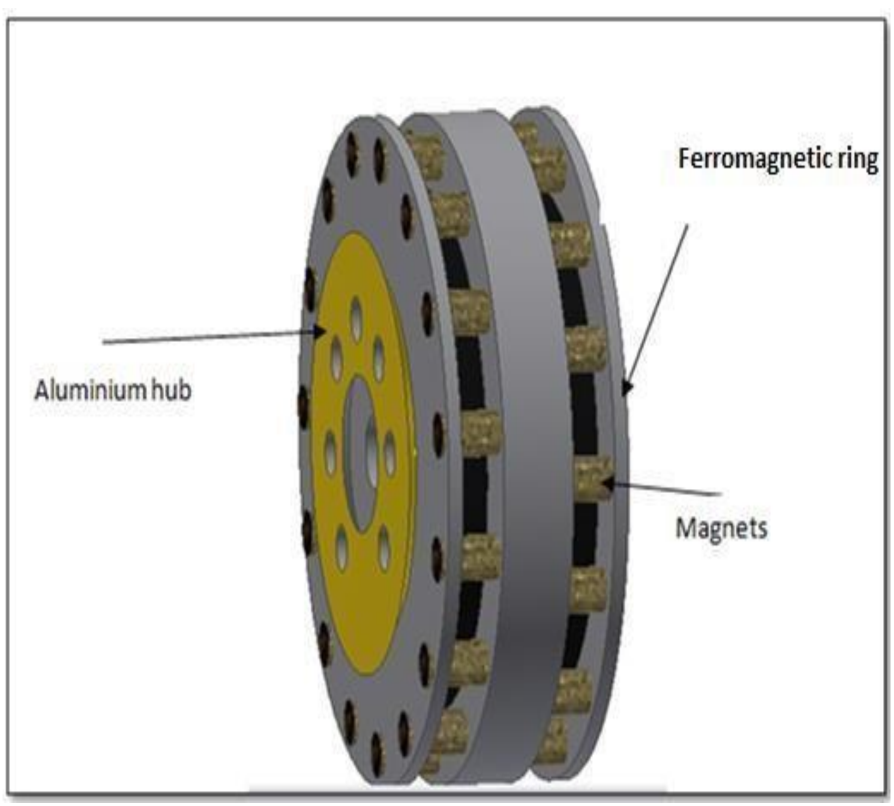

(a)

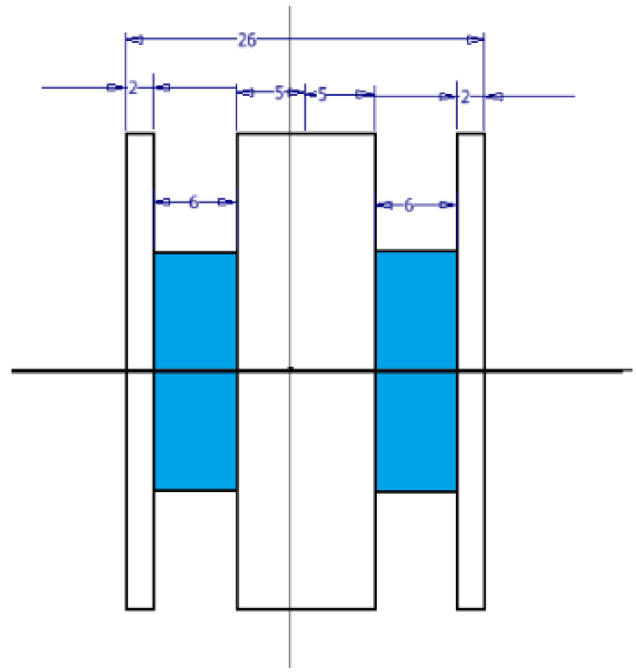

(b)

Fig.3. 9 Designed wheel model dimensions in (a) 2D (b) 3D model

In keeping with the earlier design, a thick steel ring measuring 10 mm was positioned between two ferromagnetic steel rings that were 2 mm thick on either side of the wheel. The size and diameter of the magnets have undergone substantial modification. Between the steel rings are two 6mm-thick holes for the installation of tiny cylinder-shaped magnets. During wheel rotation, the Zig-Zag pattern of cylindrical magnets increases adhesion forces. Figure 3.9 depicts the diameter of the wheel and the zigzag magnet configuration. To lower the weight of the wheel assembly, the wheel's driving mechanism is coupled to an aluminum hub. A 1mm-thick rubber covering was placed to the magnetic rings to boost the gripping forces and overall frictional force to prevent slippage. Here, figure 3.10(a) displays a three-dimensional model of a rubber-coated magnetic wheel. In addition, the wheel's measurements are shown below in fig. 3.10(b)

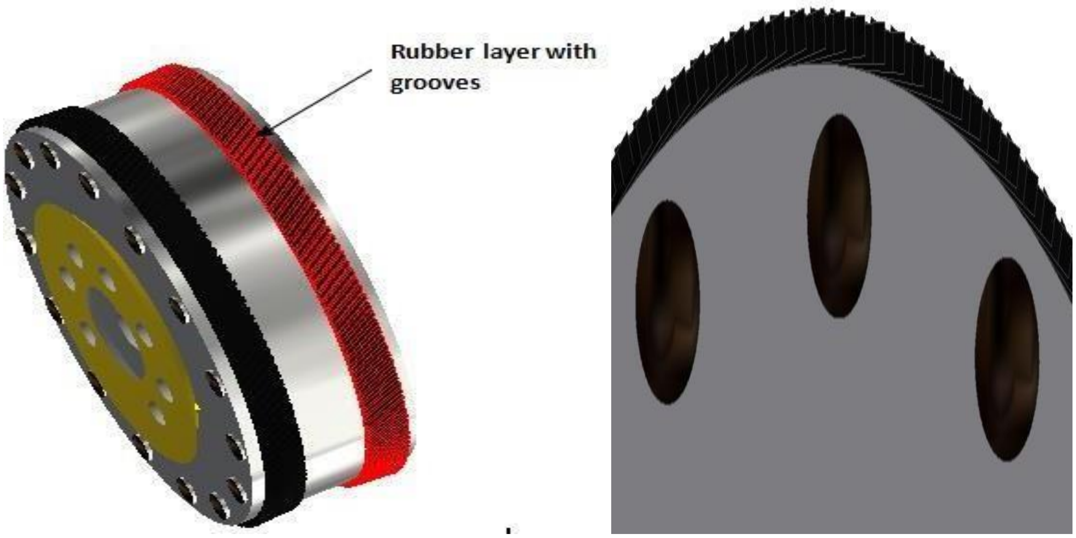

(a)

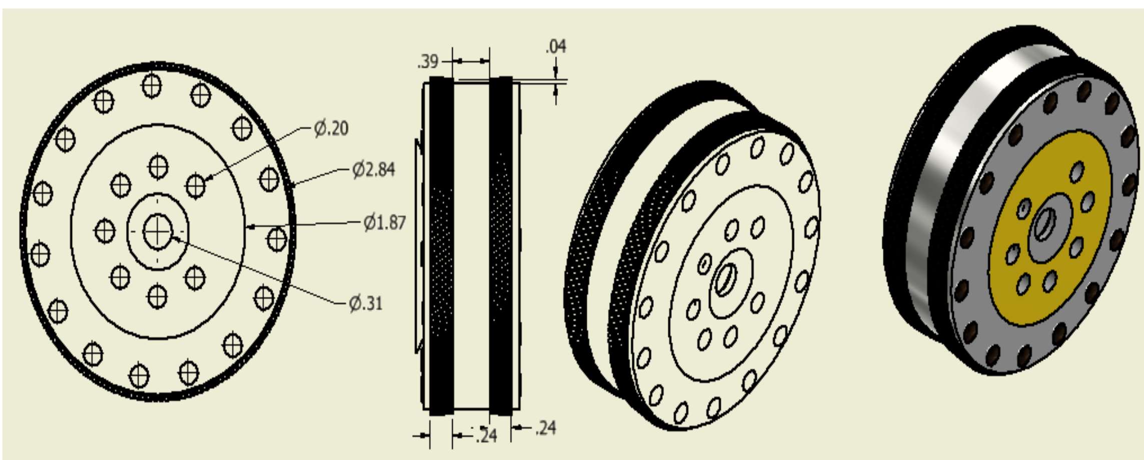

(b)

Fig.3. 10 Wheel with an outer covering of rubber layer (b) Side view of wheel with dimension

Table 3-5 DIMENSIONS OF THE MULTI MAGNET WHEEL

Dimension	Value	Material
Outer Diameter	75mm	Stainless Steel
Inner Diameter	50mm	
Total wheel Width	26mm	
Magnet Diameter	5mm	Neodymium N35
Magnet length	10mm	
Number of magnets	30	

The only drawback of the above designed wheel, heavy weight and uneven adhesion forces during the rotation of wheel on the surface. In order to maintain the grip on the vertical surfaces, adhesion force should be constant through the rotation of the wheel. Due to this limitation, it was required to create some lightweight wheel, that can maintain constant adhesion forces during the inspection process.

3.3 Final wheel design

Two failed magnetic wheel designs gave us valuable lessons about how to address the issue of decreasing adhesion forces between the wheel and the inspection surface. An innovative method for creating an efficient magnetic wheel is presented in this section. The robot's ability to climb is mostly dependent on its wheels. A lot of research has been done on the magnetic wheel's construction. In this case, the magnetic wheels are provided for two purposes: first, as a climbing aid, and second, as a magnetic field generator for a non-destructive flaw diagnosis technique. When developing the magnetic wheel, it is necessary to keep the weight of the magnetic wheel as light as possible, and the magnetic field created by the wheels should be strong during wheel rotation. To attach to the bridge's surface, it must provide adequate adhesion and friction forces to prevent slipping. This necessitates the deployment of a permanent magnet made of Neodymium Iron Boran (NDFeB) of type N48 to attain all of these attributes. A revolutionary magnetic wheel design is provided to address the significant drop in adhesion force that occurs when the wheel is coated with rubber tape.

The wheel shown in figures 3.11 and 3.12 is composed of a permanent magnet located between two ferromagnetic rings sized 3.5mm on both sides of the permanent magnet. These ferromagnetic rings are used to provide magnetic flux to the magnet.

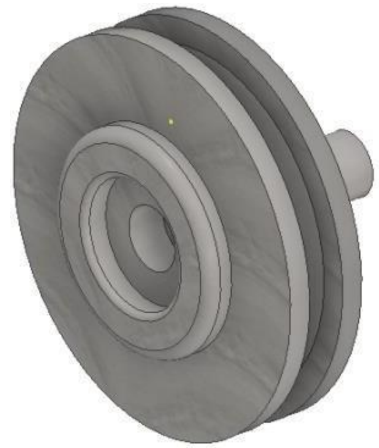

Fig.3. 11 Designed Magnetic wheel in Inventor

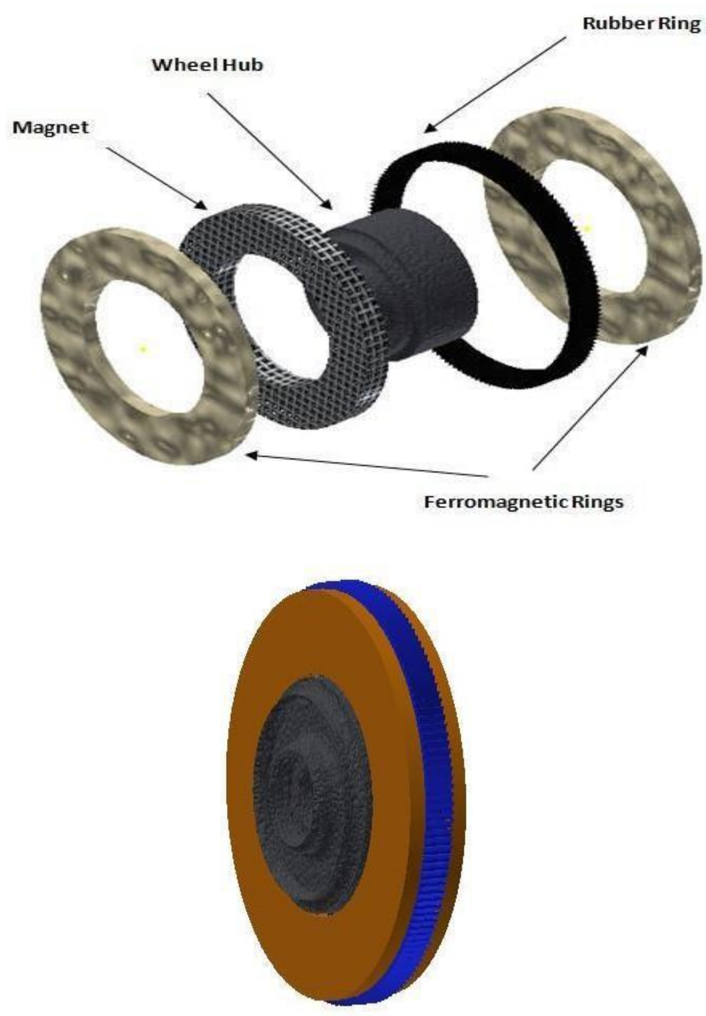

Fig.3. 12 (A)Exploded view of magnetic wheel assembly of magnetic wheel (B) Wheel with rubber covering (Yadav, A., & Szpytko, J. (2020).

A unique magnetic wheel design, seen in figure 3.12, comprises a set of ferromagnetic rings, a neodymium permanent magnet ring, a hub made of aluminium, and a rubber covering.

Both constructed ferromagnetic rings are positioned in such a way that a permanent magnet is positioned between them, leading to a magnetic flux that maintains the robot chassis on the surface of the inspection area.

To save weight, the wheel has an aluminium wheel hub. A 4 mm-wide outer rubber ring is affixed to the permanent magnet to strengthen the coefficient of friction. Initially, a simple rubber ring was in use, but it could not sustain higher frictional forces. To address this, a "V"-grooved rubber ring is developed, as seen in figure 3.13.

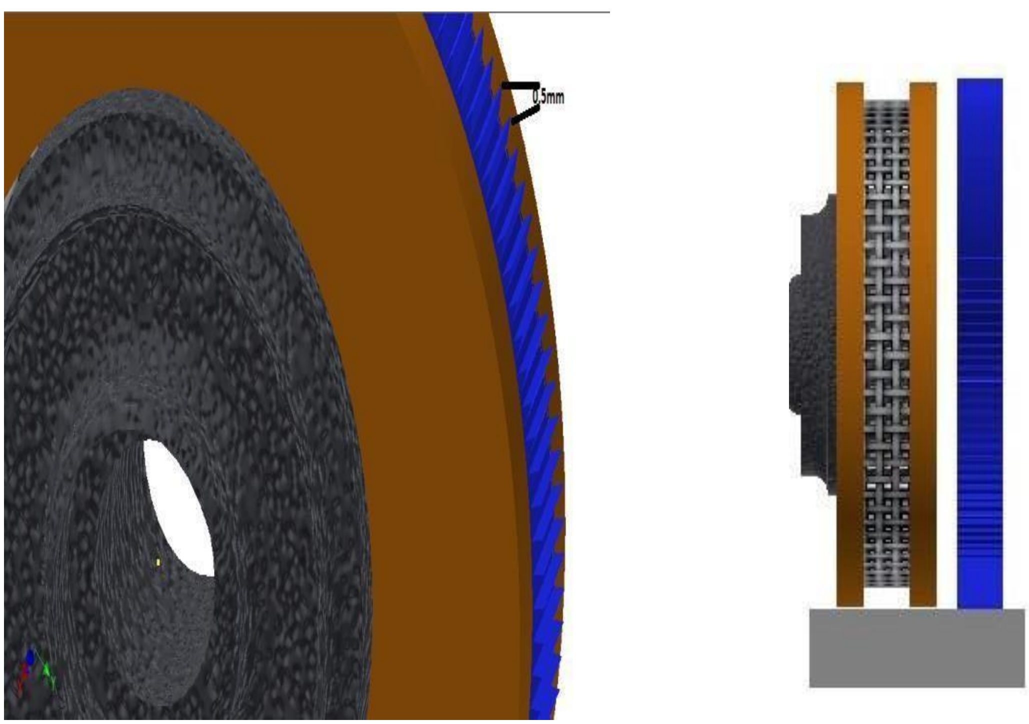

Fig.3. 13 An enlarged view of the grooved-shaped rubber ring

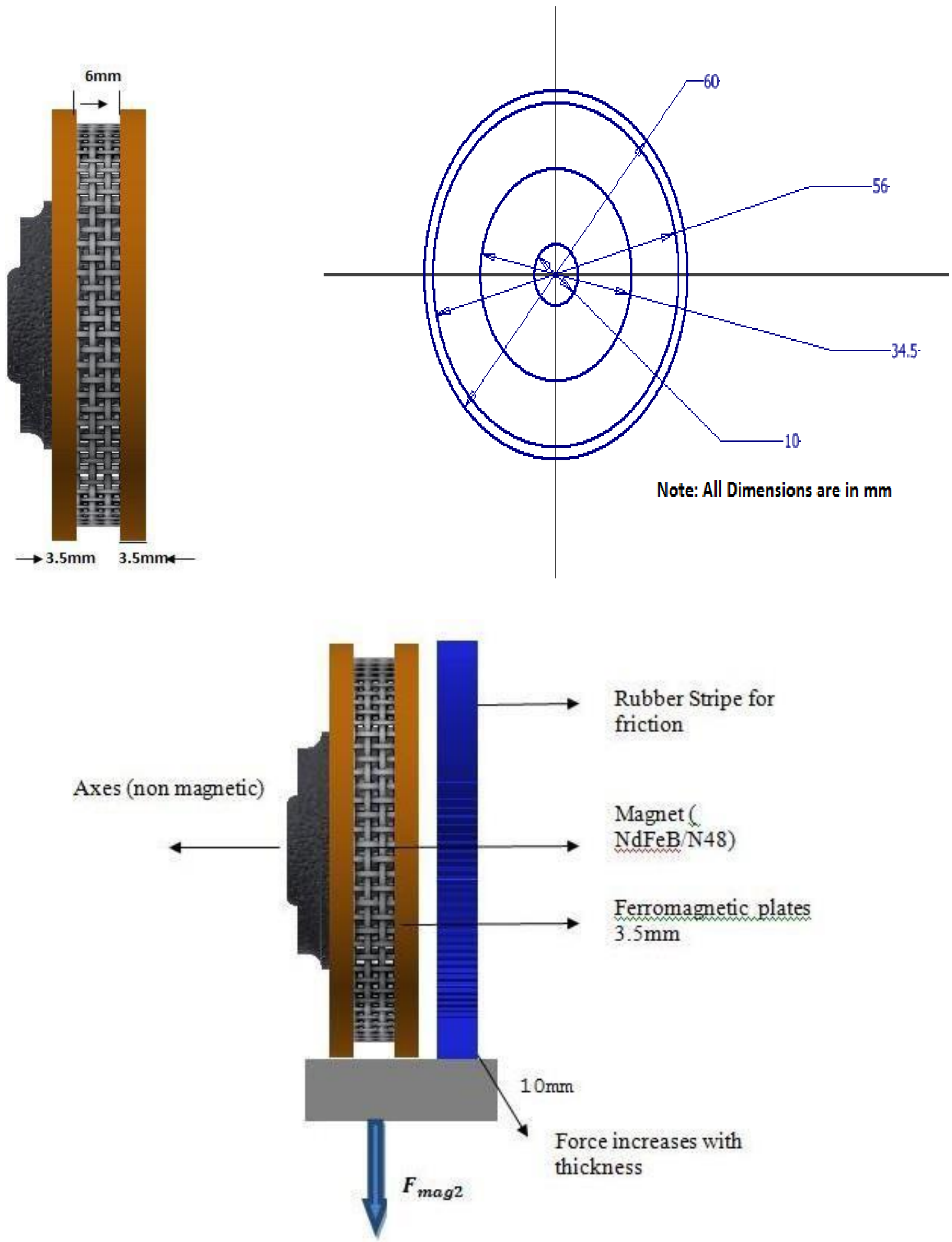

Fig.3. 14 Dimensions of the magnetic wheel(Yadav, A., & Szpytko, J. (2020).

Despite its small size, the wheel can pull a robot weighing between 5 and 6 kg by creating an attracting force of 4.4 kgf. Knowing the overall weight of the robot enables you to estimate the adhesion and frictional forces. Figure 3.14 depicts the dimensions of the magnetic wheel.

3.3.1 Calculation of magnetic flux simulation for the final wheel design

The adhesion forces, frictional forces, size, and weight of the projected magnetic wheel were all determined through a series of tests.
The adhesion forces between the wheel and the surface area must be determined. Adhesion forces need to be strong enough to hold a 5-kg robot with all of its sensors and inspection equipment attached. To find the density of magnetic flux and the flow of magnetic field lines, a simulation was run on the magnetic wheel.

Table 3-6 DIMENSIONS OF THE MULTI MAGNET WHEEL

THICKNESS	**For Steel Plate thickness 5 mm**		**For steel plate of thickn 10mm**	
FORCES	**Adhesion Force**	**Frictional force**	**Adhesion Force**	**Frictional force**
Wheel without rubber covering 	64.09 N	16	52	14
Wheel with rubber covering 	51.99 N	14	41	11

This wheel has to pass across both thick and thin inspection surfaces, therefore the thickness fluctuation of the inspection zone affects the magnetic flux density. To investigate the variation in adhesion, a specimen of steel plate with thicknesses of 5 mm and 10 mm was used.

Both specimens underwent a pull test and a simulation test to ascertain the adhesion forces. Pulling the wheel away from the test piece allowed a pull meter to quantify the adhesion and sliding forces. Table 3.6 displays the values of adhesion and friction forces in relation to specimen thickness.

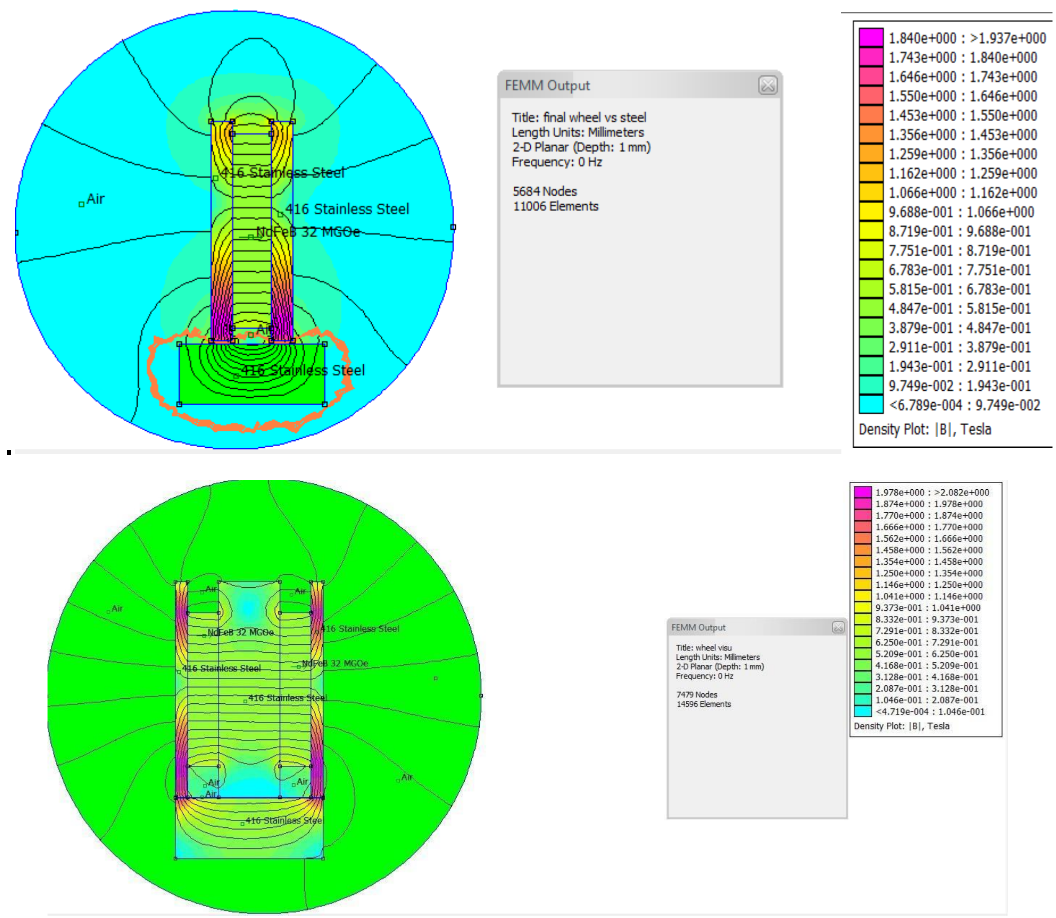

Fig.3. 15 The Finite Element method is performed on the wheel for adhesion force and magnetic flux density.

The wheel and 10-mm-thick steel plate were subjected to a finite-element analysis. The resultant magnetic flux and adhesion force among the steel plate and wheel are shown in Figure 3.15. In the picture, the point where the wheel makes contact with the steel surface is where the magnetic flux is at its highest. Figures 3.16 and 3.17 show further finite element analyses of the designs.

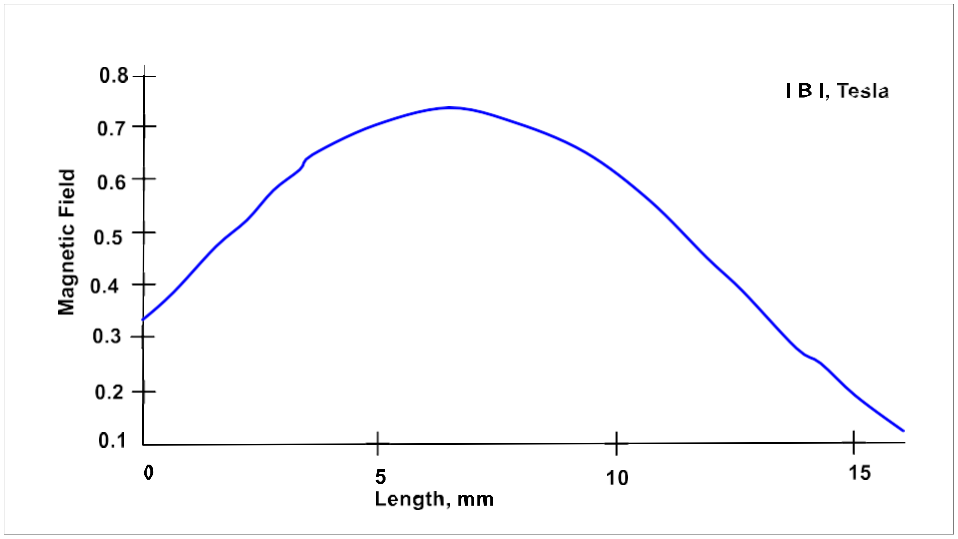

Fig.3. 16 Relationship between Magnetic Field and Length of Steel Plate

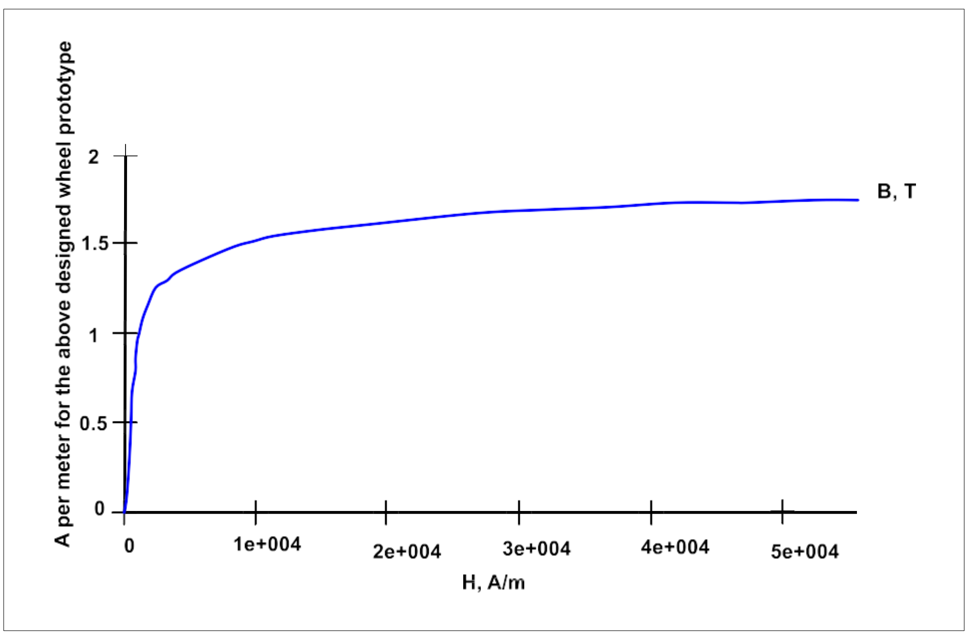

Fig.3. 17 Finite element method analysis between magnetic flux and A per meter for the above-designed wheel prototype

This designed wheel prototype can generate an adhesion force of up to 169 N, which is sufficient to support a load of up to 15 kg. A magnet and a steel surface need to be in physical touch with one another in order to create this adhesion force. In figure 3.18 are the computed results of adhesion forces between the magnet and wheel.

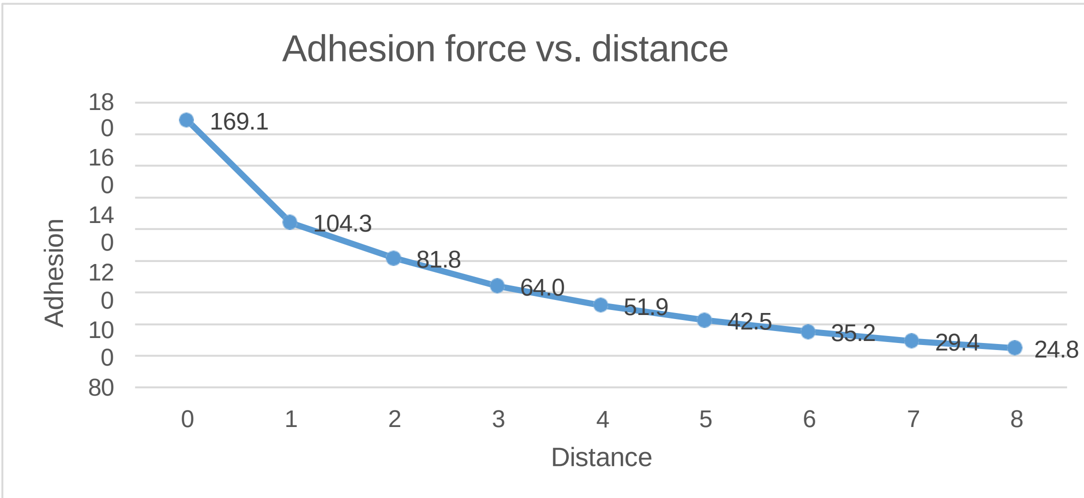

Fig.3. 18 Adhesion forces between a magnet and a wheel

There are no magnets in direct contact with the steel surface since only the 3.5 mm thick ferromagnetic rings on the wheel's sides come into interaction with the testing area. In this instance, the wheel's adhesion force holding a 7-kg robot in place is 64.9 N. This forced adhesion is produced by one of the robot's four magnetic wheels. This implies that a maximum of 26.12 kg might be supported by the four adhesion forces acting together.

The only issue with this planned prototype is while climbing very sharp turns, when the wheel must tilt owing to an uneven terrain. When a wheel is tilted at a certain degree, there is also a reduction in adhesion forces [OMNI directed]. This drop in adhesion force may cause robots to detach from the surface. When the wheel was tilted at the angle shown in figure 3.19, simulations done using software for magnetic field modeling revealed a significant reduction in adhesion forces, as seen in the graph in figure 3.19.

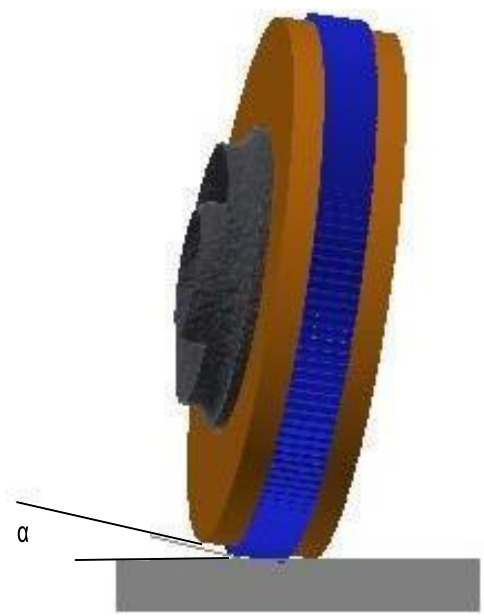

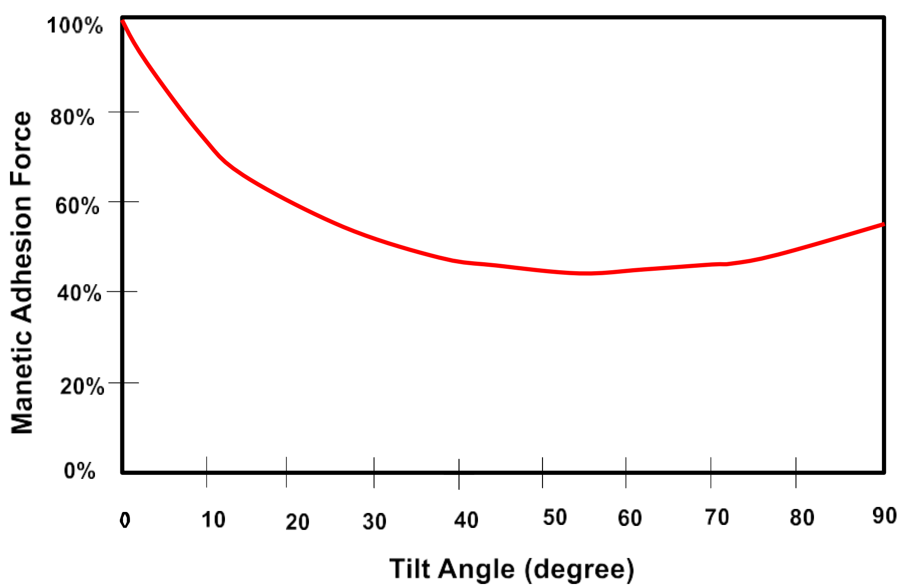

Fig.3. 19 1Relationship between Tilt Angle and Magnetic Adhesion Forces

By considering the different thicknesses of the steel inspection area, and obstacles, this designed magnetic generates enough adhesion forces to keep the robot on work during the inspection process. Their adhesion and frictional forces were enough to hold the robot adhered to in the inspection area.

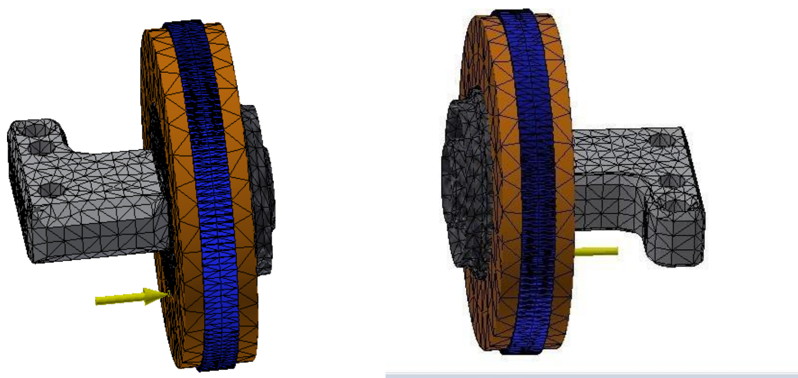

Fig.3. 20 Meshed View of Magnetic wheel

By considering the issue of slippage while tilting, it is required to make the wheel turn in such a way that the tilting can be avoided. In order to overcome the tilting and slippage, the centre hub of the wheel was fixed to the robotic chassis axle. Turning and steering of the wheels were performed by keeping the rear or front wheel constant. For better understanding, if the wheel has to turn left, the real wheels start moving towards it by keeping the front wheels fixed. In this way, tilting while performing inspections can be avoided. The wheels can carry a heavy robot and help in performing the inspection task. The robot design and details have been discussed in the upcoming chapter 5. For clarity and understanding, the dimensions of the robots have been presented here in Table 3.7. This is an overview of how these wheels will be carrying a robot with the below-mentioned dimensions.

Table 3-7 DIMENSIONS OF THE DESIGNED ROBOT

Parameter	**Value**
Length	35 CM
Width	25CM
Height	15CM
Control Operations	2.4GHZ Remote Control unit
Drive	4 motors. 4WD
Apprx. Total Weight	4kg (approx)

The simulation findings show that an adhesion force of 247.9 N may be produced between a 10 mm-thick ferromagnetic plate and the outer circular surface. In order to avoid corrosion and breakage, the magnets must be shielded from direct contact with the working surface during operation. The magnetic adhesion force between the ferromagnetic material and the magnetic wheel will be lessened by hiding the magnet with the rubber stripe. This chapter presents specific design highlights of the robot magnetic wheels in order to illustrate the reasoning behind the design and the aspects that were taken into account. The parts and other accessories that were used in the production of the robot's other parts are shown in the next chapter

CHAPTER 4

METHODOLOGY: COMPONENTS USED FOR ROBOT MANUFACTURING

4.1 Introduction

This section covers at the project's conceptual schematic representation as well as the creation of separate modules. Figure 4.1 depicts the Block diagram:

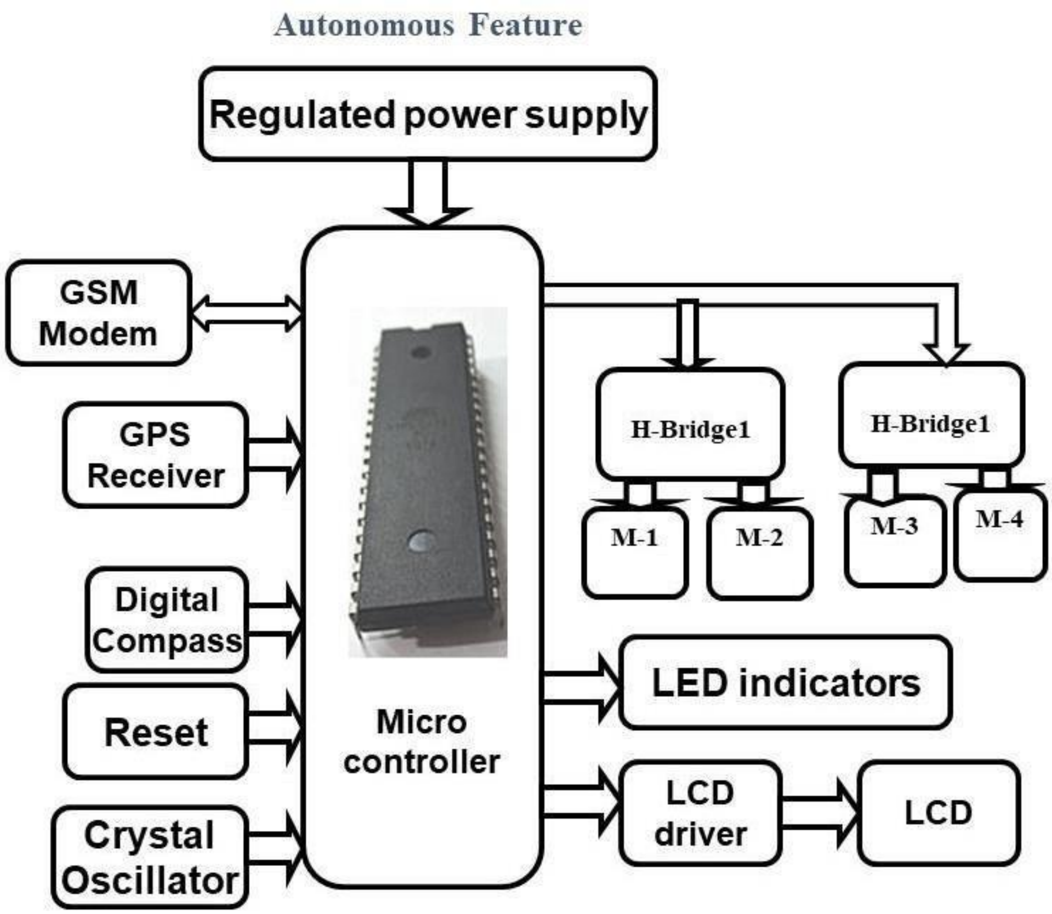

Fig.4. 1 Robots for detecting cracks with autonomous capabilities (Yadav, A., & Szpytko, J. (2020).

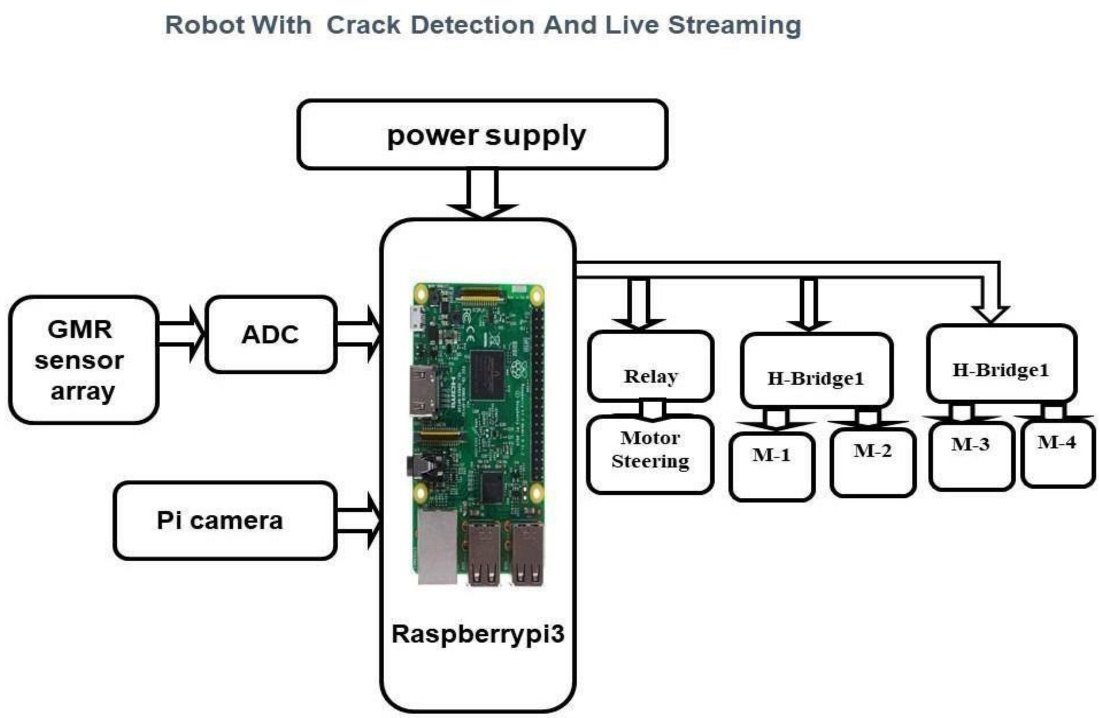

Fig.4. 2 Block schematic of the robot for crack detection (Yadav, A., & Szpytko, J. (2020).

The Autonomous crack identification robot is mostly composed of the following parts:

- Power Source.
- Microcontroller.
- Raspberrypi3 processor.
- DC motors .
- GSM moudle
- GPS
- Crystal oscillator.
- Reset.
- LED Indicators.
- Pi camera.
- Digital compass.
- LCD

- GMR Sensors
- Relay

4.2 Microcontroller

The advancement of integrated circuit technology laid the groundwork for the current state of affairs in the microcontroller industry. Thousands of transistors may now be stored on a single chip thanks to this advancement. It was a need for the manufacturing of microprocessors, and after that, external peripherals like memory, input-output lines, timers, and others were added to create the first computers. Integrated circuits were produced as a result of a further rise in package volume. These integrated circuits have peripherals and CPUs on board. That's how the first microcomputer-containing chip (PIC16F87XA Data Sheet, 2003) (Bansal et al., 2007) was created. This chip would subsequently be known as a microcontroller.
Figure 4.3 shows the PIC16F877A microcontroller that was utilized in this project.

.

Fig.4. 3 Microcontrollers

4.2.1 Pin Diagram:

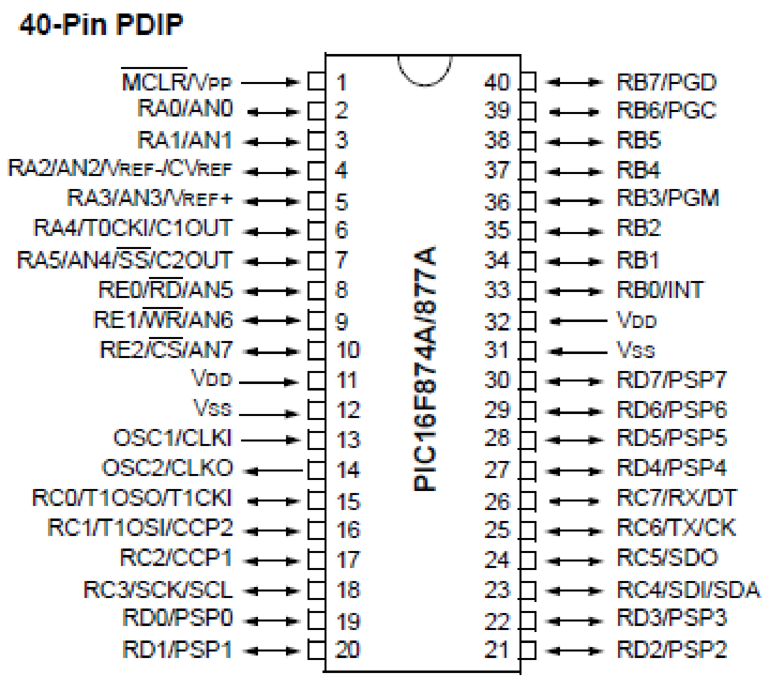

Fig.4. 4 Pin Diagram of PIC16F877

In figure 4.4 represent the PIC16F877 is a 40-pin microcontroller. It has 5 ports, port A, port B, port C, port D and port E. All the pins of the ports are for interfacing input-output devices.

Port A: It consists of 6 pins from A0 to A5

Port B: It consists of 8 pins from B0 to B7

Port C: It consists of 8 pins from C0 to C7

Port D: It consists of 8 pins from D0 to D7

Port E: It consists of 3 pins from E0 to E2

The rest of the pins are mandatory pins these should not be used to connect input/output devices.

Pin 1 is MCLR (master clear pin) pin also referred to as a reset pin.

Pin 13, 14 are used as crystal oscillators to connect and generate a frequency of about 20MHz.

Pin 11, 12 and 31, 32 are used for voltage supply Vdd (+) and Vss (-)

PIC 16F877A Specification:

RAM	368 bytes
EEPROM	256 bytes
Flash Program Memory	8k words
Operating Frequency	DC to 20MHz
I/O port	PortA, B,C,D,E

4.3 Power Source from Rechargeable Battery

To operate the robotic tool, a rechargeable battery was considered. The battery can be charged by the aid a special charger. It consists of a minimum of one electrochemical cell. An apparatus that gathers and stores energy through a reversible electrochemical process is referred to as a "accumulator". There are many different types and capacities of rechargeable batteries, from button cells to megawatt systems linked together to stabilize an electrical distribution network.

Fig.4. 5 Rechargeable battery (Yadav, Arun Kumar, and Janusz Szpytko (2022)

4.3.1 Features of the rechargeable battery

• Extremely small in both weight and size in comparison to the Ni-Cd, Ni-MH, and Lead Acid Batteries depicted in Figure 4.5.

• 180-minute completely charged using a unique adapter

• Extended lasting power with up to 1000 recharging cycles

• 3X 3.7V 2200mAh Li-Po batteries (3S1P)

• Easy to maintain

• Weight: 195 g

• Dimensions: 10.5cm*3.3cm*2.2cm

• Discharge Current (Amps): 40*2200maH = 88Amp

• Maximum Charging Current: 1 amp

4.4. LED of the Robot

LEDs contain diodes made of semiconductors that only allow one direction of current to pass across a circuit. Two different materials are combined to make a PN diode. A PN junction's P side is electron-free yet highly charged. According to Mosiori et al. (2017), the N side possesses an excess of electrons but no positive charge. The internal architecture and constituent parts of the LED are shown in figure 4.6.

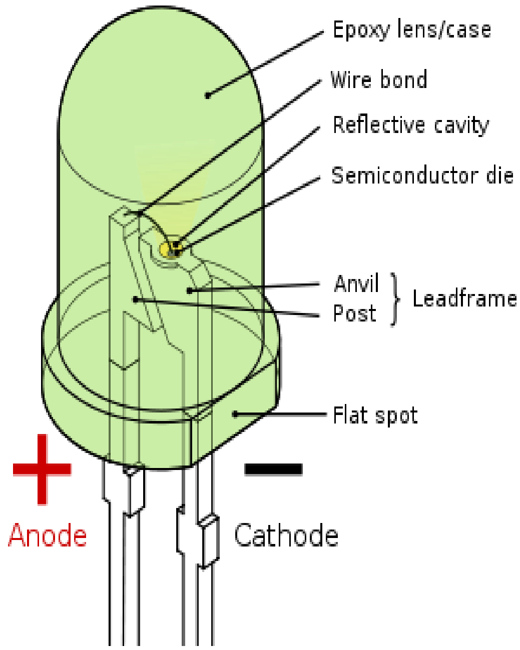

Fig.4. 6 Parts of the LED

The compact size of LEDs has allowed new text and video displays and sensors to be developed, while their high switching rates are useful in advanced communications technology (Mosiori et al., 2017). The electrical symbols and polarities of led are shown in fig: 4.7.

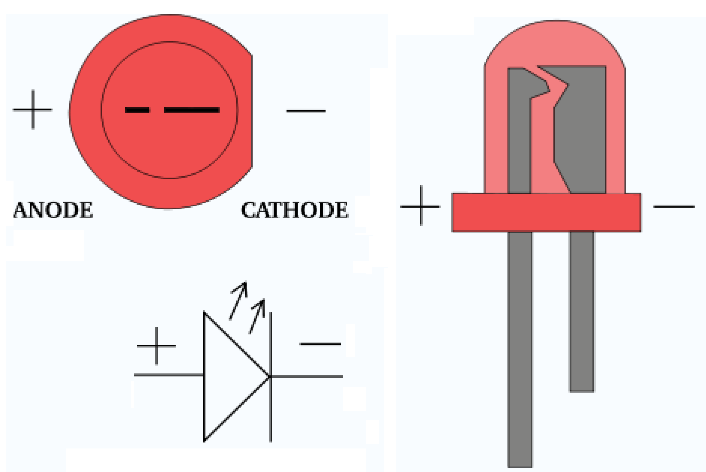

Fig.4. 7 Electrical Symbol & Polarities of LEDs

LED lights have a variety of advantages over other light sources:

- High levels of brightness and intensity
- High-efficiency
- Low-voltage and current requirements
- Low radiated heat
- High reliability (resistant to shock and vibration)
- No UV Rays
- Long source life
- Can be easily controlled and programmed

Applications for LEDs fall into three major categories:

- A visual signal application where the light goes more or less directly from the LED to the human eye, to convey a message or meaning.
- Illumination where the LED light is reflected from the object to give visual response of these objects.
- Generate light to measure and interact with processes that do not involve the human visual system.

4.5 Global Positioning System (GPS)

The Ublox NEO-6M GPS device with antenna is a low-cost GPS with exceptional performance. This module is compact (22*30 mm) and offers several connectivity options. Because the use of batteries is usually a top priority for robots that are mobile, The small design of the NEO-6M, as well as its low power usage and memory choices, render it perfect for the functioning of battery-powered mobile robots (Mosiori et al., 2017). The tiny dimension of the NEO-6 M allows for simple deployment in small spaces (Yadav, Arun Kumar, 2022).

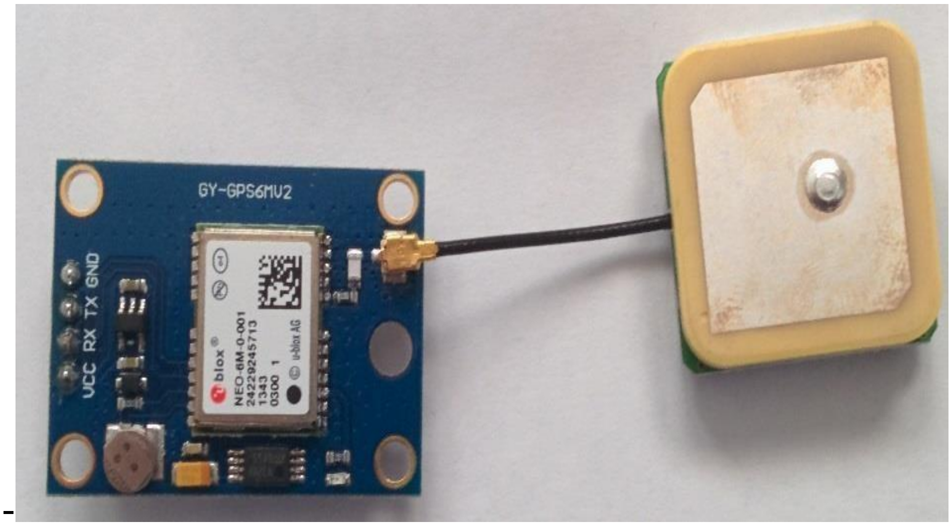

Fig.4. 8 Model of GSM module(Yadav, Arun Kumar, and Janusz Szpytko (2022).

Table 4-1 UBLOX NEO – 6M GPS SELECTION FEATURES

Mod	**Type**	**Supply**	**Interfac**	**Features**
NEO-6	Standalon GPS	2.7 V to 3.6	UART USB SPI DDC	Crystal Oscillator RTC Crystal Antenna Supply and Supervisor Configuration pin 3 Time pulse 1

4.6 Global Systems for Mobile Communication (GSM)

A SIM300 Global System for Mobile Communications (GSM) modem was used in this investigation to make the network more self-sufficient. The SIM300 GSM device has a serial interface that is simple to use. Using this device for autonomous crack detection, robots may send SMS, receive messages, and make phone calls with the help of an AT command. This modem is linked to the microcontroller via an RS232 interface. The GSM modem has a SIM card port, power management, and an external antenna.

Fig.4. 9 SIM300 GSM Module(Yadav, Arun Kumar, and Janusz Szpytko (2022).

4.6.1 SIM300 MODEM Specification

Figure 4.9 represent the SIM300, it is a tri-band GSM that works on three bandwidths of EGSM 900 MHz, DCS1800MHz, and Personal Communication System (PCS1900). It also supports the GPRS coding schemes CS-1, CS-2, CS-3, CS-4. SIM300 has a compact size of 40*33*2.85mm and also be fitted in a constrained size area.

In this work to get to know the exact location of the robot through a mobile application, a physical interface to the mobile application is made through AT command.

SIM300 provides an RF antenna interface with two alternatives: antenna connector and antenna pad.

4.6.1.1 Features of SIM300

- Tri-band GSM/GPRS900/1800/1900Mhz
- GPRS Multi-Slot Class 10

- GPRS mobile station class –B
- Complaint to GSM phase 2/2+
  - -class 4(2W @900MHz)
  - -class 1(1W @/18001900MHz)
- Dimensions: 40x33x2.85 mm
- Weight: 8gm
- Control via AT commands
- (GSM 07.07, 07.05 and SIMCOM enhanced AT Commands)
- SIM application tool kit
- supply voltage range 3.5……………v
- Low power consumption
- Normal operation temperature: -20 ’C to +55 ‘C
- Restricted operation temperature: -20 ’C to -25 ‘C and +55 ’C to +70 ‘C

CHAPTER 5

METHODOLOGY: ROBOT DESIGN

These days, the usage of inspection robots is growing, especially for huge constructions in dangerous environments and for continuous real-time monitoring in hot conditions. In this study, a climbing inspection robot is used to account for huge ferromagnetic infrastructures during inspection. Over the last 20 years, climbing robots have been used for a variety of tasks, including cleaning and painting surfaces, inspecting for corrosion, fractures, and weld joint strength (Tavakoli et al., 2013).

The crucial part in climbing robot, is to maintain the robot to stick with the surface during climbing process. Many locomotion systems have been used in the climbing robots depending on the applications as discussed in chapter 2. For easy understating, if the robot has to climb on a concrete surface or a wooden surface, the most commonly used holding mechanism is suction cups in which negative pressure is generated by the propeller (Dulimarta & Tummala, 2002). The second most common adhesion mechanism for climbing robots to climb on a ferromagnetic surface is the use of magnetic adhesion mechanisms that have been designed and discussed earlier in chapter 3.

This section explains an inventive development method for a climbing surveillance robot that finds steel bridge defects and cracks for cranes that are located overhead. The main focus of the research is on the development and use of an affordable crack detecting robot for examining large ferromagnetic constructions, particularly overhead crane girders.

Mostly overhead cranes in the industries operates under a harsh environmental condition. During the operation of cranes, it goes through continuous heavy loading and unloading. The presence of impact load and heavy vibrations, small crack formations occur into the subsurface. These sub-surfaces defects can be recognized by the inspector by visual inspection until and unless the crack appears on the surface. Upon the formation of surface crack, it can be turned into a huge crack that can result in a drastic failure of the structure.

A unique strategy is provided to limit damage to structures and reduce investigation expenses by creating a surveillance robot with magnetic wheel mobility. The proposed robot's unique feature is its excellent detection rate in detecting surface cracks and defects under the paint surface area. Because of its lightweight and small size, the robot's architecture is both reliable and easy to control.

The robot features four magnetic wheels driven by four DC motors and a lightweight aluminium frame. Servo joints are included in the robot chassis to guarantee that it may expand and contract without losing its versatility. The front suspension system with two magnetic wheels is powered by two high-torque DC motors.

Because this robot is tele operated, an examiner may operate it remotely. To control the robot from a distance, 2.4GHz wireless communication is maintained via a transmitter module on the far inspector end and a receiver module on the robot body. DC motors are controlled by electronic speed control (ESC) devices, which may be managed remotely from a distance. To lessen vibrations and enable smooth movement of the robot, a set of shock absorbers is positioned at the front axle.

Two high-torque DC motors are also mounted on the robot's back axle. The front axle of the robot has a steering mechanism installed in order to move its body. To try to make robots able to maneuver at steep and convex bends, a servo motor is added to their framework. The robot also gains additional flexibility with a rotating link connecting the frame and chassis. During sharp curves or bumps, the servo motor is adjusted to rotate in a way that brings the rear axle closer to the front axle. The robot may maintain a specific height while navigating around sharp turns.

Arrays of GMR sensors are fixed on the rear axle by maintaining a minimum fixed distance from the inspection area. The sensing and controlling parts of the robot are explained in the subsequent subsections.

Figures 5.1(a) and 5.2 show the design from the front view, side view, and top view of the inspection robot. The size and dimensional specifications are presented in Table 5.1.

(A) Top View of Root

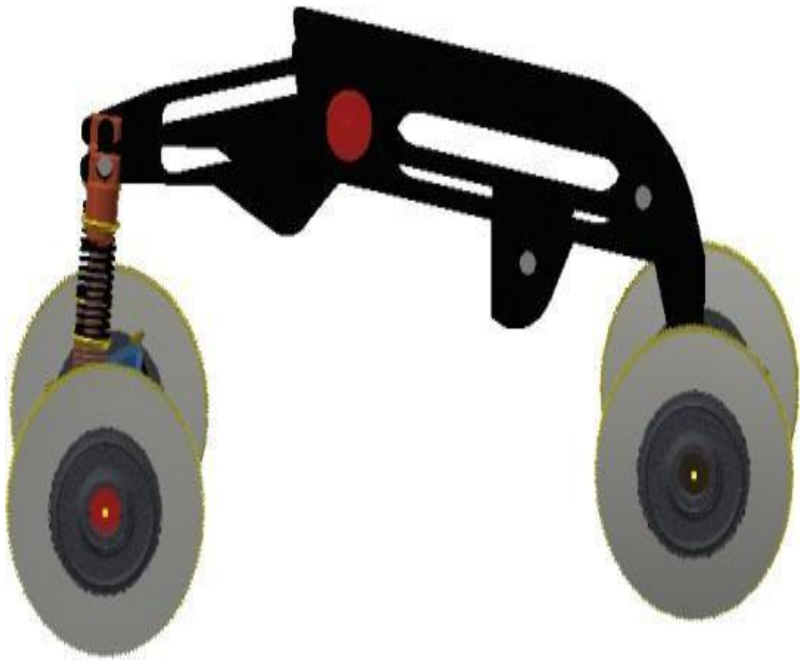

(B) Side view of the robot

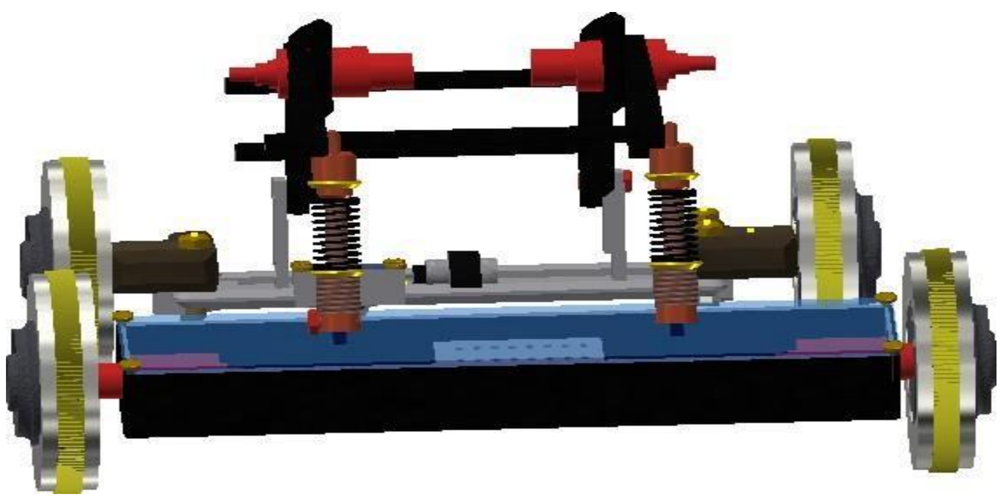

(C) Front view of the robot

Fig.5. 1Multiple views of the robots

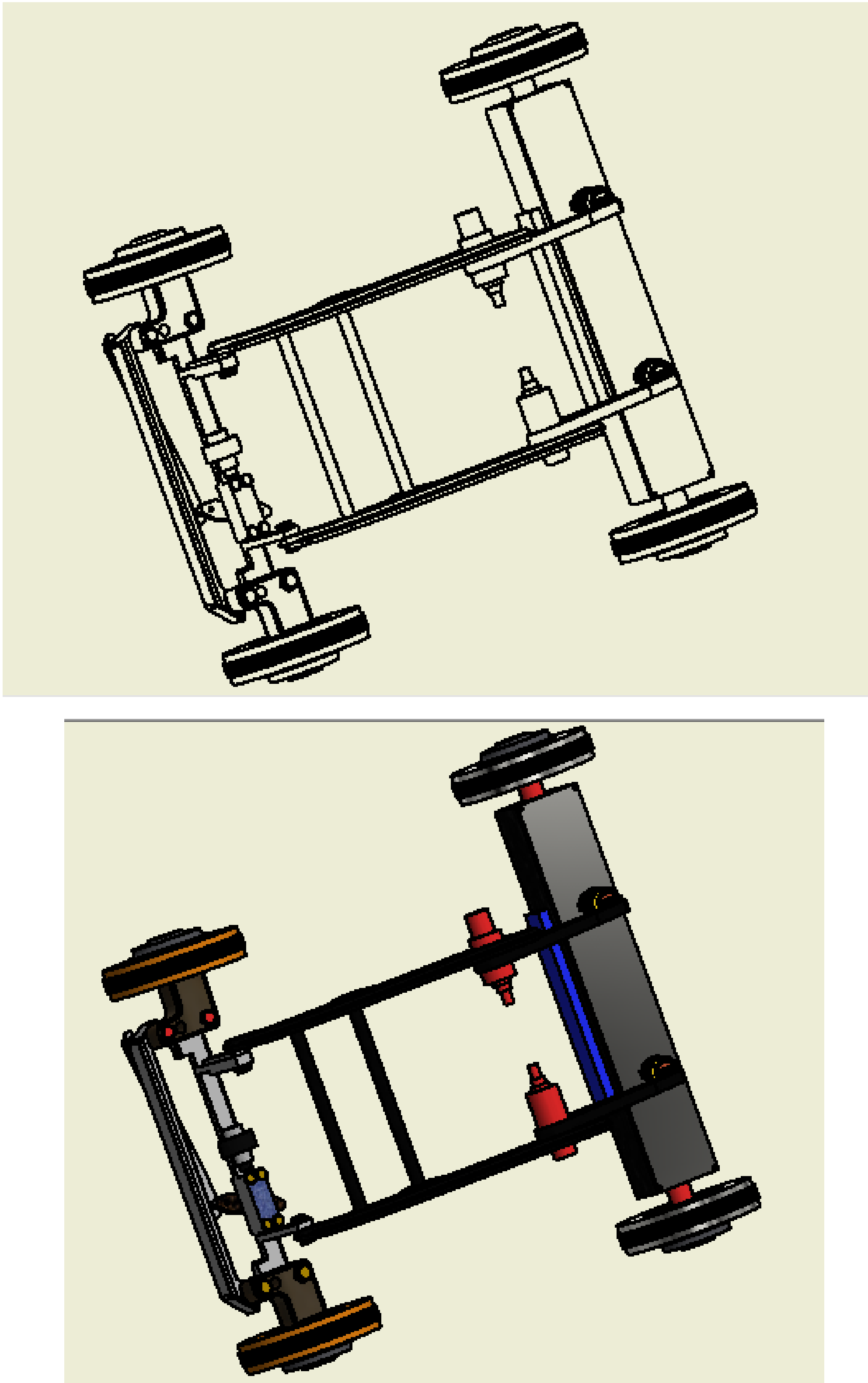

Fig.5. 2 Climbing robot design on inventor software

Table 5-1 SPECIFICATIONS OF THE ROBOT'S DIMENSIONS

Parameter	Value
Length	35 CM
Width	25CM
Height	15CM
Locomotion	Magnetic wheeled
Control Operations	2.4GHZ Remote Control unit
Drive	4 motors. 4WD
Apprx. Total Weightwithoutbattery	4kg (approx)
Maximum Travel Speed	NA
Battery	Lithium Polymer 1000mah
Controller	Beaglebone X
Operating voltage	12 V
Communication	Wireless

5.1 Transmission system

Using its magnetic wheels and sensor unit, the developed robot's main job is to inspect the inspection surface. A good motor that can deliver the appropriate torque to rotate the magnetic wheels is required in order to get the wheels to spin to the surface. Four DC motors are needed to power the robot's four magnetic wheels, which allow it to move on wheels. One often used configuration is to have four DC motors for per wheel. Here, though, the difficulty was in keeping the robot's weight low. Maintaining four DC motors might lead to increased battery usage and ultimately reduce the robot's efficiency.

To avoid these situations, a gearbox is designed for the transmission of power to the wheels. The front two wheels are powered using one DC geared motor with high torque and the rear two wheels are powered by another DC geared motor with high torque. So instead of using four motors, two motors were kept at the front and rear axle of the robot. The DC motors have to be powerful enough to provide enough driving force to the robot in any condition or position. The required motor torque must be determined before choosing any motor. The intended payload, the robot's gross weight, the size of the magnetic wheels that need to be turned, and safety considerations are only a few of the variables that affect the necessary torque and should be understood. In this study project, output torque, maximum and lowest speed, and weight are the main areas of interest for an appropriate drive system.

There is no doubt that the decision to use two motors instead of four motors minimizes the weight and typicality of the system. The main problem occurs during the calculation of continuous torque when the two front wheels are in the air and not touching the surface so that robot can pass the sharp corners. In this situation, the whole force has to be execrated by the rear wheels. Many solutions have been provided by researchers to overcome the problem of the lift-up of the wheel. Some of them are active wheel lifters and wheel in wheel methods (Tache et al. 2009). The reason for not implementing the active wheel lifter in this design is because of complexity and control.

By considering the two geared DC motors, a gearbox is designed with an axle to transmit power to the wheels.

A gear assembly is attached with a DC geared motor. The speed can be calculated by the rotation of the shaft. The reason for using the Gear DC motor here is to enhance the torque and reduce the speed. By applying appropriate combination of gears in the gear motor, the speed can be lowered to the required speed. The approach of lowering the speed of the motor to enhance the torque is known as gear reduction.

The DC motor works on the level of voltage, the greater the voltage level, higher will be the RPM (rotation per minute) (Tache et al. 2009).

$$RPM = K_1 * V \tag{5.1}$$

In equation 5.1, K_1 is Induced voltage constant, V is representing voltage applied in motor.

$$RPM\,(Rounds\ per\ \min ute) = \frac{1}{Torque} \tag{5.2}$$

In equation 5.2, represent the calculation of round per minute of DC motor.

The main principle of working of DC geared motor is conservation of angular momentum. Gears with minor radius will cover more RPM than gear with a major radius. The gear with major radius circulates more torque to minor size gears. The comparison of the angular velocity of gear that transmits energy to output gear is called a gear ratio. Here, the concept of pulse modulation is applied to geared DC motors.

5.1.1. Calculation of DC Geared Motor

1) Speed (n) of motor

$$Speed\ of\ motor = \frac{T_m}{R} \tag{5.3}$$

In equation 5.3, T_m is torque of Dc motor, R is the reduction ratio of gear.

2) Torque(T) of motor

$$Torque of\ motor = \frac{T_m * I * \eta g}{1000} \tag{5.4}$$

In equation 5.4, T_m represents the DC motor output torque, I represent the entire reduction gear ratio; ηg is represent the entire efficiency is huge.

3) Input Power (P_i) of the motor

$$P_i = U * I(W) \tag{5.5}$$

In equation 5.5, U represents the Voltage (V), I represents the current flowing in the motor.

4) Output Power (Po) of the motor

$$P_o = \frac{T_m * n}{97.5} \qquad \textbf{(5.6)}$$

In equation 5.6, T_m represent the torque (kg-cm) of motor; n is representing the number of rpm

On the bases of the above equations, a DC geared motors work on7.2 V were considered. In a condition of not loading the dc geared motor has 3000 rpm. By adding gear reduction this rpm can be reduced and high torque can be achieved. After performing some tests on the motor, the maximum output torque of the motor that can be achieved is 0.02Nm

Suppose a geared dc motor has 12,000 rpm and provides a torque of 0.1kg-cm. By adding a 225:1 gear reduction ration, will increase the torque 0.1* 225 = 22.5 kg-cm and reduces the rpm 12000/225 = 53.5 rpm.

Table 5-2 PARAMETERS OF THE ROBOT'S INPUT AND OUTPUT

Input Paramètres	Output Paramètres
Weight of robot = 4kg	Minimum Angular velocity = 15rpm
Number of drive motors= 2	Torque requirement =1.5 Nm at 90% efficienc
Drive wheel radius = 3 inch	Maximum current = 0.2980 A
Velocity = 0.1 m/s	Battery pack = 0.198 Ah
The maximum incline angle = 90degree	
Supply voltage = 7volts	
Required acceleration = 0.1 m/s2	
Required operating time = 20mins	

5.2 Ackermann Steering System

One of the critical elements of proper chassis alignment is the steering system. For a proper turn, the front two wheels must work together so that they can produce the greatest amount of traction to turn the robot.

The steering system in any robot having wheeled locomotion allows the driver to monitor and to be in charge of the direction of the climbing robot through an arrangement, which connects the steering mechanism with the front wheels. A good steering system must perform functions:

1. Change direction of vehicle
2. Not cause excessive wear to the tire
3. Not transmit excessive shock to the chassis

Generally, for an any robot with two or four wheels, three main steering methods can be used these are:

1. Differential steering method
2. Ackermann steering method
3. Skid steering method

No specialized steering mechanism is needed for the differential steering approach. The arrangement of the robot's two wheels on either side determines how it moves in this system. The robot rotates left or right based on the two wheels' differing speeds. The differential steering method is quite useful in the case of the two-wheeled robot.

In Cai et al., 2017, the author designed a differential speed steering control for four-wheel robot independent driving electric vehicles.Skid steering mechanism discussed in article (Dixon, 2001)(Morin & Samson) suggest that the research examines that skid steering is sparse. According to previous articles reviewed in this regard, not so much has been explained about the control of vehicles in case of slippage phenomenon is necessary because of the driving mechanism. Vehicles with such a wheeled mechanism are known as skid steering systems. A skid steering is tough task as the wheels must slide in order to go around the curved path. The only problem with this method is if the projection of the instantaneous center of rotation of the vehicle along the longitudinal axis becomes more the robot can lose stability and skidding will take place (Kozłowski & Pazderski, 2004).

Ackermann Steering method: It is the most commonly used steering method for steering four-wheeled robots. This method is a geometric grouping of interconnection in the steering of a robotic system built in order to pivot the inner and outer wheels at the significant angle. Unlike Skid steering mechanism, this method is useful in avoiding the wheel side slippage during a curved path passage.

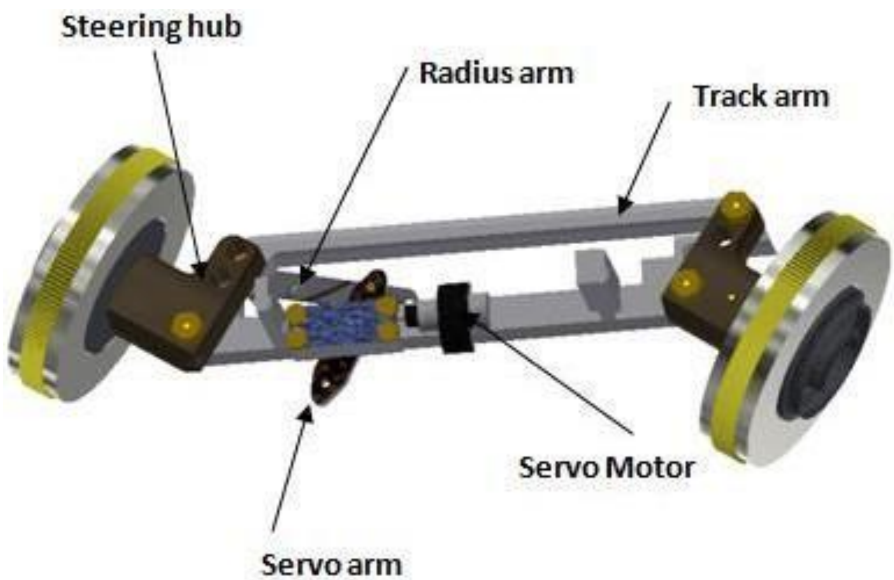

Fig.5. 3 Steering system of the robots. (Top view)

Figure 5.3 represent the steering system of the designed robot where the front axle of the climbing robot is provided with a steering mechanism based on Ackermann steering. The figure 5.4 represent the 2D drawing of the front axle with steering method. The illustration in figure 5.5 represent the 2D and 3D view of axle wheel.

The front axle with the steering method is responsible for turning the robot in the left and right directions. A servo motor is mounted on the front axle chassis. Instead of using any steering handle, the servo motor will be performing the same operation as the steering handle of a car. The Servo motor shaft is connected to the servo arm. The primary task of the servo arm is to transfer the torque from the servo shaft to the radius arm. The servo motor is fixed like that rotates the same in the left and right direction and transmits power to the radius arm. With the help of this arrangement, it is possible to steer the wheel's maximum up to 60 degrees. According to experimental research, servo motors on the steering system can generate a torque of up to 1.96Nm. An array of sensors is placed just below the rear axle chassis, on some height, from the ground for the detection of cracks. Sensor parts used in the robot design are discussed in the next chapters.

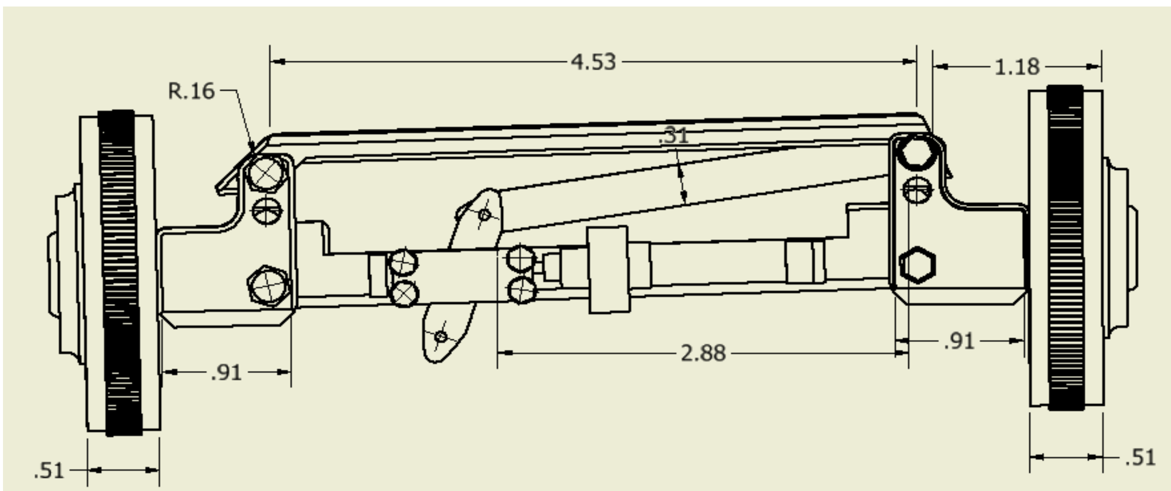

Fig.5. 4 Drawing of the front axle with steering method

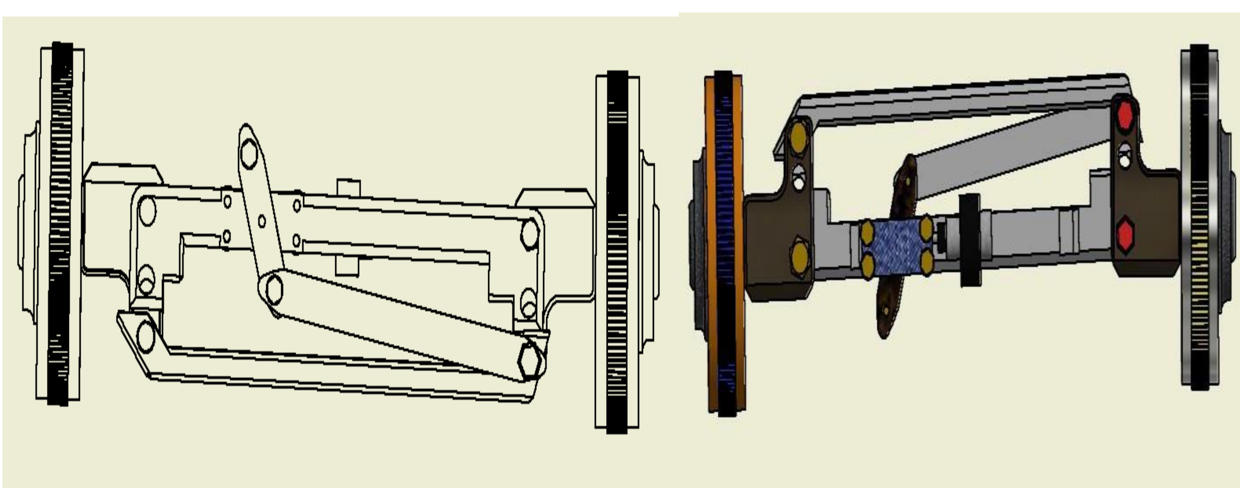

Fig.5. 5 2 D drawing of front axle (down view) (b) 3D view of front axle (top view)

5.3 Obstacles Overcome by Flexible Joint

During the structure design process, it was prioritized to make the structure capable of passing over obstacles and sharp convex corners. It is worth noting that the overhead crane girder bridge has enormous barriers, 90-degree convex corners, and nuts and bolts. The problem of convex corners can be overcome by using a flexible connection between the front and rear axles and maintaining the wheel size and dimension constant. Changing the size of the wheel and making it smaller will result in lower adhesion forces and possibly stability difficulties.

The structure is classified into three main modules.

1. Front axle module
2. Rear axle module
3. Flexible middle joint.

When the robot moves around a 90-degree convex corner, the space between the inspection surface area and the robot chassis should be sufficient for the robot's body to pass through. Figure 5.6 depicts the issue encountered during the passing of the 90-degree convex corner.

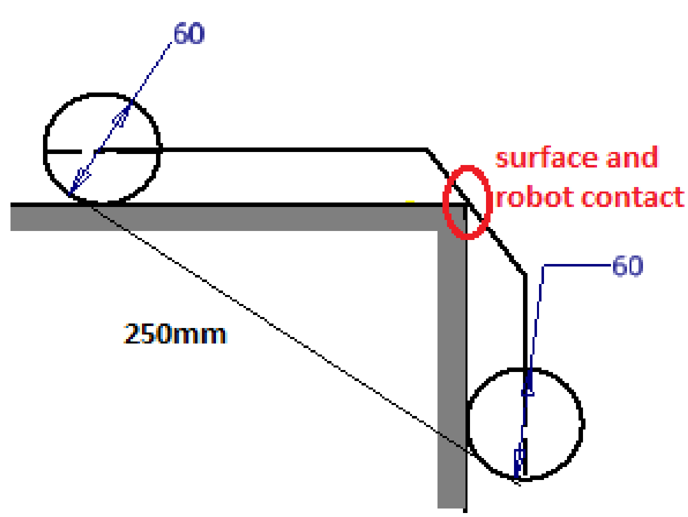

Fig.5. 6 6Model of robot and corner negotiation problem

A convex corner causes the robot to become stuck because the robot's center frame makes direct touch with the corner when it navigates around it. Insufficient pitch flexibility between the front and one wheel is the cause of the second problem. Surface contact is lost by the front wheel as it passes over a large height bolt obstruction, and the back side wheel also loses surface contact because of insufficient pitch flexibility.

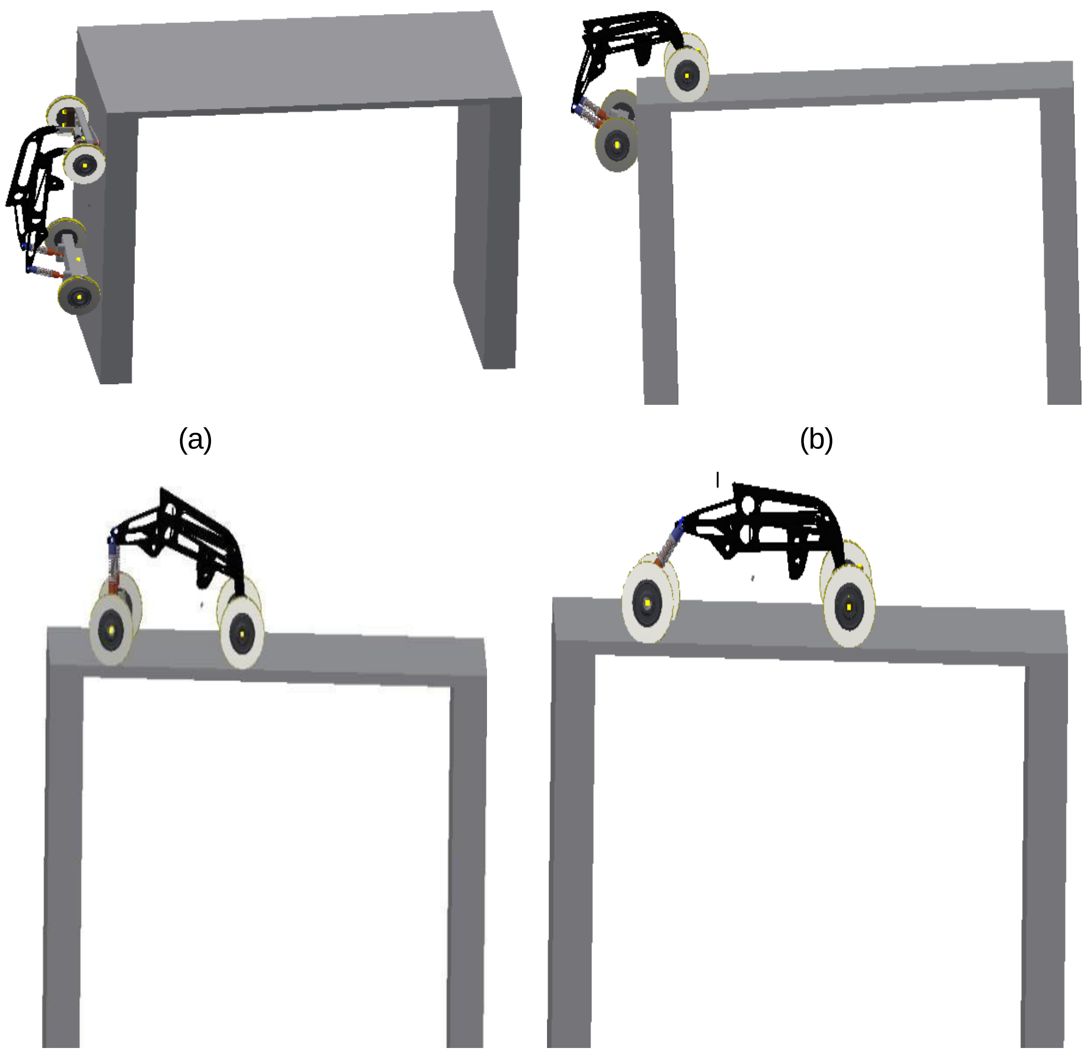

(a) (b)

(c) (d)

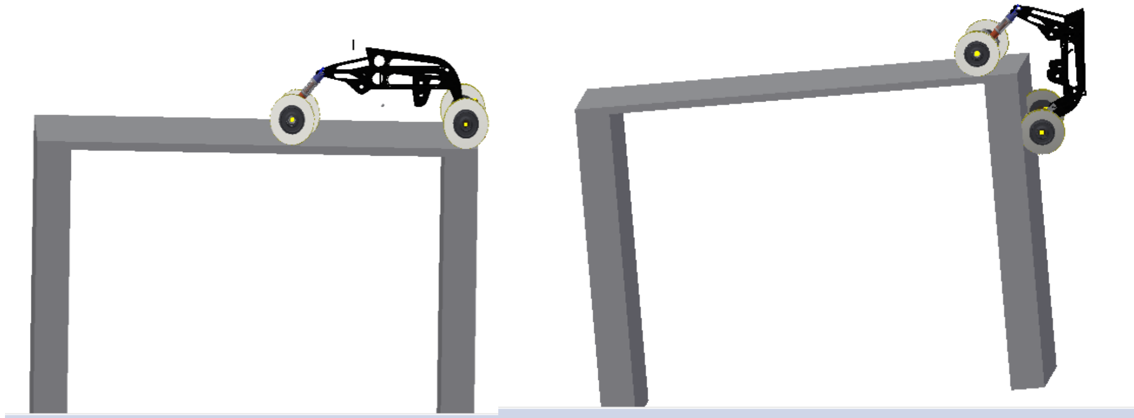

(e) (f)

Fig.5. 7 Various motion of robot on surface. (a) climbing on vertical surface (b) Avoiding corner obstacle while climbing up (c)Motion on horizontal surface (d) Expansion of robotic chassis (e) Preparation to avoid corner obstacle (f) Corner obstacle avoidance

To counteract adverse situations, the robot body is fitted with a movable linkage joint that connects the front wheels the rear wheels. This resolves the issue of contact between the inspection region and the robot chassis and greatly increases the pitch flexibility of robot designs. Various motion of designed robot on varying surfaces have been presented in figure 5.7.

In order to resolve corner negotiation concerns, Zhu et al. (2010) developed a mobile sensing node with a compliant beam as part of a sensing system for monitoring the health of structures. The movable sensor node has flexibility in the transmission situation between two structural parts thanks to its compliant beam. The authors of this study (Lee et al., 2011) developed a climbing robot equipped with a compliant track with transitional skills and a big load capacity. The robot was composed of five compliant R- joints. This designed robot has a compliant joint that is used to provide the degree of freedom to a front axle and a rear axle of the robot so that the robot can overcome the corner negotiation problem and pitch flexibility. This compliant joint has a servo motor for the adjustment of rear axle wheels. As the robot has a magnetic wheel climbing mechanism, it is necessary all the time to maintain proper contact between wheels and ferromagnetic surfaces. The easiest way to fix cornering problems is to move the rear axle wheels closer to the leading wheels while keeping the front axle immobile.

The kinematic model of the compliant joint and rear wheel is shown in figure 5.8.

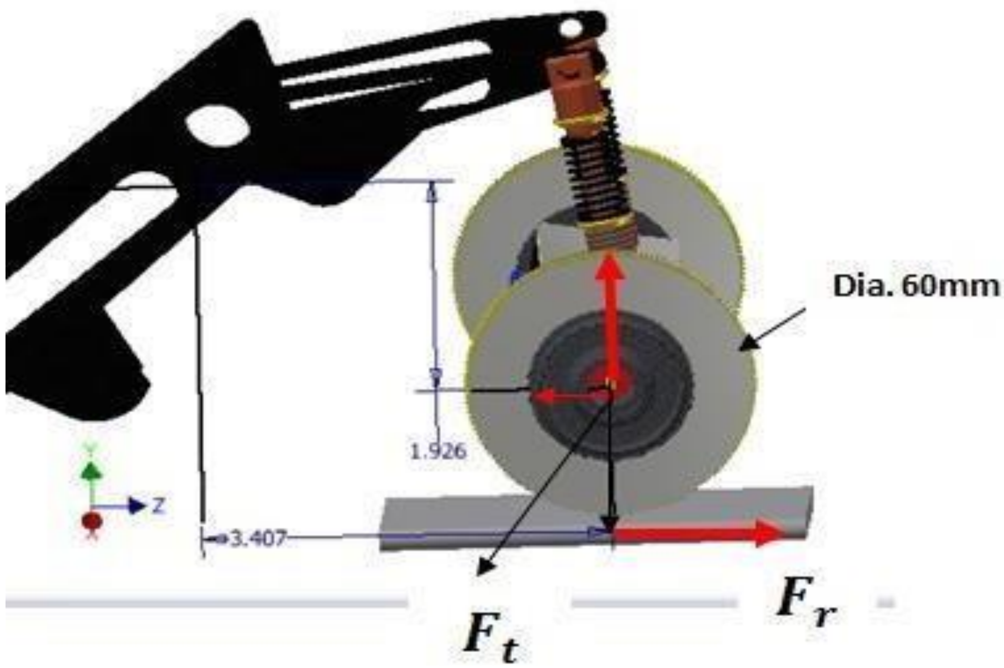

Fig.5. 8 Model of Kinematics of rear-wheel and compliant joint.

The folding mechanism of the climbing robot is seen in Figure 5.9. As illustrated in Figure 5.9, the servo motor must generate a substantial amount of torque to bend the robot's structure as it pushes the rear axle wheel towards the front axle wheel. When considering the adhesion and frictional forces of magnetic wheels as well as the frictional forces of gearboxes, it is difficult for the servo motor to resist these forces. The force F_(t) of almost 35.5 N was calculated based on the experiments done in Chapter 3 on magnetic wheels for adhesion and frictional forces on different thicknesses of steel plate.

By doing calculations based on the kinematic model of rear-wheel and compliant joint servo motor, it has to generate at least 145 Nm torque to rotate the body of the robot. To generate this much torque, there is need for a very heavy servo motor that is fairly impossible to mount in this designed structure.

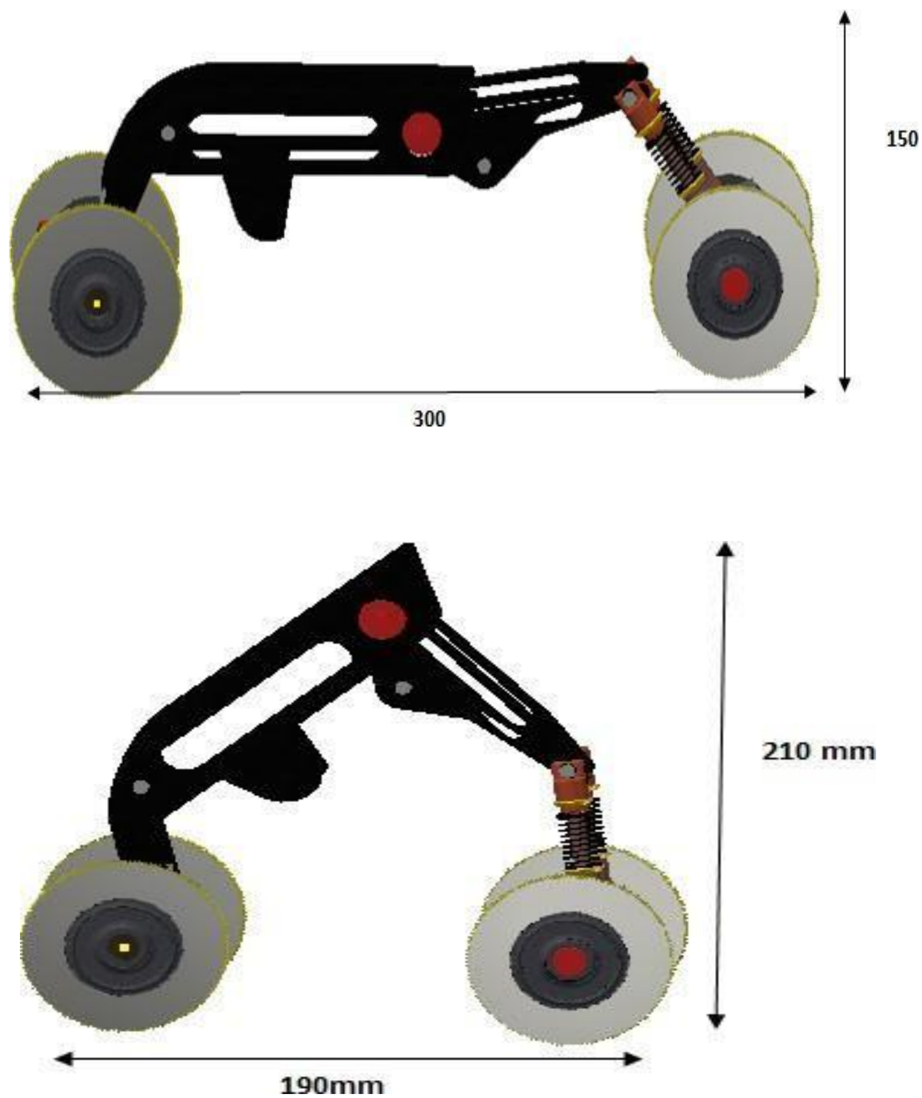

Fig.5. 9 Folding Mechanism of climbing robot

5.4 Kinematics Modelling and Calculations

Because the robot must climb diverse surfaces and navigate numerous obstacles, the kinematics of robot movement must be calibrated. Adhesion forces and frictional forces were determined using static analysis. These computed forces aided in the prediction and resolution of robot movements during obstacles. The kinematic equations may be used to investigate the necessary adhesion forces, frictional forces, motor torque, and stability using built-in robots. To accomplish a climbing action, the robot must travel through a variety of conditions, such as (Hussain et al., 2012)

1. Movement of robots on horizontal to vertical plane
2. Movement of robots on vertical plane
3. Movement from vertical to an inverted horizontal plane
4. Movement of inverted horizontal plane
5. Movement from an inverted horizontal to a vertical plane

In this section, all the above situation of the robot is represented and some mathematical operations are performed so that the robot can satisfy these equations and achieve the desired path by crossing the obstacles.

Case 1. Calculation of frictional forces and adhesion forces on horizontal to vertical plane:

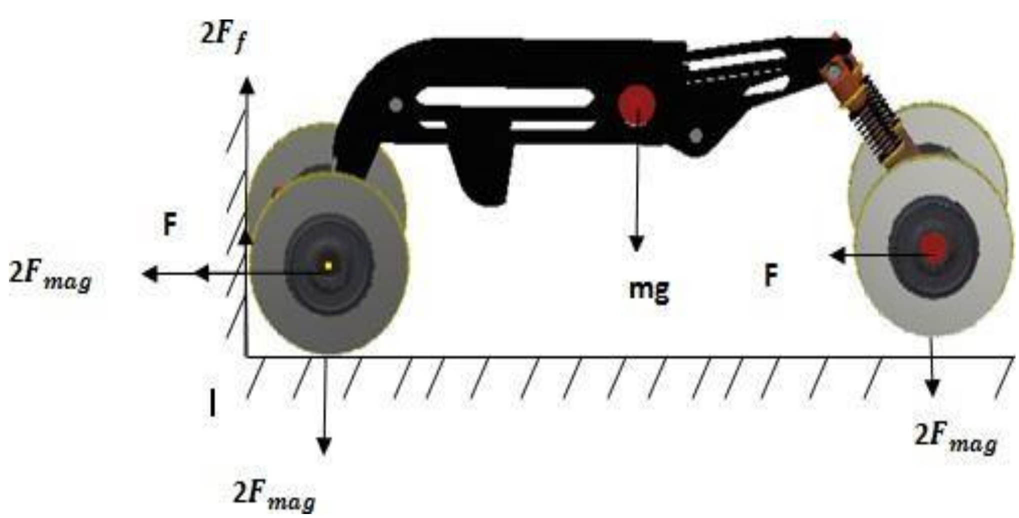

Fig.5. 10 Mathematical forces analysis on robot wheels

F= Driving force of front and rear axle

F_f= force of friction between the wheel and surface

2□□□□= Adhesion force of two wheels

mg= gravity

μ = coefficient of friction

For the calculation purpose, we suppose that the effect of gravity is only present at the axles of the robot. Climbing on a vertical surface gravitational forces are also countable (mg). In the above mathematical model, F represents the force exerted on a particular axle by the drive motor to move the wheels in the forward direction. If you climb on a vertical surface frictional force F_f should be sufficient to conquer the adhesion forces F_{mag} between the wheel and the inspection area. To satisfy this condition

$$\mu(F + F + 2F_{mag}) \geq \frac{mg}{2} + 2F_{mg} \qquad (5.1)$$

For the proper maneuver of the robot on the surface, the driving motors have to build up enough torque to rotate the wheel by overcoming the adhesion and frictional forces. The equation below is as follows

$$F \leq \mu(\frac{mg}{2} + 2F_{mag}) \qquad (5.2)$$

For the calculation of robots to move on vertical plane from the above two equations 1 and 2 must satisfy

$$\mu(\frac{mg}{2} + 2F_{mag}) \geq F \geq \frac{1-\mu}{\mu} F_{mag}) + \frac{mg}{4\mu} \qquad (5.3)$$

Case 2. Vertical surface climb

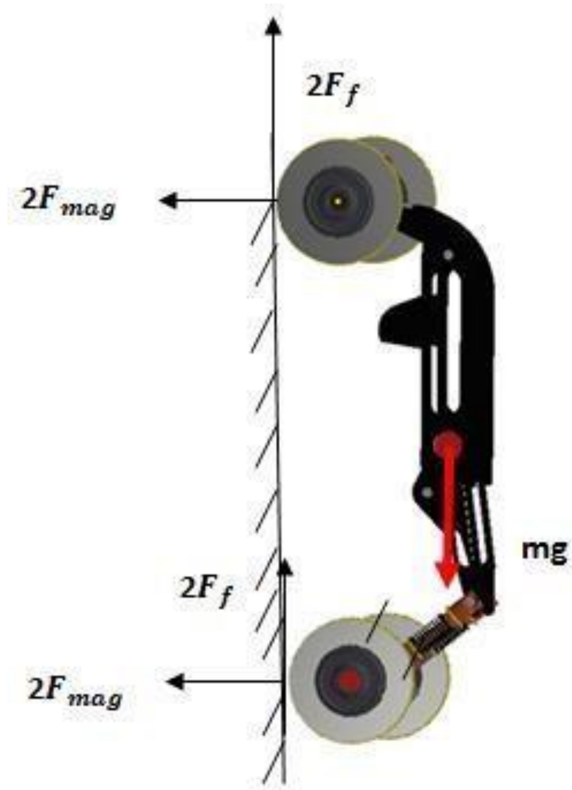

Fig.5. 11 Mathematical force calculation for vertical climbing

In case the robot maneuver on a horizontal plane, it has to overcome only frictional forces and adhesion forces. But in the case of vertical climbing gravity, the mass of robots comes into play. During vertical climbing, robots must have more frictional and adhesion forces so that they can overcome the gravitational forces and keep the robots adhered to on the surface. In figure 5.11, it is shown the direction force that applied on wheel.

$4\mu F_{mag} \geq mg$ (5.4)

Avoid the wheels getting slipped from the inspection surface.

$2\mu F_{mag} \geq F$ (5.5)

To climb on vertical surface frictional forces and adhesion forces must satisfy this equation:

$F \leq 2\mu F_{mag}\ F_{mag} \geq \frac{mg}{4\mu}$ (5.6)

Case 3: Movement of the robot from vertical plane to sharp horizontal corner:

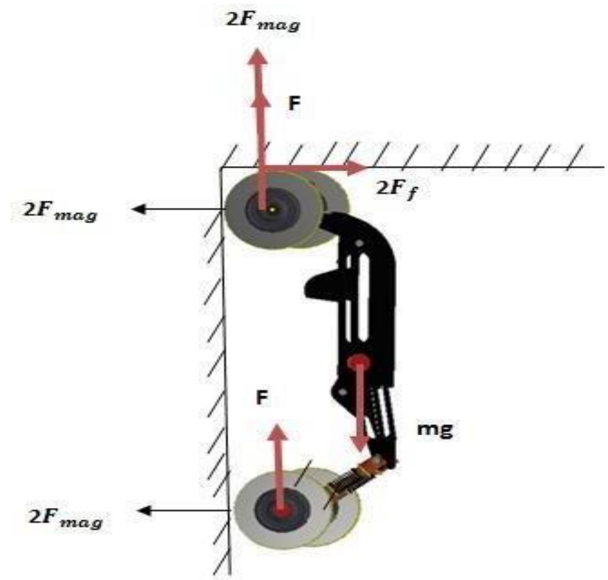

Fig.5. 12 Mathematical analysis of forces from vertical to horizontal sharp corners

The force action at steep, vertical-to-horizontal corners is seen in Figure 5.12. Maintain the same settings as in the past observations, taking into account the gravity on just two axles. The robot's front axle must move the front vertical wall to a sharp corner and then go to an inverted horizontal plane in order to get out of this scenario. The robot faces a challenging circumstance where its front wheels must counteract the adhesion force from the vertical plane, which might lead to instability and a potential collapse.

Figure 5.12 depicts the gravitational and adhesive forces exerted by the magnetic wheels in opposite directions. To accomplish the situation, frictional forces should satisfy this equation:

$\mu(F+F+2F_{mag}-mg) \geq 2F_{mag}$ (5.7)

Avoid magnetic wheels falling from the surface

$F \leq 2\mu F_{mag}$ (5.8)

For the smooth motion of the robot on the inverted plane, frictional forces and adhesion forces have to be satisfied:

$2\mu F_{mag} \geq F \geq \frac{1-\mu}{\mu} F_{mag} + \frac{mg}{2}$ (5.9

Case 4: Movement on an inverted horizontal plane

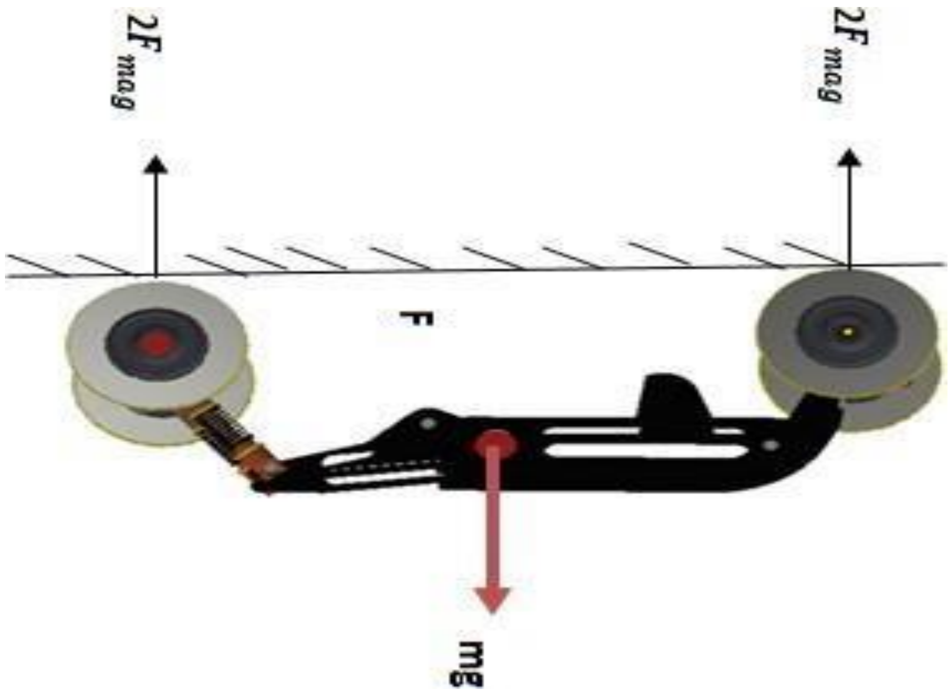

Fig.5. 13 Mathematical analysis of forces on inverted horizontal plane

In this case, the robot has to adhere to an inverted horizontal plane and has to avoid slippage of wheels from the surface by maintaining the required adhesion forces and frictional forces so that it can overcome the gravitational forces. To achieve that robot has to satisfy the equations mentioned below

$4F_{mag} \geq mg$ (5.10)

$\mu(F_{mag} - \frac{mg}{2}) \geq F$ (5.11)

For the movement on the inverted horizontal plane F_{mag} and μ has to satisfy

$F \leq \mu(2F_{mag} - \frac{mg}{2})$ $F_{mag} \geq \frac{mg}{4}$ (5.12)

All the forces graphical representation is shown in figure 5.13.

Case 5: Movement of the robot from inverted horizontal to a vertical plane

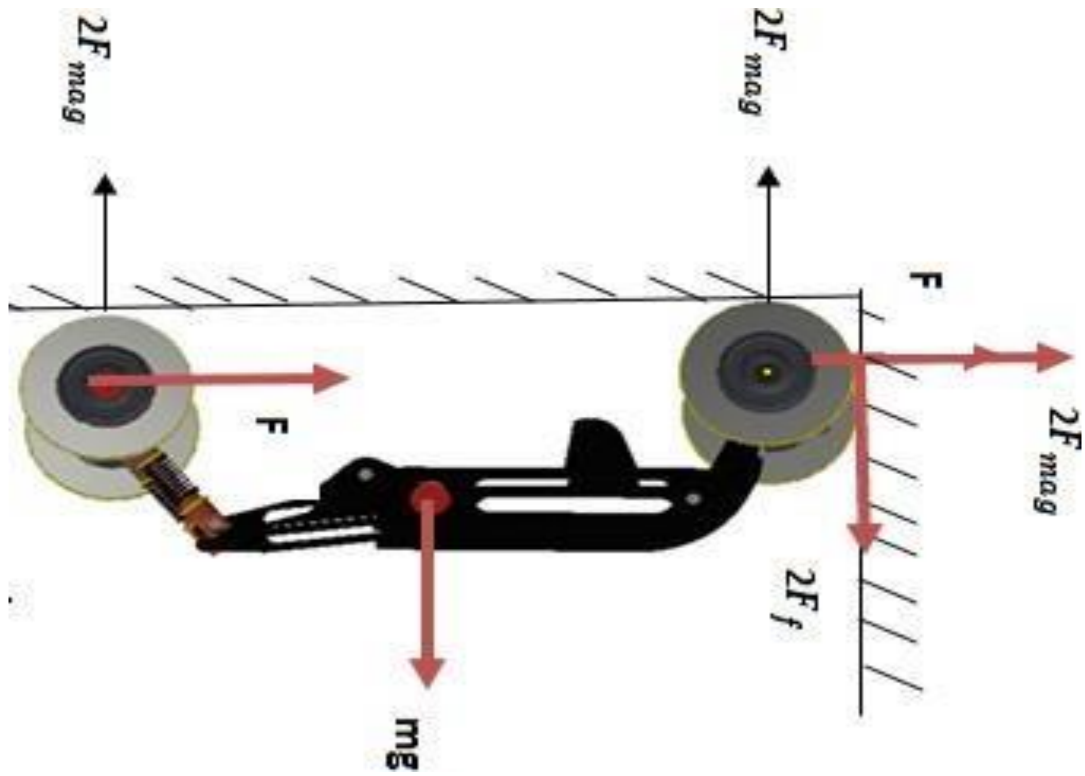

Fig.5. 14 Mathematical analysis of forces on an inverted horizontal plane to the vertical plane

$\mu(F_{mag} + 2F) \geq 2F_{mag} - \frac{mg}{2}$ (5.13)

Avoid slippage on magnetic wheels

$\mu(2F_{mag} - \frac{mg}{2}) \geq F$ (5.14)

$F_{mag} \geq \frac{mg}{4}$ (5.15)

From the above equations 5.13, 5.14 and 5.15, the frictional forces and adhesion forces should satisfy the

$\mu(2F_{mag} - \frac{mg}{2}) \geq F \geq \frac{1-\mu}{\mu} F_{mag} - \frac{mg}{4\mu}$ (5.16)

$F_{mag} \geq \frac{mg}{4}$

Case 6: Movement of the robot from vertical plane to horizontal plane:

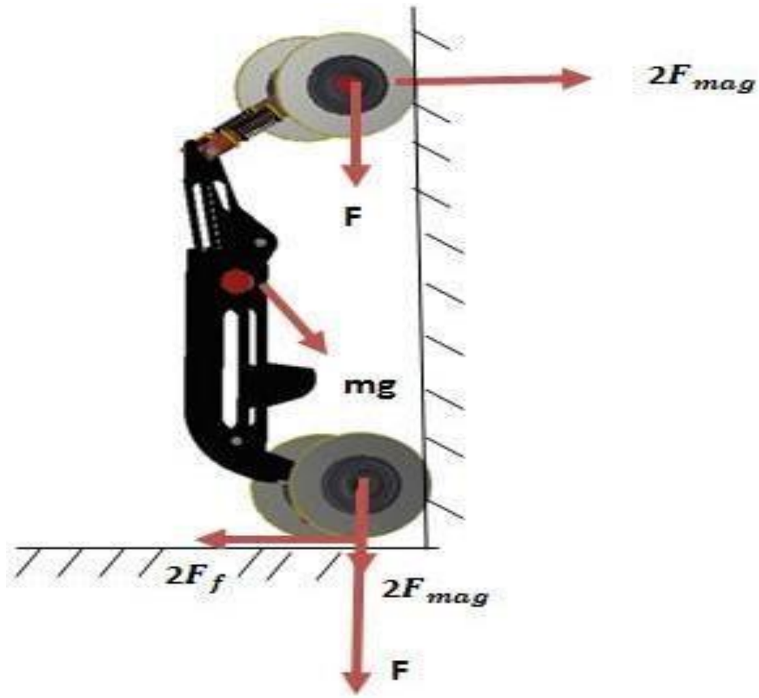

Fig.5. 15 Mathematical analysis of forces on a vertical plane to the horizontal plane

In case the robot is moving from a vertical plane to a horizontal plane, it is necessary to maintain stability (Lee et al. 2011).

$\mu\,(mg + 2F + 2F_{mag}) \geq 2F_{mag}$ (5.17)

$F \leq 2\,\mu\,F_{mag}$ (5.18)

From the above equations:

$2\,\mu\,F_{mag} \geq F \geq \frac{1-\mu}{\mu} F_{mag} - \frac{mg}{2}$ (5.19)

By solving the kinematics equations for several scenarios of robot motion, we ensured that the developed robot satisfied all of the equations. After ensuring that it passes through all of the movements, this design was implemented, and a robotics tool was developed for climbing operations on overhead crane girders. As a result, an automated tool for inspection purposes was created.

The design of a robotic tool for examining overhead crane girders is one of the main components of the study endeavour, and it is covered in this chapter. Through the use of flexible joints and a flexible chassis, a revolutionary design has been devised that surpasses the limitations of corner avoidance and can pass through a variety of obstacles.

With its four magnetic wheels, the self-governing robotic tool offers magnetic stickiness for scaling crane girders. The robotic tool's adaptable design offers flexibility and agility to operate on a range of inspection surfaces. The robot that has been proposed stands out for its exceptional precision in identifying both surface and subsurface defects. This robot design is novel and simple to operate due to its small size and light weight.

CHAPTER 6

ANALYSIS OF RESULTS OF DESIGNED NON-DESTRUCTIVE TESTING DEVICE USING GMR SENSOR

According to the prior chapters, corrosion, which leads to fatigue fracture, is one of the primary root causes of overhead crane bridge failure. Infrared thermography, magnetic flux leakage (MFL), acoustic emission, ultrasonic testing, and eddy current testing are the most commonly utilized methods for automating inspection activities. Currently, inspectors undertake visual inspections of overhead crane bridges, which is the most prevalent type of inspection. In the case of a fault underneath the painted surface area of an overhead crane bridge, the visual inspection technique is ineffective and insensitive. This is because overhead crane bridges have sophisticated geometry and design.

For large-scale companies, having hundreds of overhead cranes and visual inspection procedures is also not cost-effective. The following paragraph provides a summary of the few NDT techniques currently in use for ferromagnetic materials, along with their benefits and drawbacks. Following that, the design of a unique non-destructive testing solution based on a GMR sensor for sensing and identifying fractures and corrosion in ferromagnetic materials is presented.

6.1 Method of Eddy Current for Ferromagnetic materials

To evaluate the structural integrity of conductive surface materials, eddy current methods are frequently used in non-destructive testing (NDT) (Kral et al., 2013). Eddy current is the current produced when a driving coil is powered to produce magnetic flux (MF), in accordance with Faraday's rule (Kral et al., 2013). The driving coil's eddy current produces electromagnetic fields (EMF).

The MF connection between the primary and secondary coils and eddy current testing are explained in brief here, along with some simple techniques.

1) Changing the current generated through the coil is by the principal MF
2) Alternating primary MF generates the EC in the conductive material
3) Eddy currently creates a secondary MF in the opposite direction
4) Defects in conductive material disturb the Eddy current and reduce the secondary MF that overall varies the impedance of the coil.

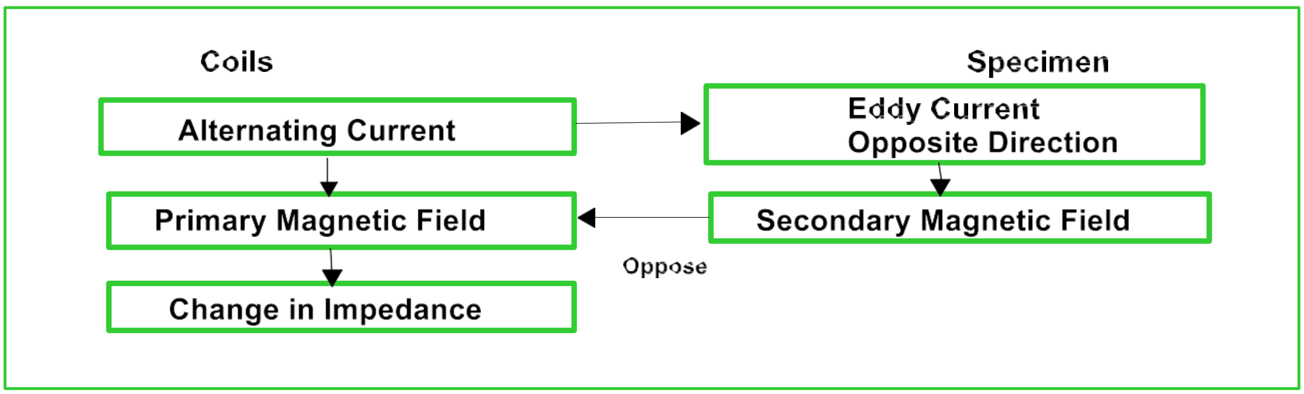

Fig.6. 1 The Main Principle for eddy current testing operation

One of the primary benefits of ECT for ferromagnetic materials is its low cost and environmental friendliness, as well as its high accuracy rate and short inspection time. The fundamental disadvantage of the ECT approach compared to current research is that it is only sensitive to surface imperfections and is only applicable to conductive surfaces

6.2. Magnetic Flux Leakage (MFL) Method

The fundamental idea of magnetic flux leakage (MFL) is that the distribution of magnetic field (MF) changes when a ferromagnetic material is positioned close to an applied magnetic field. The magnetic field uniformly disperses ahead of any flaw, avoiding the ferromagnetic material. Magnetic fields flowing through this region will be warped if the material has any faults or imperfections.

Resistance will therefore rise and reflect the magnetic field distortion in the vicinity of this fault. A magnetic leakage field will form near the damaged area, and some magnetic flux lines may bend or escape from the surface area.

By using a magnetically sensitive sensor, an electric signal can be retained by reading the magnetic fields. By analysing the obtained electric signals, the real condition of the flaw can be identified. A corrosion-related fault can manifest on both the external and interior surfaces of the material and can be detected using the Magnetic Flux Leakage (MFL) technique. But it's rather difficult to discriminate against internal and external defects using the MFL method (Wang & Kawamura, 2016).

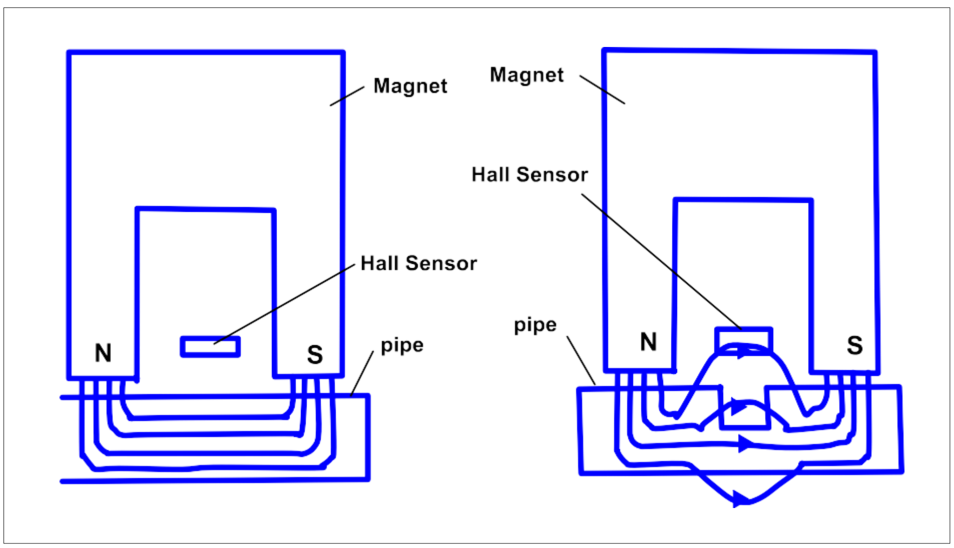

Fig.6. 2 Methods for measuring magnetic flux leakage: (a) flawless; (b) flawed. ((modified after Wang & Kawamura, 2016)

Surface cracking is a key contributor to the collapse of overhead crane structures. Most common non-destructive approaches for detecting and mapping material loss in ferromagnetic materials employ magnetic flux leakage examination. Its main advantage over other NDT methods is its ability to evaluate large surface areas quickly. Cracks are commonly generated by corrosion and are used to describe areas of material loss. To retain and prolong the life of overhead crane bridges, it is not enough to identify cracks; it is also important to determine the profile of the fault. The MFL approach is solely reliable for obtaining flaw information. It does not disclose the defect profile. The MFL is also known to completely miss some problems.An inherent ambiguity has been identified while estimating the profile of a defect by the MFL method (Person et al., 2012)(Saha et al., 2010).

6.3 Limitation of Eddy current and MFL methods for Overhead crane bridge inspection

In inspecting and monitoring, materials composed of ferromagnetic type, a few methods such as eddy current testing, and magnetic flux leakage (MFL) are prioritized. Numerous automated techniques have been created and put into use in the past for inspecting different steel bridges (Faruq Howlader & Sattar, 2015; Sahari et al., 2012). When it comes to ferromagnetic materials, the MFL approach is solely useful for fault detection. It cannot deliver effective results in cases of metal loss or corrosion examination. Automated NDT technologies are not usable in the examination of overhead crane bridges due to certain specifications and simplicity of installation. The following factors have access to some of the automated NDT parameters:

- Size
- Operational Accuracy Level
- Operational Mode
- Mode of Power Supply
- Data Collection & Sharing
- Suitability of Automation

The area should be saturated in order for the MFL technique to detect microscopic cracks and little metal loss. Magnetic leakage in the MFL technique is proportional to ferromagnetic material thickness. Because overhead crane bridges have a large thickness, this approach cannot detect metal loss.

6.3.1 Factors Affecting the Eddy Current Testing Inspection

For the inspection and monitoring of overhead crane bridges, many other factors influence eddy current testing. Instead of cracks and surface defects, the eddy current signal from the probe has a bunch of feedback from faults, surface geometry and lift off (Kral, et al.,2013).

The key drivers affecting the coil response are:

6.3.1.1 Material Magnetic Permeability:

A metal with a high permeability allows more eddy currents to enter during eddy current testing. Another example is a metal with poor permeability that permits modest eddy currents to pass through. Many additional parameters, in addition to the geometry of the test sample and the form of the faults, are affected by this component. The excitation frequency in ECT is determined by the size of the overhead crane bridge.

6.3.1.2 Conductivity of Material:

The change in the conductivity of material has a direct influence on magnetic field. The magnetic sensor probe's result is impacted by this shift in the field of magnetism. The conductivity of the material varies according to a variety of circumstances, including aging, deposition development, residual stresses, and heating. The comparison of a few materials' conductivities is displayed in table 6.1.

Table 6-1 LIST OF A FEW CONDUCTIVE MATERIALS' CONDUCTIVITY AND RESISTIVITY (KHAN ET AL., 2020)

Material	Conductivity (% IACS)	Resistivity
SS (Stainless steel)316	2.331	74.00
SS(Stainless steel) 304	2.391	72.00
Aluminum Bronze	14.00	12.32
Brass	28.00	6.20
Copper	100.00	1.72

6.3.1.3. Lift-Off

In the case of inspection of overhead crane bridges by ECT, the most common issue that comes into play is lift-off. Lift-off is the distance that lies across the specimen surface under examination and the eddy current probe.

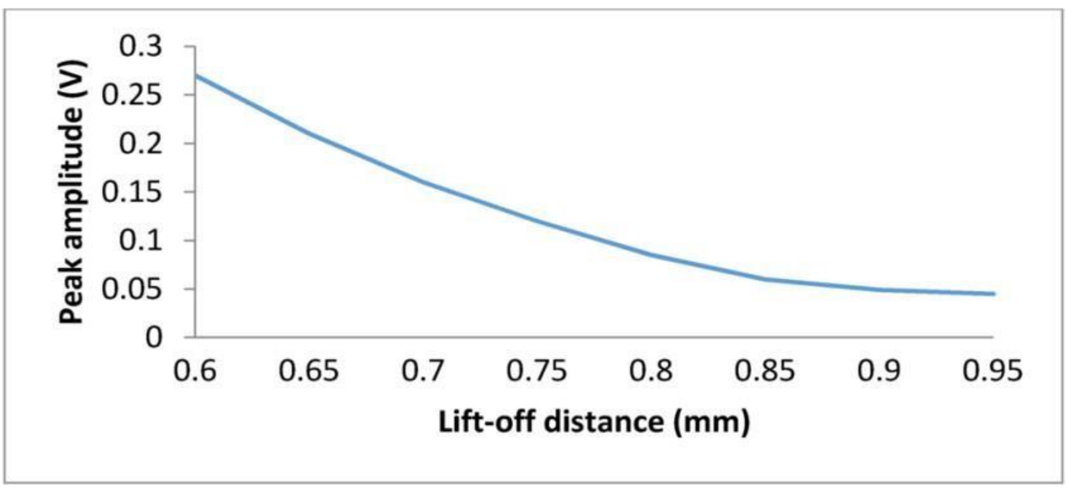

Fig.6. 3 Relation of lift-off distance and peak amplitude

Overhead crane bridge structure consists of many joints and bolts. During the movement of probe from eddy current on the bridge's surface at some point lifts off comes into play. In an experimental study by Kral et.al. (2013), Lift-off has been shown to depend on the amplitude of the output signal from the GMR sensor. An experimental link between peak amplitude and lift off distance is shown in Figure 6.3.

6.3.1.4 Effect of depth on ECT (Eddy's current testing):

In ECT, a single-current excitation coil may detect faults up to a specific depth. To detect material faults in diverse materials, eddy current testing employs sine waves as current activation coils with frequency ranging from 100 Hz to a few MHz. In eddy current method of testing for the detection of subsurface issues on overhead crane bridges, a lower frequency will be given. A highly stimulating coil frequency is also used for the identification of surface flaws. The relationship between stimulating coil frequency and penetration depth on various materials is shown in Table 6.2.

Table 6-2 RELATION BETWEEN THE EXCITING COIL FREQUENCY AND DEPTH OF PENETRATION (LIU ET AL., 2011)

Metal	**% IACS**	**Resistivity**	**Permeability**	**Depth of Penetration**					
				1KHz	**4 KHz**	**16 KHz**	**64 KHz**	**256 KHz**	**1MHz**
Copper	10	1.7	1	0.08	0.04	0.02	0.01	0.00	0.002
6061 T-6	42	4.1	1	0.12	0.06	0.03	0.01	0.00	0.00
7075 t-6	32	5.3	1	0.14	0.07	0.03	0.01	0.00	0.004
Magnesiu	37	4.6	1	0.13	0.06	0.03	0.01	0.00	0.004
Lead	7.8	22	1	0.29	0.14	0.07	0.37	0.01	0.009
Uranium	6.0	29	1	0.33	0.16	0.08	0.04	0.02	0.010
Zirconiun	3.4	70	1.02	0.51	0.25	0.12	0.06	0.03	0.016
Steel	2.9	60	750	0.01	0.009	0.004	0.002	0.002	0.000
Cast Stee	10.	16	175	0.01	0.008	0.004	0.002	0.001	0.000

The above table also illustrates that with the increase in depth of metallic materials eddy current density decreases. Eddy's current depth of penetration also relies on the test material's electrical conductivity and permeability.

6.4 Giant magneto-resistance (GMR) Sensor

This subsection present alternative to the preceding crane bridges inspections methods with a view to demonstrate the leverage the giant magneto-resistance (GMR) sensor inspection's method.

6.4.1 Working principles of GMR Effect

The phenomenon of giant magneto-resistance (GMR) develops in ultra-thin film formations made up of overlapping ferromagnetic and non-ferromagnetic layers. In recent years, several scientists have researched the magnetic field. In 1988, giant magneto-resistance (GMR) was discovered and gave researchers a fresh viewpoint on polarization carriers in ferromagnetic materials, as well as a novel way for using it for non-destructive testing [59]. The GMR sensor has a wide bandwidth and sensitivity that is irrespective of the magnetic field. As a result of these characteristics, it has attracted the attention of numerous researchers and is commonly used in a variety of applications.

Other notable aspects are the GMR sensor's low power sources and tiny size. GMR is also capable of detecting the magnetic field vector along the direction of the detecting direction axis. When the resistance of GMR and AMR (anisotropic magneto resistors) is compared, a considerable difference of 10 to 20% may be noticed in GMR materials. Compared to anisotropic magneto resistors (AMR), GMR sensors offer larger output signals and greater sensitivity. A GMR film is composed of more than two magnetic, non-magnetic layers divide the layers with a thickness of a few nanometres.

Only in the case of adequate thickness can polarized conduction electrons from an anti-ferromagnetic coupling between the adjacent ferromagnetic layers be provided by an energetic layer, allowing the magnetizations of nearby layers to align in an anti-parallelization (Chen et al., 2005). Spin-dependent scattering can help explain the physical mechanism of the GMR phenomenon. The GMR effect is caused by variations in the conduction properties of spin-up and spin-down electrons. The primary cause of metal variation is a significant difference in the density of up and down electrons.

In GMR, two magnetic layers are separated by a sufficiently thick non-ferromagnetic layer that allows electrons to travel across the layers. The flow of electrons between the layers causes a change in the magnetic layer's density state. The scattering effect is determined by the magnetization direction. For example, if the magnetization directions of two magnetic layers are parallel, their densities will be identical, and there will be no scattering effect. When the magnetization directions of the two magnetic layers are reversed, electrons that are spinning up become spin down and vice versa due to the scattering effect. Variations in resistance arise as a result of the presence of this spin-dependent scattering phenomenon.

When the magnetization of layers is parallel in the existence of an external magnetic field, then the resistance is dejected. In another case of anti-parallel magnetization layers, resistance remains at peak level. (Durai et al., 2022)

Almost all GMR sensors are composed of mainly two structures

1. Anti-ferromagnetic multi-layer unpinned sandwich
2. Anti-ferromagnetic pinned spin valves

6.4.1.1. Spin Valve Structure:

This structure is made up of two ferromagnetic layers consisting of nickel, iron, and cobalt alloys, separated by a non-ferromagnetic layer made of copper. In Fig. 6.4, the layers are linked in such a way that one ferromagnetic layer is positioned adjacent to an anti-ferromagnetic layer in a predefined direction. Figure 6.5 (a)(b) shows a spin-up electron with a yellow point and a spin-down electron with a blue point. The bent arrows in red and yellow depict electron mobility caused by scattering. The magnetization directions of both ferromagnetic layers are the same in the presence of a magnetic field provided by outside.

Since the ferromagnetic layer's magnetization is directed in the same direction as both magnetic layers, electrons spinning in it may pass through them with ease. So, for electrons, it allows an easy passage through the magnetic layer, which overall results in low resistance. If the magnetization goes in the opposite direction, lower-spin electrons face difficulty passing through the ferromagnetic layers, resulting in high resistance.

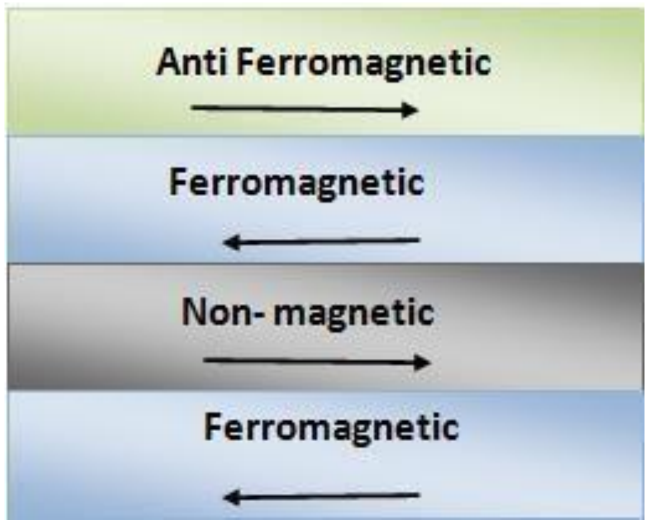

Fig.6. 4. Spin – Valve structure of GMR sensor

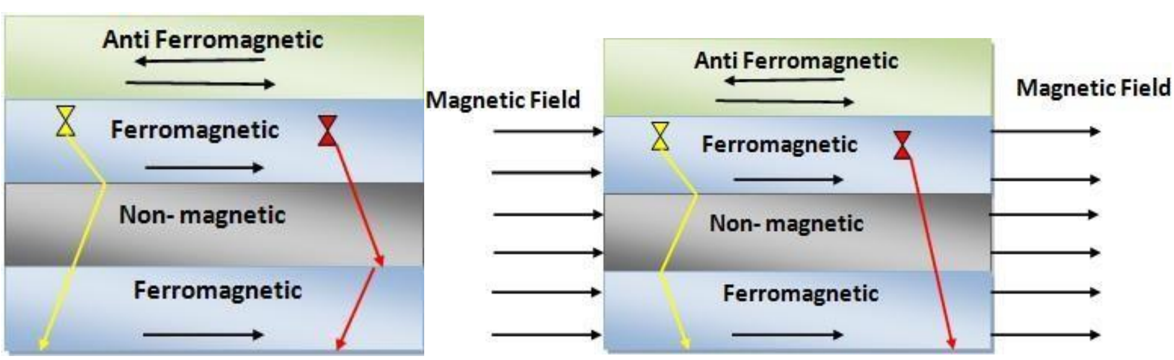

Fig.6. 5 Spin-Valve arrangement under (a)applied magnetic field (b) Without the magnetic field.

Magnetic flux leakage testing has been used for a long time to analyse and non-destructively test the structural qualities of ferromagnetic materials (Aguila-Munoz et al., 2016). This type of inspection is effective. Kataoka et al. (2002) used MFL testing to develop the first GMR sensor for use in NDT in 2001. The authors exhibited an array of 20 sensor devices in this experiment to identify mm-sized boreholes. The GMR sensor is mostly used in pipeline industries (Durai et al., 2002). Instead of the Hall element, the array of GMR sensors served as the receiver in this situation.

Hall sensors have substantially lower sensitivity and need a large electrical gain, which limits the sensor system's maximum bandwidth. The Hall sensor has no saturation effect in a strong magnetic field. Common electromagnets have been used as a source of magnetic field excitation because fields may be varied by altering the value of currents. Electromagnets were replaced with permanent magnets in an experiment conducted by Chen et al. (2005). Because the electromagnetic field requires external current to provide very high magnetic fields for examination, Permanent magnets shorten the inspection procedure. Many further examples show how to identify microscopic cracks in steel metal plates (Pelkner et al., 2022).

6.5 Literature Survey of GMR Sensors in many applications

GMR sensor has showed significant improvement in defect inspection efficiency during the previous few years. As a magnetic receiver, the GMR sensor directly monitors changes in the magnetic field and improves sensitivity to detect surface and subsurface flaws. The use of GMR sensors in non-destructive testing is gaining popularity because to its excellent sensitivity and accuracy. Du and colleagues (2010) developed a robotic pipeline inspection system based on a GMR sensor array. The creation of a GMR sensor array for utility pipe inspection is described in this work.

Four very sensitive GMR sensors (0.9-1.3 mV/V sensitivity) with built-in Wheatstone bridge and field connections are used in the system. To reduce interference with the sensors, the enclosure is composed of polycarbonate. This ring-shaped enclosure is surrounded by four GMR sensors and two permanent magnets. The PIC data collection system captures and digitizes analogue sensor data. The FET approach associates each flaw with a distinct signature with varying frequency components and amplitudes. Each distinct pattern may be utilized to describe a distinct fault.

Yang et al. (2012) conducted research to determine the quality of aeronautical constructions. The major topic of focus in this work has deviated under the riveted categories. An intense rotating magnetic field was employed to demonstrate consistent sensitivity of the GMR sensor. It demonstrates how a distinct flaw indicates different messages using mathematical modeling.

Postolache et.al., (2013) developed an advanced solution for the non-destructive solution by replacing the sensing coil with GMR's due to their high sensitivity and broadband response. They employed a number of stimulation systems and processing methods in their work, along with a neural network to determine the extent of the faults.

Xiao and Zhang (2011) introduced a magnetic scanning imaging approach for identifying faults in ferromagnetic materials. In this study, they use tiny permanent magnets to magnetize ferromagnetic surfaces and Hall sensors to quantify the vertical component of densities. The form of the faults may be defined using this way.

6.5.1 Factors Influence on Measurement of GMR Sensor

The following subsections illustrate some of the elements that impact the measurement utilizing the GMR sensor.

6.5.1.1. Structural Quality of Giant Magnet Resistance Sensor

The quality surface sheet of the GMR sensor is a significant aspect. Alpe et al. (1998) investigated the link between surface sheet quality and magnetic resistance qualities of the GMR structure layer. They determined in this investigation that heating the Fe/Cr layer at 300 °C increases magnetic resistance.
Petit et al. (2005) investigated the relationship between annealing processes at different temperatures in another investigation. The investigation of the annealing process for the GMR layer at temperatures more than 425 °C results in a 25% reduction in magnetic field and an improvement in the layer's surface quality.

6.5.1.2. Temperature

In the case of the GMR sensor, magnetic resistance decreases between a temperature of 4K and room temperature. With the temperature rise, more electrons scattering in NM layers occurs. Increased electron scatting in the NM layer leads in more electrons flowing across the GMR layers. With increasing temperature, this effect reduces the efficiency of the GMR process. Several types of study on the thermal stability of GMR structures have been conducted in recent years. Many investigations have been conducted to investigate the connection between magnetic resistance and the temperature of the GMR unit. Hossain et al. (1996) presented a NiFeCo/C GMR structure in order to improve the thermal stability of the GMR sensing unit. A thick magnetic layer is used to construct the suggested structure. Cu thickness is fixed to 2.3mm for optimal results, while material layers range from 1.7nm to 3.7nm. According to experimental results, the structure of the layer of

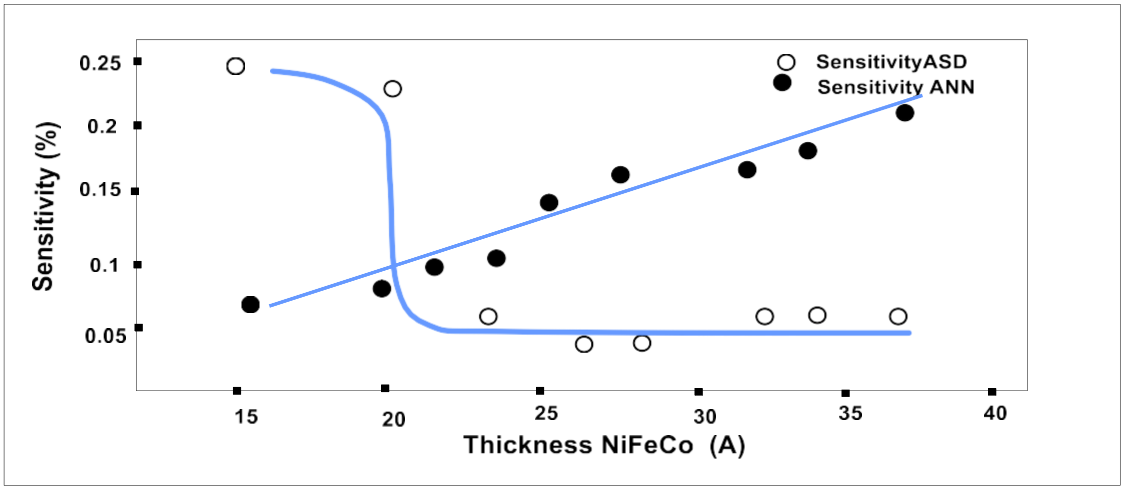

Fig.6. 6The effect of NiFeCo layer thickness on GMR sensitivity in ASD and ANN states. (Pearson et al., 2016]

thickness 3.7um as seen in the fig. 6.6 , NiFeCo has greater temperature stability and sensitivity.

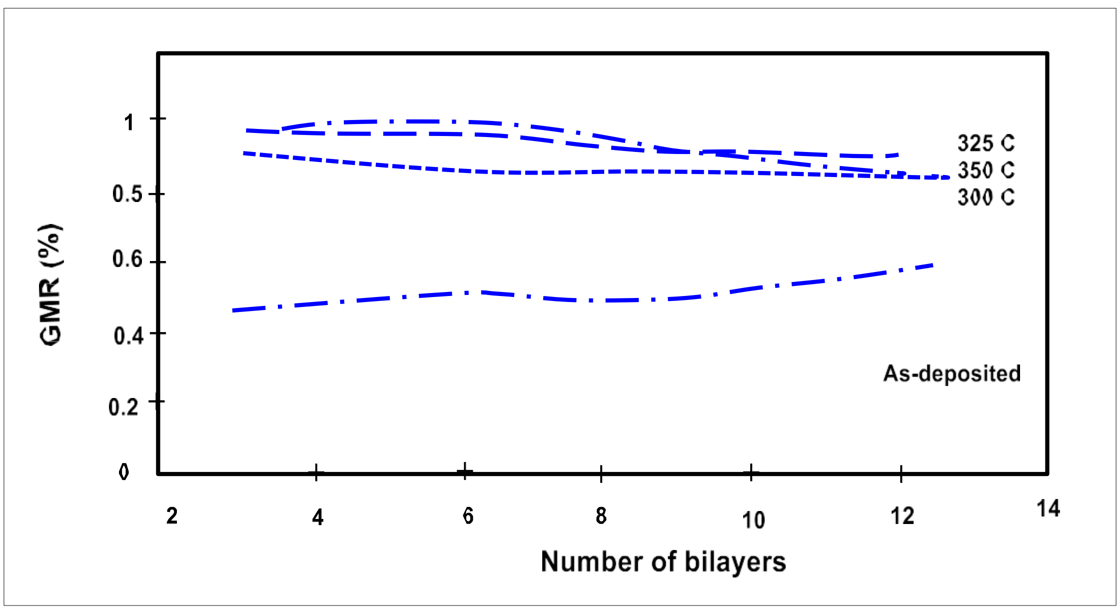

Fig.6.6 b(B) GMR multilayer structure in vacuum at 300, 325 and 350 temperature(Modified after Chen, et al., 2005)

Siritaratiwat et.al. (2000) experimented on NiFe/Cu layer of GMR structure and came out with the effect of annealing on the GMR structure. In this study, they heated the GMR structure of thickness 2.5nm for NiFe and 5nm for Cu spacer. By performing the heating process under a vacuum chamber for 2.5h at 300, 325 and 350 degrees Celsius, an improvement of 1% magnetic resistance was achieved.

Heating the GMR structure in argon medium increased the magnetic resistance qualities by 2.5% in the second instance described in Figure.6.7 (Chen et al., 2005).

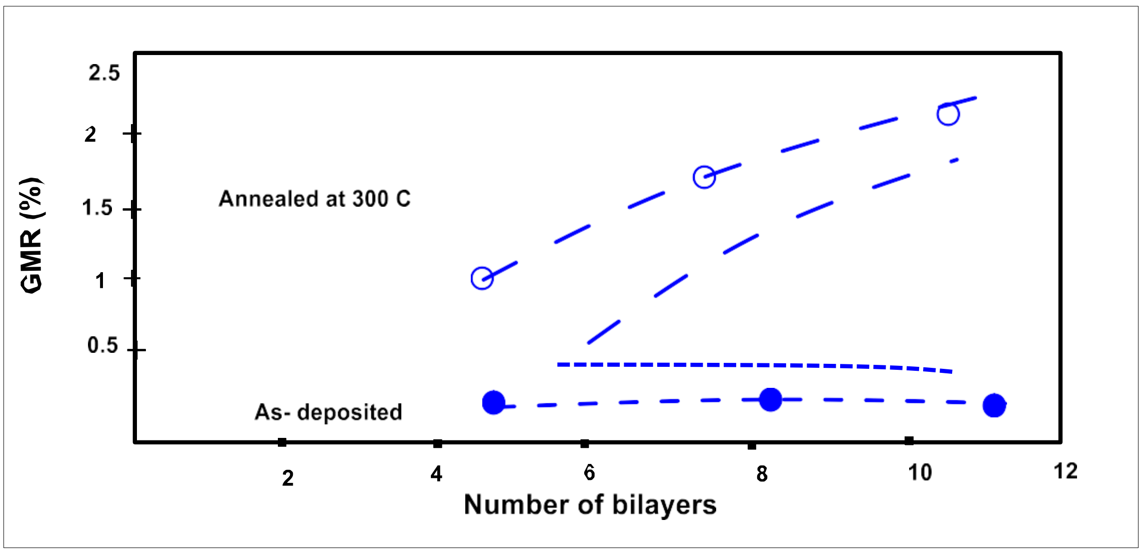

Fig.6. 7 GMR multilayer structure heating by flowing argon

6.7. Experimental Testing of GMR on the steel surface

We have examined numerous alternative sensors for fracture identification on the ferromagnetic surface when constructing the sensing portion of the robotic tool. MMM (Metal Memory Method) was one of the first usable sensors we explored. It is often used to identify cracks in metal surfaces and subsurface flaws. It has a high level of accuracy in detecting faults and errors. So we took this sensing system into account for the planned robotic instrument and conducted some laboratory trials.In the first trial, cracks and fractures were discovered inside the surface of overhead crane spans using Energodiagnostika's MMM sensor TSC-3M-12. Figure 6.8 displays two MMM sensor magnetic probes, one with a 2-channel probe sensor and the other with 4-channel probes.The TSC-3M-12 MMM sensor from Energodiagnostika is a susceptible sensor for surface defects. The operator must place the two-channel probe on the examination surface and move it gently around it to identify cracks inside the metal portion. A real-time graph will be presented on the MMM console

Fig.6. 8 (A) MMM console (B) MMM sensor TSC-3M-12 4 channel probe (C) 2 Channel probe

during the movement. A peak in the graph will be presented in the case of a stress-connected zone, which may be used for further in-depth study.

The MMM sensor's output findings are quite accurate, and the inspection procedure was also extremely speedy. It was challenging to attach the MMM console and channel probes to the robotic tool chassis due to space constraints and wiring connections. Another limitation in integrating it with the robotic body is the weight of this MMM sensor. It was difficult to place the MMM sensor on the robot since the robotic tool and wheels were designed to bear a maximum load of 5 kg. We chose the GMR sensor array after considering this difficulty.

6.8 GMR Sensor Array

A giant magneto-resistance (GMR) sensor unit was recently constructed to explore the removal of metal due to corrosion on the stainless steel surfaces of overhead crane spans. Figure 6.9 displays the GMR sensor unit setup. The GMR sensing array's architectural framework incorporates eight Hall sensors, circular Neodymium permanent magnet rings, and eight NVE AA-005-02 GMR sensors. The PCB (printed circuit board) contains all of the components. The hall sensors are covered with magnetic rings.

In addition, to maintain a homogeneous magnetic field on the surface of the steel, all magnet rings and hall sensors have been placed at identical distances. Figure 6.10 depicts the anticipated GMR sensor array, which is set up across two magnetic wheels, which also serve to magnetize the inspection region. As explained earlier in the chapter, the wheel is made of a permanent magnet that, as it spins, creates a homogenous magnetic field on the specimen's surface. Figure 6.10 depicts the position of the GMR sensor on the robot's chassis for clarity.

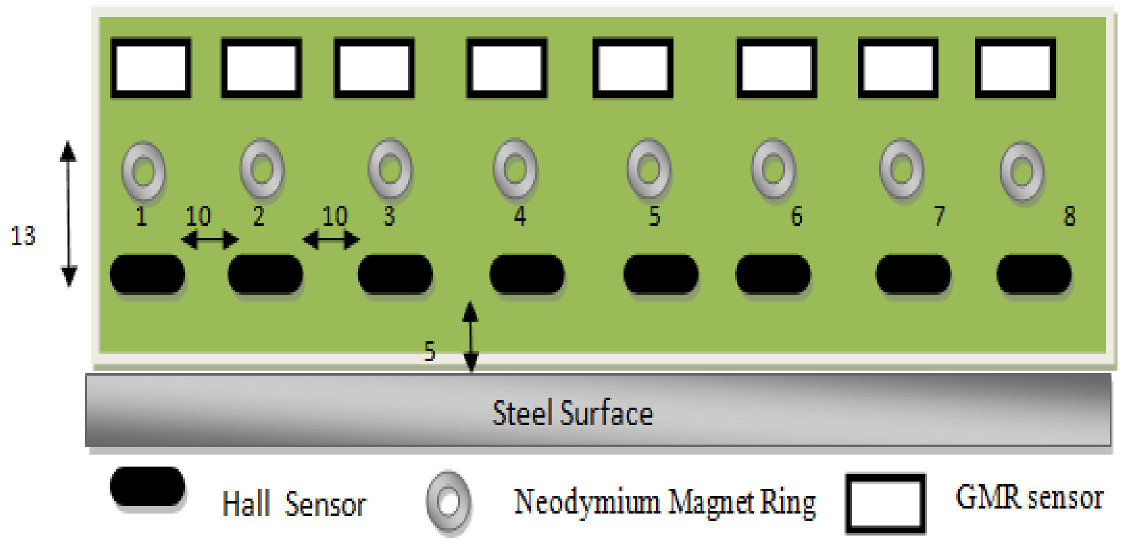

Fig.6. 9 Eight-channel Array composed of a sensor: GMR

To provide higher-quality results, the distance between the being studied surface and the GMR sensor unit is kept at 5mm. Neodymium magnet rings magnetize the steel plate.

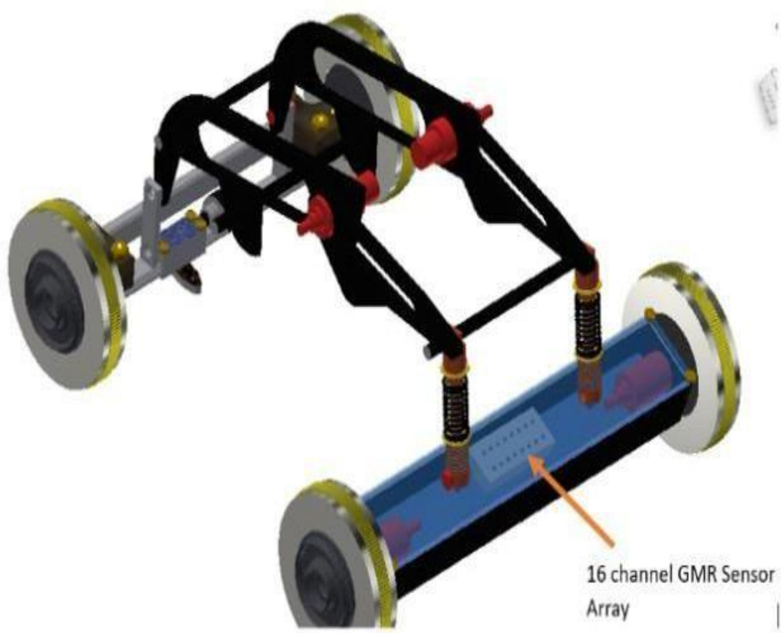

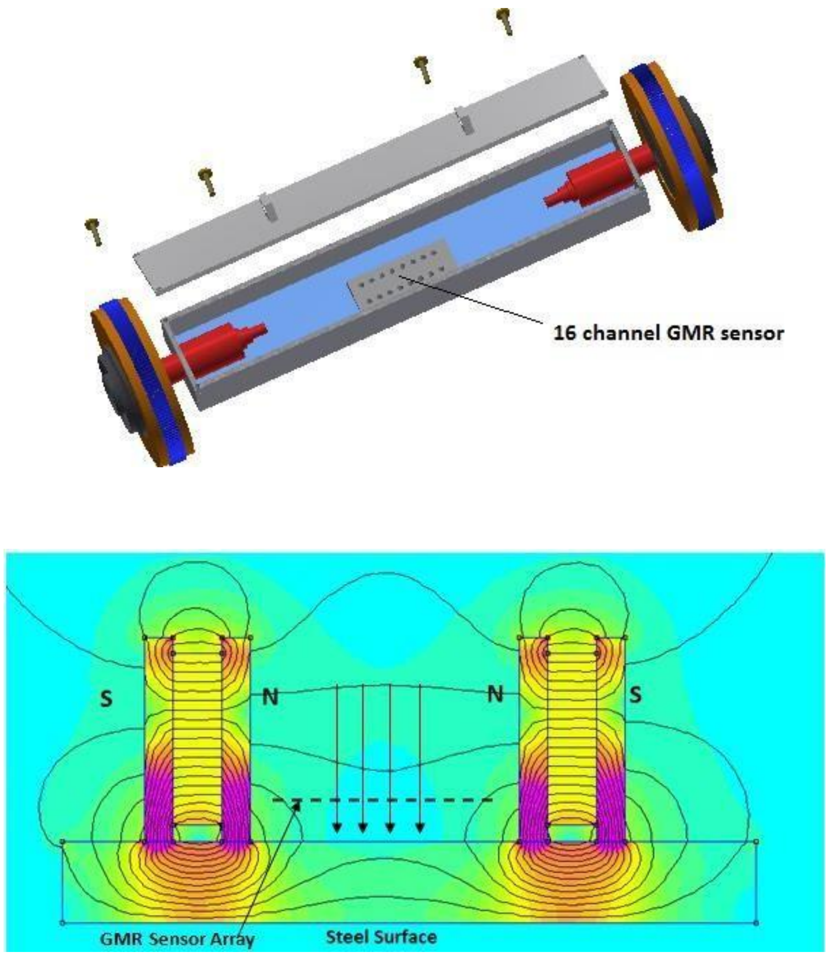

Fig.6. 10 Placement of GMR sensor array in between the robot's wheels (Yadav, A., & Szpytko, J. (2020).

Initially, a software investigation was performed using FEMM (Finite Element Method Magnetics) to examine the accuracy of the developed GMR sensor set. In order to run the test, a few settings were established at the start of FEMM. The steel surface plate on the wheel is 10mm thick, the permanent magnet is 26mm thick, and the space between the steel surface and the magnet is 5mm.

It is required to assign some values in FEMM before performing the analysis, like air space, the characteristics of steel, and wheels. During the analysis, it was noticed that magnetic lines were deformed, and the intensity of magnetic field decreased significantly in the proximity of loss of metal caused by corrosion. Here below, in Figure 6.11, two analyses have been shown. In the left region, it can be noticed that the magnetic field is uniform and consistent around the robotic magnetic wheel. Due to the existence of loss of metal in the area under examination region, an irregular flow of magnetic field lines can be noticed in the right portion.

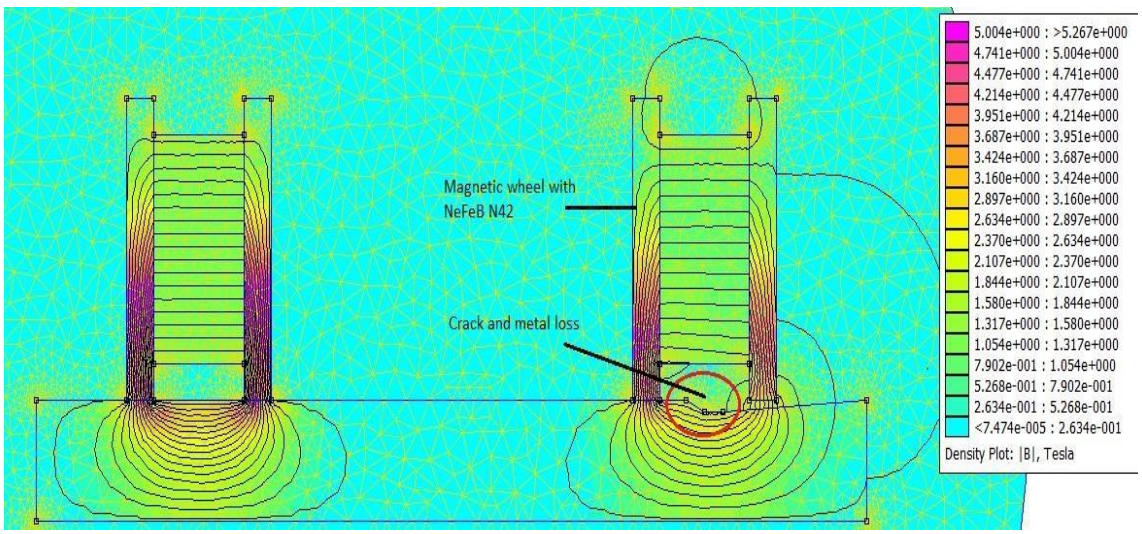

Fig.6. 11 Simulation analysis of magnetic field density using FEMM Analysis. (Left) No loss (Right) with metal loss

The distortion in magentic field is due to presence of metal loss exists under the metal surface. The simulation results show that the highest value of magnetic intensity decreases from 0.04 T to 0.03T (figure 6.12).

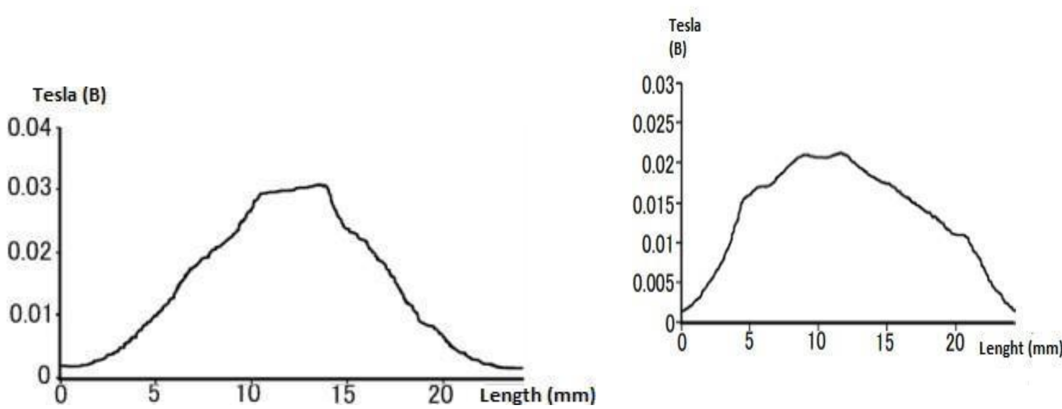

Fig.6. 12 Simulation of magnetic field density change by NDT sensor array

To make it more clear and easy to understand, a simulation result is presented below in Fig. 6.11 on a robotic magentic wheel. The wheel is kept on a inspction surface area made up of stainless steel, haing a thicknes of 10mm. A simulaton was performed to notice the direction of magentic field in absense of any cracks and defects in the inspetion area. As we can see from the fig.6.13 magnentic field are uniform around the surface area.

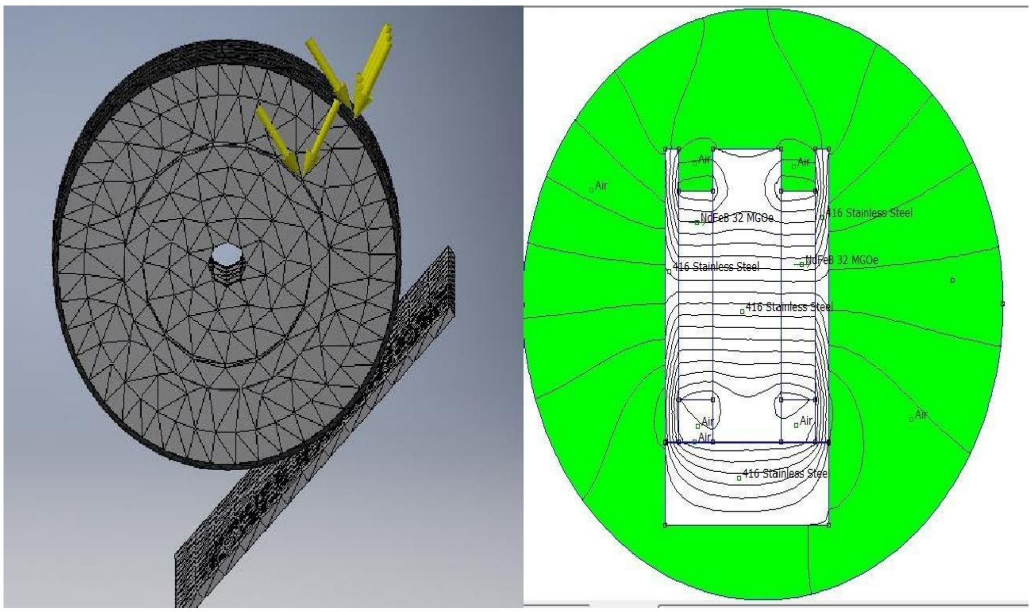

Fig.6. 13 (a) 3D meshed view of wheel on steel surface (b) Magnetic simulation on wheel

In-depth information on the presence of metal loss and corrosion is improved by the employment of a linear hall sensor between magnets and a GMR sensor. In a normal environment with no magnetic field, the hall sensor output is 2.5 volts. The Hall sensor produces an output of more than 2.5 volts in a positive magnetic field and less than 2.5 volts in a negative magnetic field.

The size of permanent magnets is critical for achieving improved precision in the measurement of magnetic flux change. The magnetic field density will be higher the larger the magnets are. However, in our situation, size is limited by the robot's weight. It is likely that the Hall sensor will be outside of its linearity range in some circumstances where the magnetic field is substantially greater. For Hall sensors to function, the magnets must be able to provide sufficient magnetic density. Neodymium magnetic rings were positioned above the hall sensors for that reason.

To calculate the distance between the magnets and the Hall sensor, an experiment has been conducted. For a particular condition, a steel surface of 10mm thickness is used to simulate the magnetic density.
The letter "X" specifies the distance that lies among the hall sensors and the inspection surface of the metal in this case. The letter "Y" represents the distance that exists between the two hall sensors.

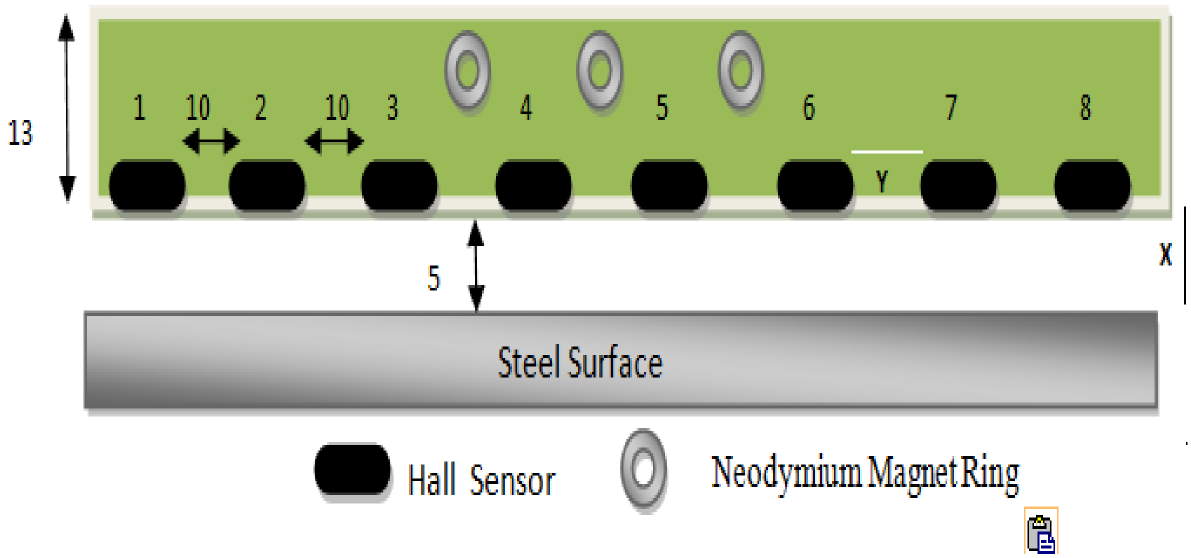

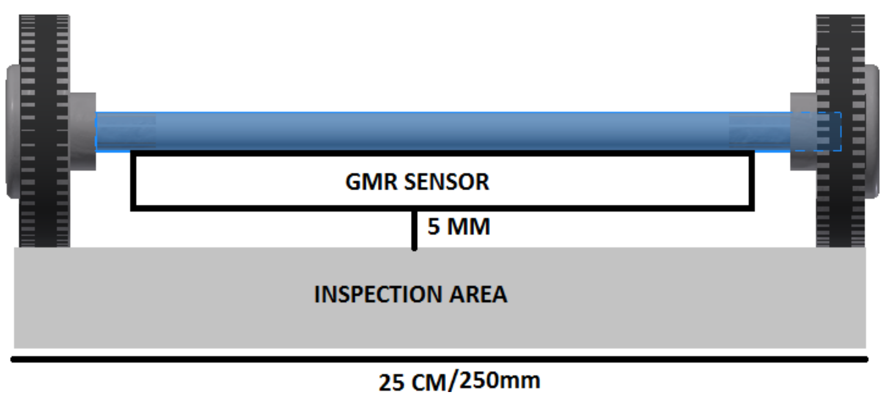

Fig.6. 14 Placement of Hall sensors and magnets in X and Y directions.

It should be noted that the Hall sensors used in this situation are inside the linearity range. The magnetic flux density fluctuates as the values of X and Y vary. As the X and Y values decrease, the magnetic field density increases. As a result, the X and Y values must be kept within a range such that Hall sensors obey the linearity scope and the value does not fall outside of it (Figure 6.14). The span between the surface of the steel and the hall sensors is shown by X in the following figure. The constant distance maintained between the hall sensors and permanent magnetic rings is denoted by Y. Maintaining an appropriate distance value for X and Y to get the proper output from the GMR sensor array is somewhat difficult here.

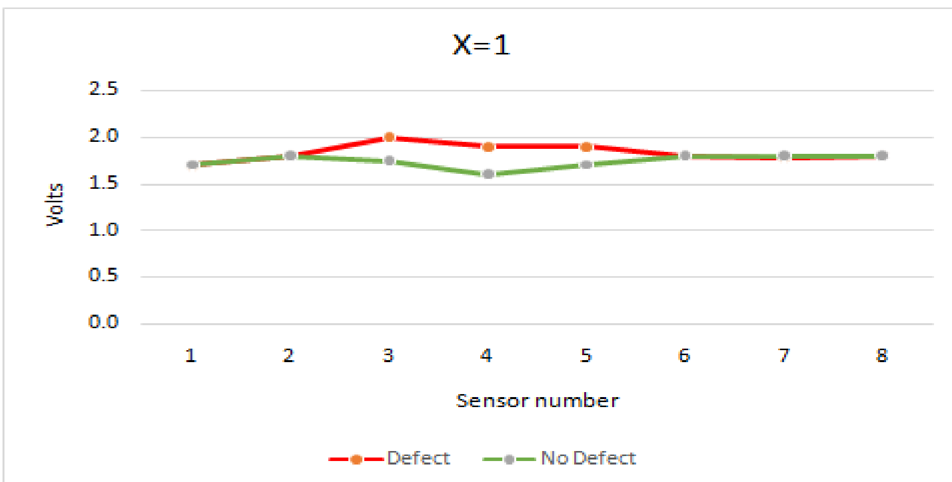

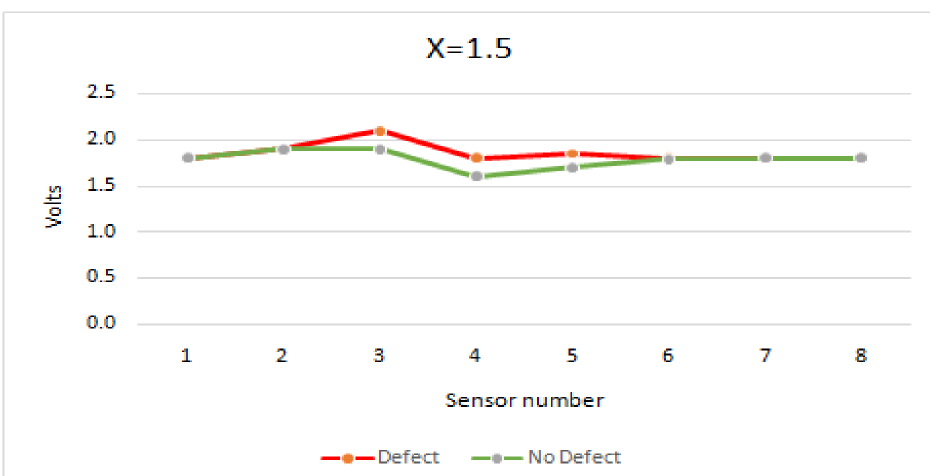

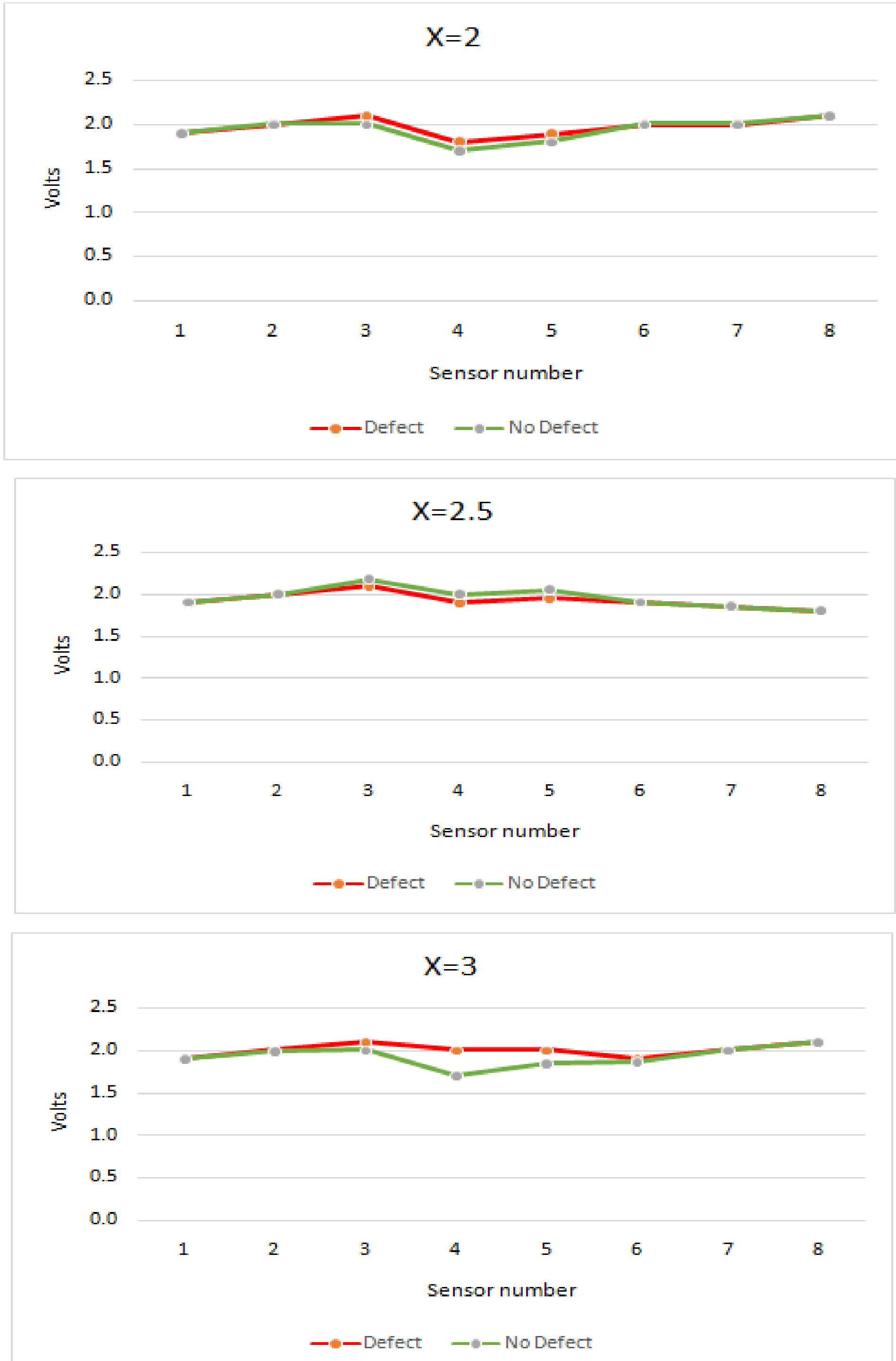

Fig.6. 15 Output of hall sensors in case of Y-5mm, and varying the values of X.

The intensity of magnetic field overcomes the linear value of Hall sensors when the x value is below than 5mm and the y value is less than 5mm. As the value of y increases, so does the sensing device's sensitivity in proportion to the value of x. The output value of a Hall sensor is shown in Figure 6.15 when the x value is adjusted while the y value is maintained constant at 5mm. By maintaining a minimal distance between the PCB board and inspection area, we can achieve maximum accurate results. In our case we did fix the x=5, to avoid any lift-off issues

6.9 Control architecture and Sensing unit

The robot is controlled by a Raspberry Pi, an Arm 11 CPU, and a microcontroller. Given that the designed robot will operate on the ferromagnetic structures of overhead crane bridges for crack detection, a lightweight sensing unit with the pi camera (25mm by 20mm by 9mm) is mounted on the robot's front axle and connects to the Raspberry Pi's Camera Serial Interface (CSI) bus connector via a flexible ribbon cable. Because the robot is controlled by two modes, the sensing unit connections must be built in accordance with the mode of operation.

- Autonomous mode
- *Semi- Autonomous Mode-Robot with remote control using Raspberry Pi Arm 11 and live video streaming*

Mode 1. Autonomous mode

In this mode of operation, a GSM SIM300 system will be connected additionally to receive the live coordinates of the robot. The GSM SIM300 module and other sensing parts have been discussed in Chapter 4. This GSM module consists of a SIM card holder. Once we insert the SIM card of any carrier in the GSM module and turn on the power supply, the LCD starts displaying the coordinates on the screen as shown below in Fig.6.16. To make the robot rover on the steel surface, the operator has to send a text message from an Android phone with a particular command format. The format of the text command consists of The command will be delivered to the robot by text message in a particular format consisting of ***"DP* Longitude*Latitude#.*** That text message will convey the location coordinates to the robot. Once the text message is delivered to the robot, it will automatically start moving to a pre-defined location coordinate and start performing the inspection operation. So, this command will provide the robot with exact location coordinates for the movement and perform the health monitoring.

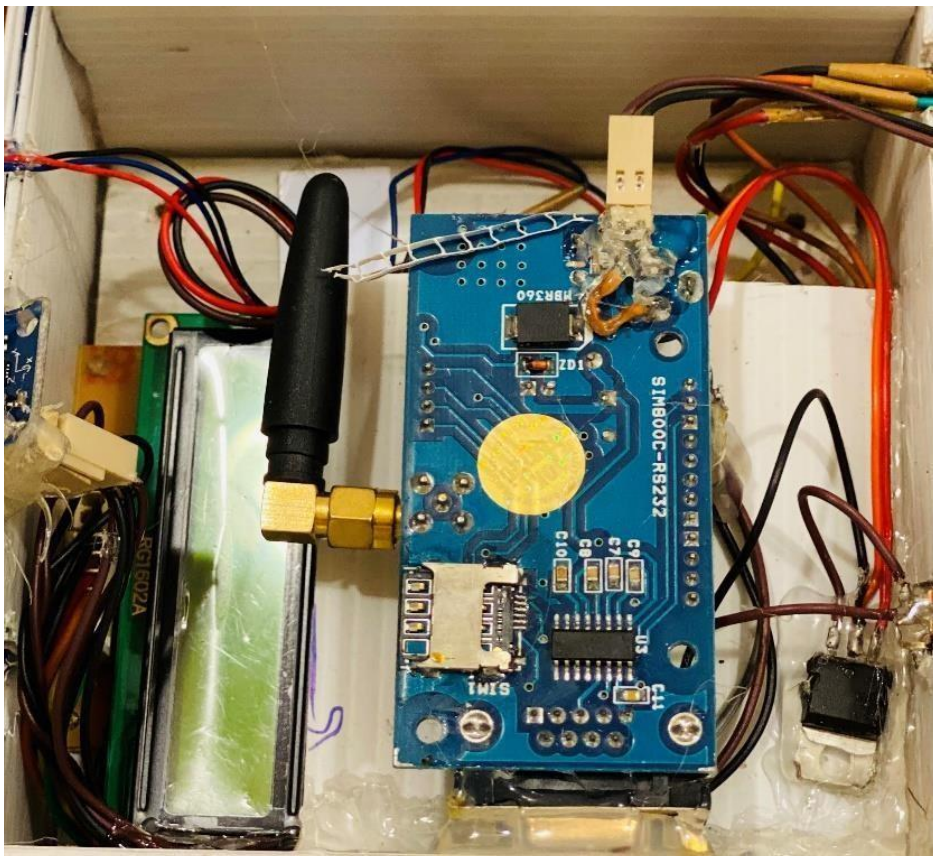

Fig.6. 16 GSM SIM 300 and LCD display

For better understanding, a screenshot of the robot command from mobile is shown in Figure 6.17.Once the robot receives this command, a return text message will be delivered to the operator to confirm that the robot has received the command, and it will be following the given location coordinates. During the movement of the robot on pre-defined location coordinates, after 2 minutes, the robot will automatically share its current location coordinates with the operator to make sure it is on the right track.

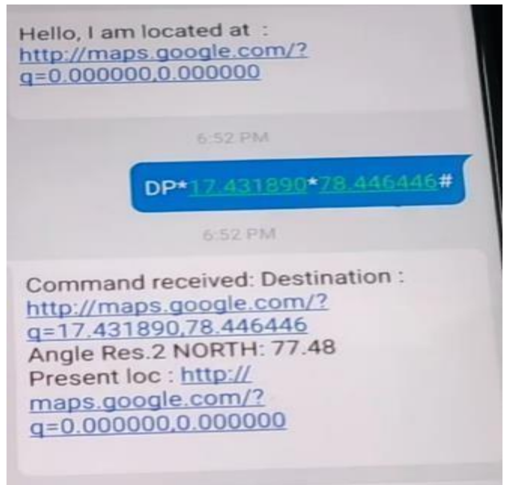

Fig.6. 17 Mobile command format from a remote location

Once the robot is at the inspection area, it can start performing the inspection of the steel bridge by using the sensing unit. Once the inspection of robot starts, the information can be accessed by using the same android phone and live video and real time live GMR sensor can be accessed.

Mode 2. Robot with remote control using Raspberry pi Arm 11 and live video streaming

In this mode of operation, the robot will be controlled by a remote operator, who can navigate the robot by accessing an Android phone. In this mode, a Raspberry Pi with a Pi camera needs to be connected to a wireless network. So it is quite necessary to turn on the wireless network and later turn on the power supply to the robot and controllers. Once the Raspberry Pi is connected to the wireless network, it is recommended to get the IP address of the Raspberry Pi. In order to set up a communication method, a software package needs to be installed on a PC. By keeping the raspberry pi address in putty, a serial connection can be setup between them. It is quite important to change the IP address in Putty, just as we have the IP address of the Raspberry Pi. By using this command, " ***sudo nano index.html,"*** we can change the IP address.

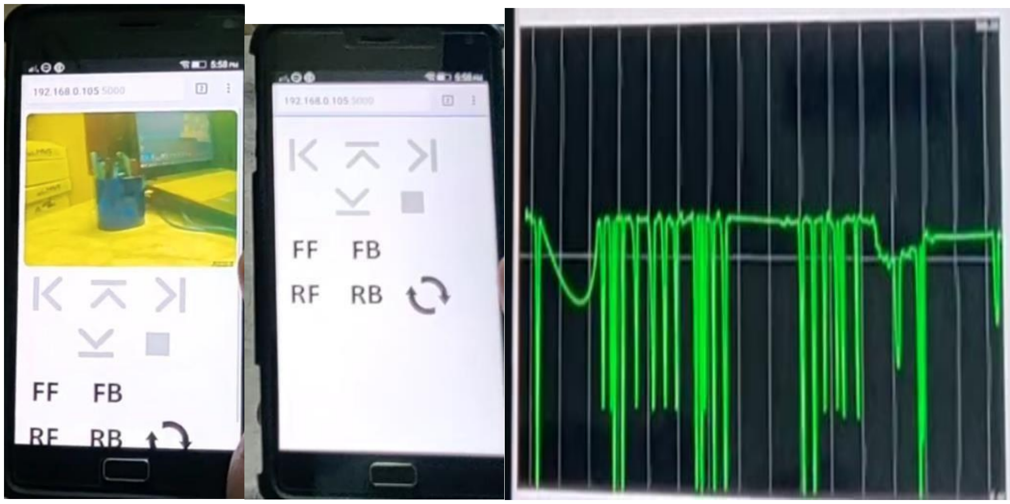

Fig.6. 18 Control Screen layout and real-time GMR sensor graph

Once the network setup is accomplished, open an internet URL with the same IP address, and we can access the robot's live location, live video monitoring, and real-time GMR sensor data on the phone screen.

One section displays the live streaming video, and the second section displays the virtual key sticks to control the robot's motion. Figure 6.18 here represents the screen layout and virtual control with the GMR sensor live real-time graph. By accessing the screen, the operator can access the robot's live location and monitor the inspection surface by live video streaming. It also allows the user to by clicking on the key indicated in table 6.3, you can regulate the robot's movement.

Table 6-3 ROBOT CONTROL BUTTONS' DESCRIPTION

Forward	Turn Left
Backward	Turn Right
FF-Front Forward	RF- Rear Forward
FB-Front Backward	RB- Rear Backward
Steering	Stop

6.9.1 Connection diagram and Programming:

Figures 6.19 and 6.20 present the connection diagram of the robot with ARM-11Raspberry Pi processor and microcontroller. It includes four DC motor, a sensor system, GMR sensor, an analog to digital converter, GPS, GSM module, Compass, LED screen, relay and motor steering.

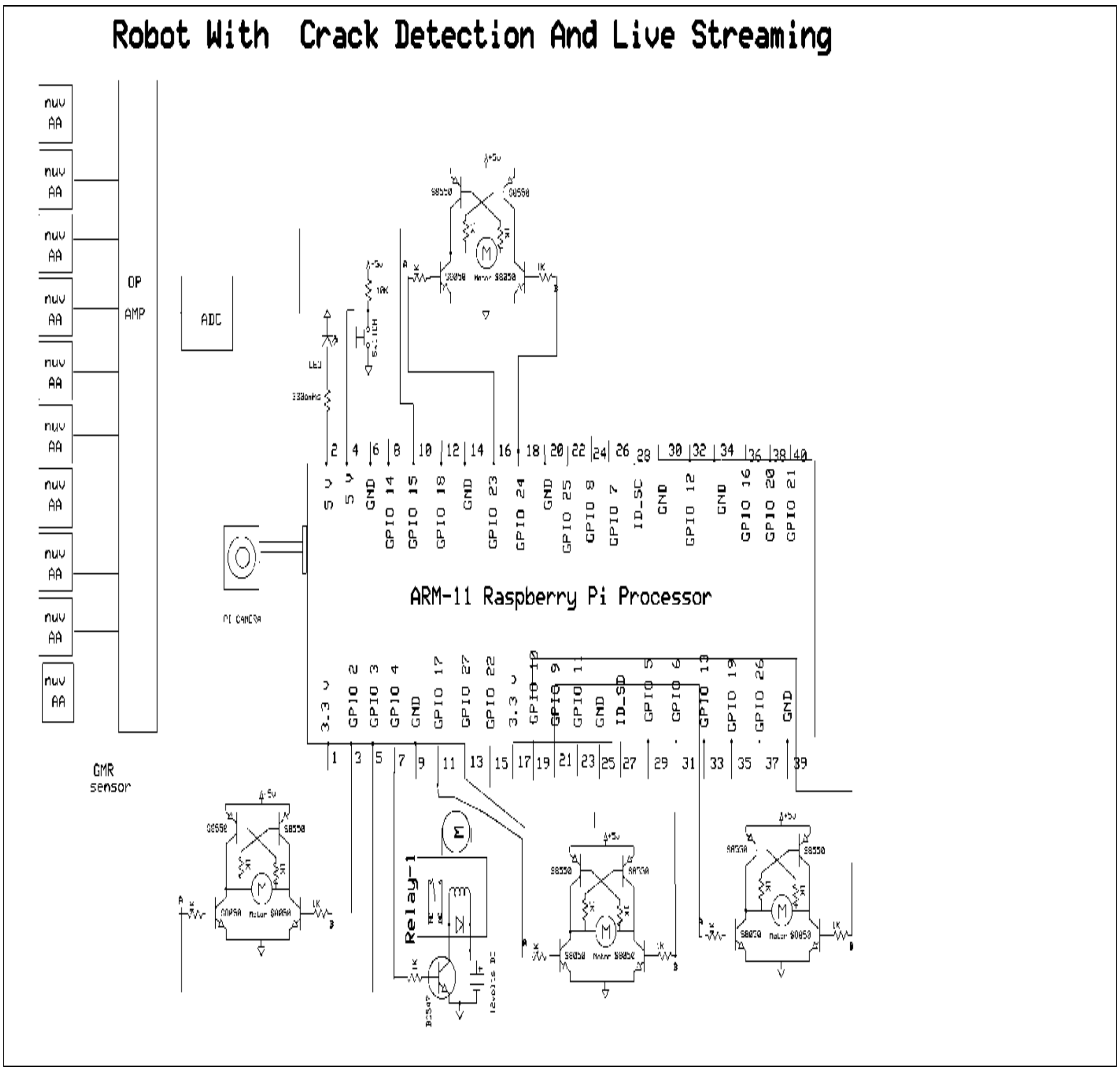

Fig.6. 19 Connection with Raspberry pi processor

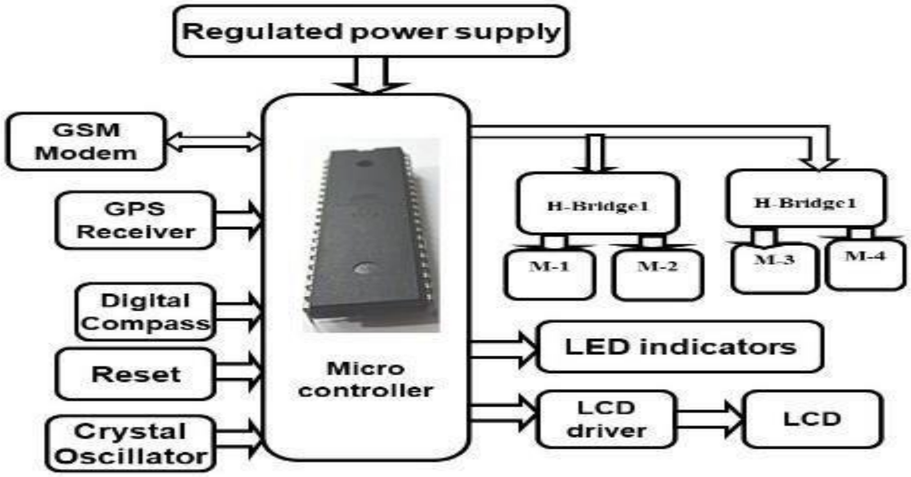

(A)

Robot With Crack Detection And Live Streaming

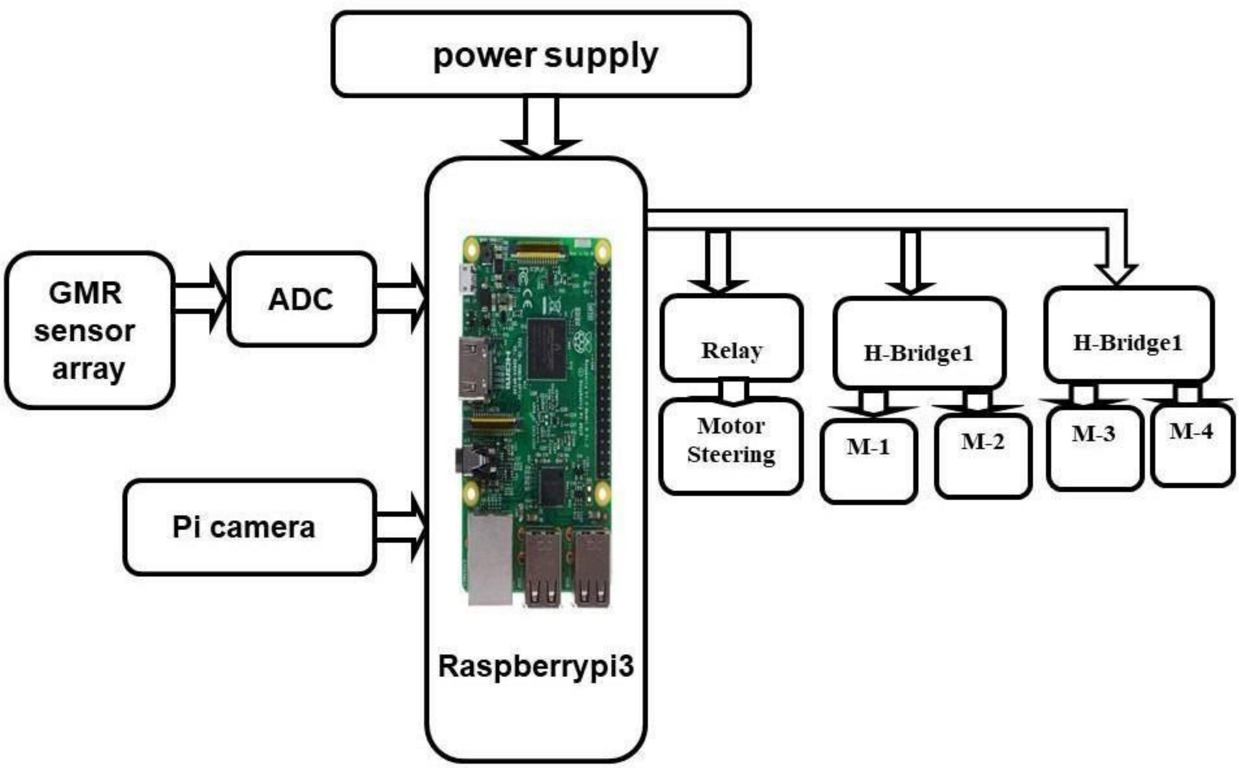

(B)

Fig.6. 20 (A)Connection with Microcontroller (B) Connection diagram with Raspberry Pi

The robotic tool has four magnetic wheels powered by four DC motors connected to H-bridges. Two H bridges are linked to the microcontroller's two pins. The microcontroller is linked to a GSM modem, GPS receiver, digital compass, reset, crystal oscillator, and LCD drivers. Another figure, 6.20(b), depicts the Raspberry Pi connection diagram. A GMR sensor with ADC and a Pi camera are attached to the Raspberry Pi for live video streaming and GMR sensor results.

6.9.2 Programming of Robot:

The robot is programmed in python language by using Jetbrains software. The motion of robot has been presented in figures 6.21.
In the images in figure 6.21 are the screenshot of the programming script

- Set up of motors

```
#Set up all as outputs
GPIO.setmode(GPIO.BCM)       # Use BCM GPIO numbers
GPIO.setup(Motor1A,GPIO.OUT)
GPIO.setup(Motor1B,GPIO.OUT)

GPIO.setup(Motor2A,GPIO.OUT)
GPIO.setup(Motor2B,GPIO.OUT)

GPIO.setup(Motor3A,GPIO.OUT)
GPIO.setup(Motor3B,GPIO.OUT)

GPIO.setup(Motor4A,GPIO.OUT)
GPIO.setup(Motor4B,GPIO.OUT)

GPIO.setup(motors,GPIO.OUT)

GPIO.output(motors,GPIO.LOW)
```

- Forward motion command for robot

```python
def forward():
    print("Going Forwards")

    GPIO.output(Motor1A,GPIO.HIGH)
    GPIO.output(Motor1B,GPIO.LOW)

    GPIO.output(Motor2A,GPIO.HIGH)
    GPIO.output(Motor2B,GPIO.LOW)

    GPIO.output(Motor3A,GPIO.HIGH)
    GPIO.output(Motor3B,GPIO.LOW)

    GPIO.output(Motor4A,GPIO.HIGH)
    GPIO.output(Motor4B,GPIO.LOW)

    sleep(0.3)
```

- Backward Motion Command

```python
def backward():
    print("Going Backwards")

    GPIO.output(Motor1A,GPIO.LOW)
    GPIO.output(Motor1B,GPIO.HIGH)

    GPIO.output(Motor2A,GPIO.LOW)
    GPIO.output(Motor2B,GPIO.HIGH)

    GPIO.output(Motor3A,GPIO.LOW)
    GPIO.output(Motor3B,GPIO.HIGH)

    GPIO.output(Motor4A,GPIO.LOW)
    GPIO.output(Motor4B,GPIO.HIGH)

    sleep(0.3)
```

- Turn left

```
def turnLeft():
    print("Going Left")

    GPIO.output(Motor1A,GPIO.LOW)
    GPIO.output(Motor1B,GPIO.HIGH)

    GPIO.output(Motor2A,GPIO.LOW)
    GPIO.output(Motor2B,GPIO.HIGH)

    GPIO.output(Motor3A,GPIO.HIGH)
    GPIO.output(Motor3B,GPIO.LOW)

    GPIO.output(Motor4A,GPIO.HIGH)
    GPIO.output(Motor4B,GPIO.LOW)

    sleep(0.3)
```

- Turn Right

```
def turnRight():
    print("Going Right")

    GPIO.output(Motor1A,GPIO.HIGH)
    GPIO.output(Motor1B,GPIO.LOW)

    GPIO.output(Motor2A,GPIO.HIGH)
    GPIO.output(Motor2B,GPIO.LOW)

    GPIO.output(Motor3A,GPIO.LOW)
    GPIO.output(Motor3B,GPIO.HIGH)

    GPIO.output(Motor4A,GPIO.LOW)
    GPIO.output(Motor4B,GPIO.HIGH)

    sleep(0.3)
```

- Front backward

```
def fb():
    print("Going FB")

    GPIO.output(Motor2A,GPIO.LOW)
    GPIO.output(Motor2B,GPIO.HIGH)

    GPIO.output(Motor4A,GPIO.LOW)
    GPIO.output(Motor4B,GPIO.HIGH)

    sleep(0.3)
```

- Rear forward (RF)

```
def rf():
    print("Going RF")

    GPIO.output(Motor1A,GPIO.HIGH)
    GPIO.output(Motor1B,GPIO.LOW)

    GPIO.output(Motor3A,GPIO.HIGH)
    GPIO.output(Motor3B,GPIO.LOW)


    sleep(0.3)
```

- Rear Backward

```
def rb():
    print("Going RB")

    GPIO.output(Motor1A,GPIO.LOW)
    GPIO.output(Motor1B,GPIO.HIGH)

    GPIO.output(Motor3A,GPIO.LOW)
    GPIO.output(Motor3B,GPIO.HIGH)

    sleep(0.3)
```

- Str command

```python
def str():
    print("Going Steering")

    GPIO.output(motors,GPIO.HIGH)
    sleep(2)
    GPIO.output(motors,GPIO.LOW)
```

- Stop Command

```python
def stop():
    print("Stopping")

    GPIO.output(Motor1A,GPIO.LOW)
    GPIO.output(Motor1B,GPIO.LOW)

    GPIO.output(Motor2A,GPIO.LOW)
    GPIO.output(Motor2B,GPIO.LOW)

    GPIO.output(Motor3A,GPIO.LOW)
    GPIO.output(Motor3B,GPIO.LOW)

    GPIO.output(Motor4A,GPIO.LOW)
    GPIO.output(Motor4B,GPIO.LOW)
```

- Command for serial communication

```python
#./websocketd --port=8085 --staticdir= --sameorigin=true tail -f log.txt
import time
import sys
import os
import serial
import re

serialport = serial.Serial("/dev/ttyS0", 9600,timeout = 0.09)
data = ""

data1 = ""

while True:
    data = serialport.readline()
    with open("log.txt", "w") as myfile:
        myfile.write(data)

    time.sleep(0.04)
```

- Command for live streaming of robot sensor data

```
project.py    index.html    motors.py

<!DOCTYPE html>
<html>
  <head>
    <script type="text/javascript" src="./smoothie.js"></script>
    <script type="text/javascript">

      var current = new TimeSeries();

      no usages
      function createTimeline() {
    var chart = new SmoothieChart({
          interpolation:'bezier',
          minValue:0,
          maxValue:500
        });
        chart.addTimeSeries(current, {
          strokeStyle: 'rgba(0, 255, 0, 1)',
          fillStyle: 'rgba(0, 0, 0, 0.2)',
          lineWidth:  2} );
        chart.streamTo(document.getElementById("chart"), 10);
      }

      // setup websocket with callbacks
      var ws = new WebSocket('ws://192.168.0.104:8085/');
      ws.onmessage = function(event) {
        var line = event.data; // get line from websocket event
```

```
      }

      // setup websocket with callbacks
      var ws = new WebSocket('ws://192.168.0.104:8085/');
      ws.onmessage = function(event) {
        var line = event.data; // get line from websocket event
        current.append(new Date().getTime(), parseFloat(line));
      };

    </script>
  </head>
  <body onload="createTimeline()">
    <h1>Welcome to HVS Technologies</h1>
    <canvas id="chart" width="800" height="400"></canvas>

        <h3>read file</h3>

  </body>
</html>
```

Fig.6. 21 Screenshot of the Programming scripts for the robot.

As shown in Fig. 6.21, the numerous programmed commands allow this constructed robot to walk across a horizontal, curved surface with bumps and irregularities. It is possible to circumvent the difficulties on the inspection surface of overhead crane bridges by using these commands. The live video streaming and real-time graphing capabilities of this robot make it user-friendly, safe, and reliable.
We can increase the robot's speed by manipulating the motors and adjusting the variables in the programming section. We reduced the robot speed to a minimum for research purposes in order to get the best data and footage. In the event of a vast inspection area, speed can be increased by keeping the motor at a high rpm and adjusting the programming variables.

The advantages of using a GMR sensor over eddy current and MFL approaches are discussed in this chapter. Because the major goal of this research is to detect cracks and corrosion on metal surfaces, a linear 8-channel GMR sensor array has been constructed in combination with a Hall sensor and neodymium permanent magnets. To reduce the lift-off effect, the developed GMR sensor array was tested between two permanent magnetic wheels at a set height of 5mm from the inspection area. To investigate the magnetic flux between the wheels, a simulation test utilizing the finite element approach was performed. The magnetization of the inspection area is performed by the robot's wheels, which are made of permanent magnets, while a GMR sensor records any change.

To cross-check the results, a few laboratory experiments have been conducted using the MMM method for detecting potential surface fractures. GMR mounting on the robot's transverse rear axis has been clarified. Both manual and automatic robot control have been covered in this chapter. This chapter has addressed the robot's controller, its wiring schematic, and its programming.

6.10 CONCLUSION

This study introduces a novel approach for detecting corrosion and cracks on the bridges of overhead cranes by combining a GMR sensor with a flexible climbing robotic framework. To overcome the current limitations to inspect the overhead crane bridges methodology, a GMR sensor array has been designed and attached to the rear axle of the robot at a fixed height of 5mm from the ground. In the inspection process of ferromagnetic structures, lift-off plays a crucial role as shown in figures 6.22 and 6.23. This graph represents the change in a magnetic field by varying the lift-off distance between the sensor and the inspection surface.

Figure 6.22(b) depicts the estimated density of magnetic flux at the location of the GMR sensor unit, as calculated by simulation. For the purposes of this experiment, the lift-off value was kept at 5mm. In the simulation, a perfectly symmetrical and parabolic magnetic flux density may be observed in the absence of flaws. That curve is the standard of excellence for describing the distribution of magnetic flux densities in regions with no defects. Several simulation results with different lift-off values are shown in figure 6.23. For the purpose of calculating the lift-off effect, three scenarios have been considered: 2mm, 5mm, and 10mm.

The magnetic flux density is found to be almost constant. At a lift-off value of 10 mm, the density of magnetic flux ceased to points perpendicular to the specimen's surface. Magnetic field fluctuations in the vertical direction cause a shift in the GMR sensor data. The output generated by the GMR sensing array appears to be reasonably insensitive to fluctuations in lift-off value, at least within a 10 mm range.

A linear array of 8 GMR sensors has been mounted to the robot's rear axle for quick inspection of the steel surface in order to examine the bridges of overhead cranes. To produce the best results, the GMR sensor array was held at a constant height of 5mm from the steel surface to reduce the lift-off effect. The sensing system comprises of an array of eight NVW AA-005-02 GMR sensors that provide the intended system with exceptional sensitivity to slight changes in the magnetic field. The primary benefits of GMR sensors is their inexpensive cost, ease of installation, and low power consumption.

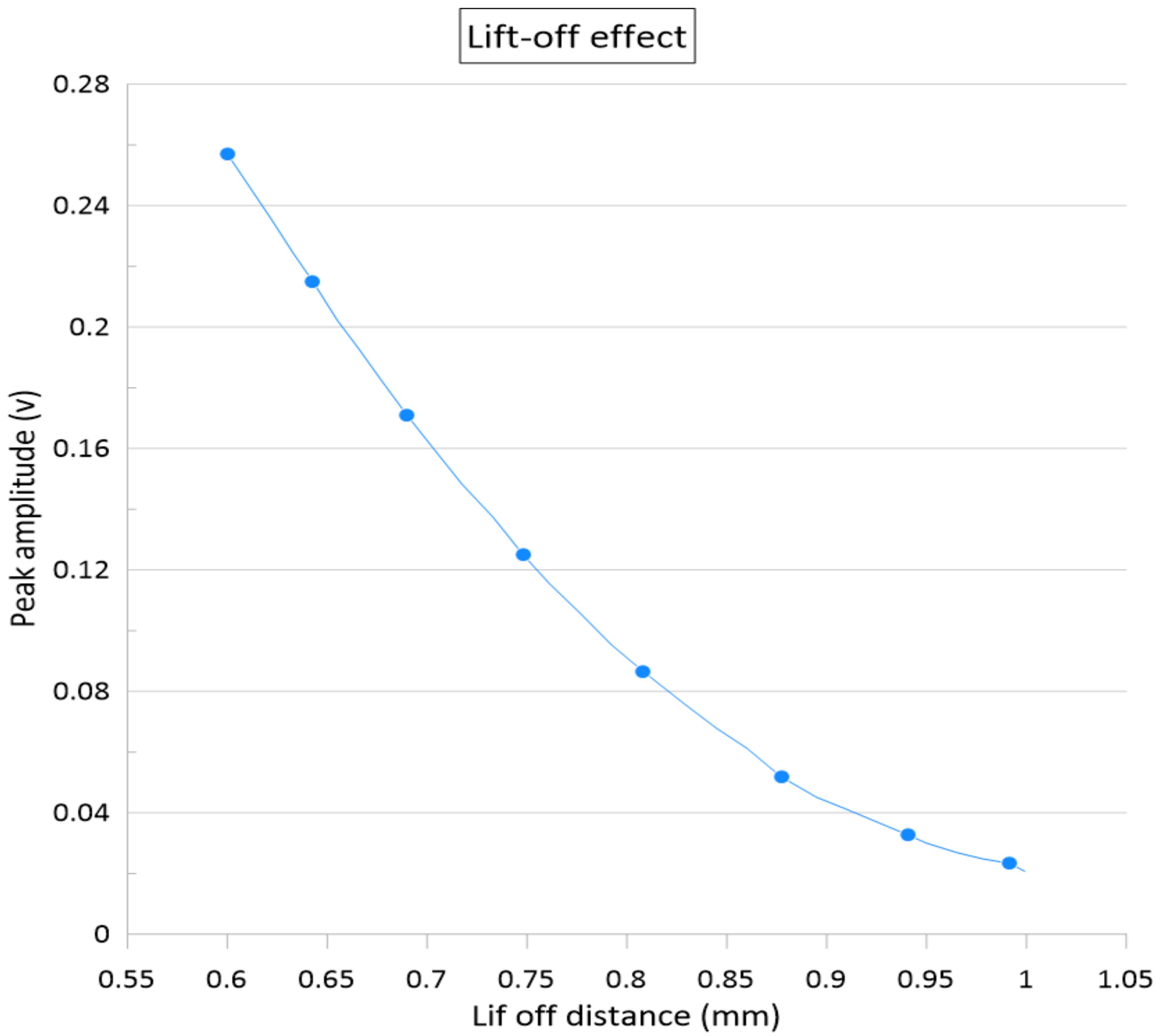

(a)

Fig.6. 22 Simulation result of Lift off effect of GMR sensor with distance and magnetic field (a) Overall lift off effect (b) Lift off effect at 5mm

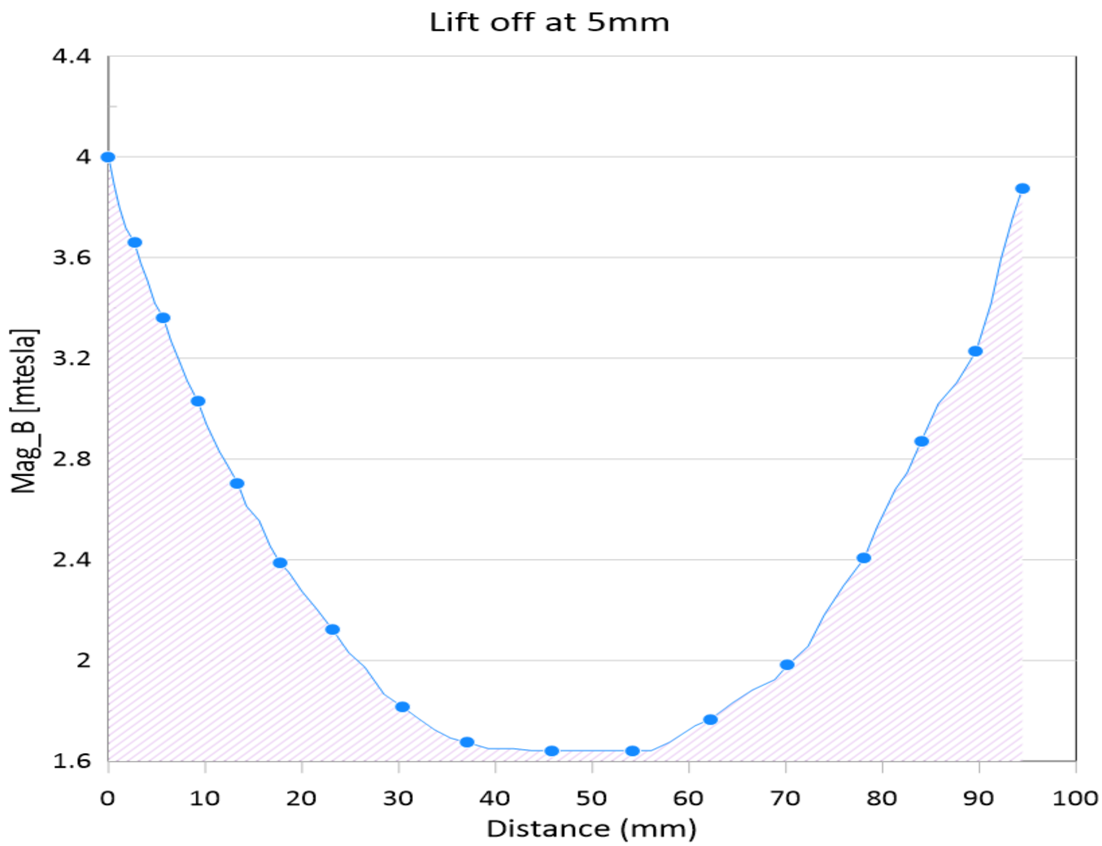

Fig. 6.22 (b) Lift off effect at 5mm

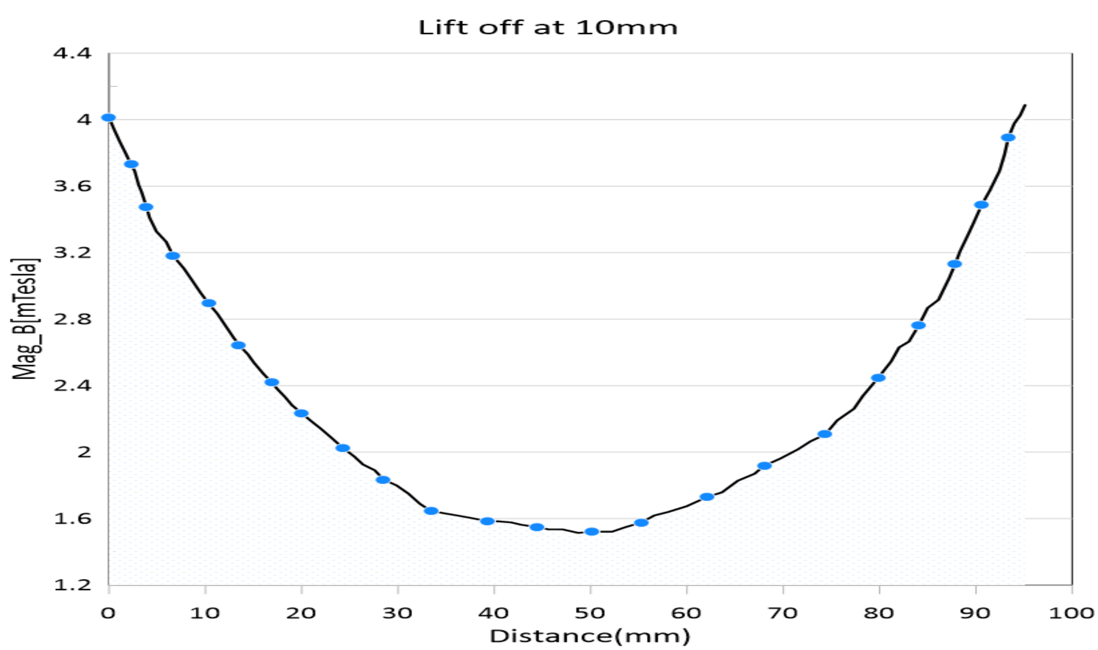

Fig.6.22 (C) Lift off effect with distance and magnetic field at 10mm

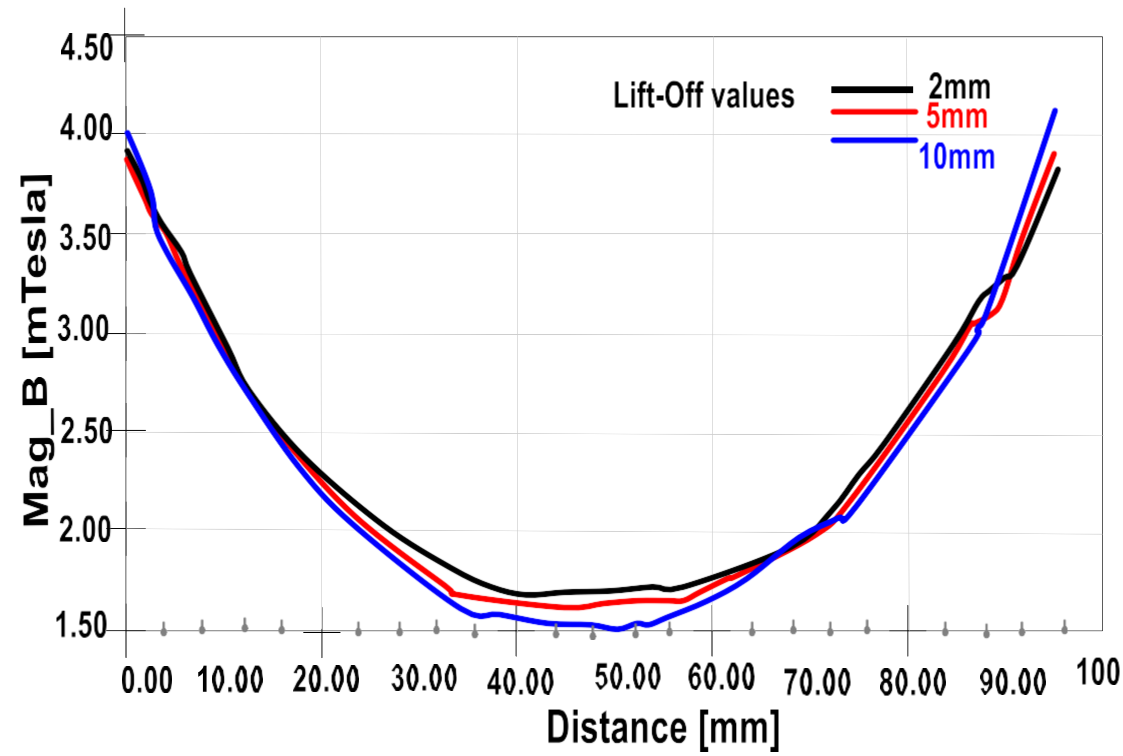

Fig.6. 23Simulation results of lift-off effect on various distances

When the sensing unit moves on the inspection steel area, due to lift-off effect the accuracy level varies. Figure 6.23 represents the variation in magnetic field with distance, in case when the lift of value varies from 2mm to 10mm. In order to minimise the lift-off effect, during the robot motion, all the sensing units were kept in a way that the minimum effect of lift-off will come and proper results can be achieved.

The proposed inspection robot with permanent magnetic wheels, the GMR sensor array, and other sensing units is depicted in Figure 6.24(a)(b). The robotic tool was created and tested in a lab to ensure that it satisfied all

requirements for inspecting overhead crane girders.
A robotic tool with four specifically designed magnetic wheels and a sensing unit for the examination of overhead crane girder design is implemented and built for the inspection duty, as shown in figure 6.24(a)(b). Lightweight aluminium is used to construct the robotic framework, which incorporates a flexible joint to provide an additional degree of freedom for the robotic chassis' contraction and extension.

The four wheels of the robotic chassis are fastened in a way that makes it simple to remove them for cleaning and reinstall them by simply inserting them into the axle shaft. The controlling and sensing part of robotic tool has been covered in detail in the chapter 5 &6. The designed wheels offer enough adhesion forces so that robot can overcome obstacles and inspect various surfaces.

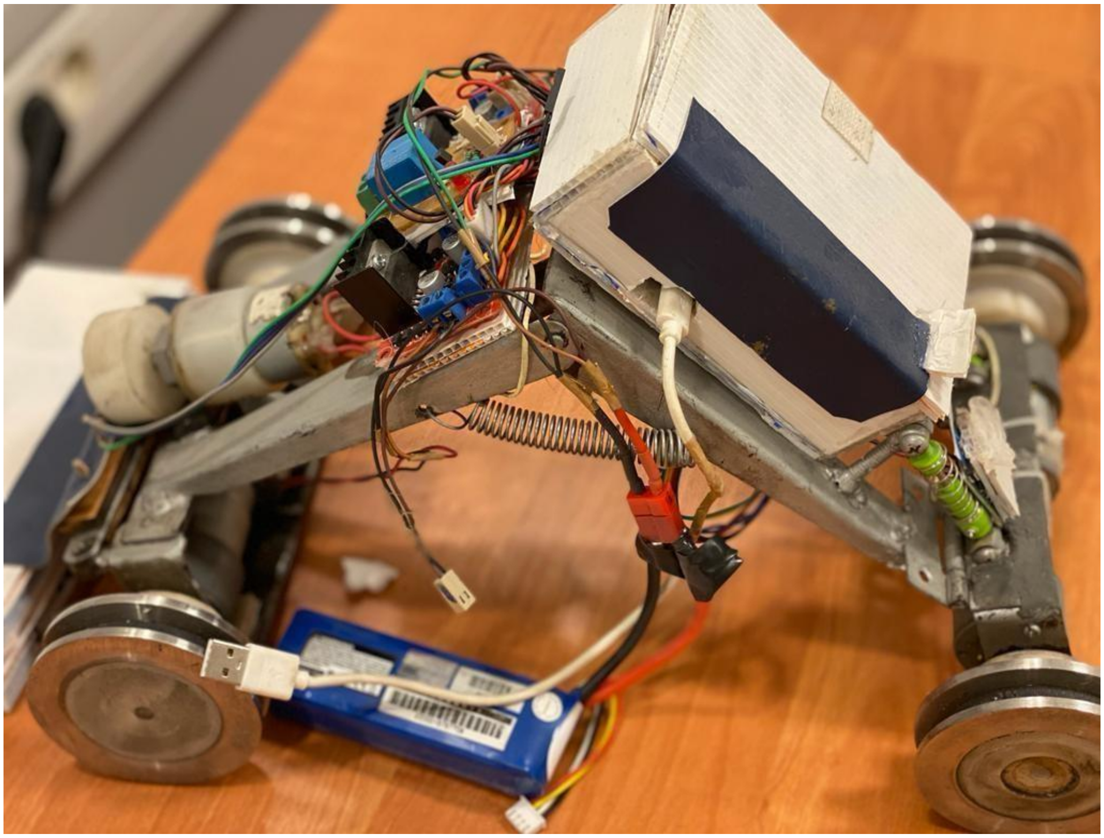

Fig.6. 24(a) Developed robotic tool with sensor unit and power supply

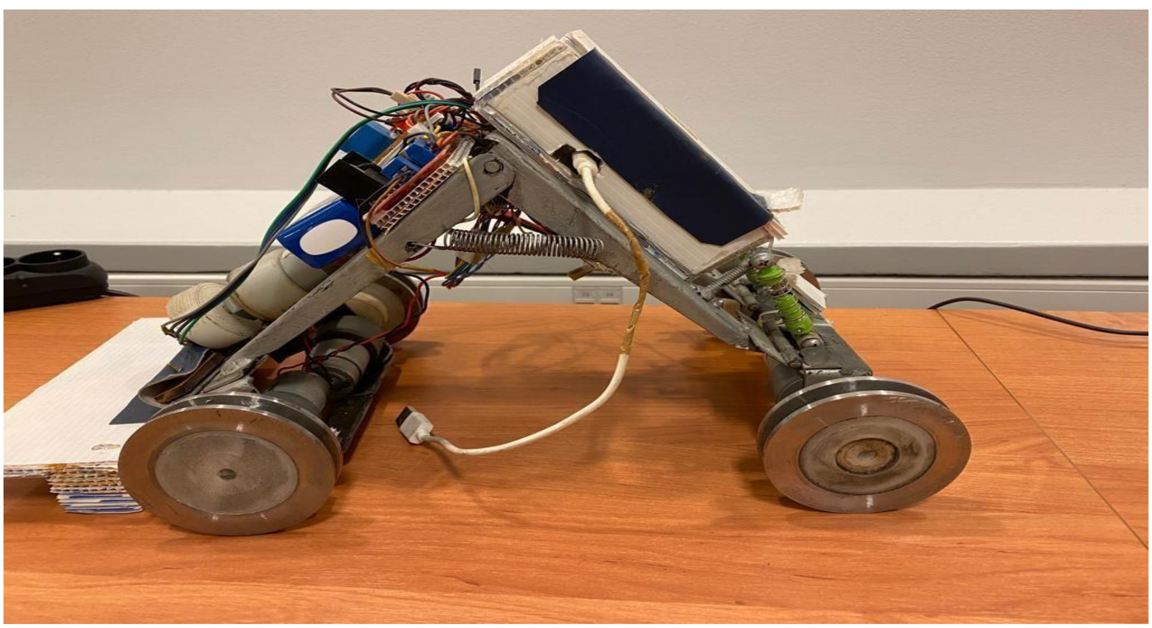

Fig. 6.24 (b) Robotic framework folding mechanism with a flexible joint.

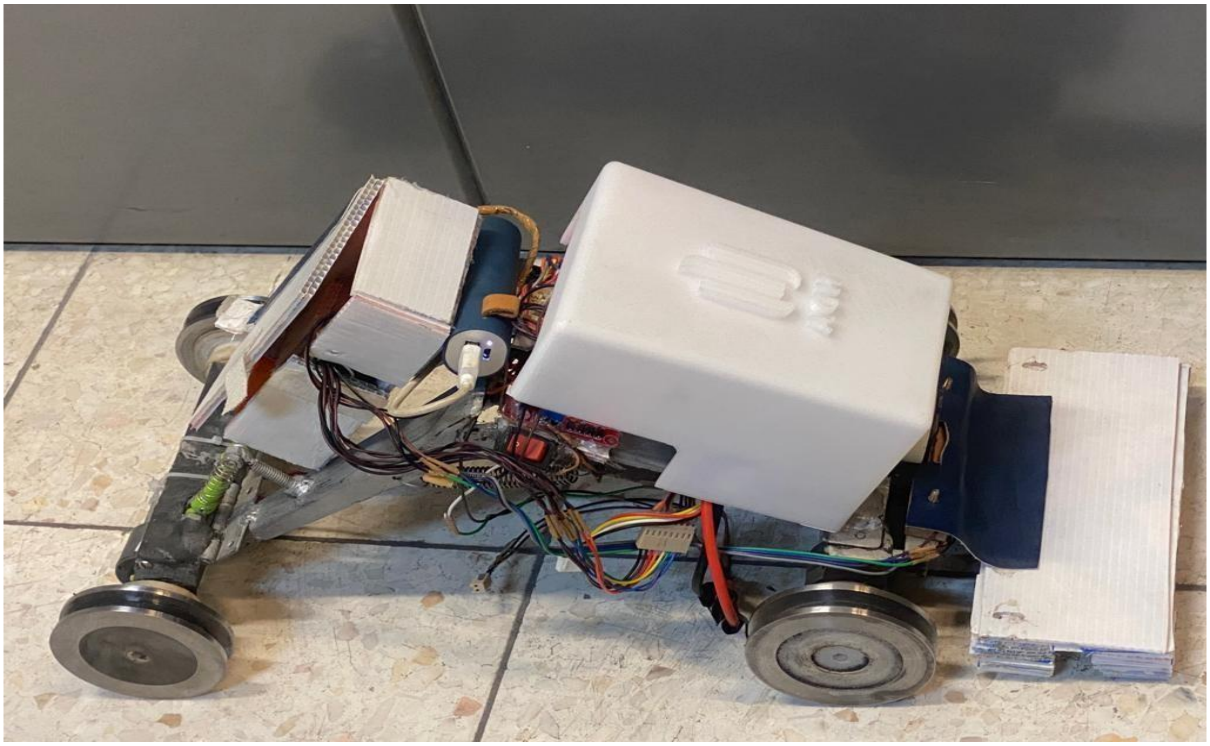

Fig.6. 25 Designed climbing inspection robot equipped with sensing unit and GMR sensor

In Figure 6.25, we can easily see on the rear axle a white stripe of sensing unit is kept at particular height of 5mm. In order to maintain that height, few magnets are placed on the corners of GMR sensor array unit, so that the sensing array will be sticking to the inspection area, in case of bumpy areas. For the experimental purpose, sensing unit is screwed with the robotic chassis, with a blue color leather stripe. The reason of keeping a leather material, is to avoid any extra weight on the GMR sensor unit. Another reason of keeping it simple and easy to mount and dismount the sensing unit on robotic chassis.

The created robot, with the assistance of magnetic wheels, can climb on the metallic surface, a few experiments were conducted to check the adhesion forces and movement of robot on the various cranes surface. Below figure 6.26(A)shows the experimental movement of robot on various surfaces.

Fig.6. 26 (A) Movement of robotic tool on the vertical surface of overhead bridge

Fig. 6.26(B) Movement of robotic tool on an inverted surface against gravity.

The robot's main goal as an inspection robotic tool is to examine the surface for flaws and fractures. For the robotic tool to adhere to the inspection area and complete the inspection duty, it must ascend on the vertical surface against gravity while maintaining sufficient adhesion forces. The robot on the overhead crane bridge is seen in Figure 6.26(a) here, maintaining its robot weight stick on the surface in defiance of gravity. By doing this experiment in lab, we can say that robotic design satisfies the kinematic equation discussed earlier in the chapter 5 and full fills the requirement for inspection

the inspection duty without falling on the ground, it must also roll on the surface to perform inspection.

Figure 6.26 (C) also depicts another case of robot movement on the gantry crane by holding adhesion forces. fractures and metal loss. Making the robot stay on the surface in the face of absolute gravity was the biggest challenge in this project. A complete different view of the robot in motion on the inverted surface of an overhead crane bridge is shown in Figure 6.26(B). It is necessary to examine the bridge and glider from all angles and surfaces to look for any

It is necessary to confirm that the robot satisfies all climbing criteria before beginning the overhead inspection assignment. Numerous experiments were carried out in the lab to verify the movement of the robot at different angles and on different surfaces. In order to confirm that the adhesion forces are enough on varied thickness surfaces, several experiments were also carried out on a variety of surfaces with diverse thicknesses

Fig. 6.26 (C) Movement of robotic tool on the gantry crane

As the robot start rolling on the steel surface, adhesion mechanism provided by magnetic wheels provides sufficient adhesion forces to keep the robot adhere to the steel surface. Once the steel surface gets magnetized by robotic wheels, GMR sensor array, starts inspecting the surface for the any cracks and defects.

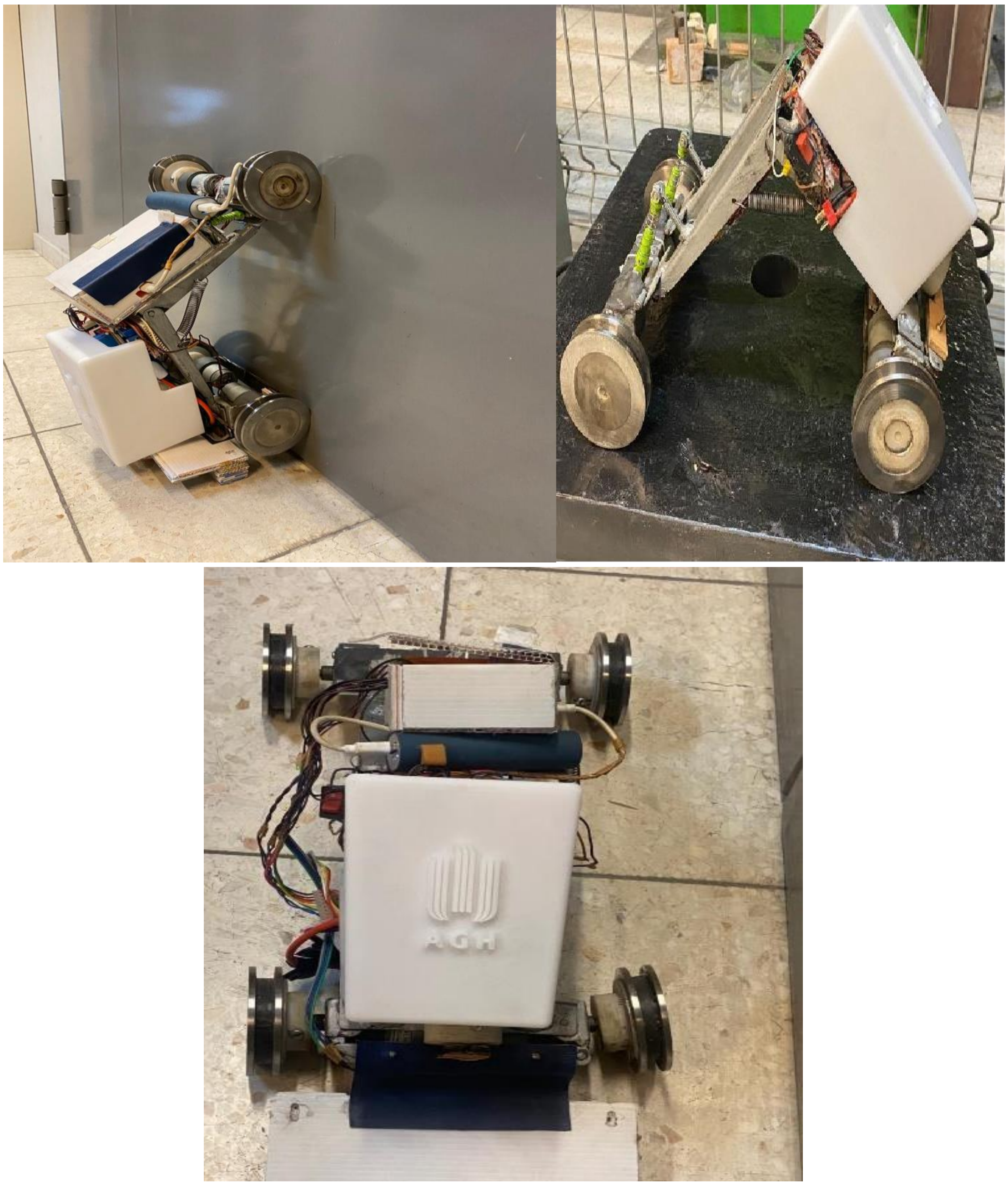

Fig.6. 27 (D) Robot Movement on various surfaces of varying thickens

As we have mentioned earlier, robot is controlled by wireless communication through a mobile phone. Below fig.6.28 depicts the results display and control virtual sticks panel. The functioning and features of virtual key sticks has been covered in table 6.3.

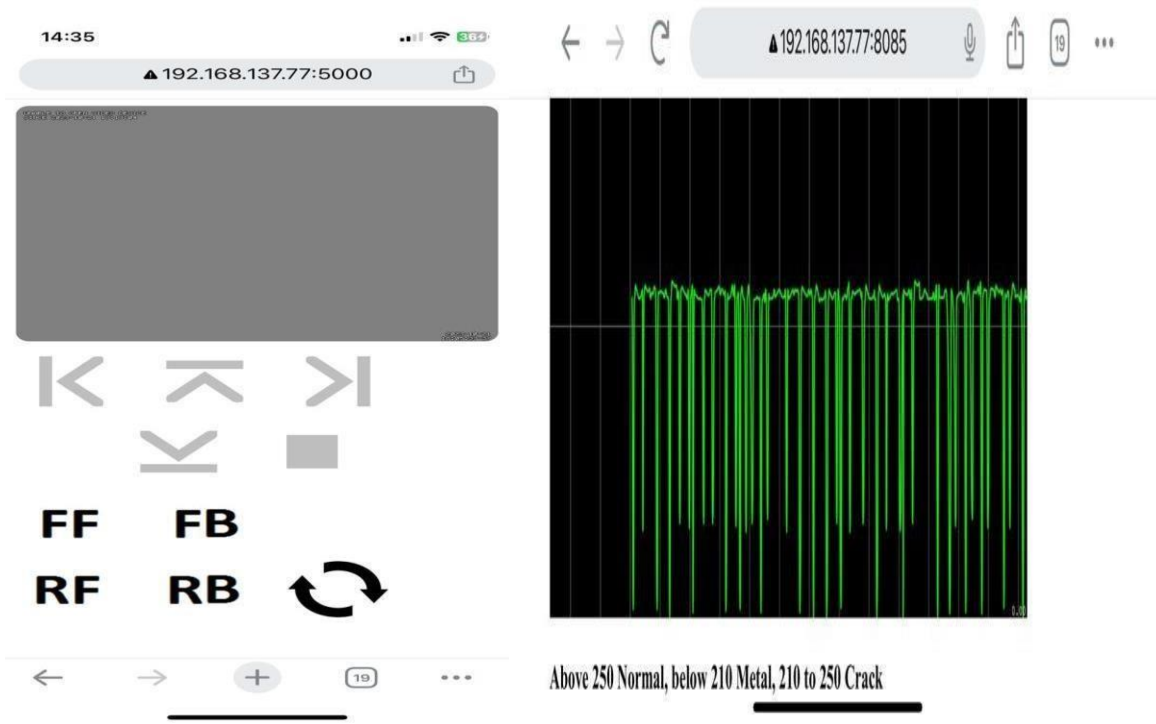

Fig.6. 28 Real time video streaming and real time GMR sensor array results on mobile screen.

Hall sensors and permanent magnets constitute the GMR sensor. The GMR output from the sensors will be transmitted to a distant location and, if necessary, amplified using an instrumentation amplifier. For experimental purposes, a 10-mm-thick steel plate with artificial fractures for characterization was positioned at varying angles (90°, 60°, 45°, and 30°) to the scanning direction. The cracks in the 10-mm-thick inspection steel plate have nominal widths of 0.25 mm, 0.5 mm, 1 mm, and 1.5 mm and depths of 0.5 mm, 1 mm, and 1.5 mm. The GMR sensor array is symmetrically arrayed on a PCB and moves independently in the direction of the robot. In this instance, the magnetic field is perpendicular to the steel plate's surface, and the sensitivity axes of GMR sensors are parallel to it. As the fig. 6.29 (A) depicts the relationship curve the output voltage(Vout) and displacement (mm) with a crack width of 0.5mm(Wn).

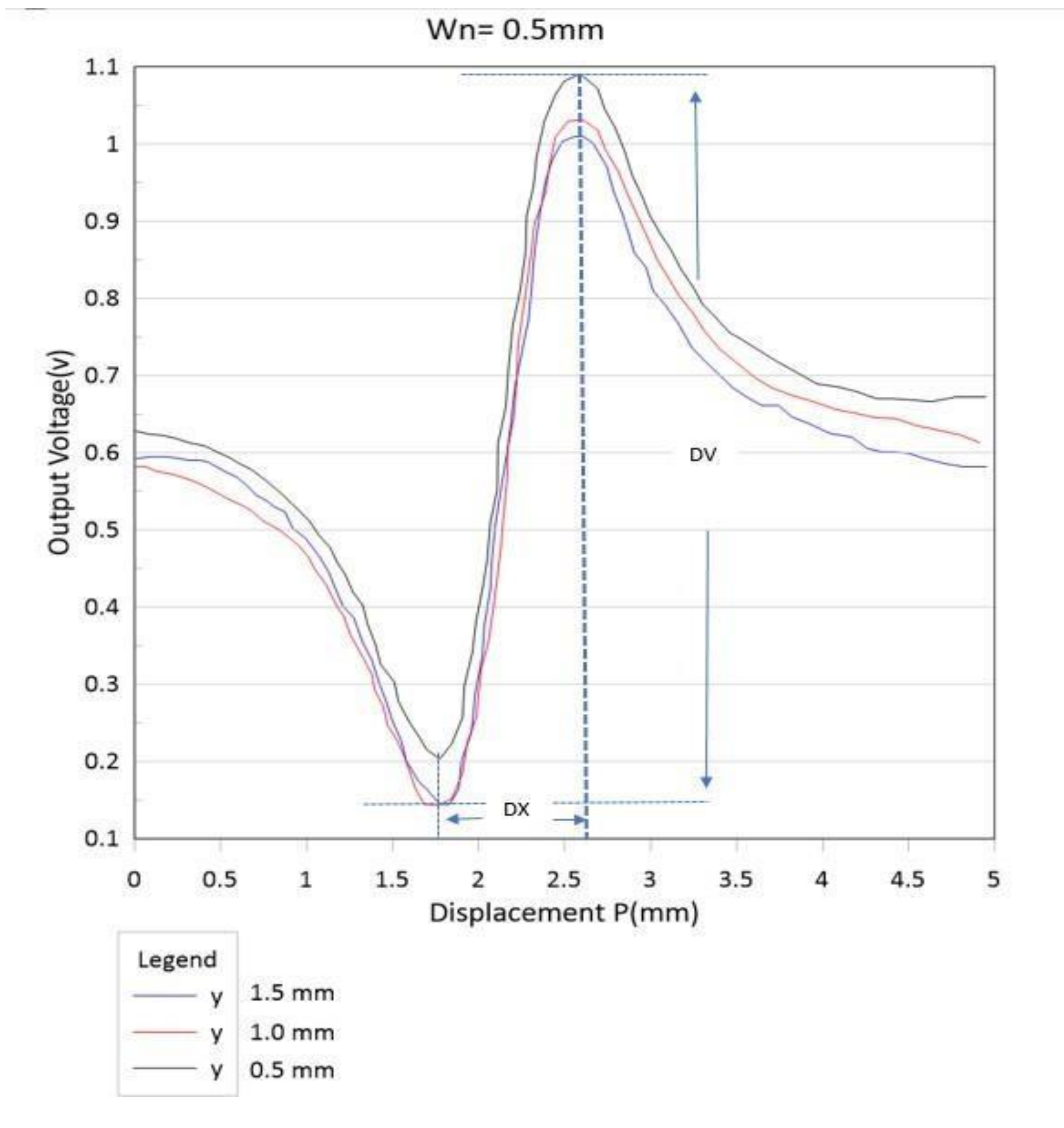

Fig.6. 29(A) GMR Sensor output graph with output voltage and displacement with a width of 0.5mm

We have considered three cracks depth (y) i.e.0.5mm, 1.0mm, 1.5mm. The parameters DV and DX are defined after considering different profiles acquired from graphs. (See Figure 6.29(a)). The voltage variation (DV) and position difference (DX) across peaks are parameters used to investigate the link between the GMR sensor's output voltage and crack feature.

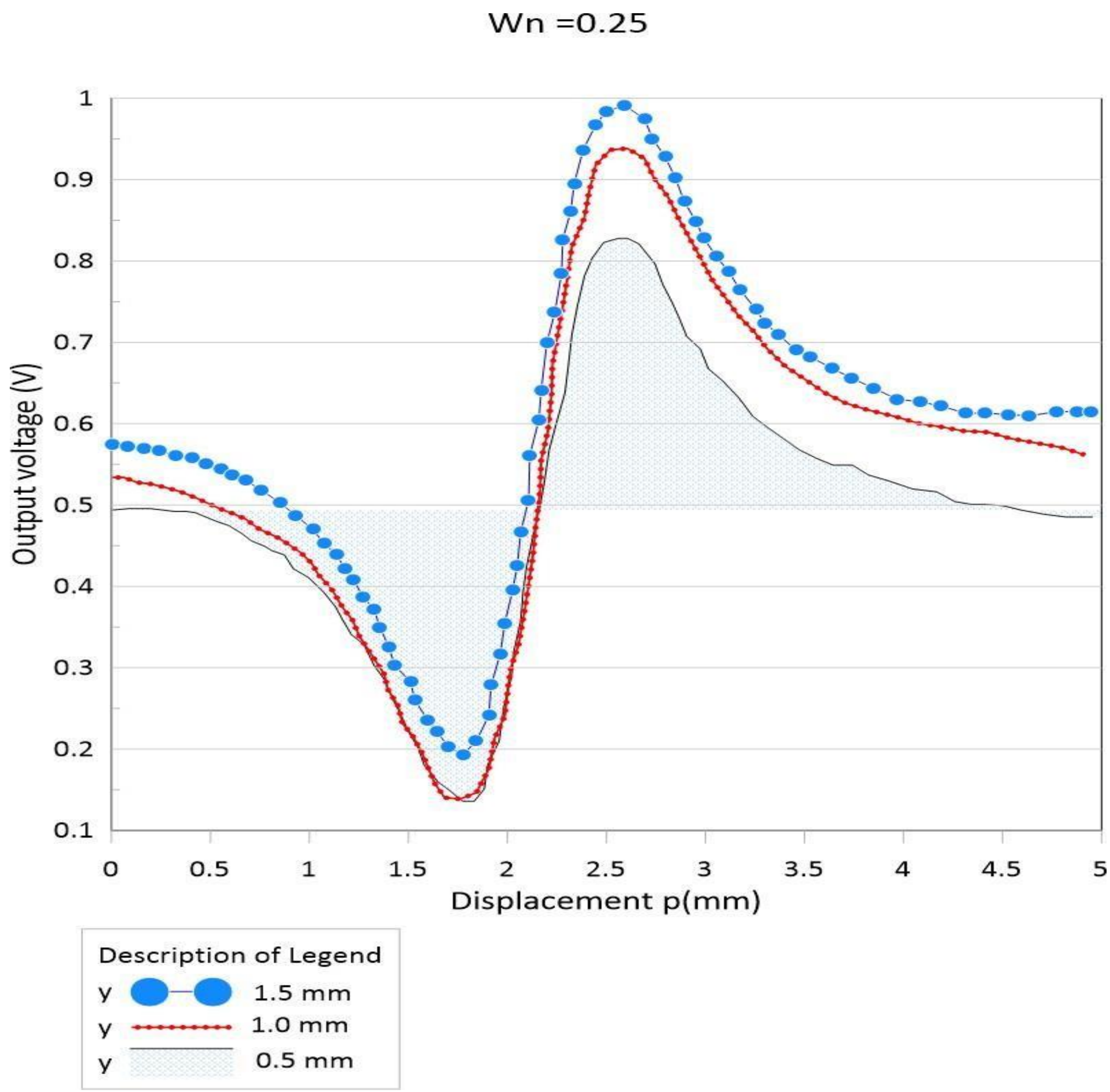

Fig. 6.29 (B) GMR Sensor output graph with output voltage and displacement with a width of 0.5mm

Figures 6.29 (A) and (B) show a symmetrical signal profile centered on the operating point.

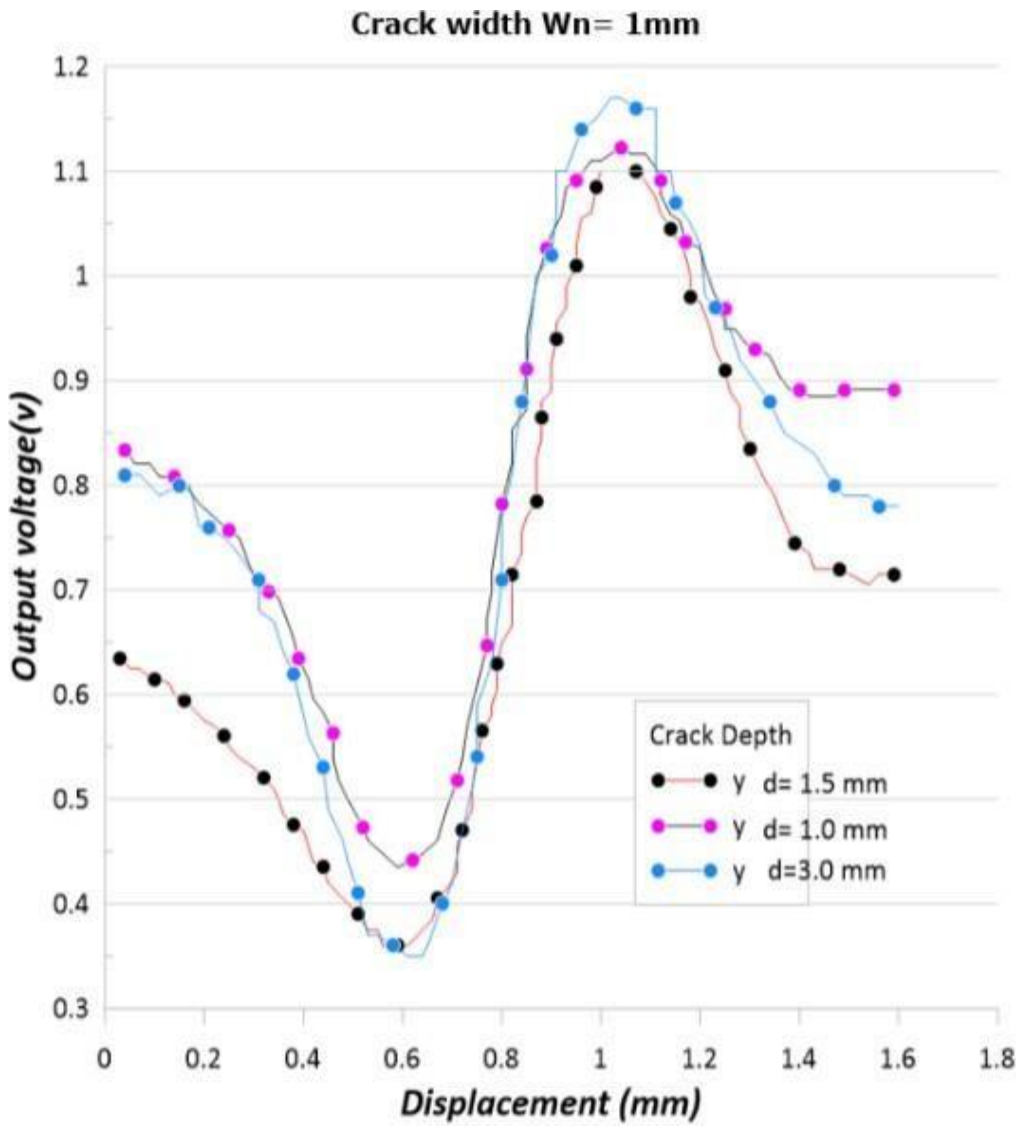

Fig. 6.29 (C) GMR Sensor output graph with output voltage and displacement with a width of 1 mm.

Figures 6.29 (C, D) also represents the graphical relationship between the output voltage and displacement. Here crack width Wn= 1mm, and Wn= 1.5 mm were considered for three crack depths i.e. 1mm,1.5, 3mm. During the experiment, a specimen of a 10 mm thickness steel plate was taken into consideration.

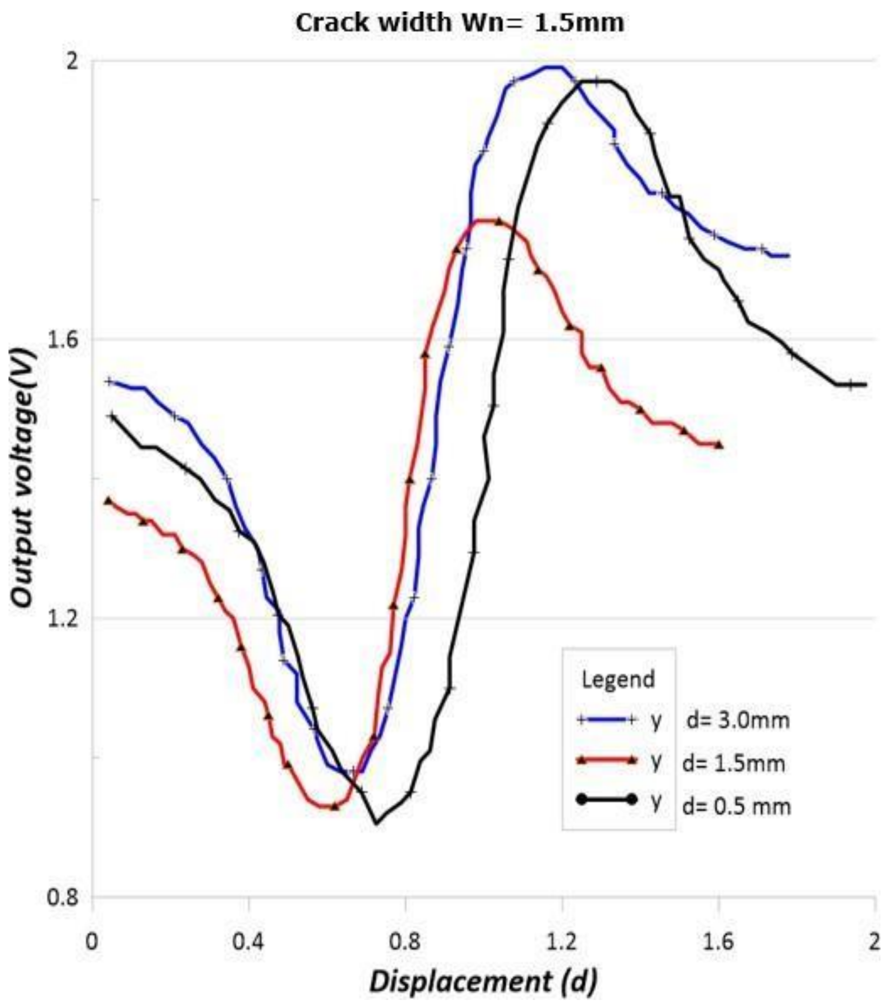

Fig.6.29 (D) GMR Sensor output graph with output voltage and displacement with a width of 1.5 mm

Figure 6.29 depicts the output voltage of the GMR sensor with the axis perpendicular to the fracture length. The graphs show the experimental curves of cracks with nominal widths of 0.25mm, 0.5mm, 1.00mm, and 1.5mm

A supply voltage of variable of 5.5V was supplied to the GMR sensor array to observe the digital output of the GMR sensor. Figure 6.30 presents the experimental output of the GMR sensor on three ferromagnetic steel plates consisting of three cracks of W= 0.25mm, 1.0mm, 1.5mm and crack depths (d)= 0.5mm, 1.0mm, 1.5mm.

The major function of the robotic tool with the GMR sensor configuration is to detect concealed fractures and faults on the surface of overhead crane girders. We ran a few tests before deploying this robotic equipment for inspection to ensure its accuracy and the sorts of problems it can detect. For this aim, we investigated three distinct stainless steel surfaces with established dimensions of fissures, metal loss, and corrosion. Fig. 6.30 also gives an overview of GMR sensor output in the presence of any cracks. The graphs here depict the variation in the sensor voltage with the variation of distance. Figure 6.30 (A) depicts the fluctuation in output voltage of a GMR sensor with a fracture width of 1mm and depths of 0.25, 1.0, and 1.5mm.

The rotating permanent magnetic wheel magnetizes the magnetic surface of the inspection region. Magnetic field lines wrap around the magnetized surface and magnetic wheels in a loop. In the presence of a flaw in the metal surface, the magnetic field of lines becomes distorted, resulting in a variance in magnetic field intensity. The role of GMR sensor setups begins here. Once the GMR sensor detects a change in the magnetic field, the output of the GMR sensor may be observed to be distorted using hall sensors and amplification. The same results for various crack widths presented in fig. 6.30 (B &C).

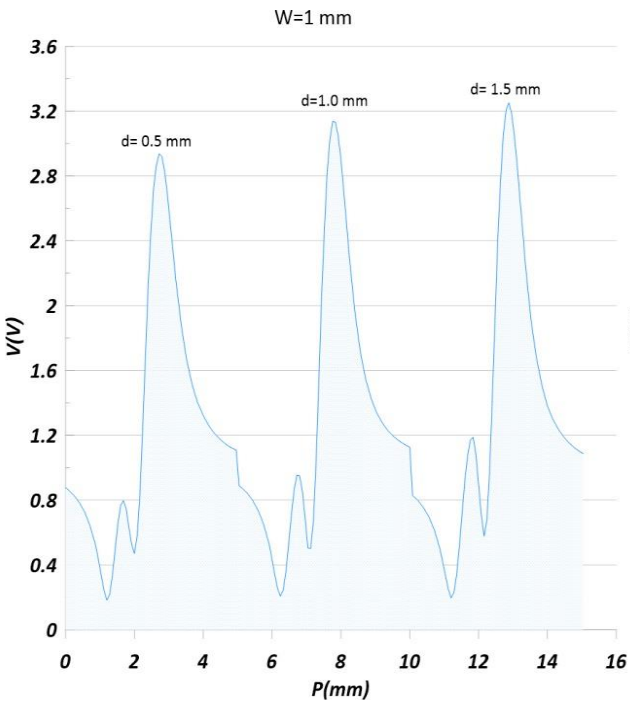

(A)

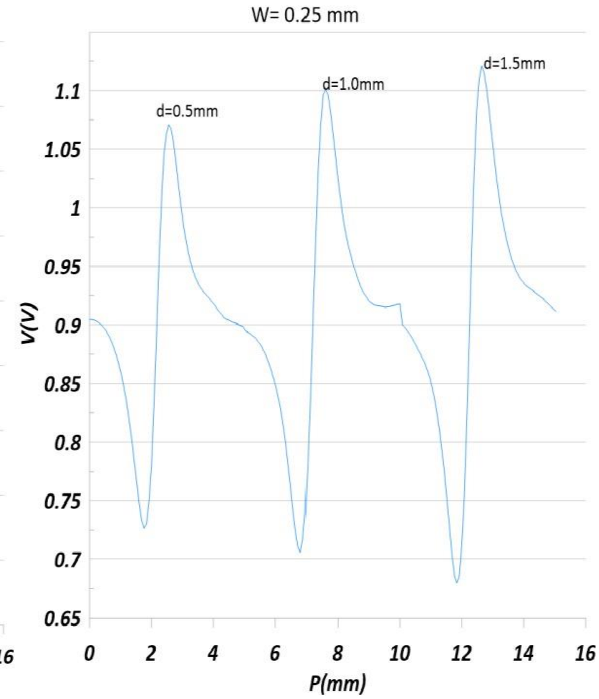

(B)

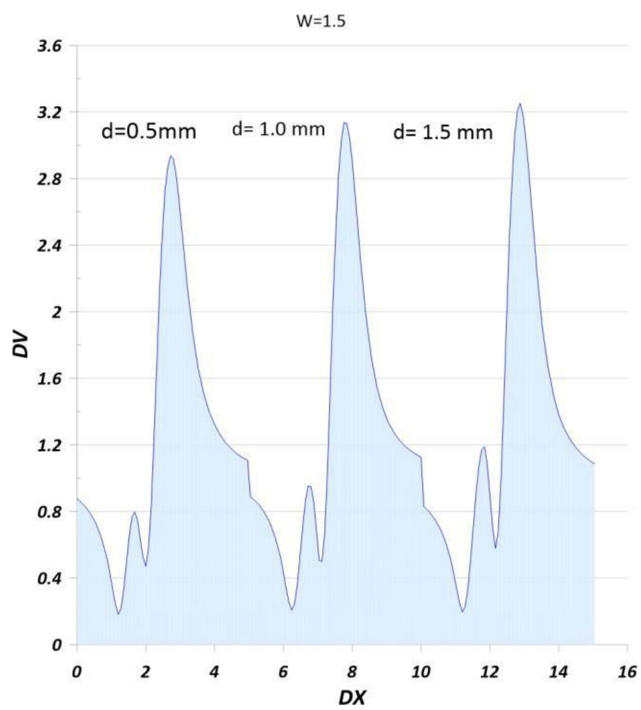

(C)

Fig.6. 30 GMR sensor signals for three ferromagnetic steel plates consisting three cracks with varying cracks depth and crack width

According to past research, this robotic tool can climb on various surfaces and overcome various huddles during climbing. It also satisfies and can detect fractures of variable depth and width on the steel surface Another test is required to determine whether the developed robotic tool with a GMR sensor setup is capable of identifying corrosion and metal loss.

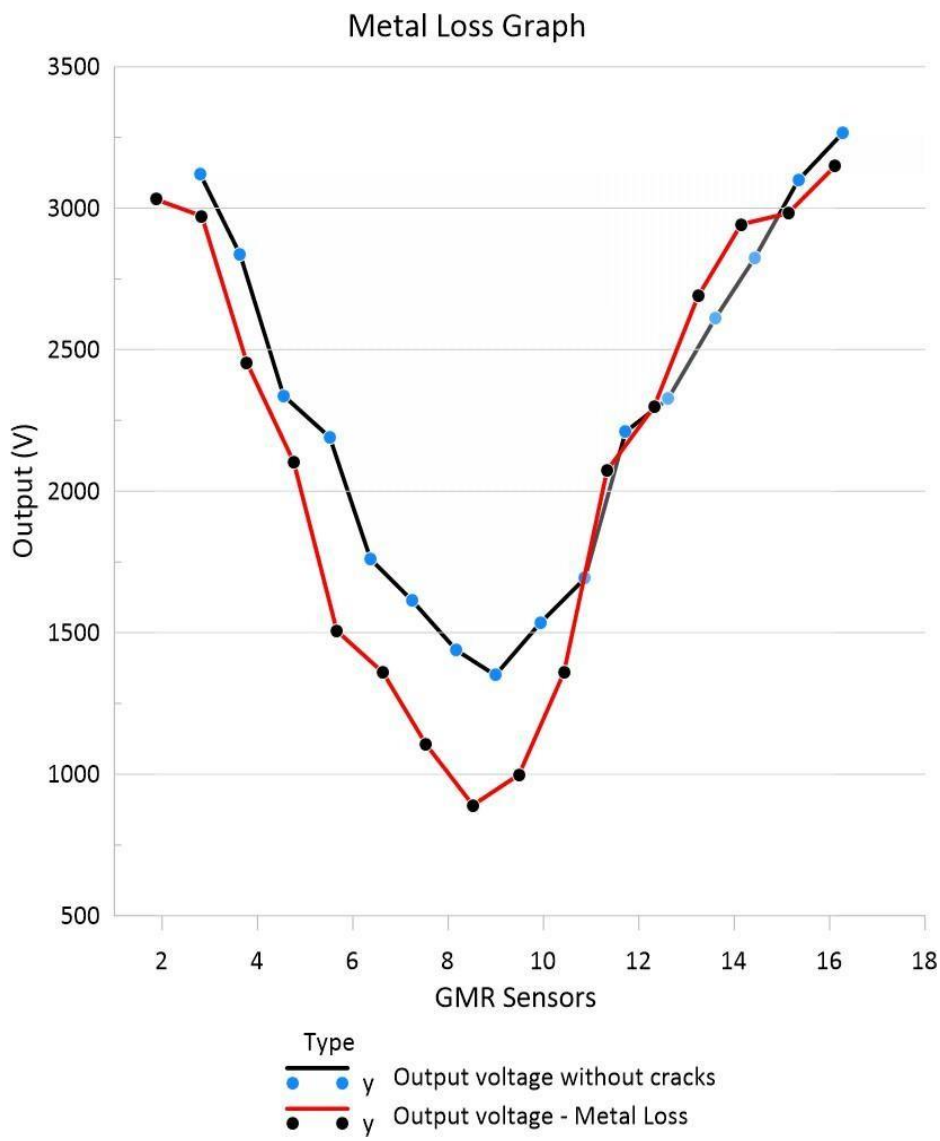

Fig.6. 31 Output voltage signals in case of (a)Metal loss

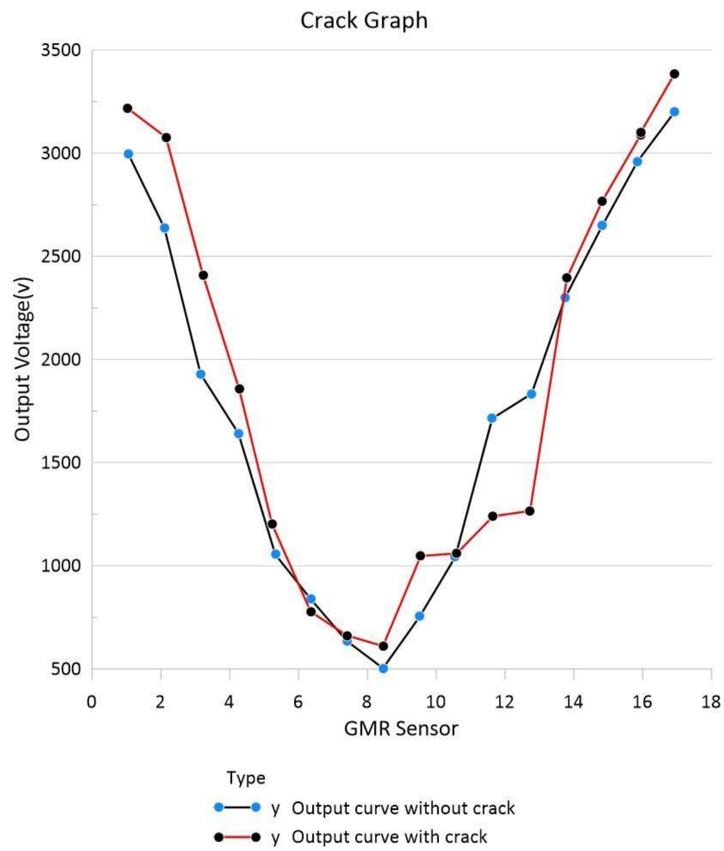

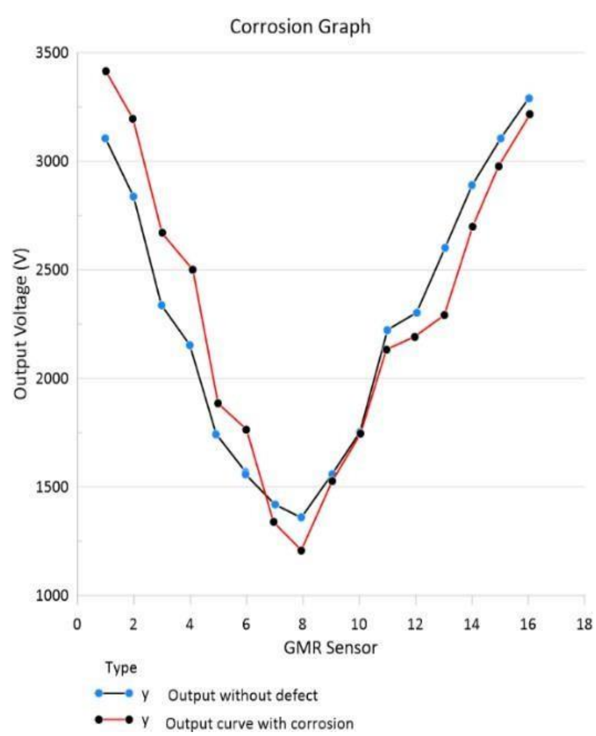

Fig.6.31 Output voltage signals in case of (a)Metal loss (b)Cracks (c)Corrosion

The presence of any cracks on the surface forms a peak in the graph. The peak value indicates that the magnitude of the GMR sensor value is directly proportional to the crack depth. In the second peak is evidenced by the fact that with the increase in depth of the crack, a minor deviation in the output voltage of the GMR sensor unit. Simply by measuring the difference between the maximum peak and minimum peak of GMR output voltage the estimation of crack depth can be determined. By experimental results, we can clearly find out the metal loss due to corrosion, surface and sub-surface defects on the bridge, and girders of the overhead crane

As overhead cranes operate in a variety of environments, it is fair to conclude that the majority of the parts suffer from corrosion, resulting in metal loss. The most difficult issue in detecting corrosion is that it frequently happens under the paint surface region. The surface seems normal upon visual inspection. However, the metal section beneath the paint is losing strength, resulting in the creation of cracks and metal loss.

Fig. 6.31 (a) present the experimental result of GMR sensor in case of metal loss. The graphical red curve shows the relation between the output voltage and GMR sensor in case of metal loss. Similarly, 6.31. (b) (c) depicts the output in case of cracks and corrosion. From the experiments and simulation, it is clear that the robotic tool can automate the inspection process of overhead cranes girders by detecting the cracks, metal loss and corrosion.

CHAPTER 7

FINAL REMARKS AND CONCLUSION

In our day-to-day lives, it is unpredictable to notice the behaviour of overhead cranes under mechanical and environmental loads. With the passage of time, these loads cause the deterioration of overhead crane bridges and spans. Many industrial cranes operate in harsh environmental conditions and fall into the category of structurally deficient before the work life cycle time period due to a lack of inspection and monitoring. Also considering the catastrophe accidents in the past, it is quite critical to introduce some automated real-time health monitoring system to monitor and report where and when maintenance operations are required.

By introducing such a system, we can minimize or avoid catastrophic accidents and extend the lifecycle of overhead cranes at some extend. As of now, a periodic inspection of overhead cranes is performed through a visual inspection by some skilled professionals. The results of inspection vary from person to person in terms of capabilities and experience. When talking about large industries consisting of hundreds of cranes, a visual inspection is not cost-effective and time-consuming. The downtime for the inspection of cranes reduces production and overall loss to the companies. Secondly, the availability of skilled workers in a given time frame is also sometimes another challenge.

The safety and security of the inspection person are another important factor that inspired me to undertake this task. It is a risky job for the inspector to check the enormous crane in a dangerous environment. Sometimes the inspection areas are inaccessible to perform the inspection work.

Overall, to perform this research work, it was considered necessary to purposefully design a systematic and automated approach to monitor and inspect the overhead crane bridges. This research work offers an automated robotic tool with a non-destructive methodology employing a developed GMR sensor array to detect fractures and faults in the construction of overhead crane bridges. This proposed system is cost-effective, sustainable, and offers reliability and safety in order to perform the inspection task. As the inspection task is performed by the robot, human errors and mistakes can be minimized and highly accurate results can be achieved. The system offers real-time monitoring data that can be live streamed to a remote location and stored for future case studies.

Therefore, the primary reason for doing this research is to develop a sophisticated automated robotic with a GMR sensing unit for the non-destructive examination of overhead crane bridges and girders. By doing this, we can reduce the cost of inspection, improve inspection accuracy, prevent significant accidents, boost the safety and dependability of overhead crane operations, and reduce the amount of time overhead cranes are out of service during inspection.

This full research work is primarily divided into two parts based on functionality and design. The first section was the design and fabrication of the flexible structure of the robot tool with the specifically designed magnetic wheels composed of permanent magnets.
The second part consists of the development and design of electronic parts, sensing systems, controlling and monitoring, networking, and programming. The GMR sensor array was used to create an effective sensing system for detecting metal loss, flaws, and fractures.

This doctoral dissertation is organized into seven chapters in general. Chapter 1: Thesis Introduction, Overview of Cranes, Classification of Cranes, and Main Crane Components with problem.

Chapter 2. It includes the earlier work that academics have done on inspection robots for various purposes and sectors. The designs and sensing technology utilized for the inspection work were demonstrated in the earlier study. A range of inspection robots, including some flying robots, crawling robots, and climbing robots, have been thoroughly described in this chapter. In-depth coverage is also given to the modes of functioning and climbing mechanisms. An overview of the drawbacks is provided in this chapter by evaluating the prior studies. The overall result of the literature review is then provided.

Chapter 3: The first half of this chapter, which describes our revolutionary research endeavor, discusses the creation of a specific magnetic wheel employing permanent Neodymium magnets. The magnetic wheels for climbing robots that have previously been created are shown at the beginning of each chapter. A list of the shortcomings of earlier wheel designs is also provided. A few designs for magnetic wheels were suggested using the influence of earlier designs. The specifications needed for our climbing robot were taken into account when creating a specific design and wheel. Additionally, some experimental findings of magnetic flux change via FEMM are shown.

Chapter 4: The components needed to build the robotic system are thoroughly described in this chapter. Described in this chapter are mostly electronics components and their intended uses.

Chapter 5: It comprises and encompasses the creation of a flexible robotic structure, which is the initial phase of the research project. The steering mechanism, adhesion mechanisms, and kinematics of the robot on various angles and surface areas have all been demonstrated together with a robotic design for climbing on overhead cranes.

Chapter 6: The study of the non-destructive device's data using the GMR sensor is the primary emphasis of this chapter. The merits and disadvantages of a few NDT procedures, including eddy current testing, ultrasonic testing, and others, were reviewed at the beginning of the chapter. The GMR sensor sensing technology's properties and benefits of employing GMR sensors for sensing in robotic systems have been given. This chapter includes discusses the conceptualization of the GMR sensing array as well as the sensor array's output during the experiment. The controlling, architecture, and flow diagrams of robotic systems are explored in the later part of this chapter. This section contains information on the GMR sensor output graphs, the lift-off impact on the sensor array, and the robot control arrangement with programming.

Chapter 7: This chapter conclude the motivation of this research work and also offer future recommendations to enhance the research work by implementing some future modifications in this research work.

The flexible robot construction in Chapter 5 not only allows the robot to climb solely on flat surfaces, but it also avoids corners. This allows the robot to operate on both concave and convex surfaces. In order to ascend vertical surfaces, specially developed magnetic wheels, as stated in Chapter 3, have been utilized to maintain correct adhesion forces. Once the tool is ready to roll on the steel girder, a sensing part has been designed to inspect the cracks in the metal structure. In Chapter 6, a very effective, efficient, and reliable GMR sensor array was created by using a configuration of hall sensors and permanent magnetic rings that can recognize any change in magnetic flux during the inspection procedure.

In order to navigate the robot and collect real-time results, a wireless communication system was established. To make this inspection process user-friendly, a graphic user interface has been provided on a mobile phone. The user can control the robot by using the virtual joysticks on their mobile phone and get the real-time GMR sensor graph on the phone screen. The detailed communication connections and architecture have been covered in Chapter 6.

This study introduces a novel approach for detecting corrosion and cracks on the bridges of overhead cranes by combining a GMR sensor with a flexible climbing robotic framework. The mobility flexibility given by this robot design enables considerably quicker, more secure, and more complete inspections to be performed at a lower cost.

A magnetic-based GMR sensor array mounted on a climbing robot is proposed for detecting corrosion and fracture inspection on overhead crane steel bridges.

This thesis presents a various distinct design for magnetic wheels that can be used on the climbing robot. The fundamental issue of magnetic wheel design in past research was to keep the wheel light while yet providing appropriate adherence and friction force. Previous studies always covered the magnetic wheel's tread with a rubber tire to boost its friction coefficient. The adhesion force, however, drops noticeably due to the rubber tire's increased friction coefficient. An innovative magnetic wheel design is introduced to address this issue. When a magnetic circuit is combined with a rubber tire with a serrated tread, the adhesion force and friction coefficient are greatly improved. The magnetic wheel, as demonstrated in the studies, can create an adhesion force equivalent to 26 its own weight, and the coefficient of friction can be increased to 0.7-0.85. The wheel is under 200g in weight.

The portability, light weight, and responsive control of these robots are significant benefits. System designs include those for driving, steering, bending, twisting, and suspension. The robot is capable of achieving a remarkable variety of obstructions, including stairs, slanted and sloping walls, and bolts. The robot can now manoeuvre around concave curves thanks to a bending technology that incorporates an active-passive compliant joint. The robot weighs only 4.5 kg and measures 35 cm by 25 cm by 15 cm. To verify the robot's mobility and identify its limits, experimental testing is carried out in the real world. The robot can travel at a top speed of 0.32 m/s and can travel at a steady 0.18 m/s on average. The highest bolt that can be overcome by the robot is 30mm.

Non-destructive testing techniques such as eddy current and magnetic flux are commonly used to check the steel girders of overhead cranes. However, as we have seen in previous chapters, each of these techniques has limits when it comes to inspecting steel bridges. Both approaches are ineffective in detecting corrosion and early metal loss on a large metal surface. A GMR sensor array paired with a Hall sensor has been designed to detect metal loss in its early phases.

Modern inspection procedures rely heavily on lift-off values, which must be kept constant during the test. The built GMR sensor array positioned above the robot's back axle wheel offers precise results when analysing the conditions of the two sites. The GMR sensor measures the fluctuation in magnetic flux lines to identify any metal loss or fractures, and the fault is shown as a peak on the graph.

The newly designed robot may function in either autonomous or semi-autonomous modes. The user uses a specific syntax to send an SMS command from any carrier. When the robot receives the precise instructions with the coordinates for the inspection region, it will travel there and begin the inspection operation. Real-time data can be viewed on a user's phone or computer screen. In our experiment, a real-time graph will be displayed on the user's display screen, which is a phone.

In another mode of operation, a person may control the robot's movement via a cell phone's display. The screen is split into two halves. The first portion has virtual control sticks, while the second shows a real-time graph of the GMR sensor's data. We can spot metal loss and corrosion on the surface using the graph data and take the appropriate steps.

An automated specialized robot for detecting cracks, corrosion and other types of defects in crane girders using non-destructive testing techniques was developed and build. The robot is equipped with a series of giant magnetoresistance (GMR) sensors, it can also carry other types of specialized sensors, collect measurement data and send them to a remote station for collecting and processing test results in real time for decision-making purposes.

By merging all of the study chapters, we arrived at the anticipated output of this research work, which is an entirely novel approach for crane girder inspection. A novel way for damage identification in overhead crane girders has been devised using the robot as a tool and GMR sensing, a non-destructive testing methodology. The primary goal of this study was to provide a solution and approach for automating the inspection process. The objective of the research was achieved by combining a flexible-structure robot with four magnetic wheels and an array of GMR sensor

Future work can be done by equipping the robot with a cleaning mechanism. As steel bridges are exposed to the environment, dirt and other debris accumulate on their surfaces. This robot can inspect the surface of steel, but if the surface is dirty or greasy, a cleaning mechanism must be implemented. Future work can incorporate an efficient scrubbing mechanism into the same design to enable this robot to operate on a variety of surfaces. Another addition that can be done for the future work is to integrate the MMM sensor on the robotic structure. As the MMR sensor also offers accurate result, it will be noticeable and effective to integrate the MMM sensor with this designed robotic tool. In addition, at this moment, this research is particularly focused for the inspection of overhead crane girders only. But in future using the same robotic tool and methodology, this inspection approach can be implemented for the inspection in various industries for another equipment's as well.

In the end it is right to mention by performing this research, a cost-efficient, flexible versatile, safe and reliable, and faster inspection methodology came in the real time monitoring and inspection for the overhead crane girders.

REFERENCES

1. **Aguila-Muñoz, J., Espina-Hernández, J. H., Pérez-Benítez, J. A., Caleyo, F., & Hallen, J. M. (2016).** A magnetic perturbation GMR-based probe for the non-destructive evaluation of surface cracks in ferromagnetic steels. *NDT & E International*, *79*, 132-141. doi: 10.1016/J.NDTEINT.2016.01.004.
2. **Ahmed, M., Eich, M., & Bernhard, F. (2015).** Design and control of MIRA: A lightweight climbing robot for ship inspection. *International Letters of Chemistry, Physics and Astronomy*, *55*, 128-135. doi: 10.18052.
3. A**lper, M., Attenborough, K., Hart, R., Lane, S. J., Lashmore, D. S., Younes, C., & Schwarzacher, W. (1993).** Giant magnetoresistance in electrodeposited superlattices. *Applied physics letters*, *63*(15), 2144-2146. doi: 10.1063/1.110567.
4. **Balaguer, C., Virk, G., & Armada, M. (2006)**. Robot applications against gravity. *IEEE Robotics & Automation Magazine*, *13*(1), 5-6. doi: 10.1109/MRA.2006.1598045.
5. **Bansal, N., Lahiri, K., & Raghunathan, A. (2007,)**. Automatic power modeling of infrastructure ip for system-on-chip power analysis. In *20th International Conference on VLSI Design held jointly with 6th International Conference on Embedded Systems (VLSID'07)* (pp. 513-520). IEEE. doi: 10.1109/VLSID.2007.46.
6. **Burmeister, A., Pezeshkian, N., Talke, K., Ostovari, S., Everett, H. R., Hart, A., ... & Nguyen, H. G. (2014).** *Design of a multi-segmented magnetic robot for hull inspection*. SPACE AND NAVAL WARFARE SYSTEMS CENTER PACIFIC SAN DIEGO CA.
7. **Cai, J., He, K., Fang, H., Chen, H., Hu, S., & Zhou, W. (2017**). The design of permanent-magnetic wheeled wall-climbing robot. In *2017 IEEE International Conference on Information and Automation (ICIA)* (pp. 604-608). IEEE. doi: 10.1109/ICINFA.2017.8078979.
8. **Chen, L., Que, P. W., & Jin, T. (2005).** A giant-magnetoresistance sensor for magnetic-flux-leakage non-destructive testing of a pipeline. *Russian Journal of Non-destructive Testing*, *41*, 462-465. doi: 10.1007/S11181-005-0193-7.
9. **Ciszewski, M., Wacławski, M., Buratowski, T., Giergiel, M., & Kurc, K. (2015).** Design, modelling and laboratory testing of a pipe inspection robot. *Archive of mechanical engineering*, *62*(3), 395-407. doi: 10.1515/MECENG-2015-0023.
10. **Deraemaeker, A. (2010)**. Vibration Based Structural Health Monitoring Using Large Sensor Arrays: Overview of Instrumentation and Feature. *New Trends in Vibration Based Structural Health Monitoring*, *520*, 19. doi: 10.1007/978-3-7091-0399-9_2.
11. **Dixon, W. E. (2001)** "Nonlinear control of wheeled mobile robots," p. 195.
12. **Dogaru, T., & Smith, S. T. (2001).** Giant magnetoresistance-based eddy-current sensor. *IEEE Transactions on magnetics*, *37*(5), 3831-3838. doi: 10.1109/20.952754.

13. **Dryanovski, I., Valenti, R. G., & Xiao, J. (2013).** An open-source navigation system for micro aerial vehicles. *Autonomous Robots*, *34*, 177-188. doi: 10.1007/S10514-012-9318-8.
14. **Du, W., Nguyen, H., Dutt, A., & Scallion, K. (2010, November)**. Design of a GMR sensor array system for robotic pipe inspection. In *SENSORS, 2010 IEEE* (pp. 2551-2554). IEEE. doi: 10.1109/ICSENS.2010.5690126.
15. **Dulimarta, H., & Tummala, R. L. (2002, June)**. Design and control of miniature climbing robots with nonholonomic constraints. In *Proceedings of the 4th World Congress on Intelligent Control and Automation (Cat. No. 02EX527)* (Vol. 4, pp. 3267-3271). IEEE. doi: 10.1109/WCICA.2002.1020138.
16. **Durai, M., Lan, C. W., & Chang, H. (2022).** In-line detection of defects in steel pipes using flexible GMR sensor array. *Journal of King Saud University-Science*, *34*(2), 101761.
17. **Eich, M., & Vögele, T. (2011, June**). Design and control of a lightweight magnetic climbing robot for vessel inspection. In *2011 19th Mediterranean Conference on Control & Automation (MED)* (pp. 1200-1205). IEEE. doi: 10.1109/MED.2011.5983075.
18. **eLCOSH (2022):** Crane-Related Deaths in Construction & Recommendations for Their Prevention." https://www.elcosh.org/document/1781/d000823/Crane-Related+Deaths+in+Construction+%2526+Recommendations+for+Their+Prevention.html (accessed May 04, 2022).
19. **F.Howlader., & Sattar, T. P. (2015)**. Novel adhesion mechanism and design parameters for concrete wall-climbing robot. In *2015 SAI Intelligent Systems Conference (IntelliSys)* (pp. 267-273). IEEE. doi: 10.1109/INTELLISYS.2015.7361153.
20. **Fernández, R., González, E., Feliú, V., & Rodríguez, A. G. (2010, November).** A wall climbing robot for tank inspection. An autonomous prototype. In *IECON 2010-36th Annual Conference on IEEE Industrial Electronics Society* (pp. 1424-1429). IEEE. doi: 10.1109/IECON.2010.5675473
21. **Ferreira, C. Z., Conte, G. Y. C., Avila, J. P. J., Pereira, R. C., & Ribeiro, T. M. C. (2014), November).** Underwater robotic vehicle for ship hull inspection: control system architecture. In *International Congress of Mechanical Engineering*. Accessed: Jan. 22, 2022. [Online]. Available: http://www.eca-robotics.com/ftp/ecatalogue/216/Roving-Bat.pdf.
22. **Fischer, W., Tâche, F., & Siegwart, R. (2007, October).** Inspection system for very thin and fragile surfaces, based on a pair of wall climbing robots with magnetic wheels. In *2007 IEEE/RSJ International Conference on Intelligent Robots and Systems* (pp. 1216-1221). IEEE. doi: 10.1109/IROS.2007.4399060.
23. **Fondahl, K., Eich, M., Wollenberg, J., & Kirchner, F. (2012, April)**. A magnetic climbing robot for marine inspection services. In *Proceedings of 11th International*

Conference on Computer and IT Applications in the Maritime Industries. [Online]. Available: http://202.114.89.60/resource/pdf/5160.pdf.

24. **Hillenbrand, C., & Berns, K. (2006).** Inspection of surfaces with a manipulator mounted on a climbing robot. In *37th International Symposium on Robotics (ISR)* (p. 8).
25. **Hossain, S. A., Pirkle, B. H., & Parker, M. R. (1996)**. Design and fabrication of GMR multilayers with enhanced thermal stability. *Journal of magnetism and magnetic materials*, *156*(1-3), 303-305. doi: 10.1016/0304-8853(95)00877-2.
26. **Hussain, S., Sattar, T., & Salinas, E. (2012).** Parameter analysis and design framework for magnetic adhesion wall climbing wheeled robot. *International Journal of Intelligent Systems Technologies and Applications*, *11*(1-2), 102-116. doi: 10.1504/IJISTA.2012.046546.
27. **Ishizu, K., Sakagami, N., Ishimaru, K., Shibata, M., Onishi, H., Murakami, S., & Kawamura, S. (2012).** Ship hull inspection using a small underwater robot with a mechanical contact mechanism. In *2012 Oceans-Yeosu* (pp. 1-6). IEEE. doi: 10.1109/OCEANS-YEOSU.2012.6263543.
28. **Jahanshahi, M. R., Shen, W. M., Mondal, T. G., Abdelbarr, M., Masri, S. F., & Qidwai, U. A. (2017).** Reconfigurable swarm robots for structural health monitoring: a brief review. *International Journal of Intelligent Robotics and Applications*, *1*, 287-305. doi: 10.1007/S41315-017-0024-8
29. **Kalra, L. P., & Gu, J. (2007).** An autonomous self-contained wall climbing robot for non-destructive inspection of above-ground storage tanks. *Industrial Robot: An International Journal*. doi: 10.1108/01439910710727469/FULL/XML.
30. **Kataoka, Y., Murayama, S., Wakiwaka, H., & Shinoura, O. (2002)**. Application of GMR line sensor to detect the magnetic flux distribution for non-destructive testing. *International Journal of Applied Electromagnetics and Mechanics*, *15*(1-4), 47-52. doi: 10.3233/JAE-2002-427.
31. **Khan, A. H., Li, S., & Luo, X. (2019).** Obstacle avoidance and tracking control of redundant robotic manipulator: An RNN-based metaheuristic approach. *IEEE transactions on industrial informatics*, *16*(7), 4670-4680. doi: 10.1109/TII.2019.2941916.
32. **Kozłowski, K., & Pazderski, D. (2004).** Modeling and control of a 4-wheel skid-steering mobile robot. *International journal of applied mathematics and computer science*, *14*(4), 477-496.
33. **Kral, J., Smid, R., Ramos, H. M. G., & Ribeiro, A. L. (2013).** The lift-off effect in eddy currents on thickness modeling and measurement. *IEEE Transactions on Instrumentation and Measurement*, *62*(7), 2043-2049. doi: 10.1109/TIM.2013.2247713.
34. **Krampfner, Y. D. (1988).** Flexible substrate eddy current coil arrays. *Review of Progress in Quantitative NDE, A*, *7*, 471-478. Accessed: Jan. 29, 2022. [Online]. Available: https://ci.nii.ac.jp/naid/10024610487.

35. **La, H. M., Dinh, T. H., Pham, N. H., Ha, Q. P., & Pham, A. Q. (2019).** Automated robotic monitoring and inspection of steel structures and bridges. *Robotica*, *37*(5), 947-967. doi: 10.1017/S0263574717000601.
36. **Lee, G., Seo, K., Lee, S., Park, J., Kim, H., Kim, J., & Seo, T. (2011, December).** Compliant track-wheeled climbing robot with transitioning ability and high-payload capacity. In *2011 IEEE International Conference on Robotics and Biomimetics* (pp. 2020-2024). IEEE. doi: 10.1109/ROBIO.2011.6181588.
37. **Lim, R. S., La, H. M., & Sheng, W. (2014).** A robotic crack inspection and mapping system for bridge deck maintenance. *IEEE Transactions on Automation Science and Engineering*, *11*(2), 367-378. doi: 10.1109/TASE.2013.2294687.
38. **Liu, K. P., Luk, B. L., Tong, F., & Chan, Y. T. (2011).** Application of service robots for building NDT inspection tasks. *Industrial Robot: An International Journal*, *38*(1), 58-65. doi: 10.1108/01439911111097850/FULL/XML.
39. **Liu, Q., & Liu, Y. (2013, December)**. An approach for auto bridge inspection based on climbing robot. In *2013 IEEE International Conference on Robotics and Biomimetics (ROBIO)* (pp. 2581-2586). IEEE. doi: 10.1109/ROBIO.2013.6739861
40. **Lu, Q., Wang, L., Xin, J., Tian, H., Wang, X., & Cui, Z. (2020).** Corrosion evolution and stress corrosion cracking of E690 steel for marine construction in artificial seawater under potentiostatic anodic polarization. *Construction and Building Materials*, *238*, 117763. doi: 10.1016/J.CONBUILDMAT.2019.117763.
41. **Mancoff, F. B., Dunn, J. H., Clemens, B. M., & White, R. L. (2000).** A giant magnetoresistance sensor for high magnetic field measurements. *Applied Physics Letters*, *77*(12), 1879-1881. doi: 10.1063/1.1311316.
42. **Meystre, P., (2008)** Sears and Zemansky's University physics: with modern physics., 12th ed. /., vol. 333, no. 6044. San Francisco: Pearson Addison Wesley.
43. **Morin, P., & Samson, C. (2003).** Practical stabilization of driftless systems on Lie groups: the transverse function approach. *IEEE Transactions on Automatic control*, *48*(9), 1496-1508. doi: 10.1109/TAC.2003.816963.
44. **Mosiori, C. O., Oeba, D. A., & Shikambe, R. (2017).** Determination of Planck's Constant using Light Emitting Diodes. *Traektoriâ Nauki= Path of Science*, *3*(10), 2007-2012. doi: 10.22178/pos.27-2.
45. **Michael M.** (**2010).** Understanding crane accidents failures: A report on cause of death in crane-related accidents. CPWR, Centre for construction Research and Training.
46. **Nguyen, S. T., & La, H. M. (2018).** Development of a steel bridge climbing robot. In *2019 IEEE/RSJ International Conference on Intelligent Robots and Systems (IROS)* (pp. 1912-1917). IEEE. doi: 10.1109/IROS40897.2019.8967748.
47. **Öztürk, S., İcin, K., Öztürk, B., Topal, U., Karaağaç, Ö., & Köçkar, H. (2018).** The role of wheel surface quality on structural and hard magnetic properties of Nd–Fe–B permanent magnet powders. *Journal of Superconductivity and Novel Magnetism*, *31*, 3025-3041. doi: 10.1007/S10948-018-4561-7.

48. **PIC16F87XA Data Sheet (2003)**28/40/44-Pin Enhanced Flash Microcontrollers,”.
49. **Pearson, N. R., Boat, M. A., Priewald, R. H., Pate, M. J., & Mason, J. S. (2012, April).** A study of MFL signals from a spectrum of defect geometries. In *18th World Conference on Non-destructive Testing* (pp. 16-20). Accessed: May 08, 2022. [Online]. Available: http://www.ndt.net/?id=12649.
50. **Pearson, N.R., Boat, M.A., and J. S. D. Mason, J.S.D. (2016)** “Bandwidth of MFL in steel plate inspection,” .
51. **Pelkner, M., Pohl, R., Erthner, T., Kreutzbruck, M., & Commandeur, C. (2014)**. Detection of hidden defects in thin steel plates using GMR sensor arrays. In *Proc. 11th Eur. Conf. Non-Destructive Test.* (pp. 1-9). Accessed: May 08, 2022. [Online]. Available: www.ndt.net/?id=16559.
52. **Petit, F., Juraszek, J., Youssef, J. B., Teillet, J., Dekadjevi, D. T., & Le Gall, H. (2005)**. Effect of annealing on the structural and magnetic properties of giant magnetostrictive multilayers. *Journal of magnetism and magnetic materials*, *290*, 839-842. doi: 10.1016/J.JMMM.2004.11.389.
53. **Postolache, O., Ribeiro, A. L., & Ramos, H. G. (2013).** GMR array uniform eddy current probe for defect detection in conductive specimens. *Measurement*, *46*(10), 4369-4378. doi: 10.1016/J.MEASUREMENT.2013.06.050
54. **Roberts, J. F., Stirling, T., Zufferey, J. C., & Floreano, D. (2007).** Quadrotor using minimal sensing for autonomous indoor flight. In *European Micro Air Vehicle Conference and Flight Competition (EMAV2007)* (No. CONF). Accessed: Dec. 16, 2021. [Online]. Available: https://infoscience.epfl.ch/record/111485
55. **Saha, S., Mukhopadhyay, S., Mahapatra, U., Bhattacharya, S., & Srivastava, G. P. (2010)**. Empirical structure for characterizing metal loss defects from radial magnetic flux leakage signal. *Ndt & E International*, *43*(6), 507-512. doi: 10.1016/J.NDTEINT.2010.05.006.
56. **Sahari, K. S. M., Anuar, A., Mohideen, S. S. K., Baharuddin, M. Z., Ismail, I. N., Basri, N. M. H., ... & Ahmad, B. (2012, November).** Development of robotic boiler header inspection device. In *The 6th International Conference on Soft Computing and Intelligent Systems, and The 13th International Symposium on Advanced Intelligence Systems* (pp. 769-773). IEEE. doi: 10.1109/SCIS-ISIS.2012.6505345.
57. **San-Millan, A. (2015, June).** Design of a teleoperated wall climbing robot for oil tank inspection. In *2015 23rd Mediterranean Conference on Control and Automation (MED)* (pp. 255-261). IEEE. doi: 10.1109/MED.2015.7158759.
58. S**choeneich, P., Rochat, F., Nguyen, O. T. D., Caprari, G., Moser, R., Bleuler, H., & Mondada, F. (2010, October**). Tubulo—A train-like miniature inspection climbing robot for ferromagnetic tubes. In *2010 1st International Conference on Applied Robotics for the Power Industry* (pp. 1-5). IEEE. doi: 10.1109/CARPI.2010.5624462.

59. S**hin, I. J. (2015)**. Factors that affect safety of tower crane installation/dismantling in construction industry. *Safety science*, *72*, 379-390. doi: 10.1016/J.SSCI.2014.10.010.
60. **Shin, J. U., Kim, D., Kim, J. H., & Myung, H. (2013, August)**. Micro aerial vehicle type wall-climbing robot mechanism. In *2013 IEEE RO-MAN* (pp. 722-725). IEEE. doi: 10.1109/ROMAN.2013.6628398.
61. **Siritaratiwat, A., Hill, E. W., Stutt, I., Fallon, J. M., & Grundy, P. J. (2000).** Annealing effects on GMR multilayer films. *Sensors and Actuators A: Physical*, *81*(1-3), 40-43. doi: 10.1016/S0924-4247(99)00112-0.
62. **Song, W., Jiang, H., Wang, T., Ji, D., & Zhu, S. (2018)**. Design of permanent magnetic wheel-type adhesion-locomotion system for water-jetting wall-climbing robot. *Advances in Mechanical Engineering*, *10*(7), 1687814018787378. oi: 10.1177/1687814018787378.
63. **Stramigioli, S., Mahony, R., & Corke, P. (2010, May).** A novel approach to haptic tele-operation of aerial robot vehicles. In *2010 IEEE International Conference on Robotics and Automation* (pp. 5302-5308). IEEE. doi: 10.1109/ROBOT.2010.5509591.
64. **Tâche, F., Fischer, W., Caprari, G., Siegwart, R., Moser, R., & Mondada, F. (2009).** Magnebike: A magnetic wheeled robot with high mobility for inspecting complex-shaped structures. *Journal of Field Robotics*, *26*(5), 453-476. doi: 10.1002/ROB.20296
65. **Tavakoli, M., Viegas, C., Marques, L., Pires, J. N., & De Almeida, A. T. (2013)**. OmniClimbers: Omni-directional magnetic wheeled climbing robots for inspection of ferromagnetic structures. *Robotics and Autonomous Systems*, *61*(9), 997-1007. doi: 10.1016/j.robot.2013.05.005.
66. **Wang, R., & Kawamura, Y. (2016)**. An automated sensing system for steel bridge inspection using GMR sensor array and magnetic wheels of climbing robot. *Journal of Sensors*, *2016*. doi: 10.1155/2016/8121678.
67. **Wang, R., & Kawamura, Y. (2016)**. Development of climbing robot for steel bridge inspection. *Industrial Robot: An International Journal*, *43*(4), 429-447. doi: 10.1108/IR-09-2015-0186/FULL/XML.
68. **Xiao, C., & Zhang, Y. (2011)**. A method of magnetic scanning imaging for detecting defects in ferromagnetic materials. *Measurement Science and Technology*, *22*(2), 025503. doi: 10.1088/0957-0233/22/2/025503.
69. **Xiao, P., Guo, R., Luan, Y., Wang, H., Li, L., Zhang, F., & Pang, D. (2013)**. Design of a laser navigation system for substation inspection robot. In *2013 10th IEEE International Conference on Control and Automation (ICCA)* (pp. 739-743). IEEE. doi: 10.1109/ICCA.2013.6564880.
70. **Xu, X. J., Chen, H. D., Yang, Z. Y., Hu, S. C., & Yan, Y. (2020)**. Magnetic linear driving method for high-voltage direct current inspection robot. *International*

Journal of Advanced Robotic Systems, *17*(3), 1729881420930933. doi: 10.1177/1729881420930933.

71. **Yadav, A., & Szpytko, J. (2020).** Development of Portable Wireless Non-Destructive Crack Identification Method by Using GMR Sensor Array for Overhead Crane Bridges. 11th International Symposium on NDT in Aerospace, Nov 2019, Paris-Saclay, France. e-Journal of Non-destructive Testing Vol. 25(2). https://www.ndt.net/?id=25059
72. **Yadav, A., & Szpytko, J. (2020).** Magnetic Wheeled Automated Robot for Structural Health Monitoring of Overhead Crane by using NDT method. Singapore International NDT Conference & Exhibition, 4-5 Dec 2019. e-Journal of Non-destructive Testing Vol. 25(4). https://www.ndt.net/?id=25147
73. **Yadav, A., & Szpytko, J. (2019)**. Design of an automated magnetic wheeled robot for crack inspection of overhead cranes by using NDT GMR sensor. NDE 2018 Conference & Exhibition of the society for NDT (ISNT), 19-21 December 2018, Mumbai, India. e-Journal of Non-destructive Testing Vol. 24(6). https://www.ndt.net/?id=24361
74. **Yadav, A. Kumar, & Szpytko J. (2022).** "Method of increasing reliability of large dimensional bridge-type structures." Journal of KONBiN 52.2 (2022): 47-62.
75. **Yadav,A., & SZPYTKO J. (2020)** Interoperability tool to the non-destructive testing: crane bridge case study W: Projektowaniei eksploatacjamaszynroboczych, Cz. 2 / red. nauk. Tadeusz Łagoda, Marta Kurek, Andrzej Kurek. — Opole: Oficyna Wydawnicza Politechniki Opolskiej, 2020. — (Studia i Monografie / Politechnika Opolska ; ISSN 1429-6063 ; z. 542). — ISBN: 978-83-66033-84-9. — S. 283-294.
76. **Yadegari, A. M., Moini, R., Sadeghi, S. H. H., & Mazlumi, F. (2010).** Output signal prediction of an open-ended rectangular waveguide probe when scanning cracks at a non-zero lift-off. *NDT & E International*, *43*(1), 1-7. doi: 10.1016/J.NDTEINT.2009.08.004.
77. **Yang, G., Zeng, Z., Deng, Y., Liu, X., Udpa, L., & Dib, G. (2012).** Sensor-tilt invariance analysis for eddy current signals. *NDT & E International*, *52*, 1-8. doi: 10.1016/J.NDTEINT.2012.08.006.
78. **Zhu, D., Yi, X., Wang, Y., Lee, K. M., & Guo, J. (2010)**. A mobile sensing system for structural health monitoring: design and validation. *Smart materials and structures*, *19*(5), 055011. doi: 10.1088/0964-1726/19/5/055011.

Appendix 1:

1. **Yadav, Arun Kumar, and Janusz Szpytko.** "Advanced communication system: for the survey of rail tracks to improve safety of rail transportation." Journal of KONES 24.2 (2017): 315-322.

   Abstract: Railway transportation is a backbone of any country for transporting people and cargo. At present Indian railway is the largest network in Asia. So that safety is always big concern. Here in this article low cost railway track surveillance and monitoring system is proposed which will identify drastic and minor changes into the railway track. It consists a high-resolution CMOS camera mounted on robot. It is designed like: it can easily roll on railway track. In case of any obstacle or train coming on track, robot folds itself and provides a path to pass the train. It is controlled by wireless control system, which can be operated from remote location or station. For accurate results, a live video streaming is done to the remote station for future references and comparison of results. On the assembly of robot, a GPS (Global Positioning System) is mounted to know the location of robot on the rail track. An obstacle detector sensor is also mounted on the front of the robot to detect any coming obstacle. In this article ultrasonic method (Non-Destructive Method) is also explained to detects presence of cracks on rail track in real time. Overall, power utilization of this system will be very low by operating this system by solar power. Signal processing and wireless communication system is used as technology, which cuts off the overall cost. By implementing this surveillance system, we can improve the safety parameters of Indian railway by minimizing the errors and reducing the time and cost.

2. **Yadav, Arun Kumar, and Janusz Szpytko.** " *Design of an automated magnetic wheeled robot for crack inspection of overhead cranes by using NDT & GMR sensor* / // W: *NDE-India 2018 [Dokumentelektroniczny]* : *conference & exhibition of the society for NDT (ISNT) : 19–21 December 2018, Mumbai, India*.

   Abstract: Overhead crane plays a vital role in almost all industries, and work under many harsh environmental conditions. Repetitive heavy loading and harsh environmental situations cause structural failure of overhead crane bridges. Corrosion is one of the major causes of structural failures. Regular and effective monitoring can contribute to minimizing the structural failures. This research work proposed an automated robot MILA3D for the inspection of steel structures, particularly for overhead crane bridges. MILA3D can perform crack detection and corrosion detection by using NDT technique and 16 channel GMR (Giant Magneto-Resistance) sensor array. Designed magnetic wheel not only provides adhesion

forces to climb on a vertical surface but also contribute to the detection of defects & flaws into steel surface by emitting a magnetic field. The MILA3D robot have some special features like compact & flexible structure, fully autonomous, collects data and send back to the remote location station for real-time monitoring as well as also enables to create a 3D map of the inspection area. The proposed method provides a noticeable contribution in deprecating the limitations of recent overhead crane bridges inspection methods by providing a cost economical and effective solution by using the GMR sensor and NDT technologies.

3. ***Yadav, A., & Szpytko, J.*** *(2020). Development of Portable Wireless Non-Destructive Crack Identification Method by Using GMR Sensor Array for Overhead Crane Bridges . 11th International Symposium on NDT in Aerospace, Nov 2019, Paris-Saclay, France. e-Journal of Non-destructive Testing Vol. 25(2). https://www.ndt.net/?id=25059*.

Abstract: Structural Health monitoring of overhead cranes bridges by the traditional inspection system with wired and bulky instrumental technologies face many challenges during the harsh environment and under working condition. This paper proposes a portable wireless and efficient NDT method using the GMR sensor array technique for the identification of fatigue cracks in the bridges of travelling overhead cranes. In this paper, to enhance the efficiency of overhead cranes by minimizing the inspection time, a portable wireless robot combined with GMR (Giant Magnet Resistive) sensor and NDT technique is developed. This novel solution offers mobility, high accuracy and low power consumption. For the detection of cracks and defects in overhead crane bridge eight GMR (Giant Magneto Resistive) sensors NVE (AA006-02) placed linearly on a PCB board with equal distance. Two magnetic wheel of neodymium N42 located on both side of the GMR sensor array to magnetize the steel surface for accurate defect reorganization. Unlike MPI (Magnetic Particle Inspection) where a global magnetization requires for further inspection, this automated detection system only magnetize the surface area under the vicinity of GMR sensor array. The instrumentation circuit including eight high speed multiplexer, Operational amplifier, and one 8 bit analog to digital converter. A PIC 877A microcontroller and raspberry pie was used to perform local data storage, data processing and controlling. In order to verify its performance and efficiency few experiments have been conducted in laboratory. This presented testing solution is quick and offers a step towards automated testing of overhead crane bridges. However, it improves the work efficiency and can meet the serious challenges within the inspection of overhead crane bridges.

4. ***Yadav, Arun Kumar, and Janusz Szpytko**. "How to Connect Hyperloop Technology with the Smart City Transportation Concept." Electric Mobility in Public Transport—Driving Towards Cleaner Air. Cham: Springer International Publishing, 2021. 201-216.*

Abstract: The paper is trying to find the answer for the following question: how to connect Hyperloop technology with the green-based transportation concept, as well as discussing the implementation of Hyperloop technology concept to improve communication for smart cities. The paper discusses also the possibilities of developing smart cities using the potential of innovative electrical-based transport technologies with use the vacuum transport system for carrier passengers, as well any types of loads in the carriage in pipes with reduced air pressure.

5. **Yadav, A. K., and J. Szpytko**. "Impact of transportation telematics to sustainable development, India and Poland case study." *Archives of Transport System Telematics* 11 (2018).

Abstract: This paper presents the positive impacts of telematics system in the sustainable development of any country. With the growing population and urbanization, high demand of movement of people and goods are occurring. From last few years in India, transportation system network is expanding rapidly and contributing a huge role into the economic growth. Due to the enhancement of traffic flow, there is need of implementation of telematics system so that the negative effects caused by the increased traffic can be converted in sustainable development of the country. Use of Telematics system in India and Poland can helps to improve the efficiency of transport system by minimize the fuel consumption which overall results into sustainable development by reducing the environmental effect by transportation. This paper outlines how the telematics system into transportation system aims to contribute in achieving sustainable development in country with the case studies of India and Poland.

6. ***Yadav, A. K., and J. Szpytko**. "Implementation of intelligent vehicle safety system eCall type, India case study." Archives of Transport System Telematics 11 (2018).*

Abstract: *T*he Indian government is still promoting eCall to minimize the number of roadway disaster by reducing the response time when an accident has occurred. The eCall system is combination of an In Vehicle System(IVS), consisting of a device with a GSM cell phone and GPS (Global Positioning System)for location Tracking facility and it all consist of corresponding infrastructure of Public Safety Answering Points (PSAPs).This Intelligent Vehicle Safety System uses information and communication technologies for providing solutions for improving road safety in particular in the pre-crash phase when the accident can still be

avoided or at least its severity significantly reduced. By using this system which can operate either manually or autonomously on-board the vehicle, the number of accidents and their severity can be reduced. The implementation of on board emergency call (eCall) is an ITS (Intelligent Transport System) service which has been already been deployed in different countries. Several private and public initiatives have already resulted into preliminary and pure private eCall services, mainly to the car industry. Location, enhanced emergency calls like in vehicle eCall have their primary benefit to society of saving lives and in offering an increased sense of security significance.

7. **Yadav, Arun Kumar, and Janusz Szpytko.** *Interoperability tool to the non-destructive testing: crane bridge case study* W: *Projektowaniei eksploatacjamaszynroboczych*, Cz. 2 / red. nauk. Tadeusz Łagoda, Marta Kurek, Andrzej Kurek. — Opole : Oficyna Wydawnicza Politechniki Opolskiej, 2020. — (*Studia i Monografie* / Politechnika Opolska ; ISSN 1429-6063 ; z. 542). — ISBN: 978-83-66033-84-9. — S. 283-294.

Abstract: The paper presents a method of testing the girder of a bridge crane using a specialized measuring type robot. The girder of the bridge crane is an example of a largesize structure. The bridge structure of the crane is a critical subsystem of the transport device due to its operational safety. The purpose of the overhead crane girder tests is to increase the reliability of the structure and operational safety. The proposed solutions indeed comply with the standards in force. Also, they increase their frequency and effectiveness of concluding in terms of predicting possible causes of threats to the safety and reliability of the structure

8. ***Yadav, Arun Kumar, and Janusz Szpytko***. *"Method of increasing reliability of large dimensional bridge-type structures." Journal of KONBiN 52.2 (2022): 47-62.*

Abstract: This paper presents a method of testing the girder of a bridge crane using a specialized measuring type robot. The girder of the bridge crane is an example of a large-size structure. The bridge structure of the crane is a critical subsystem of the transport device due to its operational safety. The purpose of the overhead crane girder tests is to increase the reliability of the structure and operational safety. The proposed solutions indeed comply with the standards in force. Also, they increase their frequency and effectiveness of concluding in terms of predicting possible causes of threats to the safety and reliability of the structure.

9. ***Yadav, Arun K., and Janusz Szpytko***. *"Safety problems in vehicles with adaptive cruise control system." Journal of KONBiN 42.1 (2017): 389-398.*

***Abstract*:** In today's world automotive industries are still putting efforts towards more autonomous vehicles (AVs). The main concern of introducing the autonomous technology is safety of driver. According to a survey 90% of accidents happen due to mistake of driver. The adaptive cruise control system (ACC) is a system which combines cruise control with a collision avoidance system. The ACC system is based on laser and radar technologies. This system is capable of controlling the velocity of vehicle automatically to match the velocity of car, bus or truck in front of vehicle. If the lead vehicle gets slow down or accelerate, then ACC system automatically matches that velocity. The proposed paper is focusing on more accurate methods of detecting the preceding vehicle by using a radar and LIDAR sensors by considering the vehicle side slip and by controlling the distance between two vehicles. By using this approach i.e. logic for calculation of former vehicle distance and controlling the throttle valve of ACC equipped vehicle, an improvement in driving stability was achieved. The own contribution results with fuel efficient driving and with safer and reliable driving system, but still some improvements are going on to make it more safe and reliable.